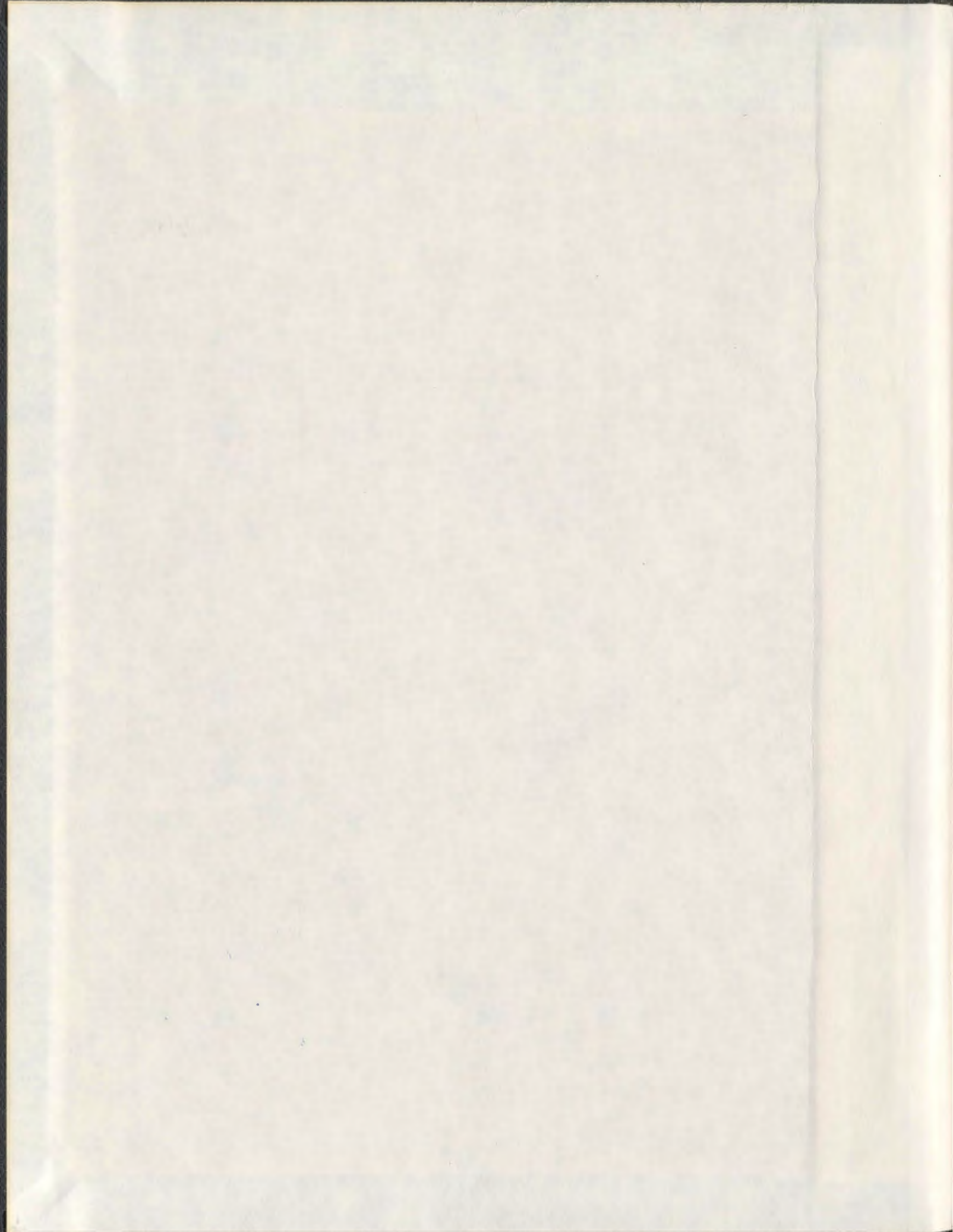


MULTIMETALLIC LITHIUM AND CHROMIUM
COMPLEXES OF AMINE-BIS(PHENOLATE) LIGANDS
AS POLYMERIZATION CATALYSTS

REBECCA DEAN



**Multimetallic Lithium and Chromium Complexes of Amine-bis(phenolate) Ligands
as Polymerization Catalysts**

by

© Rebecca Dean

A Thesis submitted to the School of Graduate Studies
in partial fulfillment of the requirements for the degree of

Doctor of Philosophy

Department of Chemistry

Memorial University of Newfoundland

October 2012

St. John's

Newfoundland

ABSTRACT

The synthesis of biodegradable and/or bioassimilable plastics has been growing in importance throughout the past decade. The steadily decreasing supply of fossil fuels, coupled with increased environmental awareness, has spurred an interest in alternative, renewable feedstocks for use in a variety of applications. The plastics industry is no exception. Therefore, an investigation of lithium and chromium complexes was undertaken for the catalytic synthesis of polyesters and polycarbonates from renewable feedstocks.

The ligands used in this thesis were tetradentate tripodal amine-bis(phenolates), where the substituents on the phenolate groups and pendant arm could be varied. The synthesis and characterization of mono- and dimeric lithium complexes was performed. The lithium complexes were then used to synthesize a series of chromium(III) complexes by two methods. Salt-metathesis and protonolysis/oxidation routes were used to produce mono- and dimeric, paramagnetic Cr(III) complexes. The isolated complexes were characterized by NMR (where appropriate), IR, UV-Vis spectroscopy, mass spectrometry, magnetometry, cyclic voltammetry and elemental analysis. In addition, an attempt was made to synthesize Cr amide and alkyl complexes of these ligands.

The polymerization of *rac*-lactide to yield polylactide, was studied with lithium-salts of amine-bis(phenolate) ligands. Polymerization studies found that ring-opening polymerization of *rac*-lactide was possible in the presence or absence of an alcohol as a co-initiator. As well, the copolymerization of propylene oxide and cyclohexene oxide with CO₂ to yield polycarbonates was investigated with chromium(III) amine-

bis(phenolate) complexes. Polymers synthesized were shown to have high selectivity, great CO₂ incorporation and low polydispersities. Polymer analysis involved ¹H and ¹³C NMR, mass spectrometry, GPC, DSC and TGA.

ACKNOWLEDGEMENTS

First I would like to thank my supervisor Dr. Chris Kozak for giving me the opportunity to work on this exciting research project, his guidance and support and for his meticulous reading of my thesis chapters. As well, I would like to thank Dr. Fran Kerton for helpful discussions in group meeting throughout my program and for her valuable comments as a committee member. I also thank my co-supervisor, Dr. Karen Hattenhauer and my other supervisory committee member Dr. Sunil Pansare for useful suggestions throughout my studies.

I am also very grateful to have had the opportunity to work with a great group of people from all over the world in the Green Chemistry and Catalysis Group. Not many days would go by where there wasn't a great discussion going on in the lab or office. I have learned a lot from all of you! Specifically, I would like to thank Nduka, Hassan, Kamrul and Hu who were always around from the beginning of my program to lend a hand or have a chat. As well, my thanks to Justin and Katalin for their help in scanning or sending me files from St. John's. I am also very thankful to Stephanie Granville, an undergraduate who worked very hard synthesizing compounds with me during the summer of 2008, Angela Crane and Amy Reckling who also made my lab and social life in St. John's something to remember.

I am also thankful to everyone in C-CART for their knowledge and advice for the many instruments I used and to Lidan Tao in GaP. A special thank-you to Dr. Celine Schneider, Dr. Louise Dawe and Dr. Brent Myron in C-CART.

I would especially like to thank all the funding agencies who allowed me to complete my degree and attend many conferences during my program. NSERC (PGS award), SGS, Department of Chemistry, Dean of Science and GSU.

Last but not least, I thank my family and friends for their continued support throughout my educational life. To my parents, I am forever grateful for always allowing and encouraging me to follow my dreams and helping me financially in whatever way you could. To Rodney Smith, my fiancé who has always been there for me during the ups and downs and has made me a better person, I thank-you for your patience and guidance during my thesis writing.

Table of Contents

Abstract	ii
Acknowledgements	iv
List of Tables	xi
List of Figures	xiii
List of Schemes	xx
List of Abbreviations and Symbols.....	xxiii
List of Appendices	xxxi
Chapter 1. Introduction	1-68
1.1 Amine-bis(phenolate) Ligands.....	1
1.1.1 Group 4 Complexes (Ti and Zr)	2
1.1.2 Group 5 Complexes (Vanadium)	6
1.1.3 Group 6 Complexes (Chromium)	8
1.1.4 Group 7, 8 and 9 Complexes (Manganese, Iron and Cobalt)	9
1.2 Chromium(III) Catalysis	11
1.2.1 Introduction to the Element Chromium	11
1.2.2 Overview of Chromium Coordination Compounds.....	13
1.2.3 Chromium(II/III) β -Diketiminato Complexes.....	17
1.2.4 Chromium Organometallic Complexes for Olefin Polymerization	23
1.2.5 Chromium Salen Complexes	26
1.3 Copolymerization of Epoxides and Carbon Dioxide	32
1.4 Ring-Opening Polymerization of Lactide	46

1.5 Objectives.....	59
1.6 References.....	61
Co-Authorship Statement	69-71
Chapter 2. Synthesis of Amine-bis(phenolate) Ligands and Lithium Amine-bis(phenolate) Complexes	72-112
2.1 Introduction.....	72
2.2 Results and Discussion.....	76
2.2.1 Synthesis of Ligands and Lithium Complexes	76
2.2.2 Structural Characterization	78
2.2.3 NMR Spectroscopy.....	84
2.2.4 Mass Spectrometry	94
2.3 Experimental	98
2.3.1 General Experimental Conditions.....	98
2.3.2 Synthesis of Ligands and Lithium Compounds.....	99
2.3.3 X-ray Crystallography	106
2.4 Conclusion	109
2.5 References.....	110
Chapter 3. Ring-opening Polymerization of Cyclic Esters with Lithium Amine-bis(phenolate) Complexes	113-146
3.1 Introduction.....	113
3.2 Results and Discussion.....	114
3.2.1 Synthesis	114
3.2.2 Structural Characterization of Polymers.....	116

3.2.2.1 NMR Spectroscopy.....	127
3.2.2.2 Mass Spectrometry	133
3.2.2.3 Gel Permeation Chromatography	135
3.2.3 Mechanistic Proposal	137
3.3 Experimental	139
3.3.1. General Experimental Conditions.....	139
3.3.2. Polymerization Procedure	140
3.3.3. MALDI-TOF Mass Spectrometry	142
3.3.4. Gel Permeation Chromatography	142
3.4 Conclusions.....	143
3.5 References.....	144
Chapter 4. Synthesis and Structure of Chromium(III) Amine-bis(phenolate)	
Complexes	147-204
4.1 Introduction.....	147
4.2 Results and Discussion.....	148
4.2.1 Synthesis of Cr(III) Complexes	148
4.2.2 Structural Characterization	151
4.2.2.1 MALDI-TOF Mass Spectrometry	151
4.2.2.2 Single Crystal X-ray Diffraction	157
4.2.3 UV-Visible Spectroscopy	168
4.2.4 Magnetometry	173
4.2.5 Cyclic Voltammetry.....	177
4.2.6 Attempted Synthesis of Cr Amide and Alkyl Complexes	180

4.3 Experimental	186
4.3.1 General Experimental Conditions	186
4.3.2 Synthesis of Cr(III) Compounds	188
4.3.2.1 Reaction of CrCl complexes with salt metathesis reagents	193
4.3.3 X-ray Crystallography	194
4.4 Conclusion	199
4.5 References	200
Chapter 5. Chromium Amine-bis(phenolate) Complexes for the Copolymerization of Epoxides and Carbon Dioxide	205-251
5.1 Introduction	205
5.2 Results and Discussion	207
5.2.1 Synthesis	207
5.2.2 Copolymerization of Propylene Oxide and CO ₂	207
5.2.2.1 NMR Spectroscopy	213
5.2.2.2 Mass Spectrometry	217
5.2.2.3 Gel Permeation Chromatography	220
5.2.2.4 Thermal Analysis (DSC & TGA)	220
5.2.3 Copolymerization of Cyclohexene Oxide and CO ₂	222
5.2.3.1 NMR Spectroscopy	229
5.2.3.2 Mass Spectrometry	232
5.2.3.3 Gel Permeation Chromatography	235
5.2.3.4 Thermal Analysis (DSC & TGA)	236
5.2.4 Copolymerization of Styrene Oxide and CO ₂	238

5.2.5 Mechanistic Proposal	241
5.3 Experimental	244
5.3.1 General Experimental Conditions	244
5.3.2 Polymerization Procedure	245
5.3.3 Mass Spectrometry.....	246
5.3.4 Gel Permeation Chromatography	246
5.3.5 Differential Scanning Calorimetry	247
5.3.6 Thermal Gravimetric Analysis.....	247
5.4 Conclusions.....	248
5.5 References	249
Chapter 6. Conclusions and Future Projects	252-260
6.1 Conclusions and Future Remarks	252
6.2 References	259
Appendices	261-309

List of Tables

Table 2.1. Selected bond angles ($^{\circ}$) for 2.1 and 2.2	80
Table 2.2. Selected bond lengths (\AA) for 2.1 and 2.2	81
Table 2.3. Selected bond lengths (\AA) and angles ($^{\circ}$) for 2.3	84
Table 2.4. Chemical shifts δ (ppm), peak width at half height (Hz) and peak areas for complexes 2.1 and 2.2 in solution (^7Li) and solid state ($^6,7\text{Li}$) NMR	92
Table 2.5. Crystallographic and structure refinement data for 2.1 , 2.2 and 2.3	108
Table 3.1 ROP of <i>rac</i> -LA initiated by complexes 2.1 , 2.2 , 3.1 and 3.2	120
Table 3.2 ROP of <i>rac</i> -LA initiated by complexes 2.1 and 2.2	122
Table 3.3 Rate constants for the ROP of LA initiated by 2.1 and 2.2	126
Table 4.1 Selected bond lengths (\AA) and angles ($^{\circ}$) for 4.1 and 4.2	160
Table 4.2 Selected bond lengths (\AA) and angles ($^{\circ}$) for 4.5 and 4.6	164
Table 4.3 Selected bond lengths (\AA) and angles ($^{\circ}$) for 4.4	168
Table 4.4 Half wave potentials for oxidation of complexes 4.1 , 4.2 , 4.6 and L3	179
Table 4.5 Selected bond lengths (\AA) and angles ($^{\circ}$) for 4.7	183
Table 4.6 Selected bond lengths (\AA) and angles ($^{\circ}$) for 4.8	186
Table 4.7 Crystallographic and structure refinement data for 4.1 , 4.2 , 4.4 , 4.5 and 4.6 ..	197
Table 4.8 Crystallographic and structure refinement data for 4.7 and 4.8	198
Table 5.1. Results of the Copolymerization of PO and CO ₂ catalyzed by 4.4	211
Table 5.2. Coupling reaction of PO and CO ₂ initiated by L6 and complexes 4.2 and 4.3	212

Table 5.3. Results of the Copolymerization of CHO and CO ₂ for catalyst 4.4 with PPNX salts.	225
Table 5.4. Results of the Copolymerization of CHO and CO ₂ for catalyst 4.4 with DMAP.	228
Table 5.5. Copolymerization of CHO and CO ₂ initiated by complexes 4.2 and 4.3	229
Table 5.6. Results of the coupling reaction of SO and CO ₂ for complex 4.4	240

List of Figures

Figure 1.1. Tetradentate diaminobisphenol "salan" ligand, $H_2[ONNO]^{RR}$	3
Figure 1.2. Vanadium(IV) and (V) (when X = O) diamine-bis(phenolate) complexes.....	7
Figure 1.3. $V(=O)(OMe)[ONO]$ aminobisphenolato complex (1.5).	7
Figure 1.4. Homoleptic, six-coordinate $\{Cr[ONO]_2\}^-$ complex (1.6).	9
Figure 1.5. Examples of Fe(III) amine-bis(phenolate) complexes.	10
Figure 1.6. Examples of mono-, di- and tri-metallic Co amine-bis(phenolate) complexes.	11
Figure 1.7. A small selection of bi- and tetradentate N and O donor ligands.....	17
Figure 1.8. Monomeric $CrCl_2(THF)_2(Ph_2nacnac)$ complex (1.14).	19
Figure 1.9. ORTEP drawing of the molecular structure of T- (left) vs. Y-shaped (right) monomeric Cr alkyls. Thermal ellipsoids at 50% probability with H-atoms excluded for clarity. Images generated using CIF data provided in reference [46].	26
Figure 1.10. Salen and salan ligands.....	27
Figure 1.11. $[Cr(salen)(OH_2)_2]^+$ complex (1.23).	28
Figure 1.12. Jacobsen's chiral salen ligand.	29
Figure 1.13. $Cr(salen)$ complexes for asymmetric epoxidation.	30
Figure 1.14. Monometallic (1.27) and bimetallic (1.28) azide $Cr(salen)$ catalysts for ARO.	31
Figure 1.15. $Cr(salen)Cl$ complex (1.30) for the coupling of CO_2 and epoxides.....	38
Figure 1.16. $CrN_3(salen)$ complex (1.31).	41

Figure 1.17. Highly active Co(salen) complex (1.32) for CO ₂ /PO copolymerization.....	41
Figure 1.18. CrCl(salalen) complexes (1.33).....	42
Figure 1.19. CrX(salan) complex (1.34) for the copolymerization of CO ₂ and PO.	43
Figure 1.20. CrCl(salan) complex (1.35).....	44
Figure 1.21. Monometallic (1.36) and bimetallic (1.37) CrCl(salphen) complexes.....	45
Figure 2.1. Dimeric tetralithium complexes by Chen (1.46), (1.47), (1.48) and O'Hara (2.0).....	74
Figure 2.2. Kerton, Kozak {Li ₂ [O ₂ N ₂] ^{BuBu} (dioxane) _{1.5} } ₂ complex (2.0a) and single unit of {Li ₂ [O ₂ NN'] ^{BuBu} (dioxane)} _∞ complex (2.0b).....	75
Figure 2.3. ORTEP diagrams of the molecular structures and partial numbering schemes of 2.1 (left) and 2.2 (right). Ellipsoids are shown at 50% probability. Hydrogen atoms were omitted for clarity. Symmetry operation used to generate equivalent atoms for 2.2 : 1-x, y, ½-z.	78
Figure 2.4. ORTEP diagram of the molecular structure and partial numbering scheme of 2.3 . Ellipsoids are shown at 50% probability. Hydrogen atoms were omitted for clarity.	82
Figure 2.5. ¹ H NMR spectrum of 2.1 in C ₆ D ₆ at 298 K (500 MHz).....	86
Figure 2.6. ¹ H NMR spectrum of 2.1 in D ₈ -Tol at 298 K (500 MHz).....	87
Figure 2.7. Portion of the VT ¹ H NMR spectrum of 2.1 in D ₈ -Tol from 248 – 378 K, corresponding to methyl and <i>tert</i> -butyl peaks (300 MHz).....	88
Figure 2.8. ¹ H NMR spectrum of 2.1 in D ₅ -Py at 298 K (500 MHz).	89
Figure 2.9. ⁷ Li NMR spectra at 7.04 T for complex 2.2 in D ₅ -Py (top) and C ₆ D ₆ (bottom).	91
Figure 2.10. VT ⁷ Li NMR spectra at 7.04 T for complex 2.1 in D ₈ -Tol.	92

Figure 2.11. ^7Li MAS (20 kHz) and ^6Li MAS (15 kHz) spectra of complex 2.2 at 14 T.	94
Figure 2.12. MALDI-TOF mass spectrum of $\{\text{Li}_2[\text{O}_2\text{NO}]^{\text{BuMe}}\}_2$ (2.1).	96
Figure 2.13. Experimental and theoretical MALDI-TOF MS isotopic distribution pattern for 2.1 (top = monomer, bottom = dimer).	97
Figure 3.1. Lithium amine-bis(phenolate) complexes 3.1 and 3.2 .	115
Figure 3.2. ^1H NMR spectrum for an attempted ROP reaction of β -BL, where M = monomer and P = polymer (in CDCl_3).	117
Figure 3.3. % conversion vs. time for the ROP of LA at 40 °C initiated by 2.1 .	121
Figure 3.4. Plots of $\ln[\text{LA}]_0/[\text{LA}]_t$ vs. time and $1/[\text{LA}]_t$ vs. time, $[\text{LA}]_0/[\mathbf{2.1}]_0 = 100$, $[\text{Li}] = 17.2$ mM; (a) $\bullet = 26$ °C (BnOH) ($R^2 = 0.97_6$), $\circ = 26$ °C (no BnOH) ($R^2 = 0.98_2$), $\blacktriangledown = 40$ °C (BnOH) ($R^2 = 0.98_9$), and (b) $\blacksquare = 60$ °C (BnOH) ($R^2 = 0.98_5$), $\Delta = 80$ °C (BnOH) ($R^2 = 0.99_9$).	124
Figure 3.5. Plots of $\ln[\text{LA}]_0/[\text{LA}]_t$ vs. time and $1/[\text{LA}]_t$ vs. time, $[\text{LA}]_0/[\mathbf{2.2}]_0 = 100$, $[\text{Li}] = 14.7$ mM; (a) $\bullet = 26$ °C (BnOH) ($R^2 = 0.97_4$), $\circ = 26$ °C (no BnOH) ($R^2 = 0.97_4$), $\blacktriangledown = 40$ °C (BnOH) ($R^2 = 0.99_7$), $\Delta = 60$ °C (BnOH) ($R^2 = 0.96_7$), and (b) $\blacksquare = 80$ °C (BnOH) ($R^2 = 0.99_4$).	124
Figure 3.6. ^1H NMR spectra of the methine region for aliquots taken from ROP of LA initiated by complex 2.1 at 60 °C (300 MHz, CDCl_3).	127
Figure 3.7. Typical ^1H NMR spectrum of $[\text{LA}]:[\text{Li}]:[\text{BnOH}] = 1:100:1$ in CDCl_3 , 300 MHz (entry 9, Table 3.1).	129
Figure 3.8. Typical ^{13}C NMR spectrum of PLA in CDCl_3 , 75 MHz (entry 2, Table 3.2).	130

Figure 3.9. Typical ^1H NMR spectrum of $[\text{LA}]:[\text{Li}]:[\text{BnOH}] = 1:50:0$ in CDCl_3 , 300 MHz (entry 8, Table 3.1), where M = monomer.....	131
Figure 3.10. (Left) ^{13}C NMR spectrum (75.49 MHz, CDCl_3) and (Right) $^1\text{H}\{^1\text{H}\}$ NMR spectrum (500 MHz, CDCl_3) of the methine region of PLA produced by $[\text{LA}]_0:[\mathbf{2.1}]_0:[\text{BnOH}]_0 = 100:1:1$ in toluene.	133
Figure 3.11. Typical MALDI-TOF mass spectrum of PLA (entry 9, Table 3.1).	135
Figure 4.1. MALDI-TOF mass spectrum of $\text{CrCl}(\text{THF})[\text{O}_2\text{NO}]^{\text{BuMe}}$ (4.1).	152
Figure 4.2. Experimental and theoretical MALDI-TOF MS isotopic distribution pattern for 4.1	153
Figure 4.3. Lower mass region of the MALDI-TOF mass spectrum of $\{\text{CrCl}[\text{O}_2\text{NN}']^{\text{BuBu}}\}(\mu\text{-HO})\{\text{CrCl}[\text{HO}_2\text{NN}']^{\text{BuBu}}\}$ (4.6).	154
Figure 4.4. Experimental and theoretical MALDI-TOF MS isotopic distribution pattern for $\text{CrCl}[\text{O}_2\text{NN}']^{\text{BuBu}}$ fragment in 4.6	155
Figure 4.5. MALDI-TOF mass spectrum of $\{\text{CrCl}[\text{O}_2\text{NN}']^{\text{BuBu}}\}_2$ (4.4).	156
Figure 4.6. Experimental and theoretical MALDI-TOF MS isotopic distribution pattern for monomer fragment in 4.4	157
Figure 4.7. Molecular structures (ORTEP) and partially labelled numbering scheme of 4.1 (top) and 4.2 (bottom). Ellipsoids are shown at 30% and 50% probability, respectively. Hydrogen atoms are omitted for clarity.	159
Figure 4.8. Molecular structures (ORTEP) and partially labelled numbering scheme of 4.5 (left) and 4.6 (right). Ellipsoids are shown at 50% probability and hydrogen atoms are omitted for clarity, except for H(117) and H(118) on 4.6 . Symmetry operation used to generate equivalent atoms in 4.5 : $\frac{1}{2}\text{-x}, y, \frac{1}{2}\text{-z}$	162

Figure 4.9. Molecular structure (ORTEP) and partial numbering scheme of $\{\text{CrCl}[\text{O}_2\text{NN}^{\text{BuBu}}]\}_2$ (4.4). Ellipsoids are drawn at 50% probability and hydrogen atoms are omitted for clarity. Symmetry operation used to generate equivalent atoms: 1-x, -y, 1-z.....	167
Figure 4.10. UV-Vis absorption spectra of 4.1 (top) and 4.2 (bottom).	170
Figure 4.11. UV-Vis absorption spectra of 4.3 (top) and 4.6 (bottom).	172
Figure 4.12. Magnetic susceptibility (per mole of bimetallic complex) vs. temperature plot (top) and magnetic moment vs. temperature plot (bottom) for 4.6 . The solid line (–) was generated using the Heisenberg dimer model with $J = -16.5 \text{ cm}^{-1}$, $g = 1.92$ and $P = 0.0079$. Experimental data were corrected for $TIP = 23.0 \times 10^{-4} \text{ cm}^3 \text{ mol}^{-1}$. The dashed line (--) was generated using a biquadratic function with $J = -18.2 \text{ cm}^{-1}$, $j = -0.69 \text{ cm}^{-1}$, $g = 2.10$ and $P = 0.011$	176
Figure 4.13. Magnetic moment vs. temperature plot for 4.4	177
Figure 4.14. Cyclic voltammograms of 4.1 , 4.2 and 4.6 [$(n\text{-Bu})_4\text{N}]\text{PF}_6$) at 20 °C and a scan rate of 200 mV s^{-1}	179
Figure 4.15. Cyclic voltammogram of L3 in CH_2Cl_2 (0.1 M [$(n\text{-Bu})_4\text{N}]\text{PF}_6$) at 20 °C and a scan rate of 200 mV s^{-1}	180
Figure 4.16. Molecular structure (ORTEP) and partially labelled numbering scheme of $\text{Cr}(\text{NMe}_2)\text{NHMe}_2[\text{O}_2\text{NO}]^{\text{BuMe}}$ complex 4.7 . Ellipsoids are shown at 50% probability and hydrogen atoms other than H(2) are omitted for clarity.	182
Figure 4.17. Molecular structure (ORTEP) and partially labelled numbering scheme of a single $\text{Cr}_2\text{Li}_2\text{O}_5$ moiety of complex 4.8 . Ellipsoids are shown at 50% probability and	

hydrogen atoms were omitted for clarity. Symmetry operation used to generate equivalent atoms: -x, -y, -z.	184
Figure 4.18. Molecular structure (ORTEP) and partially labelled numbering scheme of the “window pane-like” Cr ₂ Li ₂ O ₅ core of complex 4.8 . Ellipsoids are shown at 50% probability and hydrogen atoms were omitted for clarity.	185
Figure 5.1. Common co-catalysts used in epoxide/CO ₂ copolymerization reactions.	208
Figure 5.2. ¹ H NMR of the copolymerization of PO and CO ₂ (Table 5.1, entry 3, 300 MHz, CDCl ₃).	214
Figure 5.3. ¹ H NMR of the depolymerization of PPC to PC with time (300 MHz, CDCl ₃).	215
Figure 5.4. Carbonyl region of the ¹³ C NMR spectrum (75.5 MHz, CDCl ₃) of PO/CO ₂ copolymer prepared with PPNCI (Table 5.1, entry 7).	216
Figure 5.5. Possible regiochemistry of PPC.	217
Figure 5.6. (A) MALDI-TOF MS of PPC produced by 4.4 (Table 5.1, entry 7). (B) Magnified region of the spectrum (n = 44-48). Modeled isotopic masses (when n = 47) and images for polymer chains with end groups (a-c).	219
Figure 5.7. Representative DSC trace of PPC produced by 4.4 , 2 nd heat cycle (Table 5.1, entry 7).	221
Figure 5.8. Representative TGA trace and derivative plot of PPC produced by 4.4 (Table 5.1, entry 7).	222
Figure 5.9. Typical ¹ H NMR spectrum of PCHC in CDCl ₃ (Table 5.4, entry 12).	230
Figure 5.10. Carbonyl region of the ¹³ C NMR spectrum (75.5 MHz, CDCl ₃) of CHO/CO ₂ copolymer prepared with DMAP (Table 5.4, entry 5).	231

Figure 5.11. Stereochemistry of PCHC.	232
Figure 5.12. (A) MALDI-TOF MS of PCHC produced by 4.4 (Table 5.4, entry 13). (B) Magnified region of the spectrum (n = 26-29). Modeled isotopic masses (when n = 27) and images for polymer chains with end groups (a-d).....	234
Figure 5.13. Representative TGA curve of PCHC produced by 4.4 (Table 5.4, entry 5).	237
Figure 5.14. Representative DSC trace of PCHC produced by 4.4 , 2 nd heat cycle (Table 5.4, entry 5).	238
Figure 5.15. ¹ H NMR spectrum of an aliquot from the reaction mixture of SO/CO ₂ in CDCl ₃ (Table 5.6, entry 3).....	239
Figure 6.1. Potential examples of amine-bis(phenol) ligands for Li and Cr complexes..	253

List of Schemes

Scheme 1.1. Synthesis of $\text{Ti}(\text{O}^i\text{Pr})_2[\text{O}_2\text{NN}^i]$ complex (1.1).....	2
Scheme 1.2. Synthesis of $\text{ZrCl}_2[\text{O}_2\text{NN}^i]^R$ (1.2) and $\text{Zr}\{[\text{O}_2\text{NN}^i]^{Mc}\}_2$ (1.3) complexes.....	4
Scheme 1.3. Zr amine-bis(phenolate) complex (1.4) featuring a tetrahydrofuranlyl pendant donor side-arm on the ligand.	5
Scheme 1.4. Synthesis of Zr salan complexes.	5
Scheme 1.5. Synthesis of the first Cr β -diketiminate complexes (1.11 , 1.12a , 1.12b and 1.13).	18
Scheme 1.6. Synthesis of dimeric $\text{Cr}(\text{III})(\mu\text{-Cl})\text{nacnac}$ complexes (1.15) and (1.16).	20
Scheme 1.7. Attempted synthesis of Cr alkyls giving mono- (1.17 and 1.18) and dimeric (1.19) Cr nacnac complexes.....	21
Scheme 1.8. Attempted synthesis of dialkyls produced disproportionation to 1.17 and CrPh_4 , as well as $\text{Cr}(\text{Ph}_2\text{nacnac})_2\text{Ph}$ (1.20).	22
Scheme 1.9. Synthesis of cationic $\text{Cr}[(2,6\text{-Me}_2\text{Ph})\text{nacnac}]$ alkyls as single-site polymerization catalysts.....	25
Scheme 1.10. General reaction of common epoxides and CO_2 producing cyclic carbonate and/or polycarbonate. PO = propylene oxide, CHO = cyclohexene oxide, and SO = styrene oxide.	32
Scheme 1.11. Proposed general catalytic cycle for the copolymerization of CO_2 /epoxides.	34
Scheme 1.12. Proposed bimetallic initiation pathway for a model salen complex.....	34

Scheme 1.13. Synthesis of CrTFPPCl complex (1.29).....	35
Scheme 1.14. Stereochemistry of PPC derived from PO/CO ₂ copolymerization.....	38
Scheme 1.15. The coordination-insertion mechanism for PLA synthesis.	48
Scheme 1.16. Intermolecular and intramolecular transesterification.....	48
Scheme 1.17. Synthesis of hexalithium clusters (1.38), (1.39) and (1.40).	51
Scheme 1.18. Synthesis of octalithium (1.41) and tetralithium (1.42) complexes.	52
Scheme 1.19. Synthesis of mono- (1.43), (1.45) and dilithium (1.44) complexes.	53
Scheme 1.20. Synthesis of tetralithium complexes (1.46), (1.47) and (1.48).....	54
Scheme 1.21. Synthesis of dimeric lithium complexes (1.49), (1.50), (1.51), (1.52) and monomeric-BnOH adduct (1.53).	56
Scheme 1.22. Synthesis of monomeric lithium complex (1.54).	57
Scheme 1.23. Synthesis of di- (1.55), (1.57), (1.59), (1.60), (1.61) and tetra- (1.56) and (1.58) lithium and sodium complexes.....	58
Scheme 2.1. Synthesis of amine-bis(phenol) ligands.	76
Scheme 2.2. Synthesis of lithium complexes 2.1 and 2.2.....	77
Scheme 3.1. Synthetic procedure for the ROP of LA, CL and β-BL.	116
Scheme 3.2. Proposed mechanism of the ROP of <i>rac</i> -LA initiated by {Li ₂ [O ₂ NO] ^{RR'} } ₂	138
Scheme 4.1. Synthetic routes to Cr(III) complexes, <i>Method A</i> : salt metathesis and <i>Method B</i> : protonolysis/oxidation by air.....	150
Scheme 4.2. Attempted synthesis of Cr(III) amide and alkyl complexes.....	181
Scheme 5.1. Copolymerization of PO and CO ₂	207
Scheme 5.2. Copolymerization of CHO and CO ₂	223

Scheme 5.3. A proposed route to the chain transfer reaction.	235
Scheme 5.4. Copolymerization of SO and CO ₂	239
Scheme 5.5. Proposed mechanism for the copolymerization of CO ₂ with PO and CHO with Cr amine-bis(phenolate) complexes.	243
Scheme 5.6. Formation of propylene carbonate <i>via</i> back-biting mechanism.	244
Scheme 6.1. Generic synthesis of a poly(ester- <i>co</i> -carbonate).	258

List of Abbreviations and Symbols

CH₃CN: acetonitrile

acac: acetylacetonato

E_a: activation energy

et al.: and co-workers

Å: Angstrom (10⁻¹⁰ m)

ARO: asymmetric ring-opening

amu: atomic mass unit

BnOH: benzyl alcohol

j: biquadratic exchange constant

BPA: bisphenol A

salan: N,N'-bis(phenolato)-1,2-diaminoethane

salen: N,N'-bis(salicylaldehyde)ethylenediamine)

salphen: N,N-bis(salicylidene)-1,2-diaminobenzene

PPNN₃: bis(triphenylphosphoranylidene)iminium azide

PPNCl: bis(triphenylphosphoranylidene)iminium chloride

μ_B: bohr magneton

br: broad

BuLi: butyllithium

β-BL: β-butyrolactone

CaH₂: calcium hydride

CL: ϵ -caprolactone
cm: centimetre (10^{-2} m)
CT: charge transfer
 δ : chemical shift
Cl⁻: chloride ion
CHCl₃: chloroform
J: coupling constant
 θ : Curie-Weiss term
CV: cyclic voltammetry
CHC: cyclohexene carbonate
CHO: cyclohexene oxide
Cp: cyclopentadienyl
Da: Dalton
(°): degree
C₆D₆: deuterated benzene
CDCl₃: deuterated chloroform
D₅-Py: deuterated pyridine
D₈-Tol: deuterated toluene
D₂O: deuterium oxide
CH₂Cl₂: dichloromethane
Et₂O: diethyl ether
DSC: differential scanning calorimetry
DHBA: 2,5-dihydroxybenzoic acid

BDI: β -diketiminate

DMAP: (4-dimethylamino)pyridine

Ph₂nacnac: N,N'-diphenyl-2,4-pentanediiiminate

d: doublet

dd: doublet of doublets

μ_{eff} : effective magnetic moment

ESI: electrospray ionization

Et: ethyl

EDBP: 2,2'-ethylidene-bis(4,6-di-*tert*-butylphenol)

tbptamd: N-ethyl-N'-*tert*-butylbis(3,5-di-*tert*-butylpyrazol-1-yl)acetamidinate

ϵ : excitation coefficient ($\text{M}^{-1}\text{cm}^{-1}$)

FT: Fourier transform

GPC: gel permeation chromatography

T_g : glass transition temperature

GOF: goodness of fit

g: gram

HH: head-to-head

HT: head-to-tail

Hz: hertz

HOMO: highest occupied molecular orbital

h or hr: hour

H₂O₂: hydrogen peroxide

OH⁻: hydroxyl ion

ICP: inductively coupled plasma

IR: infrared

in situ: “in the reaction mixture”

K: Kelvin

kHz: kilohertz (10^3 Hz)

LA: lactide

g: Landé splitting factor

Dq (Δ_o): ligand field splitting energy

LMCT: ligand to metal charge transfer

MAS: magic angle spin

χ : magnetic susceptibility

MS: mass spectrometry

m/z: mass-to-charge ratio

MALDI-TOF: matrix assisted laser desorption ionization time-of-flight

λ_{max} : maximum wavelength (nm)

MHz: megahertz (10^6 Hz)

MeOH: methanol

Me: methyl

MAO: methylaluminumoxane

N-MeIm: 1-methylimidazole

μL : microlitre (10^{-6} L)

μs : microsecond (10^{-6} s)

mg: milligram (10^{-3} g)

mL: millilitre (10^{-3} L)
mmol: millimole (10^{-3} mol)
mV: millivolt (10^{-3} V)
min: minute
M: molar (mols/L)
 χ_M : molar susceptibility
m: multiplet (in NMR) and medium (in IR)
nm: nanometre (10^{-9} m)
NMR: nuclear magnetic resonance
 M_n : number average molecular weight
ORTEP: Oak Ridge thermal-ellipsoid plot program
trans: “on the other side”
cis: “on the same side”
P: paramagnetic impurity
ppm: parts per million
Cp*: pentamethylcyclopentadienyl
Ph: phenyl
PCL: poly(caprolactone)
PCHC: poly(cyclohexene carbonate)
PCHO: poly(cyclohexene oxide)
PDI: polydispersity index
PE: poly(ethene)
PHA: poly(hydroxyalkanoate)

PLA: poly(lactic acid) or polylactide
PPC: poly(propylene carbonate)
PPO: poly(propylene oxide)
PSC: poly(styrene carbonate)
PVCHC: poly(vinylcyclohexene carbonate)
E: potential
 P_r : probability of racemic enchainment
PC: propylene carbonate
PO: propylene oxide
 B : Racah parameter
rac: racemic
ROP: ring-opening polymerization
SCE: saturated calomel electrode
sh: shoulder (in UV-vis)
s: singlet (in NMR) and strong (in IR)
H: spin Hamiltonian
 λ : spin-orbit coupling constant
 T_2 : spin-spin relaxation time
SC: styrene carbonate
SO: styrene oxide
SQUID: superconducting quantum interference device
scCO₂: supercritical carbon dioxide
TT: tail-to-tail

TIP: temperature independent paramagnetism

O'Bu: *tert*-butoxide

t'Bu: tertiary-butyl

T: tesla

TBABr: tetrabutylammonium bromide

[(*n*Bu)₄N]PF₆: tetrabutylammonium hexafluorophosphate

THF: tetrahydrofuran

tmeda: *N,N,N',N'*-tetramethylethylenediamine

TMS: tetramethylsilane

TFPP: tetra(pentafluorophenyl)porphyrin

TPP: *meso*-tetra-phenylporphyrinato(2-)

TGA: thermal gravimetric analysis

t: time

td: triplet of doublets

TPB: tris(pyrazolyl)borate

TOF: turnover frequency

TON: turnover number

UV-Vis: ultraviolet-visible

VHPO: vanadium haloperoxidase

VT: variable temperature

vs.: "versus"

w: weak (in IR)

*M*_w: weight average molecular weight

Ligands used in this work:

$\text{H}_2[\text{O}_2\text{NO}]^{\text{MeMe}}$ (**L1**): 2-tetrahydrofurfurylamino-*N, N'*-bis(2-methylene-4,6-methylphenol)

$\text{H}_2[\text{O}_2\text{NO}]^{\text{BuMe}}$ (**L2**): 2-tetrahydrofurfurylamino-*N, N'*-bis(2-methylene-4-methyl-6-*tert*-butylphenol)

$\text{H}_2[\text{O}_2\text{NO}]^{\text{BuBu}}$ (**L3**): 2-tetrahydrofurfurylamino-*N, N'*-bis(2-methylene-4,6-*tert*-butylphenol)

$\text{H}_2[\text{O}_2\text{NN}']^{\text{MeMe}}$ (**L4**): 2-pyridylamino-*N, N'*-bis(2-methylene-4,6-methylphenol)

$\text{H}_2[\text{O}_2\text{NN}']^{\text{BuMe}}$ (**L5**): 2-pyridylamino-*N, N'*-bis(2-methylene-4-methyl-6-*tert*-butylphenol)

$\text{H}_2[\text{O}_2\text{NN}']^{\text{BuBu}}$ (**L6**): 2-pyridylamino-*N, N'*-bis(2-methylene-4,6-*tert*-butylphenol)

List of Appendices

Appendix A: NMR Spectroscopy

Figure A1.1. ^1H NMR spectrum of L1	261
Figure A1.2. ^{13}C NMR spectrum of L1	262
Figure A1.3. ^1H NMR spectrum of L2	263
Figure A1.4. ^{13}C NMR spectrum of L2	264
Figure A1.5. ^1H NMR spectrum of L3	265
Figure A1.6. ^{13}C NMR spectrum of L3	266
Figure A1.7. ^1H NMR spectrum of L4	267
Figure A1.8. ^{13}C NMR spectrum of L4	268
Figure A1.9. ^1H NMR spectrum of L5	269
Figure A1.10. ^{13}C NMR spectrum of L5	270
Figure A1.11. ^1H NMR spectrum of L6	271
Figure A1.12. ^{13}C NMR spectrum of L6	272
Figure A1.13. ^1H NMR spectrum of 2.1 in CDCl_3	273
Figure A1.14. ^1H NMR spectrum of 2.2 in CDCl_3	274
Figure A1.15. ^1H NMR spectrum of 2.2 in C_6D_6	275
Figure A1.16. ^1H NMR spectrum of 2.2 in D_8 -toluene.....	276
Figure A1.17. ^1H NMR spectrum of 2.2 in D_5 -pyridine.....	277
Figure A1.18. ^{13}C NMR spectrum of 2.2 in D_5 -pyridine.....	278
Figure A1.19. ^{13}C NMR spectrum of 2.1 in D_5 -pyridine.....	279

Figure A1.20. ^7Li NMR spectra at 7.04 T for complex 2.1 in $\text{D}_5\text{-pyridine}$ (top) and C_6D_6 (bottom).	280
Figure A1.21. ^7Li MAS (20 kHz) and ^6Li MAS (15 kHz) spectra of complex 2.1 at 14 T.	281
Figure A1.22. ^1H NMR spectrum from aliquot sample of PCHC in CDCl_3 (Table 5.5, entry 1).	282
Figure A1.23. ^1H NMR spectrum from aliquot sample of PCHC in CDCl_3 (Table 5.5, entry 2).	283
Figure A1.24. Carbonyl region of the ^{13}C NMR spectrum (75.5 MHz, CDCl_3) of CHO/ CO_2 copolymer prepared with PPNCl (Table 5.3, entry 6).	284
Figure A1.25. Carbonyl region of the ^{13}C NMR spectrum (75.5 MHz, CDCl_3) of CHO/ CO_2 copolymer prepared with PPNN_3 (Table 5.3, entry 12).	285

Appendix B: MALDI-TOF MS

Figure B1.1. MALDI-TOF mass spectrum of $\{\text{Li}_2[\text{O}_2\text{NO}]^{\text{BuBu}}\}_2$ (2.2).	286
Figure B1.2. Experimental and theoretical MALDI-TOF MS isotopic distribution pattern for 2.2 (top = monomer, bottom = dimer).	287
Figure B1.3. MALDI-TOF mass spectrum of $\text{CrCl}(\text{THF})[\text{O}_2\text{NO}]^{\text{BuBu}}$ (4.2).	288
Figure B1.4. Experimental and theoretical MALDI-TOF MS isotopic distribution pattern for 4.2	289
Figure B1.5. MALDI-TOF mass spectrum of $\text{CrCl}[\text{O}_2\text{NN}]^{\text{BuMe}}$ (4.3).	290
Figure B1.6. Experimental and theoretical MALDI-TOF MS isotopic distribution pattern for 4.3 (top = monomer, bottom = dimer).	291

Figure B1.7. Experimental and theoretical MALDI-TOF MS isotopic distribution pattern for dimer fragment in 4.4 . Poor resolution is due to very weak signal intensity.....	292
Figure B1.8. MALDI-TOF mass spectrum of $\{\text{CrCl}[\text{O}_2\text{NN}^{\text{MeMe}}](\mu\text{-HO})\{\text{CrCl}[\text{HO}_2\text{NN}^{\text{MeMe}}]\}$ (4.5).....	293
Figure B1.9. Experimental and theoretical MALDI-TOF MS isotopic distribution pattern for 4.5 (top = monomer, bottom = dimer).	294
Figure B1.10. MALDI-TOF mass spectrum of $\{\text{CrCl}[\text{O}_2\text{NN}^{\text{BuBu}}](\mu\text{-HO})\{\text{CrCl}[\text{HO}_2\text{NN}^{\text{BuBu}}]\}$ (4.6).....	295

Appendix C: Conversion Plots for the ROP of LA

Figure C1.1. % conversion vs. time for the ROP of LA at 26 °C initiated by 2.1 without BnOH.....	296
Figure C1.2. % conversion vs. time for the ROP of LA at 26 °C initiated by 2.1	297
Figure C1.3. % conversion vs. time for the ROP of LA at 60 °C initiated by 2.1	298
Figure C1.4. % conversion vs. time for the ROP of LA at 80 °C initiated by 2.1	299
Figure C1.5. % conversion vs. time for the ROP of LA at 26 °C initiated by 2.2 without BnOH.....	300
Figure C1.6. % conversion vs. time for the ROP of LA at 26 °C initiated by 2.2	301
Figure C1.7. % conversion vs. time for the ROP of LA at 40 °C initiated by 2.2	302
Figure C1.8. % conversion vs. time for the ROP of LA at 60 °C initiated by 2.2	303
Figure C1.9. % conversion vs. time for the ROP of LA at 80 °C initiated by 2.2	304

Appendix D: UV-Visible Spectroscopy

Figure D1.1. UV-Vis absorption spectrum of 4.4	305
---	-----

Figure D1.2. UV-Vis absorption spectrum of 4.5	306
---	-----

Appendix E: Infrared Spectra

Figure E1.1. IR spectrum of complex 4.3	307
--	-----

Figure E1.2. IR spectrum of complex 4.5	308
--	-----

Figure E1.3. IR spectrum of complex 4.6	309
--	-----

Chapter 1

Introduction

1.1 Amine-bis(phenolate) Ligands

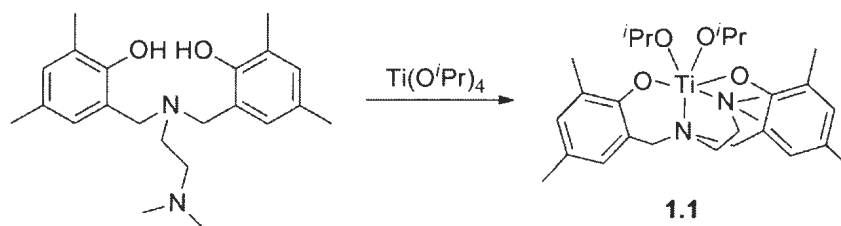
Ligand design in coordination chemistry is crucial for the control of reactivity at metal centres. Ligands can coordinate to metals in various fashions. For example, ligands can be mono-, bi-, tri-, tetra- or multidentate. Amine-bis(phenolate) ligands are chelating (chelate comes from the Greek word *chelè*, meaning claw) ligands where the donor atoms can surround the metal in a cavity or cup-like formation. These ligands can be electronically or sterically modified to suit the properties required for the specific task.

Specifically, the ligands studied in this thesis involve tetradentate tripodal ligands of the amino-bis(phenolate) variety $[\text{ONOL}']^{\text{RR}'}$, where L' is N or O, which represents the nature of the neutral pendant donor functionality, and R/R' can be varied to include alkyl or heteroatom containing groups such as Cl or NO₂ at the *ortho* and *para* positions of the phenolate ring. The ligand of choice is not new; it has been used in the literature since Hinshaw *et al.* introduced it in 1989.¹ Since the late 80s, a wide range of metals has been complexed with aminobisphenols. Most complexes are still based on groups 3 and 4 of the periodic table, as well as the lanthanides, with the majority of research being performed in the late 90s and 2000s.² A modified Mannich condensation reaction is the most common method for synthesising these ligands as the synthesis can be performed in a one-pot fashion. However, this has proven to be more difficult when trying to incorporate two different phenols or when the phenols do not have substituents in the

para-positions.² The focus of this section is not to give a comprehensive review of every transition metal aminobisphenolato complex reported, but to mention relevant references which pertain to the research presented in this thesis. A recent review article of this area was published in *Coordination Chemistry Reviews* in 2012.²

1.1.1 Group 4 Complexes (Ti and Zr)

Titanium aminobisphenolato complexes were first explored by Moshe Kol and co-workers to try and avoid the formation of homoleptic Ti complexes previously observed when incorporating various chelating ligands. It was found that a tridentate [ONO] ligand yielded a homoleptic Ti complex, $\text{Ti}[\text{ONO}]_2$. The addition of an extra donor arm ($L' = \text{N}$), in this case $\text{CH}_2\text{CH}_2\text{NMe}_2$, formed a tetradentate $[\text{O}_2\text{NL}']$ ligand, which produced a mononuclear, heteroleptic octahedral $\text{Ti}(\text{O}^i\text{Pr})_2[\text{O}_2\text{NN}']$ complex (**1.1**) shown in Scheme 1.1.³ These results led to a new search for polymerization catalysts for α -olefins. Specifically, for Ti it was found that some tri- and tetradentate amine-bis(phenolate) complexes were active for the polymerization of 1-hexene.⁴



Scheme 1.1. Synthesis of $\text{Ti}(\text{O}^i\text{Pr})_2[\text{O}_2\text{NN}']$ complex (**1.1**).

Zirconium coordination chemistry was also explored by Kol and co-workers but unlike Ti, Zr homoleptic species were not formed when coordinated with the [ONO] ligand if bulky *tert*-butyl groups were present on the phenols. Reactivity towards 1-

hexene polymerization by Zr complexes showed a significant increase when a tetradentate ligand was employed over the tridentate type.⁵ The extra side-arm nitrogen donor altered the steric and electronic environment of the metal centre, which proved useful in polymerization catalysis.

Further modification of the $[O_2NN']$ ligand type saw the development of dianionic tetradentate $[ONNO]$ salan type ligands (Figure 1.1). Complexes of these with zirconium also showed high reactivity for the synthesis of isospecific poly(1-hexene).⁶

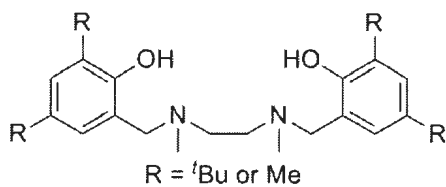
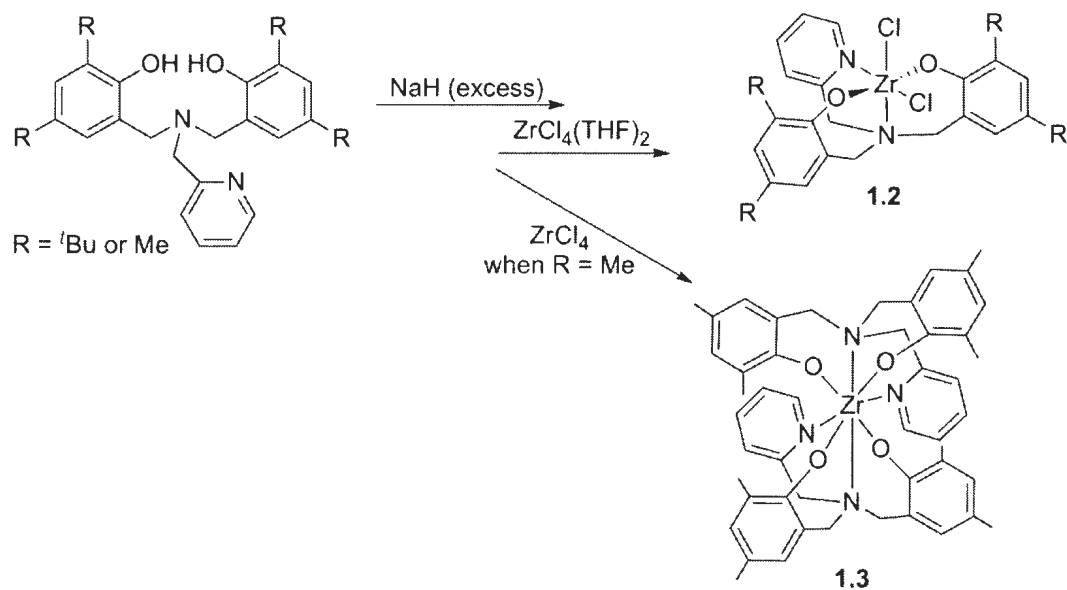


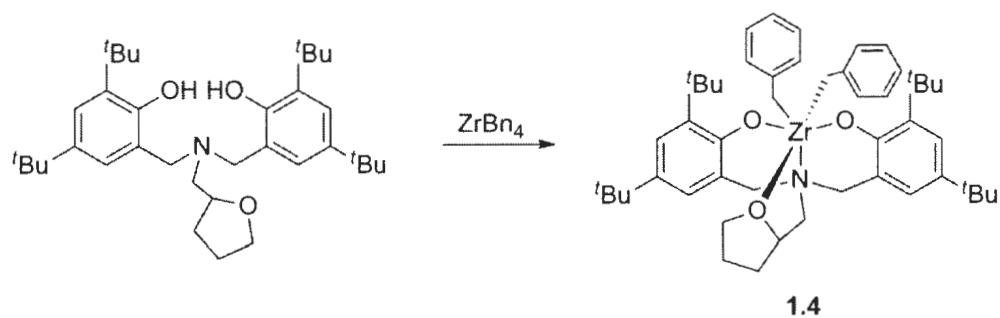
Figure 1.1. Tetradentate diaminobisphenol “salan” ligand, $H_2[ONNO]^{RR}$.

Mountford and co-workers⁷ used derivatives of these diamine-bis(phenolate) ligands of the form $[O_2NN']^R$, where $N' = \text{pyridyl}$ and $R = \text{Me or 'Bu}$, for coordination to Zr (Scheme 1.2). Complexes were commonly six-coordinate (**1.2**), but homoleptic eight-coordinate complexes (**1.3**) could be obtained when $R = \text{Me}$.



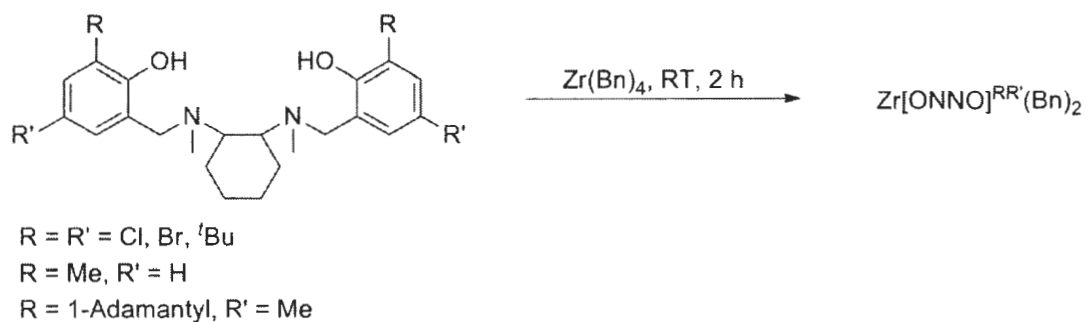
Scheme 1.2. Synthesis of $\text{ZrCl}_2[\text{O}_2\text{NN}']^{\text{R}}$ (**1.2**) and $\text{Zr}\{[\text{O}_2\text{NN}']^{\text{Me}}\}_2$ (**1.3**) complexes.

Continued ligand design advancements from Kol and co-workers provided the introduction of a new sidearm donor. An oxygen donor, such as tetrahydrofuran, was incorporated into the ligand. This amine-bis(phenolate) ligand was synthesised in a one-pot Mannich condensation reaction and was easily complexed to group 4 metals. The single-site zirconium complex (**1.4**), as shown in Scheme 1.3, showed high activity towards the catalytic polymerization of both 1-hexene and 1-octene.⁸ Minor steric or electronic adjustments in these amine-bis(phenolate) ligands has permitted a wide range of reactivities in olefin polymerization.



Scheme 1.3. Zr amine-bis(phenolate) complex (**1.4**) featuring a tetrahydrofuranyl pendant donor side-arm on the ligand.

Isospecific polymerization catalysis has become increasingly important in the development of new materials. Enantiomorphic ligands, such as chiral salan ligands, have provided new opportunities in the field of polymerization catalysts. The first Zr complexes of chiral salan ligands were introduced by Kol and co-workers in 2006 (Scheme 1.4). Increased stereoselectivity was observed due to bulky substituents on the phenol.⁹



Scheme 1.4. Synthesis of Zr salan complexes.

1.1.2 Group 5 Complexes (Vanadium)

A natural transition from the well-studied group 4 complexes (Ti and Zr) was to study group 5 transition metals. Specifically, vanadium complexes of amine-bis(phenolates) were studied extensively, where the metal exhibited oxidation states ranging from II-V. As with group 4 metals, vanadium has been shown to polymerize olefins such as ethene, propene and 1-hexene.¹⁰ Six-coordinate vanadium complexes are common for amine-bis(phenolate) species, where the complex has an overall neutral charge. The oxidation state of the V centre varies, depending on the nature of the co-ligands used.

A family of oxo-vanadium complexes, $V(X')(X)[ONNO]$, of the ligand type amine-bis(phenolate) has been synthesised and well characterized for oxidation states (II-V) by Lorber and co-workers (Figure 1.2).¹⁰⁻¹² The oxidation state can be varied, depending on the salt used in the synthesis of the V complex. For example, V(II) complexes were complexed with tmeda (tmeda = *N,N,N',N'*-tetramethylethylenediamine), V(III) with acetylacetonato (acac) or chloro, and V(IV) or V(V) with azido, isopropoxo or chloro groups. Vanadium(II) is generally inactive towards olefin polymerization reactions. Only one structure has been reported to date when complexed with these ligands.¹⁰ It was commonly found that the pendant donor group (NMe_2) was bound tightly to the metal no matter the oxidation state of the vanadium centre. The addition of strong coordinating donors could not displace the pendant group. Of the derivatives studied, V(III)(acac)[ONNO] was found to be the best suited for ethene and α -olefin homo- and co-polymerizations.

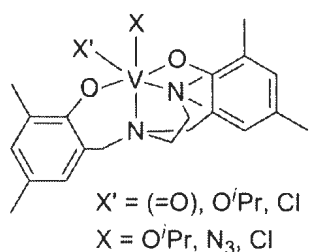


Figure 1.2. Vanadium(IV) and (V) (when X = O) diamine-bis(phenolate) complexes.

Salicylato oxovanadium(V) complexes were synthesised by Ali and co-workers¹³ where tetradentate ligands with the same donor that Lorber introduced were used. This work was followed by a study of oxovanadium(V) complexes with a tridentate (propylamine or seleno donor) ligand.¹⁴ The authors in this case were not looking at the complexes for polymerization catalysis, but rather as a model complex for bioinorganic oxidation of ascorbic acid. Ali explored these complexes because they closely resemble the active structure of vanadium haloperoxidases (VHPO). Catalytic oxidation of aromatic hydrocarbons by H₂O₂, such as toluene and isomers of xylene, were found to produce the respective carboxylic acids with good turnover numbers (TONs). The TONs ranged from 134-188 (mol product/mol V) in the presence of a five-coordinate oxovanadium(V) complex (**1.5**) (Figure 1.3).¹⁵

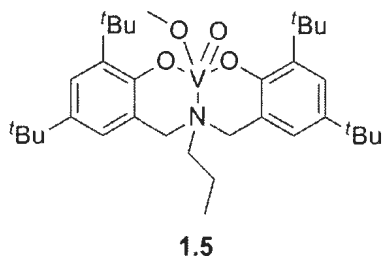


Figure 1.3. V(=O)(OMe)[ONO] aminobisphenolato complex (**1.5**).

1.1.3 Group 6 Complexes (Chromium)

Group 6 metal complexes of the amino-bis(phenolate) ligands have been less actively explored in the literature than group 4 or 5 metals. Of the group 6 metals, only chromium will be discussed here, as it is most relevant to this thesis.

Examples of chromium(III) complexes involving tetradentate diamine-bis(phenolate) ligands are limited. Springborg and co-workers explored Cr(III) complexation with salan ligands. Geometries of these complexes were observed to be dimetallic¹⁶ $\{\text{Cr}[\text{ONNO}]\text{Cl}\}_2$ giving a phenoxo-bridged dichromium(III) compound when prepared from $\text{CrCl}_3 \cdot 6\text{H}_2\text{O}$ or tetrametallic¹⁷ $\{\text{Cr}[\text{ONNO}]\text{F}\}_4$ when synthesised from *trans*- $[\text{Cr}(\text{py})_4\text{F}_2]\text{ClO}_4$.

Two other accounts of the synthesis and structural properties of chromium(III) amine-bis(phenolate) complexes have been reported in the literature to date.^{18,19} These include a homoleptic anionic octahedral compound $\{\text{Cr}[\text{ONO}]_2\}^-$ (**1.6**) where two tridentate ligands are coordinated to the metal centre (Figure 1.4).¹⁸ As well, mono- and bimetallic Cr(III) octahedral complexes have been reported recently by the Kozak group.¹⁹ These complexes contain tetradentate tripodal ligands with either a tetrahydrofuranlyl or pyridyl pendant donor arm. An in depth examination of these complexes will be discussed in Chapter 4.

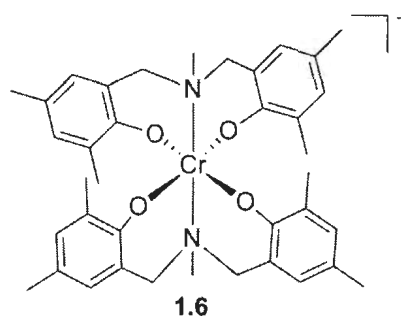


Figure 1.4. Homoleptic, six-coordinate $\{\text{Cr}[\text{ONO}]_2\}^-$ complex (1.6).

1.1.4 Group 7, 8 and 9 Complexes (Manganese, Iron and Cobalt)

Later transition metals such as manganese, iron and cobalt complexed with amine-bis(phenolate) ligands have had an increased presence in the literature in recent years. A manganese amine-bis(phenolate) complex reported by Chaudhuri and co-workers was found to have a similar structure to their Cr complex.¹⁸ The mononuclear $\{\text{Mn}(\text{III})[\text{ONO}]_2\}^-$ complex was easily oxidised in the presence of air to give a $\text{Mn}(\text{IV})[\text{ONO}]_2$ species. They also described an analogous $\{\text{Fe}(\text{III})[\text{ONO}]_2\}^-$ compound along with a dinuclear $\text{Fe}_2(\text{III})[\text{ONO}]_3$ complex, where X-ray analysis showed the existence of five- and six-coordinate iron(III) centres.¹⁸

More recently, the Kozak group has reported a number of $\text{Fe}(\text{III})$ amine-bis(phenolate) complexes (Figure 1.5) that are effective catalysts for cross-coupling of alkyl halides with aromatic Grignard reagents.²⁰⁻²⁴

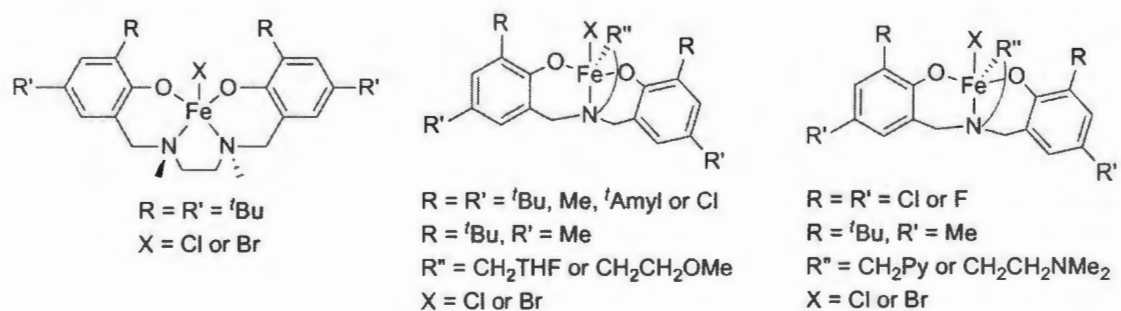


Figure 1.5. Examples of Fe(III) amine-bis(phenolate) complexes.^{20,21,23}

Cobalt complexes bearing amine-bis(phenolate) ligands have also been recently explored due to their interesting physical and structural properties, along with their redox reactivity.²⁵⁻²⁷ The Co compounds reported to date have been diverse in their nuclearity, where mono-, bi- and trimetallic compounds have been synthesised. This is contrary to what is observed in early transition metal complexes of this ligand class, which are predominantly monometallic. Monometallic Co structures were reported with oxidation states of II and III. Solvent coordination (such as methanol, acetone and propylene oxide) to the metal is also readily observed for Co(II) species (Figure 1.6).^{26,28} The majority of Co(II) compounds reported are dimeric in nature. For example when a tripodal N_2O_2 donor ligand was used, dinuclear complexes of composition $\{\text{Co}_2[\text{N}_2\text{O}_2]_2\}$ formed (Figure 1.6), where the less sterically hindered phenol acts as a bridge between the pentacoordinate Co centres.^{29,30} A trimetallic Co(II) complex has been observed when excess cobaltous acetate was present in the reaction (Figure 1.6). Two bridging acetate ligands were connected to the central Co(II), which was six-coordinate due to the addition of four methanol solvent molecules.²⁸ A mixed Co(II)/Co(III) species has also been

reported where both metal centres are six-coordinate with an acetate bridge connecting the cobalt atoms.³¹

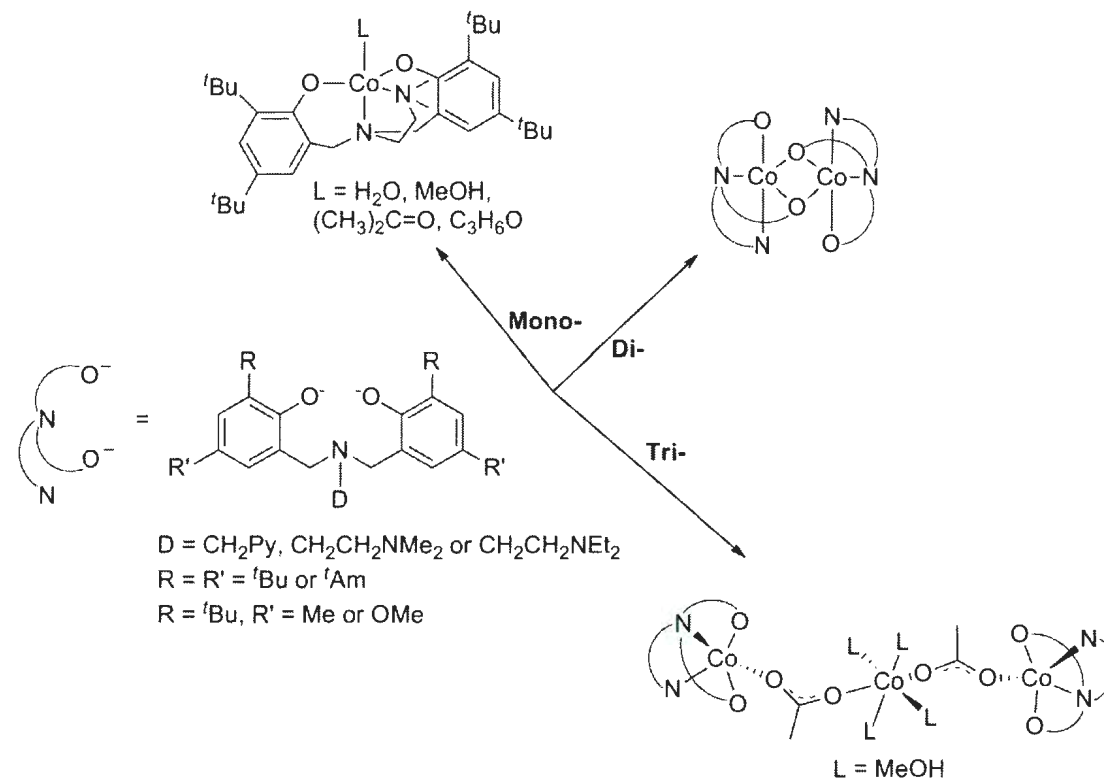


Figure 1.6. Examples of mono-, di- and tri-metallic Co amine-bis(phenolate) complexes.

1.2 Chromium(III) Catalysis

1.2.1 Introduction to the Element Chromium

Chromium was first discovered in 1797 by Louis N. Vauquelin of France. The element was initially found in crocoite (PbCrO_4), a rare mineral.³² It ranks 21st in elemental abundance in the earth's crust where the most common ore mined is in the form of chromite (FeCr_2O_4). Various other ores are found to contain Cr but in relatively minor amounts.³² Chromium was named after the Greek word "chroma" due to its various

coloured compounds and traces can be found in such gems as emeralds and rubies, which gives them their beautiful colours. Chromium compounds can exist in a wide range of oxidation states, from -IV to +VI. The most common oxidation states are +II, +III and +VI for Cr inorganic compounds. The +II oxidation state can be strongly reducing, while the highest oxidation state of Cr (+VI) is found to be a very strong oxidant.

Industrially, Cr is used on a large scale as alloys in the manufacturing of steel. For pure Cr, without Fe alloys, chromite must be first treated with molten alkali and oxygen to allow conversion of the Cr(III) to Cr(VI).^{32,33} This can then be precipitated out of water as sodium dichromate ($\text{Na}_2\text{Cr}_2\text{O}_7$) and reduced with carbon to chromium oxide (Cr_2O_3). The addition of reducing agents such as aluminium, carbon or silicon completes the process, affording elemental Cr.^{32,33} This white, hard, lustrous metal is extremely resistant to corrosion and it has been used to electroplate surfaces to protect them from corrosion. As well, Cr is often used for decorative purposes and simple Cr salts are commonly used in the dyeing of leathers. Specifically and more relevant to this thesis, heterogeneous Cr catalysts are well known for their active role in ethene polymerization.^{32,33}

Biologically, chromium(III) was once thought to be an essential element.³² A recent review by Vincent³⁴ has questioned the role of Cr in mammal, specifically human, metabolic processes. The safety of prescribing Cr supplements for glucose metabolism to improve type 2 diabetes symptoms or other related conditions is still considered controversial. Human studies are therefore required in order to provide definitive evidence around such issues. Cr(VI) compounds are suspected carcinogens.³² Exposure of the respiratory tract to Cr(VI) has been shown to cause adverse health problems (for

example, lung and nasal cancers). Such effects have appeared in industrial workers in the fields of chrome electroplating, stainless steel welding, dyeing and wood preservation.³⁵

Recently, methods involving Cr(VI) for photo-catalytic oxidation of organic substances have been shown to be useful for wastewater treatment. As well, bioremediation of contaminated soils and groundwaters using Cr(VI) has been postulated.³⁵ Although caution should be taken, as the debate is still on as to whether Cr(VI) in low doses in drinking water can lead to cancer. A lawsuit in the US related to groundwater contaminated with Cr(VI), as popularized in the movie “Erin Brockovich”, raises questions and brings attention toward the issue.³⁵

Various isotopes exist for Cr (atomic masses 45-57), although only four are stable. The most abundant is ⁵²Cr, which represents 83.79% of all chromium. Chromium possesses an NMR-active nucleus in ⁵³Cr. However, ⁵³Cr NMR can be experimentally difficult due to its low resonance frequency (16.956 MHz, ¹H = 300 MHz), quadrupole moment ($4.1 \times 10^{-30} \text{ m}^2$) and relative receptivity (8.62×10^{-5} , ¹H = 1.00). Chromium is also used as a medical tracer. Specifically, ⁵¹Cr is used because this isotope is radioactive with a half-life of 27.7 days.³²

1.2.2 Overview of Chromium Coordination Compounds

The use of chromium(III) coordination complexes has been at the forefront of early coordination chemistry research. Groundbreaking work in the late 19th century by Alfred Werner, who coordination chemists crown ‘the father of modern coordination chemistry’, led to the development of thousands of new coordination complexes including Cr compounds. He was able to demonstrate that six-coordinate octahedral complexes

were one of the most common coordination environments due to their chemical and structural stability, which initiated this now vast area of transition metal coordination chemistry.³²

Early studies of Cr coordination chemistry concentrated on Cr(II) and Cr(III) complexes and was dominated by monometallic octahedral complexes. The prevalence of Cr(III) complexes in the literature remains, due to the fact that they are inert and often the most stable oxidation state, making them easier to synthesise. The electron configuration of mononuclear d^3 octahedral Cr(III) complexes arises from the large ligand field stabilization energy of this geometry ($t_{2g}^3 e_g^0$). As chromium is the lightest element in group 6, its tendency to form cluster compounds is greatly decreased. Hence, most compounds are of octahedral geometries. More recently, other Cr oxidation states (+IV and +V) have been explored, although the majority of research is still focused on Cr(III).³²

Briefly, a number of the most common and relevant Cr(II) coordination compounds will be presented. Chromium dichloride is a grey solid and is one of the most common and most important Cr(II) starting materials. The aqua complex, bright blue $[\text{Cr}(\text{H}_2\text{O})_6]^{2+}$, is a strong reducing agent and has been widely used as a reductant in electron-transfer reactions.^{32,33,35} Most Cr(II) compounds are octahedral high-spin, d^4 complexes. These compounds exhibit Jahn-Teller distortions and have attracted much attention as they allow further examination of the classic tetragonal elongation.³² Low-spin Cr(II), octahedral complexes are in fact rarer than previously thought. Wieghardt and co-workers³⁶ have recently demonstrated that the generally accepted notion that strong-field ligands produce Cr(II) low-spin complexes is not always correct. Ligands such as

bipyridine (bipy) and phenanthroline (phen), which were previously considered low-spin Cr(II) compounds are actually better described as Cr(III) species antiferromagnetically coupled to a ligand-centered radical. Strong-field ligands at the extreme end of the spectrochemical series, for example cyanide (CN), cyclopentadienide (Cp), allyl or aryl are able to stabilize a Cr(II) ($S = 1$) centre. Furthermore, oxygen-containing Cr(II) species can be readily formed and isolated. For example, in a donor solvent such as tetrahydrofuran (THF), complexes of the form $[\text{Cr}(\text{OR})_2(\text{THF})_2]$ are produced. As well, $\text{Cr}(\text{acac})_2$ and other β -diketonates form many stable paramagnetic, high-spin d^4 electron configurations used in catalysis.^{32,33}

Thousands of Cr(III) coordination compounds have been published in the literature since Werner first introduced the foundations of coordination chemistry. A variety of ligands can be used in the synthesis of these Cr(III) complexes and the fact that they are kinetically inert has allowed a vast number of isolable complexes to be generated. Similar ligands to those described with Cr(II) compounds will be reviewed.

An important halide is CrCl_3 . This polymeric Cr(III) compound is a common starting material for many Cr(III) compounds. Adducts are easily synthesised through incorporation of donor solvents such as THF. Chromium trichloride tris-tetrahydrofuran ($\text{CrCl}_3 \cdot 3\text{THF}$) is a useful starting material for many chromium compounds, especially for the synthesis of organometallic Cr species. Further Cr(III) halides, $[\text{CrX}_4]^-$ and $[\text{CrX}_6]^{3-}$ can also be formed, for example, $\text{K}[\text{CrF}_4]$, $[\text{CrF}_6]^{3-}$ and $[\text{CrCl}_6]^{3-}$.^{32,33,35}

Chromium(III) compounds with oxygen and sulfur ligands are well known, where the harder oxygen-donor ligands dominate in comparison to the softer sulfur ligands. The violet hexaaqua ion, $[\text{Cr}(\text{H}_2\text{O})_6]^{3+}$, is also an important reagent for the production of

commercially available CrCl-salts that are used in the synthesis of new materials. Cr(acac)₃ has played an important role in the synthesis of new β-diketonate compounds. Such complexes were reported more extensively in the 80s as they provided a bridge from the well defined cyclopentadienyl (Cp) ligands to the addition of an oxygen donor species for catalysis.^{32,33,35} Oxalate chromium(III) coordination compounds (e.g. [Cr(C₂O₄)₃]³⁻) have been known for a long time. Werner introduced the first known optically active, anionic coordination compound in 1912, a chiral chromium oxalate.³² Sulfur ligands, although not as common, can be prepared through the oxidation of Cr(II)(aq) with sulfur oxidants. These complexes often suffer from 'aquation', the substitution of sulfur for water. Thiolate complexes are also common in nonaqueous media.^{32,35}

Some of the most well studied chromium coordination compounds involve ammonia and amine derivatives. Mono- and polydentate species exist, where [Cr(NH₃)₆]³⁺ is the most famously known for its ligand-exchange reactions.^{32,33,35} Complexes containing N-heterocycles also exist in large numbers, mainly with ligands such as pyridines, imidazoles, pyrazines and pyrazoles. Octahedral Cr(III) porphyrinato complexes are the most common compounds in this series. They are readily formed from the five-coordinate CrCl(TPP) (TPP = *meso*-tetra-phenylporphyrinato(2-)) through addition of solvent or donor ligands, L, and, or exchange of the Cl⁻ (X), to give a six-coordinate species, CrX(L)(TPP).^{32,35} Porphyrin systems have become less prominent in the literature since salen ligand development took over 20 years ago. The next sections will focus specifically on Cr coordination chemistry most relevant to this thesis, such as the well published Schiff-base ligands, β-diketiminato and salen, which possess nitrogen and oxygen donor ligands.

1.2.3 Chromium(II/III) β -Diketiminato Complexes

The development of new ligands has allowed the field of chromium coordination chemistry to continuously advance. Chromium diketiminates, or diiminates (**1.7**) as they are also known, were introduced after the diketonato (**1.8**), enaminketonato (**1.9**) and the porphyrinato (**1.10**) ligand (Figure 1.7). Earlier ligands such as the diketonates provided a pathway for researchers to add or modify the donor groups (for example O or N), substituents (for example hydrogen, alkyl, aryl or silyl) as well as their bonding mode on the ligand framework.³⁷

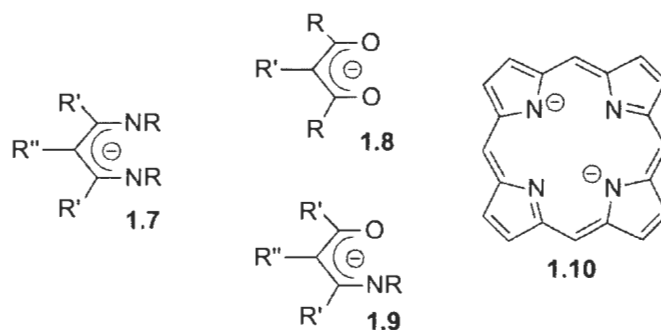
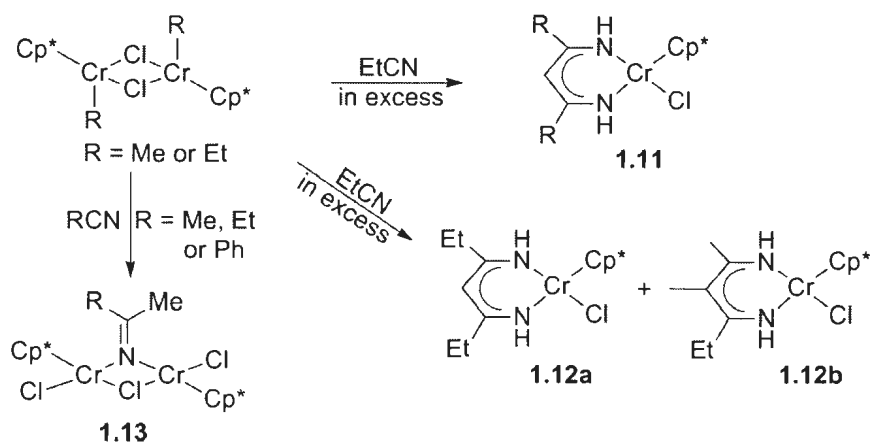


Figure 1.7. A small selection of bi- and tetradentate N and O donor ligands.

β -Diketiminates (BDI) are similar in structure to the diketonate ligand where O is replaced by a N group. The acronym associated with these ligands is derived from the diketonates or “acac” (derived from acetylacetonate) series. In the β -diketiminate ligand a deprotonated diimine allows coordination to the metal, and hence the abbreviation “nacnac”. Major advancements, in the mid 90s, led to the realization that this ligand could provide new avenues for olefin polymerization catalysis. These included strong bonding to the metal centre and high tunability to allow more sterically demanding groups to be incorporated.³⁷

Specifically, chromium β -diketiminates were first introduced by Klaus Theopold in 1989.³⁸ Dimeric $[\text{Cr}(\text{Cp}^*)(\mu\text{-Cl})\text{R}]_2$ (where $\text{R} = \text{Me}, \text{Et}, \text{Ph}$ and Bn and $\text{Cp}^* =$ pentamethylcyclopentadienyl) when reacted with excess nitrile yielded monomeric $[\text{Cr}(\text{Cp}^*)\text{Cl}(\text{R}_2\text{nacnac})]$ (Scheme 1.5).³⁸ Reaction of the ethyl-containing dimer with excess EtCN yields only the symmetric complex (**1.11**). A mixture of compounds (**1.12a**) and (**1.12b**) were observed following the reaction of the methyl dimer with excess EtCN. However, the addition of stoichiometric amounts of nitrile afforded a different mixture of products to (**1.12a**) or (**1.12b**). A crystal structure confirmed that a bimetallic complex had been synthesised, having two Cp^*CrCl compounds bridged by a chloride and a ketiminato ligand (**1.13**).³⁸



Scheme 1.5. Synthesis of the first Cr β -diketiminate complexes (**1.11**, **1.12a**, **1.12b** and **1.13**).

The initial deviation away from CrCp to Cr β -diketiminate complexes was employed in order to find a homogeneous model system for the well-known heterogeneous Phillips catalyst (Cr/SiO_2). The hard N-donors in the nacnac ligand mimic

the binding of the oxygens from the silica surface to the chromium. As well, steric protection by the substituents on the nitrogens allows protection of the active site.^{39,40}

Both Theopold³⁹⁻⁴¹ and Gibson^{42,43} produced groundbreaking work in this area, which led to the development of new organochromium complexes for olefin polymerization. The search for a ligand capable of mimicking the Phillips catalyst led Theopold and co-workers to use bulkier β -diketimines.⁴¹ Addition of the lithiated ligand precursor, $\text{Li}(\text{Ph}_2\text{nacnac})$, where $(\text{Ph}_2\text{nacnac}) = \text{N,N-diphenyl-2,4-pentanediiminate anion}$, to $\text{CrCl}_3(\text{THF})_3$ in THF yielded a mononuclear dichloride complex, $\text{CrCl}_2(\text{THF})_2(\text{Ph}_2\text{nacnac})$ (**1.14**), as shown in Figure 1.8. Homogeneous catalysis with this compound gave high molecular weight poly(ethene) in the presence of excess methylaluminoxane (MAO).

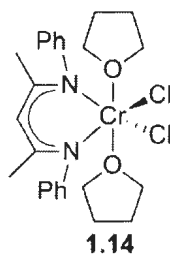
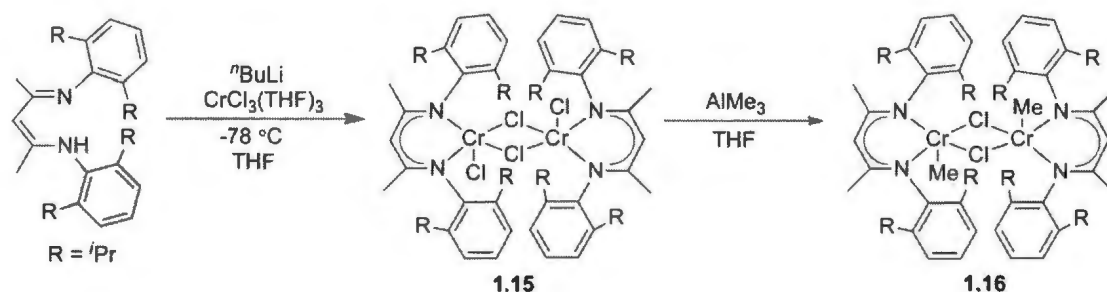


Figure 1.8. Monomeric $\text{CrCl}_2(\text{THF})_2(\text{Ph}_2\text{nacnac})$ complex (**1.14**).

Gibson was also exploring this ligand class at the same time for ethene polymerization, where the general strategy of using these ligands with bulky aryls was to protect the active metal site.⁴² The bulky monoanionic N,N-chelate ligands (when $\text{R} = \textit{i}\text{Pr}$) were found to only allow coordination of one equivalent of ligand, giving a dimeric chromium species with bridging chlorides (entries **1.15** and **1.16** Scheme 1.6).



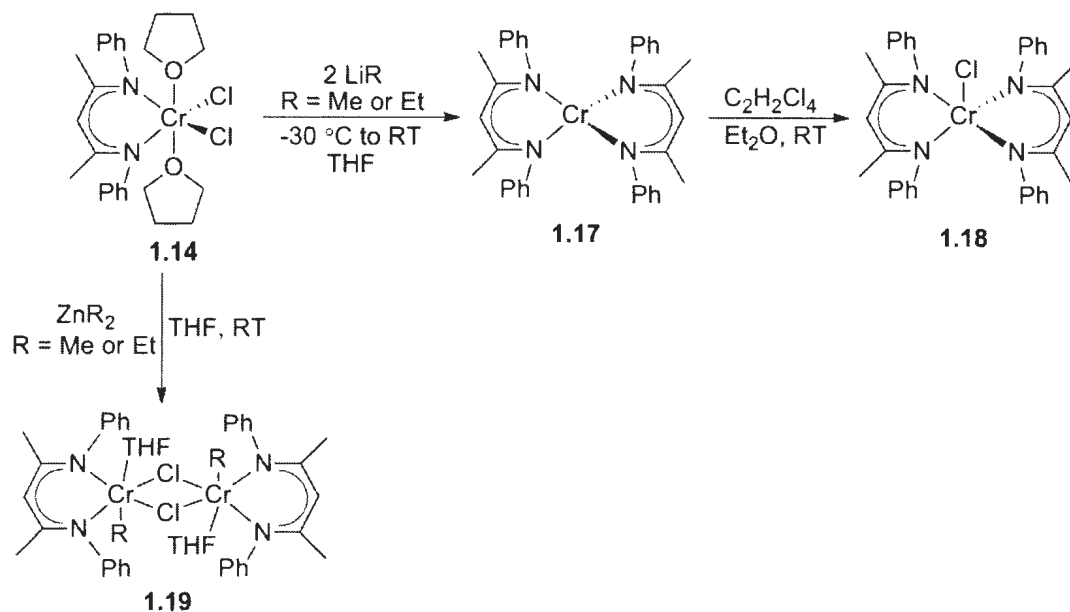
Scheme 1.6. Synthesis of dimeric Cr(III)(μ-Cl)nacnac complexes (**1.15**) and (**1.16**).

The most active catalyst was found to be **1.15**, using diethylaluminium chloride (Et₂AlCl) as the co-catalyst. For this system the co-catalyst was shown to have an important role, where MAO (the typical co-catalyst for these reactions) was observed to be less active. This complex was among only a few examples at that time of a non-cyclopentadienyl Cr catalyst for the synthesis of poly(ethene).⁴²

Gibson *et al.*⁴³ continued to examine chromium complexes of non-cyclopentadienyl ligands for ethene polymerization. As observed with their previous use of the sterically demanding ligand, [ArNC(Me)CHC(Me)NAr]⁻ (Ar = 2,6-*i*-Pr₂C₆H₃, DPP), dimeric species were also produced upon the addition of alkylating or reducing reagents, AlMe₃ or BnMgCl, respectively with **1.15**. Whereas, monomeric complexes were produced in the presence of NaO₂C(R) and Li[{O(R)C}₂CH] where R = CH₃ or Ph. High molecular weight poly(ethene) was observed from both the monomeric and dimeric complexes with the addition of aluminium activators.

Theopold and co-workers was particularly interested in the synthesis of a single-site catalyst that could polymerize ethene without the need of a co-catalyst, such as MAO. The well-defined complex **1.14** was a useful starting material for Theopold and co-

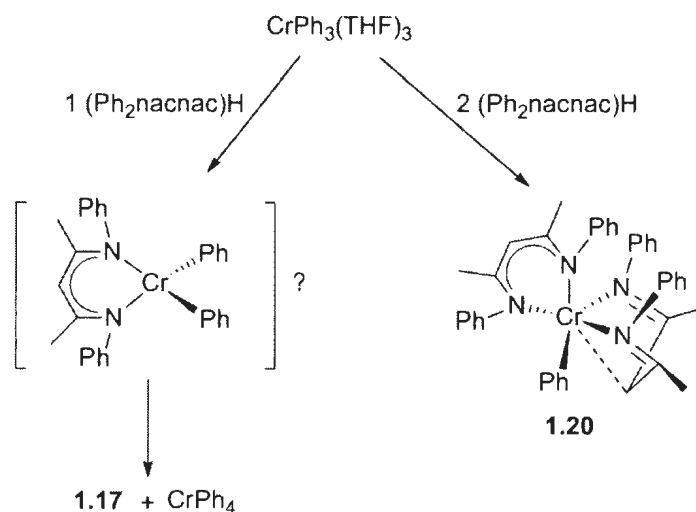
workers to use to pursue the organometallic chemistry of Cr(III) nacnac compounds. Attempts to alkylate **1.14** proved to be more difficult than originally anticipated and disproportionation and orthometalation products were observed instead.³⁹ In an attempt to alkylate **1.14** the addition of alkyllithium yielded a bis-nacnac complex, Cr(Ph₂nacnac)₂ (**1.17**), as shown in Scheme 1.7. Attempts to alkylate **1.17** using tetrachloroethane (C₂H₂Cl₄) instead led to the formation of Cr(III)chloro complex, **1.18** (Scheme 1.7). Reaction of **1.14** with an equivalent of dialkyl zinc, yielded [Cr(Ph₂nacnac)(R)(THF)(μ-Cl)]₂, where R = Me or Et, **1.19** (Scheme 1.7).



Scheme 1.7. Attempted synthesis of Cr alkyls giving mono- (**1.17** and **1.18**) and dimeric (**1.19**) Cr nacnac complexes.

Another route was explored to synthesise Cr(III) nacnac alkyl complexes (Scheme 1.8).³⁹ This time, protonolysis of Cr(III)Ph₃(THF)₃ by (Ph₂nacnac)H was attempted. However, disproportionation was likely, whereby the presumably formed

$\text{Cr}(\text{Ph}_2\text{nacnac})(\text{Ph})_2$ disproportionates to give **1.17** and $\text{Cr}(\text{Ph})_4$ as shown in Scheme 1.8. Furthermore, the addition of $\text{CrPh}_3(\text{THF})_3$ to 2 equivalents of $(\text{Ph}_2\text{nacnac})\text{H}$ produced $\text{Cr}(\text{Ph}_2\text{nacnac})_2\text{Ph}$, (**1.20**), a product that was also not expected (Scheme 1.8). Although no single-site catalyst was produced in these attempts, further research led by Theopold saw the isolation of a cationic chromium alkyl catalyst in 2005. This catalyst was found to be active without the addition of activators.⁴⁰ A more in depth discussion on this synthesis can be found in the following section.



Scheme 1.8. Attempted synthesis of dialkyls produced disproportionation to **1.17** and CrPh_4 , as well as $\text{Cr}(\text{Ph}_2\text{nacnac})_2\text{Ph}$ (**1.20**).

Research of chromium-BDI is still ongoing today, albeit less active than in the late 90s. The majority of the focus for $\text{Cr}(\text{nacnac})$ compounds remains around organometallic catalysis.^{44,45} Further discussions of important chromium organometallic species will be highlighted in the next section.

1.2.4 Chromium Organometallic Complexes for Olefin Polymerization

Chromium organometallic chemistry has roots which can be traced back to 1866, when Berthelot discovered that Cr(II) salts could reduce acetylene to ethene.⁴⁶ Today chromium-carbon bond chemistry covers a wide area, where research continues to be carried out on olefin polymerization catalysts, stereoselective (arene)chromium reagents and the fundamentals of compounds in unusual oxidation states. Specifically, the area of chromium alkyls for polymerization catalysis will be briefly discussed in this section.

Single-site catalysts capable of olefin polymerization became important after the introduction of the ill-defined heterogeneous Cr-based systems, the Phillips and Union Carbide catalysts.⁴⁷ Both catalysts are used on the industrial scale to produce polyethene. For this reason, research efforts have been focused on the development of homogeneous catalyst systems capable of improving the structural and mechanistic understanding of the polymerization process.

Important initial work involved CrCp alkyl complexes. These complexes have been shown to be effective homogeneous models to the Union Carbide system.⁴⁴ Furthermore, BDI ligands have been used to mimic the Phillips catalyst system, where Cr(II) and (III) oxidation states are the common active species in the polymerization. This discussion will focus on non-Cp chromium alkyl complexes for olefin polymerization.

Initial reports by Kim *et al.*⁴¹ and Gibson⁴² in 1998 described the first examples of BDI complexes for olefin polymerization. Theopold and co-workers found that the octahedral, $\text{CrCl}_2(\text{THF})_2(\text{Ph}_2\text{nacnac})$ complex (**1.14**), as previously shown in Figure 1.8, was capable of producing polyethene (PE) in the presence of MAO (130 equivalents).⁴¹

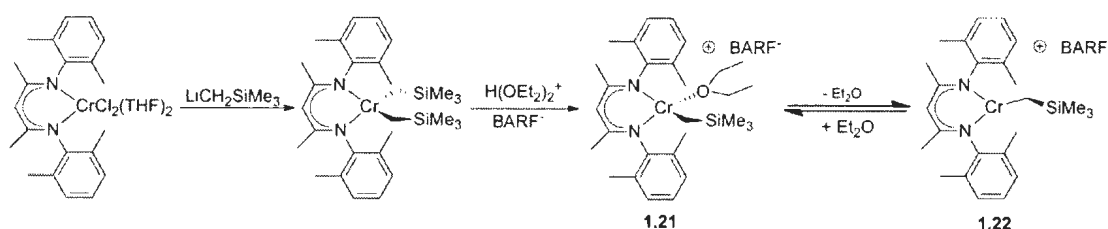
The molecular weight observed was almost 16 000 g/mol after 1 h. Complex (1.14) was also found to catalyse the copolymerization of ethene/propene. However, the M_n was observed to be significantly lower along with a low percentage of comonomer incorporation.

In the complex synthesised by Gibson *et al.*, no THF was coordinated to the chromium due to the presence of the bulkier BDI ligand.⁴² Instead, an unusual five-coordinate square pyramidal Cr(III) dimeric complex (1.15), as mentioned in Scheme 1.6 was observed. Activation of 1.15 with Et₂AlCl (30 equivalents) gave high molecular weight PE (113 000 g/mol).

Theopold and co-workers continued to study Cr-BDI complexes in pursuit of a highly active single-site catalyst. Theopold's group explored the use of chromium complexes of the moderately sterically hindered Ph₂(nacnac) ligand for olefin polymerization.³⁹ Mono- (1.18) and dimeric (1.19) species were synthesised in the presence of an alkyl chloride and dialkyl zinc, respectively (Scheme 1.7). Although these complexes could not polymerize ethene on their own, they did show high activity when activated with MAO. Broad molecular weight distributions were observed for all polymers produced from these chromium(III) derivatives. The trigonal bipyramidal CrCl(Ph₂nacnac)₂ complex (1.18) produced the highest activity for the polymerization of ethene. However, like other Cr-BDI species, the copolymerization of ethene with hexene yielded poor incorporation of comonomer.

Theopold and co-workers continued their search for a catalyst, which would not require activation by a co-catalyst, such as MAO. They successfully achieved this result after synthesising a cationic Cr(III) alkyl complex in the presence of a more sterically

hindered nacnac ligand.⁴⁰ The synthesis, as shown in Scheme 1.9, of the single-site ethene polymerization catalyst, $\{\text{Cr}[(2,6\text{-Me}_2\text{Ph})_2\text{nacnac}](\text{CH}_2\text{SiMe}_3)(\text{Et}_2\text{O})\}^+ \text{BARF}^-$ (**1.21**), was only possible through the addition of a non-coordinating counteranion, $[\text{BARF}^- = \text{B}(3,5\text{-(CF}_3)_2\text{C}_6\text{H}_3)_4^-]$ and coordination of one diethyl ether solvent molecule. The actual active species is thought to be the three-coordinate, nine-electron unsolvated complex **1.22**.



Scheme 1.9. Synthesis of cationic $\text{Cr}[(2,6\text{-Me}_2\text{Ph})\text{nacnac}]$ alkyls as single-site polymerization catalysts.

Polymerization studies using **1.21**, in CH_2Cl_2 at ambient temperature for 5-25 min, produced PE with narrow polydispersity (PDI). Additionally, this system was shown to have living polymerization characteristics rarely found in PE polymerizations. Furthermore, this catalyst was able to mimic the Phillips catalyst, producing copolymer of ethene and 1-hexene. Although the PDIs were found to be slightly higher than for the resulting PE, the M_n observed was very high (108 000 g/mol).

Inspired by Theopold's and Gibson's novel work, Baik, Mindiola and co-workers explored Cr(II) complexes with the nacnac ligand.⁴⁸ A series of interesting monomeric, three-coordinate neutral chromium complexes were observed, as shown in Figure 1.9. These complexes were shown to adopt T- or Y-shaped geometries depending on the third

ligand used. Experimental and computational studies were explored to gather insight into catalyst design and develop models useful for other three-coordinate metal complexes.

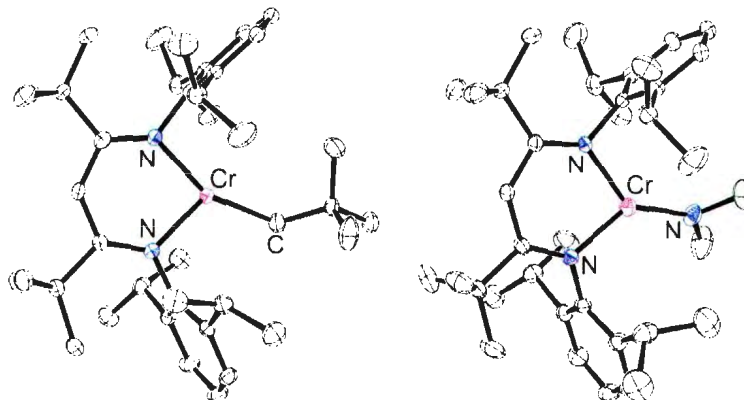


Figure 1.9. ORTEP drawing of the molecular structure of T- (left) vs. Y-shaped (right) monomeric Cr alkyls. Thermal ellipsoids at 50% probability with H-atoms excluded for clarity. Images generated using CIF data provided in reference [46].

It was found that electronic factors were most important, with sterics having a secondary role. For example, σ -donor ligands such as alkyls (CH_3) favoured the T-shaped geometry, whereas π -donors such as aryl oxide or dimethylamide favoured a Y-shaped geometry.

As observed, chromium organometallic complexes can encompass a wide range of ligand frameworks. Complexes like those mentioned above continue to be actively explored today in polymerization catalysis, towards the pursuit for a better mechanistic understanding.

1.2.5 Chromium Salen Complexes

Schiff-base ligands have proven over the years to impart great reactivity to a number of metal ions. Specifically, the salen ($\text{N,N}'$ -bis(salicylaldehyde)ethylenediamine)

ligand class is comprised of a tetradentate [O,N,N,O] Schiff-base system (Figure 1.10). A related class of ligand contains saturated N-donors (e.g. secondary or tertiary amines) rather than imines in the backbone. By analogy to the salens, these ligands are often called "salans" (Figure 1.10).

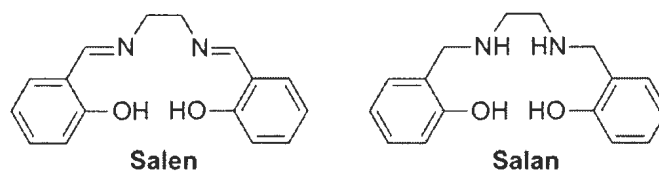


Figure 1.10. Salen and salan ligands.

The tetradentate framework of these ligands is similar to the porphyrin ligand system, but has some important advantages. First, synthetically, the salen ligands can be easily made in high yields through a condensation reaction. Second, the ease with which the substituents on the ligands can be modified has allowed the steric and electronic properties to be tailored depending on the complex required. Third, they have the ability to stabilize many transition metals in various oxidation states, as well as the possibility to coordinate more than one metal ion via the phenolate O-donors. Fourth, the rigid nature of the backbone provides protection to the active site as well as an avenue for chiral or achiral components to be incorporated.

Most metal salen complexes can be generated *in situ*, hence they are not always well characterized in the literature.^{49,50} In the case of Cr(III)-salen complexes, the generic procedure usually involves the reaction of the corresponding Cr(II)-salt with the appropriate ligand under an inert atmosphere. This is followed by exposing the resulting solution to air.³⁵ Many important Cr(III)-salen derivatives have been prepared since the

ligand was first introduced in the 19th century. The range of application for these complexes, especially as catalysts, is vast and still continues to grow today. Some procedures involving Cr(III)-salen complexes include: (1) oxidation of allylic alcohols,⁵¹ (2) cyclisation⁵² or copolymerization⁵³⁻⁵⁵ of epoxides and carbon dioxide (CO₂), (3) asymmetric ring-opening of epoxides,^{56,57} (4) enantioselective Diels-Alder reactions,⁵⁸ (5) asymmetric allylation of aromatic aldehydes,^{59,60} and (6) asymmetric epoxidation.⁶¹

The first known application of a Cr-salen complex was the active achiral cationic chromium species, which Kochi first introduced (Figure 1.11).⁶² These complexes were explored for their epoxidation of olefins with iodosylbenzene (PhIO). Optimised conditions were obtained with norbornene, resulting in the epoxidation product norbornene oxide in 70% yield.⁶²

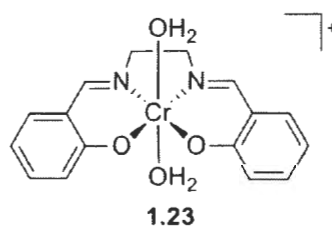


Figure 1.11. [Cr(salen)(OH₂)₂]⁺ complex (**1.23**).

The introduction of Jacobsen's chiral ligand, (R,R)-(-)-N,N'-bis(3,5-di-*tert*-butylsalicylidene)-1,2-cyclohexanediamine (Figure 1.12), caused a major increase in the use of salen ligands in the literature. After Jacobsen⁶³ showed that he was able to enantioselectively produce a chiral epoxide from an achiral alkene with this ligand complexed to manganese, its complexation to other metals followed, including chromium.

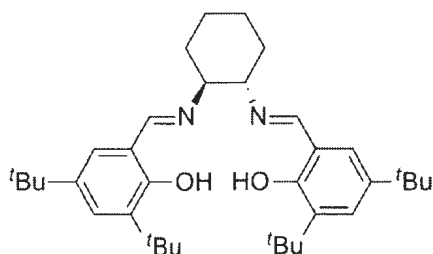


Figure 1.12. Jacobsen's chiral salen ligand.

Chiral Cr-salen catalysts have been widely employed in organic asymmetric synthesis.⁴⁹ Asymmetric epoxidation with chromium salens was investigated in depth as a result of the early fundamental work of Sharpless, Kochi and Jacobsen. Complexes such as **1.24**, shown in Figure 1.13 by Gilheany started a new synthetic route incorporating Cr as the active metal. It was found that alkenes such as (*E*)- β -methylstyrene could be epoxidized in the presence of **1.24** in 83% ee.⁶⁴

A strong solvent dependence was observed in the epoxidation of conjugated alkenes by Cr-salen complex (**1.25**), shown in Figure 1.13. Results showed that in the presence of a more polar solvent, such as acetonitrile, the *trans* enantiomer dominated. The opposite enantiomer was observed to form in less polar solvents.⁶⁵

Difficulties in isolating chiral Cr(salen)Cl complexes for epoxidation led Gilheany to use an *in situ* method instead. This led to the observation that *trans* epoxides can be formed from *cis* alkenes catalysed in the presence of Cr oxo(salen) complexes (**1.26**), shown in Figure 1.13. Additionally, if NO_3^- is replaced with the BARF^- counterion a Cr(IV) low-spin species was observed both experimentally and theoretically due to a one-electron reduction of the chromium by the tetraarylborate.⁶¹

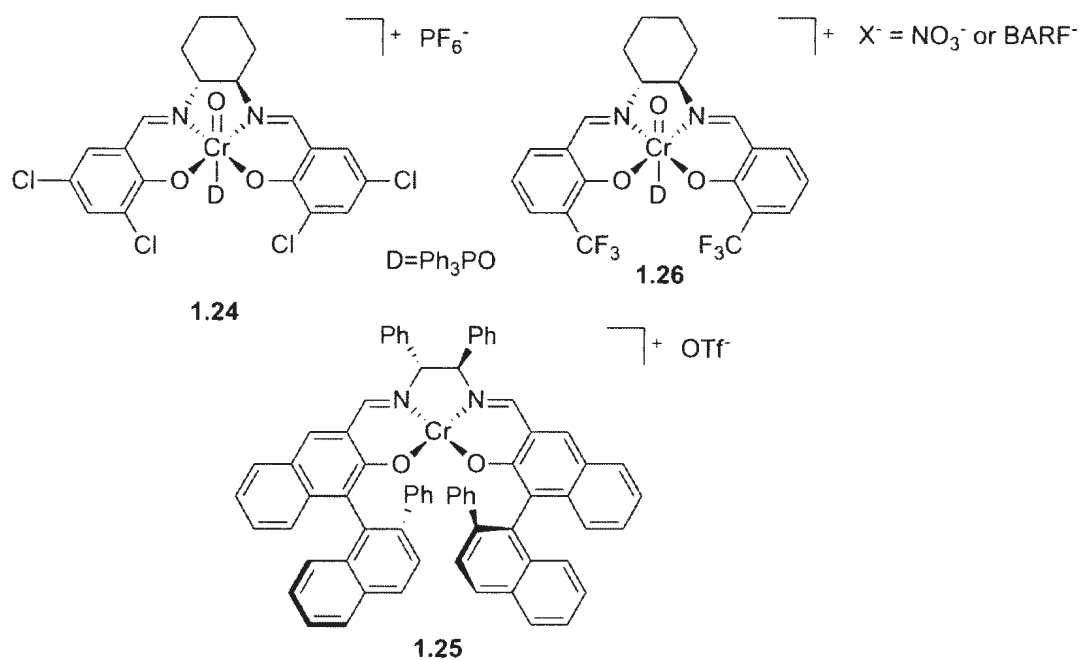


Figure 1.13. Cr(salen) complexes for asymmetric epoxidation.

Jacobsen's group explored catalysts **1.27** and **1.28** shown in Figure 1.14 for their use in asymmetric ring-opening (ARO) of epoxides.^{56,66} An important monomeric Cr(salen) alkoxide intermediate was isolated from the reaction of **1.27** with cyclopentene oxide.⁵⁶ Mechanistic studies provided evidence towards a bimetallic mechanism for the ARO of epoxides. Following this result, a study of bimetallic Cr(salen) complexes (**1.28**) was undertaken by Jacobsen.⁶⁶ It was found that the tethered catalysts were in fact more reactive than the monometallic species, on the order of 1-2 times faster and without notable loss of enantioselectivity.

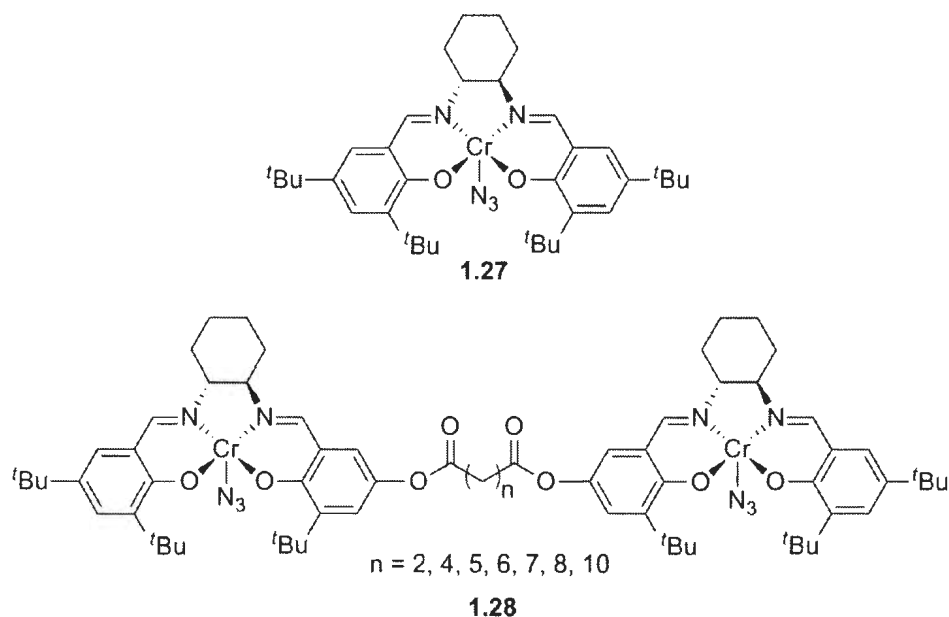


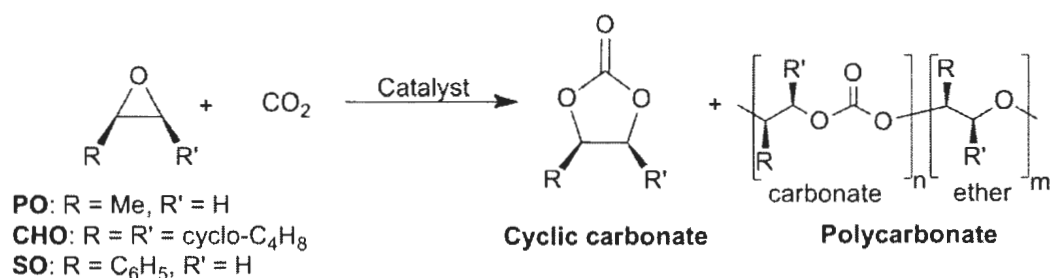
Figure 1.14. Monometallic (**1.27**) and bimetallic (**1.28**) azide Cr(salen) catalysts for ARO.

Asymmetric hetero-Diels-Alder reactions are also important reactions studied by Jacobsen and others. Chromium salen catalysts incorporating various counterions give good enantioselectivities for acyclic dienes, aromatic or aliphatic aldehydes and silyl enol ethers.^{58,67}

Chromium salen catalysts have also shown excellent activities in the copolymerization and cyclisation of epoxides and CO₂. The use of Cr-salen complexes as the active catalyst in such chemical CO₂ fixation reactions originated from the discovery that good activities in nucleophilic ring-opening of epoxides was possible, and therefore cyclisation or polymerization could be possible.⁵² The following section describes important milestones in the reaction of epoxides with CO₂ catalysed by metal-containing catalysts, including those containing chromium.

1.3 Copolymerization of Epoxides and Carbon Dioxide

Within the past decade there has been a significant amount of activity in the literature regarding the use of carbon dioxide as a co-monomer in the copolymerization of epoxides to form polycarbonates (Scheme 1.10).⁶⁸⁻⁷³ The first report of the reaction dates back to 1969. Inoue and co-workers reported a heterogeneous catalyst system, a 1:1 mixture of ZnEt_2 and H_2O was used in the synthesis of aliphatic polycarbonates.^{74,75}



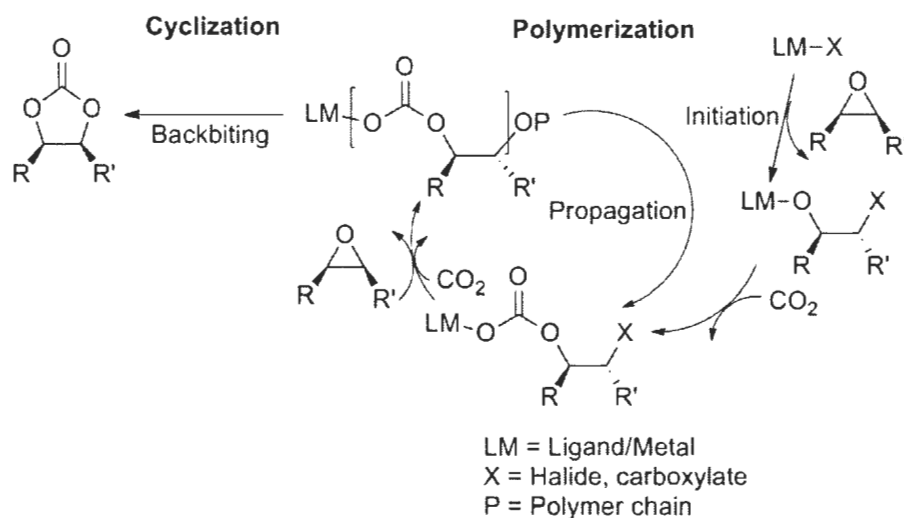
Scheme 1.10. General reaction of common epoxides and CO_2 producing cyclic carbonate and/or polycarbonate. PO = propylene oxide, CHO = cyclohexene oxide, and SO = styrene oxide.

Using CO_2 as a reactant or monomer has proven difficult due to the energy barrier required to activate the molecule. Recently, an increase in the production of polycarbonates worldwide along with growing environmental concerns has allowed CO_2 to become an attractive feedstock for the synthesis of copolymers. Advantages of using carbon dioxide include its high abundance, low toxicity, ability to act as a solvent or reagent, non-flammability, and relative low cost. As well, safety concerns surrounding the current commercial synthesis of “polycarbonate”, which uses phosgene (a toxic gas) and bisphenol A (BPA), has allowed new markets to be explored for the production of a safer polycarbonate. To date, there are a handful of companies that have developed synthetic

procedures incorporating the use of CO₂ and homogeneous catalysis for making polycarbonates. Limitations still exist because the physical properties of the plastic produced from the CO₂ method cannot yet mimic those of polycarbonates made by the conventional procedure. Catalyst design will be crucial in order to allow continued improvements in the production of cost effective and useful polycarbonates.

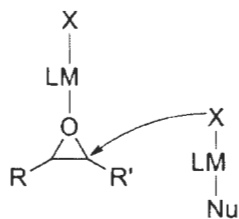
Catalysts used for the copolymerization of CO₂ and epoxides have incorporated a range of different ligand classes throughout the years. Inoue and co-workers first used organometallic catalysts such as ZnEt₂/H₂O, their most active species, to carry out novel copolymerization studies with CO₂ and propylene oxide (PO).^{74,75} The reaction was predicted to occur in the presence of a metal alkoxide species, as well as the resulting reaction of a metal carbonate and an epoxide. The initial reactions carried out by Inoue were performed either at atmospheric pressure or ~50.7 bar, and ambient temperature. Increased pressures led to higher yields and reactions, which originally took many days at atmospheric pressure, required only 24 h at 50 bar CO₂.⁷⁵ Other epoxides, such as epichlorohydrin and styrene oxide (SO), did produce some polycarbonates, albeit at much lower yields than in the case of propylene oxide.

A coordination-insertion mechanism has been the generally accepted pathway for epoxide/CO₂ copolymerization reactions. The accepted two-step process is (i) insertion of CO₂ into a metal alkoxide bond, followed by (ii) the insertion of the epoxide into the resulting metal carbonate bond. Propagation continues with sequential additions of CO₂ and epoxide. Cyclic carbonate formation arises due to a backbiting reaction of a metal alkoxide into a carbonate adjacent to it. The proposed mechanism for the formation of polycarbonates and cyclic carbonates is shown in Scheme 1.11.^{71,76}



Scheme 1.11. Proposed general catalytic cycle for the copolymerization of CO₂/epoxides.

Both monometallic and bimetallic initiation pathways for the copolymerization of CO₂/epoxides have been proposed based on spectroscopic and kinetic investigations. In the case of the bimetallic mechanism with metal salen complexes an intermolecular interaction has been proposed.⁷⁷⁻⁷⁹ Two metal complexes, one with an activated nucleophile (either X or Nu) and another with an epoxide coordinated to the metal, allow intermolecular ring-opening of the epoxide to occur (Scheme 1.12).



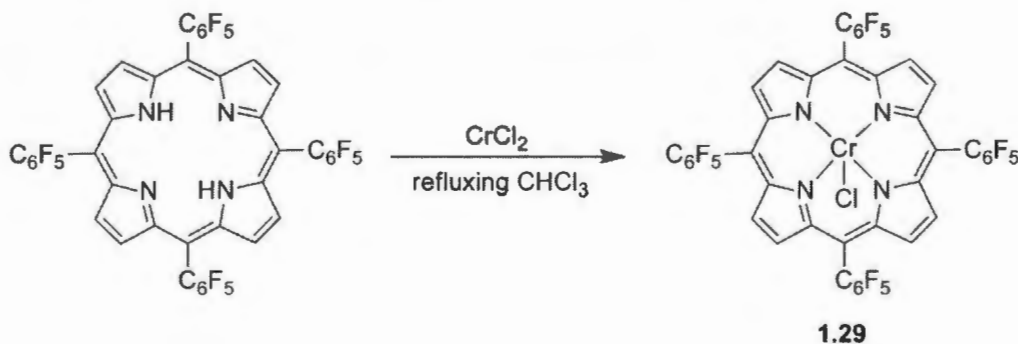
Scheme 1.12. Proposed bimetallic initiation pathway for a model salen complex.

It was not until the mid 80s that more researchers became interested in the formation of polycarbonates derived from CO₂ and epoxides. Aluminium complexes of

porphyrin ligands (tetra-*p*-tolylporphyrinate) proved capable of trapping CO₂ where, in the presence of 1-methylimidazole (N-MeIm), CO₂ and propylene oxide were observed to form propylene carbonate (PC), the cyclic carbonate species (Scheme 1.10).⁸⁰

Kruper discovered that when the metal centre is changed from Al(III) to Cr(III), specifically CrTTPCl, and combined with an amine co-catalyst, N-MeIm or (4-dimethylamino)pyridine (DMAP), the system was 4 to 5 times more active. It was also found that such chromium porphyrinates could be recycled without undergoing any loss in activity.⁸¹

After the introduction of Cr-porphyrin catalysts for the copolymerization of CO₂/epoxides, Holmes and co-workers used a supercritical carbon dioxide (scCO₂) soluble catalyst allowing for the elimination of volatile organic solvents from the reaction.⁸² The complex, tetra(pentafluorophenyl)porphyrin chromium(III) chloride, CrTFPPCl (**1.29**), was synthesised from CrCl₂ in refluxing CHCl₃ (Scheme 1.13).



Scheme 1.13. Synthesis of CrTFPPCl complex (**1.29**).

In the presence of DMAP, **1.29** was observed to produce poly(cyclohexene carbonate) (PCHC) from cyclohexene oxide (CHO) and CO₂ (Scheme 1.10). The copolymer formed was found to possess low molecular weights on the order of 3 500

g/mol. Narrow polydispersity indices (PDIs), 1.1-1.5, were observed for all copolymers produced. Temperature was found to be an important parameter in these reactions. High temperatures led to higher CO₂ incorporation while low temperatures produced only oligomeric polyethers.⁸²

Holmes and co-workers also introduced a new polymer-supported Cr(porphyrin) catalyst used in scCO₂.⁸³ The ring-opening copolymerization of CHO and CO₂ to form the polycarbonate PCHC was catalysed by an Argogel[®] (beaded solid crosslinked polymer support) Cr porphyrin. Molecular weights and PDIs were reported to be very similar to the previous scCO₂ CrTFPPCl system of Holmes and co-workers.⁸² In the case of the supported catalyst, the beads could be recycled; however, a decrease was observed in both the yield and molecular weight of the copolymer upon each re-use.

Previous catalytic reactions were generally carried out at low temperature and pressure, although the turnovers were usually very low. Darensbourg and Holtcamp⁸⁴ introduced monomeric zinc phenoxide complexes for the copolymerization or terpolymerization of epoxides (CHO and PO) and CO₂. The tetrahedral catalyst Zn(II)(diphenylphenoxide)₂(Et₂O)₂ allowed inclusion of bulky substituents on the phenolate ligand. This system was observed to copolymerize CHO and CO₂ to yield PCHC with high carbonate linkages as well as perform the terpolymerization of CHO, PO and CO₂.

A continuation of this study found that similar four-coordinate monomeric Zn(bis phenoxides) were capable of producing high molecular weight poly(cyclohexene carbonate).⁸⁵ The inability of these complexes to coordinate weak donors such as epoxides (PO or CHO) made them good catalysts for ring-opening epoxides. Less

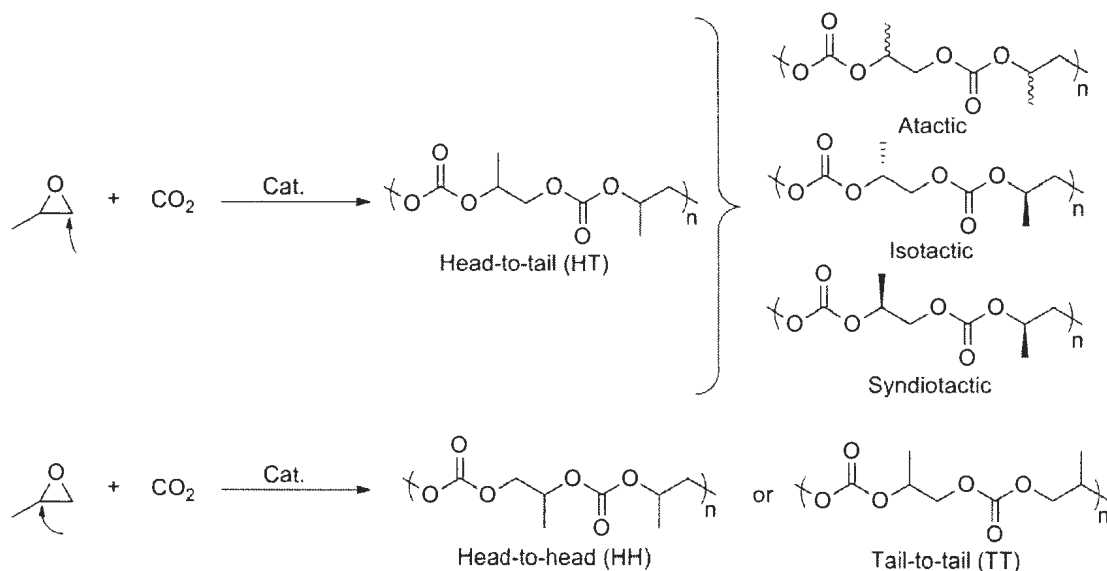
sterically demanding ligands, such as Me, resulted in higher catalytic activity as a consequence of making the metal more electron-rich. The terpolymerization of CHO, PO and CO₂ with minimal PC formation was also achieved using these derivatives.

Further modifications to Zn systems, such as the addition of an electron-withdrawing group along with non-sterically demanding substituents, produced a dimeric Zn phenoxide with fluorinated substituents effective for the copolymerization of CHO and CO₂.⁸⁶ The copolymer afforded high molecular weight of 42 000 g/mol. Although higher turnovers were observed, the turnover frequency (TOF) of 16.5 (g of polymer per g of Zn)/h was still considered low compared to industrial standards. This complex was also found to be stable in air and was actually more active for the homopolymerization of CHO, giving poly(cyclohexene oxide) (PCHO).

Highly active homogeneous Zn catalysts were explored by Coates and co-workers.⁶⁸ Zinc complexes having bulky β -diiminate (BDI) ligands were active towards the living polymerization of CO₂/epoxide copolymerization.⁸⁷ High molecular weights were also observed (15 000-23 000 g/mol). Furthermore, these reactions were shown to be effective under relatively low pressures (6.9 bar) and temperatures (20-80 °C). Contrary to what Darensbourg observed with Zn(phenoxide) complexes, Coates' Zn system showed that bulkier substituents produced a more active species.⁶⁸

Selectivity of stereospecific polymers had not previously been a priority. Jacobsen's important discovery of ARO of epoxides, as previously mentioned in Section 1.2.5, provided new opportunities in CO₂/epoxide chemistry.^{56,66} The first chiral Cr(salen) used for CO₂/epoxide studies was reported by Jacobsen and co-workers in a patent filed in 2000. Such systems opened an avenue for stereocontrolled polymers to be synthesised,

as shown for poly(propylene carbonate) in Scheme 1.14.⁸⁸ The properties of the polymer are highly dependent on its tacticity which is controlled by the stereochemistry.



Scheme 1.14. Stereochemistry of PPC derived from PO/ CO_2 copolymerization.

Paddock and Nguyen were successful in coupling CO_2 with propylene oxide, giving propylene carbonate. An added Lewis base such as DMAP was used as a co-catalyst to help make the Cr(III) centre more electron-rich in order to activate the CO_2 .⁵² Their most active Cr-salen species was observed to be **1.30**, (Figure 1.15), having a TOF of 916 h^{-1} .

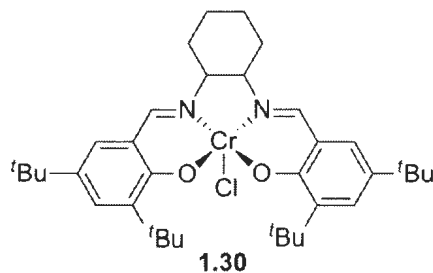


Figure 1.15. Cr(salen)Cl complex (**1.30**) for the coupling of CO_2 and epoxides.

A range of epoxides were catalysed by **1.30** in solvent-free reaction conditions at relatively low pressures (~3.45 bar) and times (1.5-12 h). Interestingly, they found that the activity of the system relied on the concentration of DMAP used. Yields were shown to increase with increased loading of DMAP, with a maximum yield being obtained when 2 equivalents of co-catalyst were used. Beyond this, DMAP was detrimental and significantly less PC was produced. Such results were proposed to be due to an increased formation of Cr(III)(salen)·DMAP species, which would have a negative effect on the rate of reaction.⁵² In this case, DMAP strongly coordinates to Cr, making the chain-end more anionic, facilitating degradation to the cyclic product.

Darensbourg has made a considerable impact in this field, developing very active chromium catalysts for the copolymerization of CO₂ and epoxides. Initially, he investigated the chiral Cr(III)Cl(salen) (**1.30**) species which Jacobsen had previously used in the ARO of epoxides. In this case Darensbourg pursued this complex for its activity in the copolymerization of CO₂ and cyclohexene oxide.⁸⁹ This air-stable, square pyramidal chromium complex was found to be effective towards the synthesis of atactic poly(cyclohexene carbonate). A TOF of 28.5 (g of polymer per g of Cr)/h was observed when carried out at 80 °C and 58.5 bar.⁸⁹ Analysis of the copolymer was shown to have a M_n of 8 900 g/mol and low PDI of 1.2.⁸⁹

Even though a chiral ligand was used in this study, the polymer did not show any evidence of stereochemical control as indicated by the characteristic peaks in the ¹³C NMR of an atactic polymer. Turnover frequencies in the presence of 1 equivalent of co-catalyst, N-MeIm, were low (10.4 h⁻¹), but additional N-MeIm gave increased TOFs. The

use of 5 equivalents produced 32.2 moles of epoxide consumed per mole of metal per hour.

Kinetic studies carried out by Darensbourg *et al.*⁹⁰ on (**1.30**) gave important energetic data, providing knowledge for future investigations on how to overcome the production of cyclic species in the synthesis of polycarbonates. Both cyclohexene oxide and propylene oxide were examined using this catalytic system. The activation energies (E_a) for the cyclic and polymeric products of CHO are 31.8 and 11.2 kcal mol⁻¹, respectively. This indicates that the formation of the cyclohexene carbonate (CHC) species has a much greater barrier to overcome, therefore making PCHC a more favourable product. Activation energies were found to be 24.0 for propylene carbonate and 16.2 kcal mol⁻¹ for poly(propylene) carbonate. For PO/CO₂ copolymerization, the small difference in E_a allows the cyclic carbonate species, PC and polymer, poly(propylene) carbonate (PPC) to form at competitive rates.

Darensbourg and co-workers sought to optimize the reaction conditions for CrN₃(salen) complex (**1.31**) with bis(triphenylphosphoranylidene) ammonium (PPN⁺) salts through altering the CO₂ pressure.⁹¹ A slight modification to one of the substituents on the phenol, where a *tert*-butyl is replaced with a methoxy group, gave rise to a significant increase in activity, reporting their most active chromium catalyst for CO₂/CHO copolymerization (Figure 1.16). In the presence of **1.31** and 1 equivalent of bis(triphenylphosphoranylidene) ammonium azide (PPNN₃) as the co-catalyst, a TOF of 1153 h⁻¹ was achievable under 34.5 bar of CO₂ and 80 °C. Not only was the activity found to be extremely high, but the M_n was found to be very high, at 50 000 g/mol, as well as having a very narrow PDI of 1.13. A high TOF (1056.8 h⁻¹) could still be afforded

in the presence of **1.31** and PPNCl, albeit slightly lower than with the azide-containing co-catalyst.⁹¹

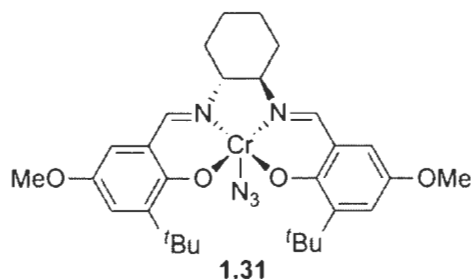


Figure 1.16. CrN₃(salen) complex (**1.31**).

Cobalt salen complexes have also shown high activity towards the copolymerization of CO₂ and epoxides.⁹²⁻⁹⁴ For example, the most active Co system gave TOFs greater than 20 000 h⁻¹ when Co(salen) complexes having quaternary ammonium groups attached to the phenol were employed.⁹³ Catalyst **1.32**, shown in Figure 1.17, was capable of producing poly(propylene) carbonate of 114 000 to 285 000 g/mol. Of particular importance was that the catalyst could be recycled simply by passing the product through a pad of silica gel. This separated catalyst could then be reused without observing much loss in activity.

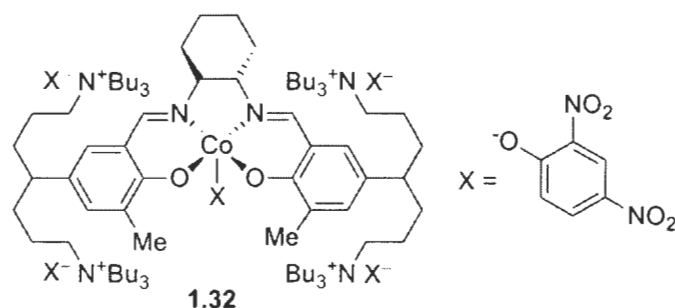


Figure 1.17. Highly active Co(salen) complex (**1.32**) for CO₂/PO copolymerization.

Very recently, Williams and co-workers reported the first use of an iron catalyst for such polymerization reactions.⁹⁵ A bimetallic Fe(III) catalyst was shown to copolymerize CO₂ and CHO. Relatively good activities with TOFs of 3-107 h⁻¹ were observed for cyclohexene oxide under low pressures of CO₂ (1-10 bar). In the presence of PO and SO, the cyclic carbonate species propylene carbonate (PC) and styrene carbonate (SC) were observed.

Alternatives to metal-salen catalysts have been explored. These include reduced analogues of the salen class, such as salalen and salan ligands. Nozaki and co-workers studied chromium complexes with the salalen ligand.⁹⁶ Specifically, the CrCl(salalen) complexes (**1.33**), (Figure 1.18) showed good activities towards the copolymerization of CHO/CO₂. The TOFs ranged from 83-230 h⁻¹ and were obtained under pressures of 13 bar to 52 bar CO₂ at 70 °C. The M_n of the copolymer was highly dependent on the structure of the ligand, but in all cases the polydispersities were observed to be low (1.05-1.17).

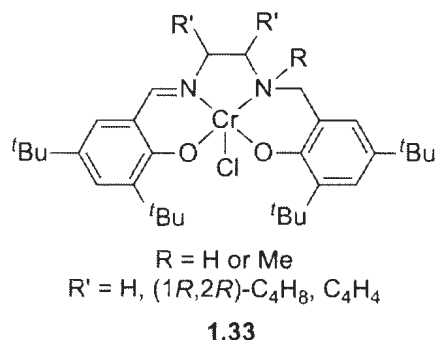


Figure 1.18. CrCl(salalen) complexes (**1.33**).

Ligands such as the salan type can be coordinated to chromium to give highly active catalysts as well.^{55,88} Li *et al.* first introduced a saturated version of the Schiff-base

salen ligand, a chiral Cr(III)(salan) complex (**1.34**) shown in Figure 1.19.⁸⁸ The catalyst afforded alternating PPC in conjunction with co-catalysts, *n*Bu₄NNO₃ or *n*Bu₄NCl at ambient temperature (25 °C) and low pressures (15 bar of CO₂). Higher activities, enantioselectivity and stereochemical control were possible with this catalyst system than with the corresponding Cr(III)(salen) complexes. High *M_n* (> 20 000 g/mol) and low PDIs (1.27) were observed. The reason attributed for increased activity for the salan system is due to the presence of sp³-hybridized amino donors and the N,N'-disubstituted groups of the chiral species, causing lower electrophilicity at the central Cr ion. Interestingly, unlike the salen system which works well with bulky ionic salts as the co-catalyst, such as PPNCl, decreased activity and enantioselectivity was found in the case of this salan system. Additionally, this system was shown to be easily tuned to favour cyclic carbonate over polycarbonate depending on the parameters used.

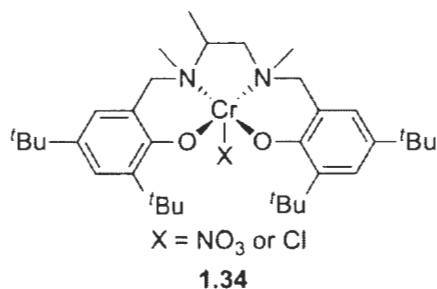


Figure 1.19. CrX(salan) complex (**1.34**) for the copolymerization of CO₂ and PO.

Lu's group also carried out an elegant MS study on both Cr(III)(salen) and Cr(III)(salan) complexes in the presence of DMAP as the co-catalyst.⁷⁸ It was found that [Cr(salen)]⁺ cations preferentially coordinated two molecules of DMAP, forming six-coordinate species. Whereas [Cr(salan)]⁺ cations coordinated only one DMAP molecule,

forming five-coordinate species. This resulted in varying activities for the different species. Cr(salan), when reacted with 1 equivalent of DMAP, proved to be approximately 30 times more active than the Cr(salen) species. This allowed them to postulate that the actual active intermediate in initiating the reaction may be the species with only one DMAP coordinated.

There has been growing interest in the use of salan based ligands due to their enhanced reactivity as catalysts. Darensbourg and co-workers described a CrCl(salan) complex (**1.35**) used for the copolymerization of CHO, PO and CO₂ (Figure 1.20).⁵⁵ They proposed that the complex adopted a geometry where three of the salan binding sites were in plane with the metal centre, while one oxygen binding site lies out of the plane. This differs from salen complexes previously studied, where all four binding sites are in plane with the Cr centre.

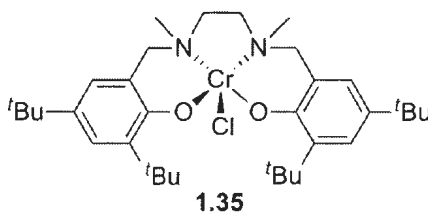


Figure 1.20. CrCl(salan) complex (**1.35**).

Complex **1.35** in the presence of 1 equivalent of PPNN₃ gave a TOF of 405 h⁻¹ when performed at 34 bar CO₂ and 60 °C. Copolymer molecular weights were found to be greater than 19 000 g/mol with low polydispersities. As well, this Cr(salan) derivative is an effective catalyst for the formation of poly(propylene carbonate) at 25 °C, which was not the case for the Cr(salen) analogue. Furthermore, this catalyst system was capable of forming diblock and triblock copolymers of PPC, PCHC and

poly(vinylcyclohexene carbonate), PVCHC. Interestingly, the Cr(salan) analogue was much easier to remove from the polymer than the Cr(salen) species, leaving an almost colourless polymer after only one methanol washing.

Only a few dimeric Cr(III)(salphen) complexes, where salphen = N,N-bis(salicylidene)-1,2-diaminobenzene, have been reported in the literature. Rieger and co-workers presented a recent report on monometallic (**1.36**) and bimetallic (**1.37**) Cr(III)(salphen) catalysts, as shown in Figure 1.21, for the copolymerization of propylene oxide with CO₂.⁹⁷

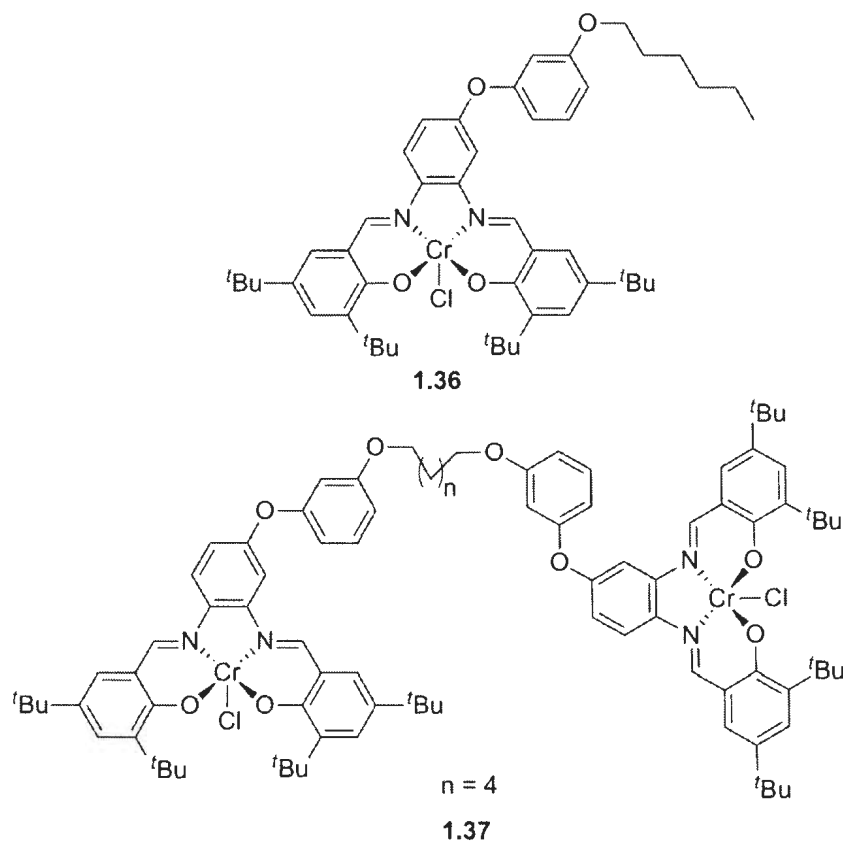


Figure 1.21. Monometallic (**1.36**) and bimetallic (**1.37**) CrCl(salphen) complexes.

The reactions were performed at 60 °C, 40 bar CO₂ for 24 hours, without the addition of any co-catalyst. They were able to achieve TOFs of 67 h⁻¹ for the monometallic complex and 82 h⁻¹ for the bimetallic complex. *M_n* were found to be greater than 50 000 g/mol, although PDIs were observed to be broad, ranging from 2.0 to 3.3. The increased activity for the bimetallic species suggests that a bimetallic mechanism may be at work here.

1.4 Ring-Opening Polymerization of Lactide

Polyesters such as poly(lactic acid) PLA are widely used and common place in the plastics industry today. An increased interest surrounding the synthesis of aliphatic polyesters, for example PLA, poly(caprolactone) (PCL) and poly(hydroxyalkanoate) (PHA) has grown in the scientific community as a result of their biodegradability and biocompatibility properties. Traditionally, polyesters were synthesised via a polycondensation reaction, where high energy costs, poor atom efficiency (needing stoichiometric amounts of reagents), as well as difficulty in producing high molecular weights were common.

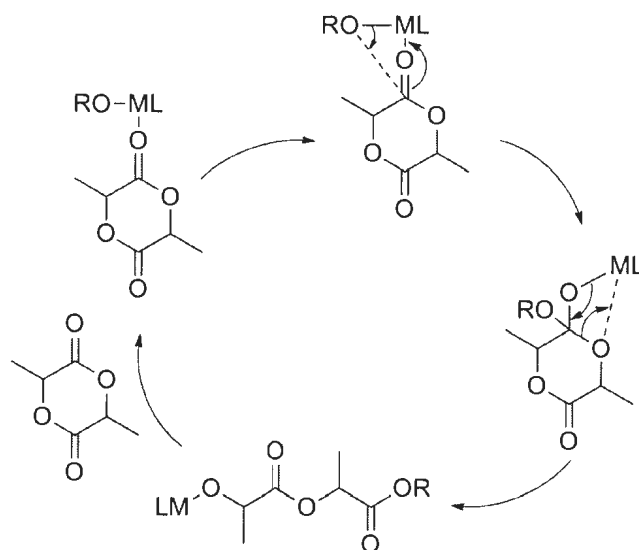
Since the 1970s, the synthesis through catalytic ring-opening polymerization (ROP) has been the chosen method.⁹⁸ The reasons for this are related to the reaction mechanism. A coordination-insertion mechanism occurs, which provides lower energy costs, higher atom efficiency (catalytic initiators being used) and allows higher molecular weight polymers to be synthesised. A variety of applications have been reported for polyesters including their use in the medical field (used in drug delivery), food packaging as well as the textiles industry.⁹⁹⁻¹⁰¹

As with any very active research area, many review articles have been published on the ROP of polyesters.^{98,99,101-104} Due to the nature of this thesis, this section will focus on the ROP of lactide (LA), specifically highlighting the use of alkali metals.

Commercialization of PLA using renewable resources, such as that based on corn, has yielded increased economic benefits. Natureworks, LLC has successfully demonstrated this with their production of PLA on a 140 000 ton industrial scale.¹⁰³

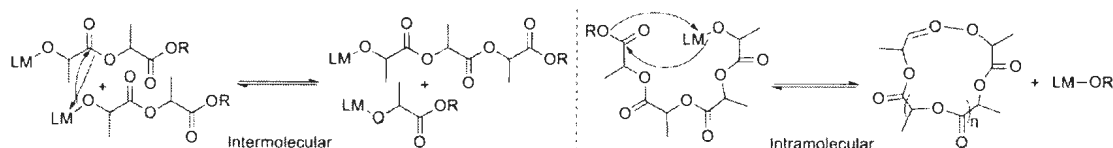
Single-site catalysts or initiators play a significant role in the production of PLA. Control over the reaction is key in order to produce high molecular weight polymers with narrow PDIs, stereoselective PLA and high rates of polymerization. Additionally, other considerations important to the development of PLAs synthetic process include cost, toxicity, minimal traces of metal catalyst in the final product, as well as a high abundance of the desired starting materials.¹⁰¹

The most common initiator is a metal alkoxide which produces PLA via a coordination-insertion mechanism. The process is thought to occur when the metal catalyst activates the lactide monomer via the alkoxide bond from the ligand within the same complex or from the addition of a co-initiator such as an aliphatic alcohol, primary amine or water (Scheme 1.15).



Scheme 1.15. The coordination-insertion mechanism for PLA synthesis.

Although ROP is the most widely used synthetic method for PLA, it is still not perfect. Side reactions such as transesterification are known to occur at elevated temperatures and in the presence of less selective and more active catalysts.⁹⁹ Transesterification is the cleavage and reformation of polymer chains leading to various molecular weights and hence broad PDIs. Both variable chain length polymers (intermolecular transesterification) and macrocyclic polymers (intramolecular transesterification) have been observed to occur (Scheme 1.16).^{99,101,105}



Scheme 1.16. Intermolecular and intramolecular transesterification.

Initial independent studies by Coates and by Chisholm using BDI supported catalysts and tris(pyrazolyl)borate (TPB) complexes, respectively, as initiators allowed

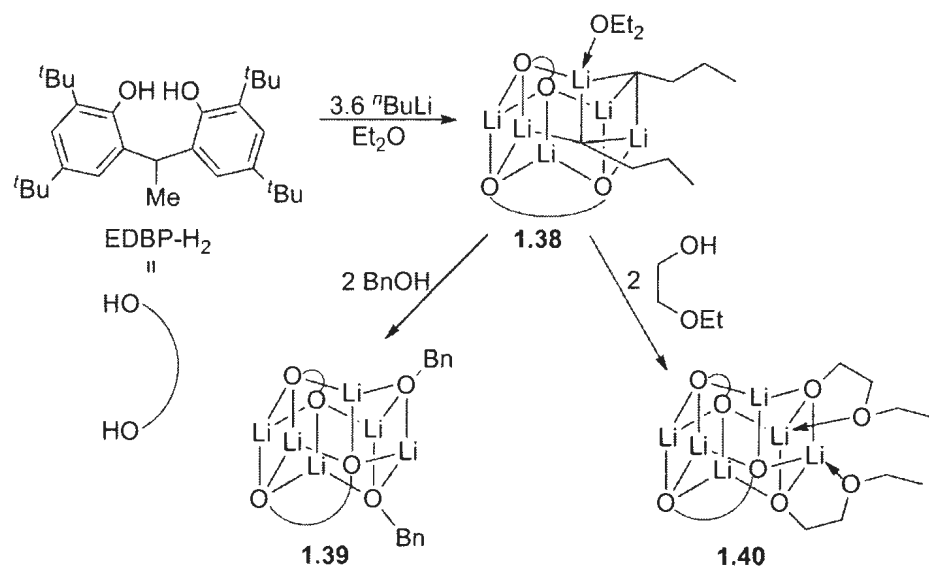
novel advancements in the polymerization of lactide.^{106,107} Various ligand frameworks have been employed towards ROP of LA, including phenolate ligands. Such systems are capable of ROP due to their steric bulk, allowing more control as well as their ability to form a metal-oxygen bond necessary in the proposed coordination-insertion mechanism for polyesters. In recent years, mono- and dianionic bis(phenolate) metal complexes have been used as potential ROP initiators. Metals such as Li, Na, K, Mg, Zn and Ca have been explored for their potential as catalysts/initiators in ROP systems.

Group 1 metal complexes including simple alkali-salts have shown activity and biocompatibility for ROP of LA. For example, lithium chloride was found to be capable of producing PLA in the presence of ethylene glycol and methyl α -D-glucopyranoside.¹⁰⁸ Although the polymerization was successful, the degree of control was poor, as broad PDIs were observed (>2.2). Due to the ionic nature of these Group 1 metals, they have a high affinity for competing side reactions.⁹⁹

Simple metal alkoxide complexes such as lithium or potassium *tert*-butoxide proved to be good initiators possessing reasonable efficiency and control of the polymerization. Kasperczyk reported M_n of 40 000 g/mol with only 0.25 mol% catalyst loading when using LiO*t*Bu as the initiator.¹⁰⁹ Stereocontrol was also reported affording heterotactic PLA. Further studies with LiO*t*Bu observed even better stereoselectivity at low temperatures (0 °C).¹¹⁰ As previously reported, lower temperatures were found to inhibit side reactions such as transesterification, which is likely what has occurred here. However, back-biting reactions led to intramolecular transesterification. This resulted in macrocycles and broad molecular weight distributions. Potassium *tert*-butoxide also showed activity towards ROP of LA.¹¹¹

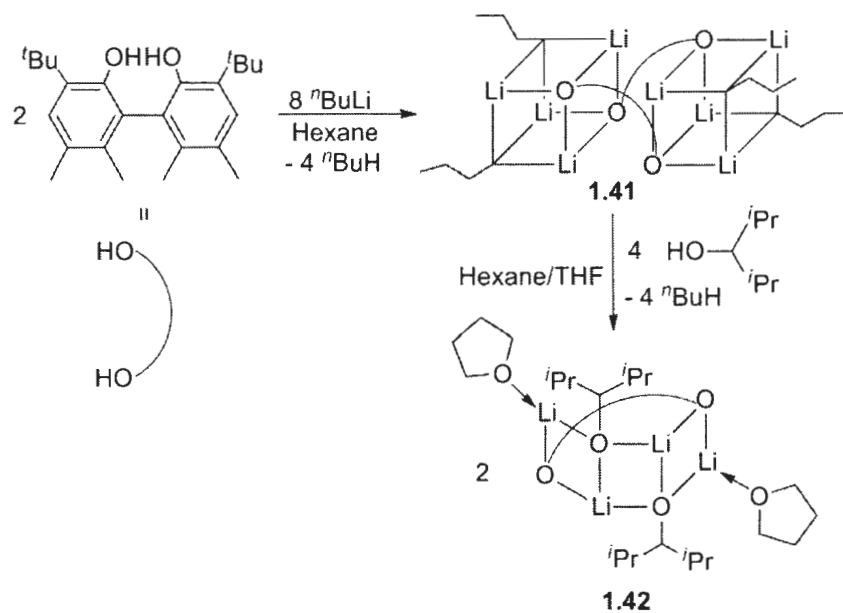
Kasperczyk and co-workers also examined the ROP of *rac*-lactide initiated by butyllithium (BuLi) in THF at 20 °C for 40 minutes. The polymer from this reaction was found to afford higher molecular weights than its magnesium analogue (M_n ranged from 7 000 – 45 000 g/mol) and gave a bias towards a syndiotactic structure.¹¹²

Initial studies by Lin and co-workers built upon the results of the alkyl lithium initiators mentioned above. However, in order to try and avoid side reactions they incorporated a bulky bis(phenolate) ligand, 2,2'-ethylidene-bis(4,6-di-*tert*-butylphenol), referred to as EDBP-H₂, into their catalytic system.¹¹³ Group 1 alkoxides are known to aggregate, therefore it was not surprising that the addition of ⁿBuLi to EDBP-H₂ produced the first example of a lithium bisphenoxide aggregate. The reaction of complex **1.38** with 2 equivalents of benzyl alcohol (BnOH) yielded **1.39**. Furthermore, the reaction of complex (**1.38**) with 2 equivalents of 2-ethoxyethanol yielded **1.40** as described in Scheme 1.17. Sterics were shown to a certain extent, to play a role in the polymerization, as complex (**1.38**) with the least sterically hindered Li ions was inactive, whereas complexes (**1.39**) and (**1.40**) in the presence of L-lactide produced PLA in a controlled manner. Mechanistic results suggest that the Li atoms coordinated to the less sterically hindered benzyl alkoxide oxygens in **1.39** are the site of initiation due to the similarity of complex (**1.40**) to that of (**1.39**).



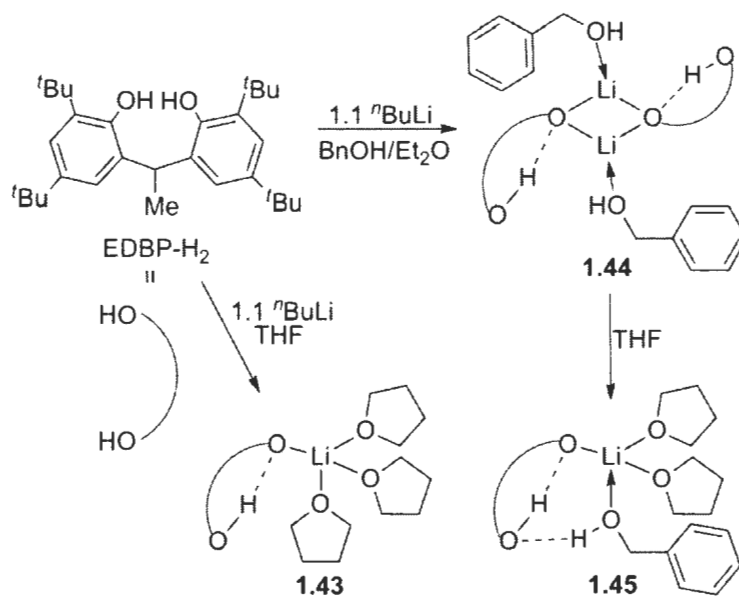
Scheme 1.17. Synthesis of hexalithium clusters (**1.38**), (**1.39**) and (**1.40**).

An octalithium cluster was also produced in the synthesis of a similar bis(phenolate) ligand with 8 equivalents of n BuLi giving complex (**1.41**) as shown in Scheme 1.18. The addition of 4 equivalents of 2,4-dimethyl-3-pentanol to **1.41** in THF gave a tetralithium complex (**1.42**). Chisholm *et al.* reported that **1.42** was able to successfully ring-open lactide in 1 h at ambient temperature. Unfortunately, atactic PLA was observed from this initiator indicative of transesterification.



Scheme 1.18. Synthesis of octalithium (**1.41**) and tetralithium (**1.42**) complexes.

Further work done by Lin and co-workers using the EDBP- H_2 ligand as mentioned previously in the presence of 1.1 equivalent of $^n\text{BuLi}$ in THF afforded complex (**1.43**) shown in Scheme 1.19.¹¹⁴ Furthermore, the addition of BnOH , $^n\text{BuLi}$ and EDBP- H_2 in diethyl ether resulted in a dimeric lithium species (**1.44**) being produced. A monomeric species (**1.45**) was also isolated following the reaction of **1.44** in a coordinating solvent such as THF at ambient temperature.

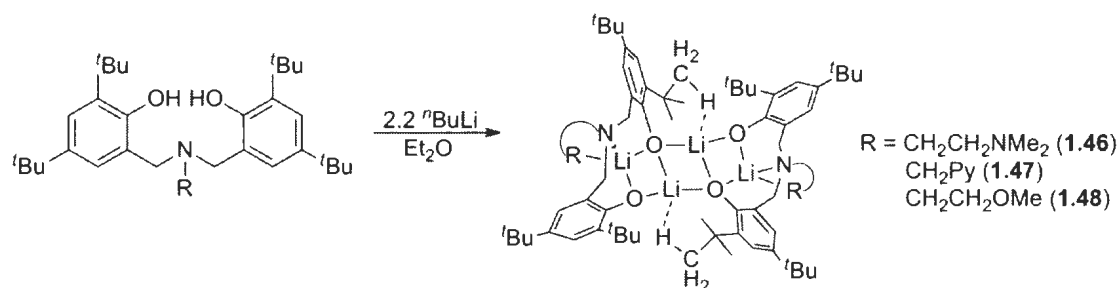


Scheme 1.19. Synthesis of mono- (**1.43**), (**1.45**) and dilithium (**1.44**) complexes.

The ROP of L-lactide with **1.44** was shown to yield PLA when performed in dichloromethane (CH₂Cl₂) at 0 and 25 °C. Living polymerization characteristics were observed, providing a linear relationship between the molecular weights (M_n) of the polymer and the molecular weight distributions (PDIs). This controlled polymerization process gave very narrow PDIs over a wide range of monomer-to-initiator ratios. M_n values ranged from low (2 200, with BnOH) to high (23 800 without BnOH) over a period of 2 h or less.

Complex (**1.45**) also showed good activity in the ROP of L-lactide, although it was not as active as **1.44**. It was suggested that this could be due to the coordinated THF hindering the insertion of the lactide. Both mono- and bimetallic lithium species proved to be more active compared to the hexalithium clusters.

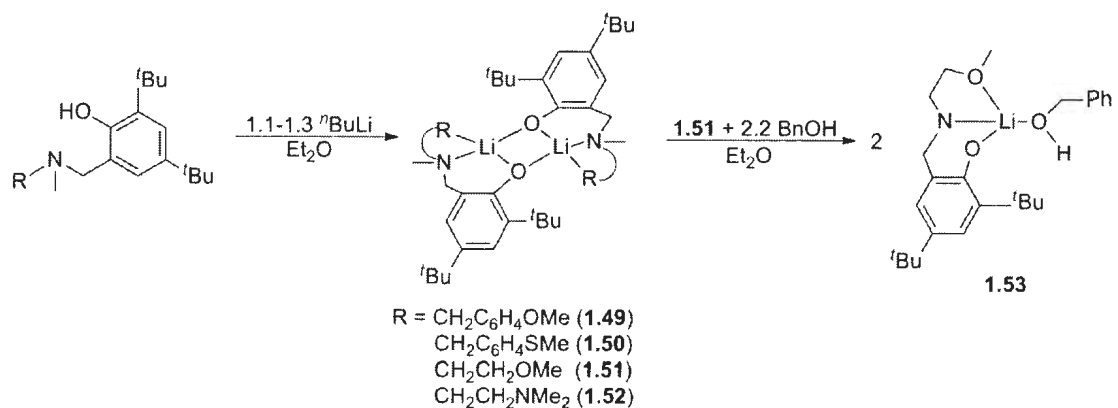
Related to the phenolate ligands mentioned above, amino-bis(phenolate) ligands containing pendant donor arms coordinated to lithium were also explored. Initial studies entailed using tetradentate ligands such as $H_2[O_2NN^i]^{Me_2}$, $H_2[O_2NN^i]^{Py}$ and $H_2[O_2NO]^{Me}$. These ligands were then reacted with 2.2 equivalents of tBuLi in Et_2O giving ladder-like motifs as tetralithium complexes $\{Li_2[O_2NN^i]^{Me_2}\}_2$ (**1.46**), $\{Li_2[O_2NN^i]^{Py}\}_2$ (**1.47**) and $\{Li_2[O_2NO]^{Me}\}_2$ (**1.48**) as shown in Scheme 1.20.¹¹⁵



Scheme 1.20. Synthesis of tetralithium complexes (**1.46**), (**1.47**) and (**1.48**).

The ROP of L-lactide with a co-initiator, BnOH, was conducted at 26.5 °C in CH_2Cl_2 . Polymer was produced with high conversions in a controlled and living manner in less than 1 h. The molecular weights observed were moderate ranging from 5 000 to 20 000 g/mol. Almost all the PDIs reported were low (1.08-1.18) when BnOH was used as a co-initiator. Without BnOH PDIs were broader in the range 1.26-1.55. Immortal character was also reported for all three complexes, whereby the polymerization could not be terminated even after the addition of a protic compound. The results allude to a mechanism similar to that proposed by Lin's group,¹¹³ whereby a benzyl oxide group inserts into the carbonyl carbon of the lactide allowing the opening of the ring. Therefore, the presence of BnOH is important in maintaining a controlled polymerization.

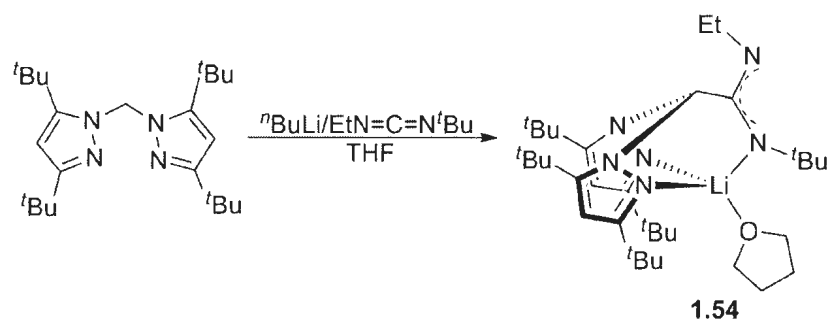
A continuation of ligand design towards a more active catalyst/initiator for ROP led Chen's group to explore asymmetric amino phenolate ligand precursors.¹¹⁶ The ligands used were $\text{H}[\text{ON}^{\text{Me}}\text{O}]^{\text{Me}}$, $\text{H}[\text{ON}^{\text{Me}}\text{S}]^{\text{Me}}$, $\text{H}[\text{ON}^{\text{Me}}](\text{CH}_2)_2\text{OMe}$ and $\text{H}[\text{ON}^{\text{Me}}](\text{CH}_2)_2\text{NMe}_2$. These ligands were reacted with 1.1-1.3 equivalents of $n\text{BuLi}$ in Et_2O giving dimeric lithium complexes $\{\text{Li}[\text{ON}^{\text{Me}}\text{O}]^{\text{Me}}\}_2$ (**1.49**), $\{\text{Li}[\text{ON}^{\text{Me}}\text{S}]^{\text{Me}}\}_2$ (**1.50**), $\{\text{Li}[\text{ON}^{\text{Me}}](\text{CH}_2)_2\text{OMe}\}_2$ (**1.51**) and $\{\text{Li}[\text{ON}^{\text{Me}}](\text{CH}_2)_2\text{NMe}_2\}_2$ (**1.52**) as shown in Scheme 1.21. These complexes were then tested for their activity in the ROP of L-lactide with BnOH at $26.5\text{ }^\circ\text{C}$ and with various solvents (CH_2Cl_2 , THF and toluene). As was the case with previous ROP results, the best controlled process was observed when CH_2Cl_2 was used as the solvent. Between the four complexes explored, complex (**1.52**) proved to be the best initiator. A similar living polymerization relationship was observed here. For example, complex (**1.52**) yielded a linear correlation between the M_n (5 600-19 100 g/mol) and PDI (1.19-1.56) as well as immortal characteristics. However, control of the polymerization was not possible upon increasing monomer-to-initiator ratio. This was suggested to be due to transesterification occurring in the later stages of the reaction as observed in the increasing PDI values.



Scheme 1.21. Synthesis of dimeric lithium complexes (**1.49**), (**1.50**), (**1.51**), (**1.52**) and monomeric-BnOH adduct (**1.53**).

A monomeric species (**1.53**) was also capable of being synthesised when **1.51** and 2.2 equivalents of BnOH were reacted in Et_2O .¹¹⁶ The BnOH was shown to coordinate to the lithium and the complex was isolated and used in the study to compare reactivities. Results found that **1.53** was as active as the dilithium complexes when generated *in situ*. Stereoselectivity was not found to be any better for **1.53** than for **1.51**, when *rac*-lactide was used as the monomer. It was also discovered that the highest activity was observed when the amino phenolate with the amino pendant (**1.52**) was employed rather than the methoxy or thioether donors (**1.49-1.51**).

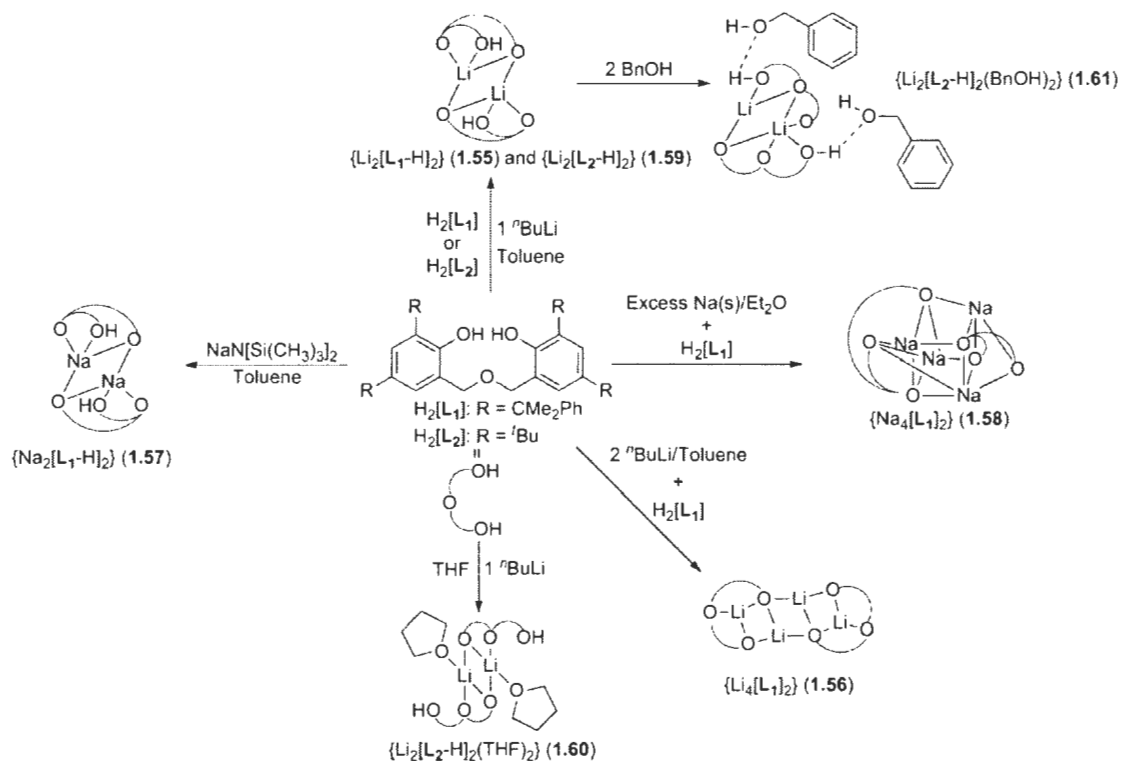
A bulky bis-pyrazolyl amidinate “heteroscorpionate” ligand framework complexed with lithium also proved to be active towards the ROP of L-lactide.¹¹⁷ The lithium acetamidinate $[\text{Li}(\text{tbptamd})\text{-(THF)}]$ (**1.54**) [tbptamd = N-ethyl-N'-*tert*-butylbis(3,5-di-*tert*-butylpyrazol-1-yl)acetamidinate] was synthesised from $n\text{-BuLi}$ in THF with good yields (Scheme 1.22).



Scheme 1.22. Synthesis of monomeric lithium complex (**1.54**).

Polymerization reactions with **1.54** were carried out at 110 °C in toluene without the need of any co-initiator. Conversions were observed to be high over a wide range of reaction times (0.75 to 36 h). Molecular weights (6 500-14 500 g/mol) and PDIs (1.28-1.45) were found to be moderate for this system.¹¹⁷

Lin and co-workers more recently described an OOO-tridentate bis(phenolate)-ether ligand used in the synthesis of lithium and sodium complexes for ROP of L-lactide.¹¹⁸ In the presence of ⁿBuLi and various solvents such as THF, toluene or BnOH, di- and tetralithium structures were isolated. Complexes {Li₂[L₁-H]₂} (**1.55**), {Li₄[L₁]₂} (**1.56**), {Na₂[L₁-H]₂} (**1.57**), {Na₄[L₁]₂} (**1.58**), {Li₂[L₂-H]₂} (**1.59**), {Li₂[L₂-H]₂(THF)₂} (**1.60**) and {Li₂[L₂-H]₂(BnOH)₂} (**1.61**), as described in Scheme 1.23, have all shown activity for the polymerization of L-lactide with BnOH in CH₂Cl₂.



Scheme 1.23. Synthesis of di- (1.55), (1.57), (1.59), (1.60), (1.61) and tetra- (1.56) and (1.58) lithium and sodium complexes.

Specifically, complex (1.58), a dimeric sodium complex had the highest reactivity. The polymerization reached completion in less than 10 min at 0 °C and 0.5 mol% catalyst loading. The sodium complexes showed much higher activities, which the authors attributed to the higher electropositive nature of sodium, but the larger ionic radius of Na could also be a contributing factor. Steric bulk around the metal also affected the activity, whereby the bulkier ligand in complex (1.55) actually decreased the activity in comparison to complex (1.59). However, it was found that the tetralithium species showed higher ROP activities than the dilithium analogues. The addition of 2 equivalents of BnOH to the reaction resulted in a faster polymerization and the M_n dropped by half,

signifying an immortal polymerization process. Furthermore, all complexes produced low PDI values (1.04-1.30), indicative of controlled polymerizations.

1.5 Objectives

The objectives of this research were to synthesise transition metal complexes for polymerization catalysis. Specifically, the syntheses of biodegradable and/or bioassimilable polymers were of interest. The focus of the research was to develop catalysts specific to (a) the polymerization of cyclic esters and (b) the copolymerization of CO₂ with epoxides. In order to achieve the objectives mentioned, studies involving 1) ligand effects, 2) metal centre, 3) co-catalyst and 4) monomers, as well as characterization of the polymers and mechanistic studies of the polymerization would be necessary to maximize yields of the desired polymers.

The ligands of interest in this thesis were tetradentate, tripodal, amine-bis(phenolates). These ligands are highly modifiable: allowing fine-tuning of their sterics by altering the substituents on the phenolate groups, and their electronic nature by changing the pendant donor arm. The geometry of the donor around the metal centre is crucial to the reactivity of the system. The ability to modify the ligand framework to suit a specific task makes them highly desirable. The synthesis of these ligands and their complexation to inexpensive transition metals is importantly straight forward and attainable in high yields. Compounds containing lithium and chromium have previously shown success in the literature for their polymerization capability. However, the use of such ligands for this purpose had yet to be investigated.

A series of Li and Cr complexes were successfully synthesised and tested for their polymerization activities. Many experimental factors, including the co-catalyst, temperature, pressure and time proved to be important in attaining the desired product. The isolated complexes were also characterized by NMR (where appropriate), IR, UV-Vis spectroscopy, mass spectrometry, magnetometry, cyclic voltammetry and elemental analysis. In addition to the catalytic and structural properties of these Cr complexes, an attempt was made to synthesise Cr alkyl amine-bis(phenolate) complexes for potential future use in polymerization catalysis.

This research has shown that both poly(lactide) and polycarbonates can be synthesised from their respective Li and Cr amine-bis(phenolate) complexes. Although, activities were not exceptional the polymers obtained did show interesting results. In the case of the ROP results the poly(lactide) obtained was found to give high activities at high temperatures but proved difficult to control. The copolymerization results found that when employing cyclohexene oxide as the monomer no cyclic species were produced and PDIs remained low. Further reactions and innovations are still necessary in order to achieve the goals set out in this research. For example, continued investigations are needed on the effect of varying the ligand; mechanistic studies of this system; additional co-catalyst modifications with the possibility of synthesising a single-site catalyst; and the exploration of other unique and environmentally benign monomers.

1.6 References

- (1) Hinshaw, C. J.; Peng, G.; Singh, R.; Spence, J. T.; Enemark, J. H.; Bruck, M.; Kristofzski, J.; Merbs, S. L.; Ortega, R. B.; Wexler, P. A. *Inorg. Chem.* **1989**, *28*, 4483-4491.
- (2) Wichmann, O.; Sillanpää, R.; Lehtonen, A. *Coord. Chem. Rev.* **2012**, *256*, 371-392.
- (3) Tshuva, E. Y.; Versano, M.; Goldberg, I.; Kol, M.; Weitman, H.; Goldschmidt, Z. *Inorg. Chem. Commun.* **1999**, *2*, 371-373.
- (4) Tshuva, E. Y.; Goldberg, I.; Kol, M.; Goldschmidt, Z. *Inorg. Chem. Commun.* **2000**, *3*, 611-614.
- (5) Tshuva, E. Y.; Goldberg, I.; Kol, M.; Weitman, H.; Goldschmidt, Z. *Chem. Commun.* **2000**, 379-380.
- (6) Tshuva, E. Y.; Goldberg, I.; Kol, M. *J. Am. Chem. Soc.* **2000**, *122*, 10706-10707.
- (7) Toupance, T.; Dubberley, S. R.; Rees, N. H.; Tyrrell, B. R.; Mountford, P. *Organometallics* **2002**, *21*, 1367-1382.
- (8) Groysman, S.; Goldberg, I.; Kol, M.; Genizi, E.; Goldschmidt, Z. *Inorg. Chim. Acta* **2003**, *345*, 137-144.
- (9) Yeori, A.; Goldberg, I.; Shuster, M.; Kol, M. *J. Am. Chem. Soc.* **2006**, *128*, 13062-13063.
- (10) Lorber, C.; Wolff, F.; Choukroun, R.; Vendier, L. *Eur. J. Inorg. Chem.* **2005**, 2850-2859.
- (11) Wolff, F.; Lorber, C.; Choukroun, R.; Donnadiou, B. *Inorg. Chem.* **2003**, *42*, 7839-7845.
- (12) Wolff, F.; Lorber, C.; Choukroun, R.; Donnadiou, B. *Eur. J. Inorg. Chem.* **2004**, 2861-2867.
- (13) Maity, D.; Ray, A.; Sheldrick, W. S.; Figge, H. M.; Bandyopadhyay, B.; Ali, M. *Inorg. Chim. Acta* **2006**, *359*, 3197-3204.
- (14) Maity, D.; Mijanuddin, M.; Drew, M. G. B.; Marek, J.; Mondal, P. C.; Pahari, B.; Ali, M. *Polyhedron* **2007**, *26*, 4494-4502.

- (15) Maity, D.; Marek, J.; Sheldrick, W. S.; Mayer-Figge, H.; Ali, M. *J. Mol. Cat. A* **2007**, *270*, 153-159.
- (16) Böttcher, A.; Elias, H.; Glerup, J.; Neuburger, M.; Olsen, C.,E.; Springborg, J.; Weihe, H.; Zehnder, M. *Acta Chem. Scand.* **1994**, *48*, 981-988.
- (17) Böttcher, A.; Elias, H.; Glerup, J.; Neuburger, M.; Olsen, C.,Erik; Paulus, H.; Springborg, J.; Zehnder, M. *Acta Chem. Scand.* **1994**, *48*, 967-980.
- (18) Weyhermüller, T.; Paine, T. K.; Bothe, E.; Bill, E.; Chaudhuri, P. *Inorg. Chim. Acta* **2002**, *337*, 344-356.
- (19) Dean, R. K.; Granville, S. L.; Dawe, L. N.; Decken, A.; Hattenhauer, K. M.; Kozak, C. M. *Dalton Trans.* **2010**, *39*, 548-559.
- (20) Chowdhury, R. R.; Crane, A. K.; Fowler, C.; Kwong, P.; Kozak, C. M. *Chem. Commun.* **2008**, 94-96.
- (21) Hasan, K.; Fowler, C.; Kwong, P.; Crane, A. K.; Collins, J. L.; Kozak, C. M. *Dalton Trans.* **2008**, 2991-2998.
- (22) Qian, X.; Dawe, L. N.; Kozak, C. M. *Dalton Trans.* **2011**, *40*, 933-943.
- (23) Reckling, A. M.; Martin, D.; Dawe, L. N.; Decken, A.; Kozak, C. M. *J. Organomet. Chem.* **2011**, *696*, 787-794.
- (24) Hasan, K.; Dawe, L. N.; Kozak, C. M. *Eur. J. Inorg. Chem.* **2011**, 4610-4621.
- (25) Rodríguez, L.; Labisbal, E.; Sousa-Pedrares, A.; García-Vázquez, J. A.; Romero, J.; Durán, M. L.; Real, J. A.; Sousa, A. *Inorg. Chem.* **2006**, *45*, 7903-7914.
- (26) Schnieders, D.; Hammerschmidt, A.; Merkel, M.; Schweppe, F.; Krebs, B. *Anorg. Allg. Chem.* **2008**, *634*, 2933-2939.
- (27) Labisbal, E.; Rodríguez, L.; Souto, O.; Sousa-Pedrares, A.; García-Vázquez, J.; Romero, J.; Sousa, A.; Yáñez, M.; Orallo, F.; Real, J. A. *Dalton Trans.* **2009**, 8644-8656.
- (28) Das, U. K.; Bobak, J.; Fowler, C.; Hann, S. E.; Petten, C. F.; Dawe, L. N.; Decken, A.; Kerton, F. M.; Kozak, C. M. *Dalton Trans.* **2010**, *39*, 5462-5477.
- (29) Mukherjee, A.; Lloret, F.; Mukherjee, R. *Inorg. Chem.* **2008**, *47*, 4471-4480.
- (30) Mukherjee, A.; Lloret, F.; Mukherjee, R. *Eur. J. Inorg. Chem.* **2010**, 1032-1042.

- (31) Singh, R.; Banerjee, A.; Gordon, Y.; Rajak, K. *Transition Metal Chemistry* **2009**, *34*, 689-694.
- (32) Theopold, K. H. In *Chromium: Inorganic & Coordination Chemistry*; King, R. B., Ed.; Encyclopedia of Inorganic Chemistry [Online]; John Wiley & Sons, Ltd.: Hoboken, NJ, 2006; pp 1-14.
- (33) Cotton, F. A.; Wilkinson, G.; Murillo, C. A.; Bochmann, M. In *The Elements of the First Transition Series*; Advanced Inorganic Chemistry; Wiley: New York, 1999; Chapter 17; pp 736-756.
- (34) Vincent, J. B. *Dalton Trans.* **2010**, *39*, 3787-3794.
- (35) Lay, P. A.; Levina, A. In *4.6 - Chromium* McCleverty, J. A., Meyer, T. J., Eds.; *Comprehensive Coordination Chemistry II* [Online]; Elsevier Pergamon: Amsterdam, 2004; Vol. 4, pp 313-413.
- (36) Scarborough, C. C.; Sproules, S.; Doonan, C. J.; Hagen, K. S.; Weyhermüller, T.; Wieghardt, K. *Inorg. Chem.* **2012**, *51*, 6969-6982.
- (37) Bourget-Merle, L.; Lappert, M. F.; Severn, J. R. *Chem. Rev.* **2002**, *102*, 3031-3066.
- (38) Richeson, D. S.; Mitchell, J. F.; Theopold, K. H. *Organometallics* **1989**, *8*, 2570-2577.
- (39) MacAdams, L. A.; Kim, W.; Liable-Sands, L.; Guzei, I. A.; Rheingold, A. L.; Theopold, K. H. *Organometallics* **2002**, *21*, 952-960.
- (40) MacAdams, L. A.; Buffone, G. P.; Incarvito, C. D.; Rheingold, A. L.; Theopold, K. H. *J. Am. Chem. Soc.* **2005**, *127*, 1082-1083.
- (41) Kim, W.; Fevola, M. J.; Liable-Sands, L.; Rheingold, A. L.; Theopold, K. H. *Organometallics* **1998**, *17*, 4541-4543.
- (42) Gibson, V. C.; Newton, C.; Redshaw, C.; Solan, G. A.; White, A. J. P.; Williams, D. J.; Maddox, P. J. *Chem. Commun.* **1998**, 1651-1652.
- (43) Gibson, V. C.; Newton, C.; Redshaw, C.; Solan, G. A.; White, A. J. P.; Williams, D. J. *Eur. J. Inorg. Chem.* **2001**, 1895-1903.
- (44) Smith, K. M. *Current Organic Chemistry* **2006**, *10*, 955-963.
- (45) Young, J. F.; MacAdams, L. A.; Yap, G. P. A.; Theopold, K. H. *Inorg. Chim. Acta* **2010**, *364*, 138-143.

- (46) Theopold, K. H.; Kucharczyk, R. R. In *Chromium: Organometallic Chemistry*; Encyclopedia of Inorganic Chemistry [Online]; John Wiley & Sons, Ltd: Hoboken, NJ, 2006; pp 1-18."Originally published in M. Berthelot, *Ann. Chim. Phys.*, **1866**, *9*, 401."
- (47) Gibson, V. C.; Marshall, E. L. In *9.1 - Metal Complexes as Catalysts for Polymerization Reactions*; Editors-in-Chief: J. A. McCleverty, T. J. Meyer, Eds.; Comprehensive Coordination Chemistry II [Online]; Elsevier: Boston, 2003; Vol. 9, pp 1-74.
- (48) Fan, H.; Adhikari, D.; Saleh, A. A.; Clark, R. L.; Zuno-Cruz, F.; Sanchez Cabrera, G.; Huffman, J. C.; Pink, M.; Mindiola, D. J.; Baik, M. *J. Am. Chem. Soc.* **2008**, *130*, 17351-17361.
- (49) Canali, L.; Sherrington, D. C. *Chem. Soc. Rev.* **1999**, *28*, 85-93.
- (50) Cozzi, P. G. *Chem. Soc. Rev.* **2004**, *33*, 410-421.
- (51) Adam, W.; Gelalcha, F. G.; Saha-Möller, C. R.; Stegmann, V. R. *J. Org. Chem.* **2000**, *65*, 1915-1918.
- (52) Paddock, R. L.; Nguyen, S. T. *J. Am. Chem. Soc.* **2001**, *123*, 11498-11499.
- (53) Darensbourg, D. J.; Mackiewicz, R. M.; Rodgers, J. L.; Phelps, A. L. *Inorg. Chem.* **2004**, *43*, 1831-1833.
- (54) Darensbourg, D. J.; Frantz, E. B.; Andreatta, J. R. *Inorg. Chim. Acta* **2007**, *360*, 523-528.
- (55) Darensbourg, D. J.; Ulusoy, M.; Karroonnirum, O.; Poland, R. R.; Reibenspies, J. H.; Çetinkaya, B. *Macromolecules* **2009**, *42*, 6992-6998.
- (56) Hansen, K. B.; Leighton, J. L.; Jacobsen, E. N. *J. Am. Chem. Soc.* **1996**, *118*, 10924-10925.
- (57) Jacobsen, E. N. *Acc. Chem. Res.* **2000**, *33*, 421-431.
- (58) Huang, Y.; Iwama, T.; Rawal, V. H. *J. Am. Chem. Soc.* **2000**, *122*, 7843-7844.
- (59) Bandini, M.; Cozzi, P. G.; Umani-Ronchi, A. *Tetrahedron* **2001**, *57*, 835-843.
- (60) Bandini, M.; Cozzi, P. G.; Melchiorre, P.; Morganti, S.; Umani-Ronchi, A. *Org. Lett.* **2001**, *3*, 1153-1155.

- (61) Brandt, P.; Norrby, P.; Daly, A. M.; Gilheany, D. G. *Chem. Eur. J.* **2002**, *8*, 4299-4307.
- (62) Samsel, E. G.; Srinivasan, K.; Kochi, J. K. *J. Am. Chem. Soc.* **1985**, *107*, 7606-7617.
- (63) Jacobsen, E. N.; Zhang, W.; Muci, A. R.; Ecker, J. R.; Deng, L. *J. Am. Chem. Soc.* **1991**, *113*, 7063-7064.
- (64) Bousquet, C.; Gilheany, D. G. *Tetrahedron Lett.* **1995**, *36*, 7739-7742.
- (65) Imanishi, H.; Katsuki, T. *Tetrahedron Lett.* **1997**, *38*, 251-254.
- (66) Konsler, R. G.; Karl, J.; Jacobsen, E. N. *J. Am. Chem. Soc.* **1998**, *120*, 10780-10781.
- (67) Ruck, R. T.; Jacobsen, E. N. *Angew. Chem. Int. Ed.* **2003**, *42*, 4771-4774.
- (68) Coates, G. W.; Moore, D. R. *Angew. Chem. Int. Ed.* **2004**, *43*, 6618-6639.
- (69) Darensbourg, D. J. *Chem. Rev.* **2007**, *107*, 2388-2410.
- (70) Darensbourg, D. J. *Inorg. Chem.* **2010**, *49*, 10765-10780.
- (71) Kember, M. R.; Buchard, A.; Williams, C. K. *Chem. Commun.* **2011**, *47*, 141-163.
- (72) Klaus, S.; Lehenmeier, M. W.; Anderson, C. E.; Rieger, B. *Coord. Chem. Rev.* **2011**, *255*, 1460-1479.
- (73) Lu, X.; Darensbourg, D. J. *Chem. Soc. Rev.* **2012**, *41*, 1462-1484.
- (74) Inoue, S.; Koinuma, H.; Tsuruta, T. *Makromol. Chem.* **1969**, *130*, 210-220.
- (75) Inoue, S.; Koinuma, H.; Tsuruta, T. *J. Polym. Sci., Polym. Lett.* **1969**, *7*, 287-292.
- (76) Anastas, P. T., Ed.; In *Handbook of Green Chemistry*; Crabtree, R. H., Ed.; Homogeneous Catalysis; Wiley-VCH: Weinheim, 2009; Vol. 1, pp 343-360.
- (77) Cohen, C. T.; Chu, T.; Coates, G. W. *J. Am. Chem. Soc.* **2005**, *127*, 10869-10878.
- (78) Rao, D.; Li, B.; Zhang, R.; Wang, H.; Lu, X. *Inorg. Chem.* **2009**, *48*, 2830-2836.
- (79) Nakano, K.; Hashimoto, S.; Nozaki, K. *Chem. Sci.* **2010**, 369-373.
- (80) Kojima, F.; Aida, T.; Inoue, S. *J. Am. Chem. Soc.* **1986**, *108*, 391-395.

- (81) Kruper, W. J.; Dellar, D. D. *J. Org. Chem.* **1995**, *60*, 725-727.
- (82) Mang, S.; Cooper, A. I.; Colclough, M. E.; Chauhan, N.; Holmes, A. B. *Macromolecules* **2000**, *33*, 303-308.
- (83) Stamp, L. M.; Mang, S. A.; Holmes, A. B.; Knights, K. A.; de Miguel, Y. R.; McConvey, I. F. *Chem. Commun.* **2001**, 2502-2503.
- (84) Darensbourg, D. J.; Holtcamp, M. W. *Macromolecules* **1995**, *28*, 7577-7579.
- (85) Darensbourg, D. J.; Holtcamp, M. W.; Struck, G. E.; Zimmer, M. S.; Niezgoda, S. A.; Rainey, P.; Robertson, J. B.; Draper, J. D.; Reibenspies, J. H. *J. Am. Chem. Soc.* **1999**, *121*, 107-116.
- (86) Darensbourg, D. J.; Wildeson, J. R.; Yarbrough, J. C.; Reibenspies, J. H. *J. Am. Chem. Soc.* **2000**, *122*, 12487-12496.
- (87) Cheng, M.; Lobkovsky, E. B.; Coates, G. W. *J. Am. Chem. Soc.* **1998**, *120*, 11018-11019.
- (88) Li, B.; Wu, G.; Ren, W.; Wang, Y.; Rao, D.; Lu, X. *J. Polym. Sci., Part A: Polym. Chem.* **2008**, *42*, 6102-6113.
- (89) Darensbourg, D. J.; Yarbrough, J. C. *J. Am. Chem. Soc.* **2002**, *124*, 6335-6342.
- (90) Darensbourg, D. J.; Yarbrough, J. C.; Ortiz, C.; Fang, C. C. *J. Am. Chem. Soc.* **2003**, *125*, 7586-7591.
- (91) Darensbourg, D. J.; Mackiewicz, R. M.; Billodeaux, D. R. *Organometallics* **2005**, *24*, 144-148.
- (92) Qin, Z.; Thomas, C. M.; Lee, S.; Coates, G. W. *Angew. Chem. Int. Ed.* **2003**, *42*, 5484-5487.
- (93) S, S.; Min, J. K.; Seong, J. E.; Na, S. J.; Lee, B. Y. *Angew. Chem.* **2008**, *120*, 7416-7419.
- (94) Ren, W.; Zhang, X.; Liu, Y.; Li, J.; Wang, H.; Lu, X. *Macromolecules* **2010**, *43*, 1396-1402.
- (95) Buchard, A.; Kemper, M. R.; Sandeman, K. G.; Williams, C. K. *Chem. Commun.* **2011**, *47*, 212-214.
- (96) Nakano, K.; Nakamura, M.; Nozaki, K. *Macromolecules* **2009**, *42*, 6972-6980.

- (97) Vagin, S. I.; Reichardt, R.; Klaus, S.; Rieger, B. *J. Am. Chem. Soc.* **2010**, *132*, 14367-14369.
- (98) Platel, R. H.; Hodgson, L. M.; Williams, C. K. *Polymer Reviews* **2008**, *48*, 11-63.
- (99) O'Keefe, B. J.; Hillmyer, M. A.; Tolman, W. B. *J. Chem. Soc., Dalton Trans.* **2001**, 2215-2224.
- (100) Auras, R., *Macromolecular Bioscience* **2004**, *4*, 835-864.
- (101) Williams, C. K.; Hillmyer, M. A. *Polymer Reviews* **2008**, *48*, 1-10.
- (102) Wu, J.; Yu, T.; Chen, C.; Lin, C. *Coord. Chem. Rev.* **2006**, *250*, 602-626.
- (103) Wheaton, C. A.; Hayes, P. G.; Ireland, B. J. *Dalton Trans.* **2009**, 4832-4846.
- (104) Stanford, M. J.; Dove, A. P. *Chem. Soc. Rev.* **2010**, *39*, 486-494.
- (105) Chisholm, M. H.; Delbridge, E. E. *New J. Chem.* **2003**, *27*, 1177-1183.
- (106) Cheng, M.; Attygalle, A. B.; Lobkovsky, E. B.; Coates, G. W. *J. Am. Chem. Soc.* **1999**, *121*, 11583-11584.
- (107) Chisholm, M. H.; Eilerts, N. W.; Huffman, J. C.; Iyer, S. S.; Pacold, M.; Phomphrai, K. *J. Am. Chem. Soc.* **2000**, *122*, 11845-11854.
- (108) Xie, W.; Chen, D.; Fan, X.; Li, J.; Wang, P. G.; Cheng, H. N.; Nickol, R. G. *J. Polym. Sci., Part A: Polym. Chem.* **1999**, *37*, 3486-3491.
- (109) Kasperczyk, J. E. *Macromolecules* **1995**, *28*, 3937-3939.
- (110) Bero, M.; Dobrzyński, P.; Kasperczyk, J. *J. Polym. Sci., Part A: Polym. Chem.* **1999**, *37*, 4038-4042.
- (111) Kricheldorf, H. R.; Kreiser-Saunders, I. *Makromol. Chem.* **1990**, *191*, 1057-1066.
- (112) Kasperczyk, J.; Bero, M. *Polymer* **2000**, *41*, 391-395. The authors do not specify which form of BuLi they use in their reaction.
- (113) Ko, B.; Lin, C. *J. Am. Chem. Soc.* **2001**, *123*, 7973-7977.
- (114) Hsueh, M.; Huang, B.; Wu, J.; Lin, C. *Macromolecules* **2005**, *38*, 9482-9487.
- (115) Huang, C.; Chen, C. *Dalton Trans.* **2007**, 5561-5566.

- (116) Huang, C.; Ho, C.; Chen, C. *Dalton Trans.* **2008**, 3502-3510.
- (117) Alonso-Moreno, C.; Garcés, A.; Sánchez-Barba, L. F.; Fajardo, M.; Fernández-Baeza, J.; Otero, A.; Lara-Sánchez, A.; Antiñolo, A.; Broomfield, L.; López-Solera, M. I.; Rodríguez, A. M. *Organometallics* **2008**, *27*, 1310-1321.
- (118) Huang, Y.; Tsai, Y.; Hung, W.; Lin, C.; Wang, W.; Huang, J.; Dutta, S.; Lin, C. *Inorg. Chem.* **2010**, *49*, 9416-9425.

Co-Authorship Statement

Chapter 2: Synthesis of Amine-bis(phenolate) Ligands and Lithium Amine-bis(phenolate) Complexes; and **Chapter 4:** Synthesis and Structure of Chromium(III) Amine-bis(phenolate) Complexes.

These chapters contain some of the results published in the full article “Structure and magnetic behaviour of mono- and bimetallic chromium(III) complexes of amine-bis(phenolate) ligands”, Dalton Transactions, **2010**, *39*, 548-559.

Authors: Rebecca K. Dean, Stephanie L. Granville, Louise N. Dawe, Andreas Decken, Karen M. Hattenhauer and Christopher M. Kozak

The first author (Rebecca Dean) contributed 60% of the content of the article as a main researcher including: designing and performing experiments, analyzing and collecting data, and writing parts of the paper (creating ORTEP images, electrochemistry and experimental sections). The PhD candidate re-wrote material from this paper included in Chapters 2 and 4. All aspects of the experimental research reported in these chapters were performed by the first author, with the exception of magnetochemistry (Chapter 4). The variable temperature magnetic data were collected by a member of Prof. L. K. Thompson's group and modeled by Prof. C. M. Kozak.

The second author (Stephanie Granville) was an undergraduate student who worked one summer alongside the first author helping in the synthesis of ligands and chromium complexes, which were synthesized *via* the protonolysis/oxidation method.

The co-authors (Louise Dawe and Andreas Decken) were crystallographers at Memorial University and University of New Brunswick, respectively, who collected XRD data and solved structures for complexes **2.1**, **2.2**, **2.3**, **4.1**, **4.2**, **4.4**, **4.5**, **4.6**, **4.7**, and **4.8**. *The co-author, Karen Hattenhauer*, provided a financial contribution to my stipend while this work was being carried out.

The corresponding author (Christopher Kozak) was the principal investigator and developed the original ideas for this research. He oversaw all aspects of the project, including the design of experiments, analysis (modeling of magnetochemistry), writing and submission of the manuscript, and responding to the questions and comments from the peer reviewers.

Chapter 3: Ring-opening Polymerization of Cyclic Esters with Lithium Amine-bis(phenolate) Complexes.

This chapter is currently in preparation for publication. Complexes **3.1** and **3.2**, were synthesized by a former undergraduate student (Amy Reckling) and used as a comparison between the differing ligand frameworks in the ring-opening polymerization of *rac*-lactide.

Chapter 5: Chromium Amine-bis(phenolate) Complexes for the Copolymerization of Epoxides and Carbon Dioxide.

Sections 5.2.2 and 5.2.4 of this chapter have been submitted as a full article to Dalton Transactions “Reaction of CO₂ with Propylene Oxide and Styrene Oxide catalyzed by a Chromium(III) Amine-bis(phenolate) Complex”.

Authors: Rebecca K. Dean, Louise N. Dawe and Christopher M. Kozak

The first author (Rebecca Dean) contributed to all aspects of the article as the researcher including: designing and performing experiments, analyzing and collecting data and writing.

The co-author (Louise Dawe) is a crystallographer at Memorial University who collected XRD data and solved the crystal structure.

The corresponding author (Christopher Kozak) was the principal investigator and developed the original ideas for this research. He oversaw all aspects of the project, suggesting initial experiments, analysis, revision and submission of the manuscript, and responding to the questions and comments from the peer reviewers.

Section 5.2.3 of this chapter has been published as a full article “Copolymerization of Cyclohexene Oxide and CO₂ with a Chromium Diamine-bis(phenolate) Catalyst”, in *Inorganic Chemistry*, **2012**, *51*, 9095-9103.

Authors: Rebecca K. Dean, Louise N. Dawe and Christopher M. Kozak

The first author (Rebecca Dean) contributed to all aspects of the article as the researcher including: designing and performing experiments, analyzing and collecting data, and writing and editing the preliminary draft of the paper.

The co-author (Louise Dawe) is a crystallographer at Memorial University who collected XRD data and solved the crystal structure.

The corresponding author (Christopher Kozak) was the principal investigator and developed the original ideas for this research. He oversaw all aspects of the project, suggesting initial experiments, analysis, revision and submission of the manuscript, and responding to the questions and comments from the peer reviewers.

Chapter 2

Synthesis of Amine-bis(phenolate) Ligands and Lithium Amine-bis(phenolate) Complexes

Parts of this chapter have been published: Rebecca K. Dean, Stephanie L. Granville, Louise N. Dawe, Andreas Decken, Karen M. Hattenhauer and Christopher M. Kozak, *Dalton Trans.*, **2010**, *39*, 548-559.

2.1 Introduction

In coordination chemistry, metal complex geometry can be controlled by ligands. Ligands also determine the reactivity of the complex, whereby steric and electronic factors can offer control in the design of a metal catalyst system. Well-defined homogeneous metal catalysts should include a rigid ligand framework, which is easily modifiable and economically viable, with a stable geometry favourable to insertion or exchange with an incoming solvent, ligand or reagent.

Chelating ligands are an important type of ligand which can offer protection to the active metal site while providing a location for catalysis to occur. Amine-bis(phenolate) ligands are chelating ligands that offer such advantages. The use of this type of ligand in synthesizing homogeneous catalysts has grown within the last couple of decades.¹ They have been used primarily with early transition metals and lanthanide based systems as a substitute to the well-known cyclopentadienyl ligand class. More recently, mid-to-late transition metals have been explored with amine-bis(phenolate) ligands.

Alkali metal compounds, particularly those of lithium and sodium, are often necessary precursors for the synthesis of transition metal complexes. These lithium and sodium complexes are commonly generated *in situ* and were therefore less explored until recently. The development of efficient, stable, cheap and nontoxic catalysts has gained increased interest in the scientific community. Lithium compounds have become increasingly important due to their biocompatibility and solubility in aqueous media. In addition to having catalytic capability, lithium compounds have also been shown to display interesting structural behaviour depending on the ligand or solvent used.²⁻⁶ The tendency for lithium compounds to form aggregates has provided an attraction for the study of structure and reactivity of these multinuclear and/or polymeric compounds.

Independent studies by Huang & Chen⁷ and Clegg *et al.*² both reported dimeric and tetranuclear lithium complexes (1.46), (1.47), (1.48) and (2.0) (Figure 2.1). Ladder-like conformations were adopted in the solid state, where compounds (1.46), (1.47), (1.48) and (2.0) were found to have two amine-bis(phenolate) ligands capped onto the end of the ladder-like core. Motifs such as these are commonly observed in lithium chemistry.⁸⁻¹⁰

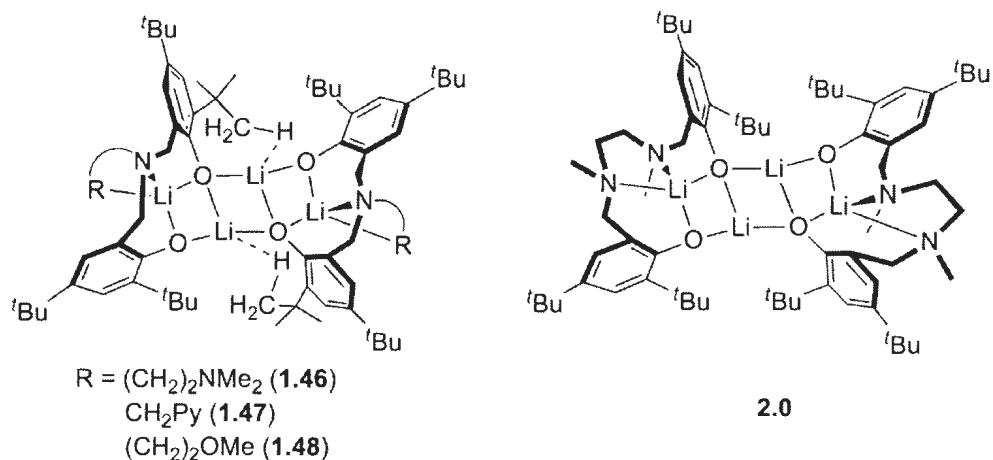


Figure 2.1. Dimeric tetralithium complexes by Chen (**1.46**), (**1.47**), (**1.48**)⁷ and O'Hara (**2.0**).²

Other alkali metal complexes (Li, Na and K) have been shown to produce interesting aggregates involving aryloxide and alkoxide ligands.^{4,6,11-13} Various structural motifs have been exhibited for such alkali metal bis(phenolate) complexes including the most common formations — dimers (M₂O₂, rings or ladders) and/or tetramers (M₄O₄, cubanes). The structures obtained can vary drastically between similar metal adducts through subtle changes in the ligand or solvent. For example Kerton, Kozak *et al.* reported a dimeric (**2.0a**) and polymeric lithium diamine-bis(phenolate) complex (**2.0b**) in the presence of 1,4-dioxane.³ The ligands used in this study were isomeric, but the solid state structures obtained were surprisingly different.

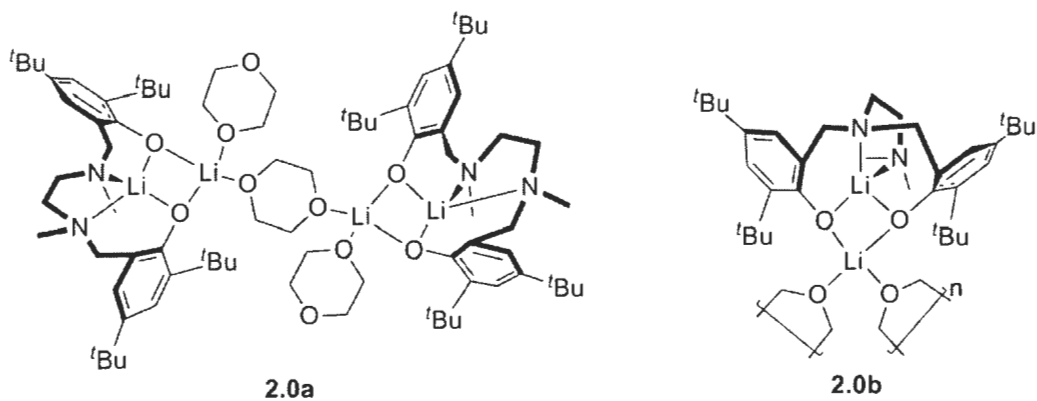


Figure 2.2. Kerton, Kozak $\{\text{Li}_2[\text{O}_2\text{N}_2]^{\text{BuBu}}(\text{dioxane})_{1.5}\}_2$ complex (**2.0a**) and single unit of $\{\text{Li}_2[\text{O}_2\text{NN}']^{\text{BuBu}}(\text{dioxane})\}_x$ complex (**2.0b**).

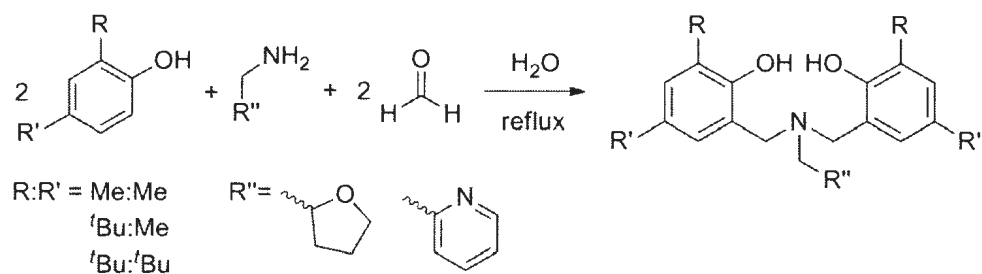
Most relevant to this work are the lithium complexes (**1.46-1.48**), (**2.0**) and (**2.0a-b**). The dimeric, dioxane bridged structure (**2.0a**) possess two distorted tetrahedral Li environments, whereas the polymeric structure (**2.0b**) exhibits two different Li environments: distorted tetrahedral and trigonal pyramidal. The base-free structures (**1.46-1.48**) and (**2.0**) both exhibit distorted tetrahedral and trigonal planar Li geometries, adopting ladder-like cores.

Specifically, tetradentate amine-bis(phenol) ligands were examined in this thesis, where the pendant donor atoms were either a nitrogen (pyridyl group) or oxygen (tetrahydrofuranyl group). This chapter describes the synthesis, structure and spectroscopy of complexes with tripodal amine-bis(phenolate) ligands coordinated to lithium.

2.2 Results and Discussion

2.2.1 Synthesis of Ligands and Lithium Complexes

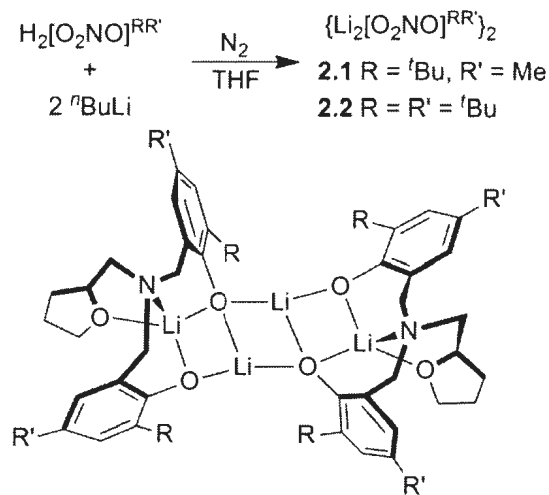
Tetradentate tripodal amine-bis(phenol) ligands were synthesized via a modified Mannich condensation reaction (Scheme 2.1).¹⁴⁻¹⁶ Kerton *et al.*^{14,17} showed that using water as the reaction medium in this ligand procedure gave higher yields and decreased reaction times over the usual route involving methanol solutions.¹⁸⁻²⁰ The ligands of interest contained substituted phenols, where either *tert*-butyl or methyl groups *ortho* and *para* to the hydroxyl group were used. Pendant donors included in this study were tetrahydrofurfurylamine and aminomethylpyridine. Refluxing a mixture of the corresponding phenol, amine and formaldehyde in water yielded $\text{H}_2[\text{O}_2\text{NO}]^{\text{MeMe}}$ (**L1**), $\text{H}_2[\text{O}_2\text{NO}]^{\text{BuMe}}$ (**L2**), $\text{H}_2[\text{O}_2\text{NO}]^{\text{BuBu}}$ (**L3**), $\text{H}_2[\text{O}_2\text{NN}']^{\text{MeMe}}$ (**L4**), $\text{H}_2[\text{O}_2\text{NN}']^{\text{BuMe}}$ (**L5**) and $\text{H}_2[\text{O}_2\text{NN}']^{\text{BuBu}}$ (**L6**) (Scheme 2.1).



Scheme 2.1. Synthesis of amine-bis(phenol) ligands.

Lithium complexes of ligands containing the tetrahydrofuran pendant donor were then synthesized by reacting 1 equivalent of the appropriate ligand with 2

equivalents of $n\text{BuLi}$ in THF, giving $\{\text{Li}_2[\text{O}_2\text{NO}]^{\text{BuMe}}\}_2$ (**2.1**), and $\{\text{Li}_2[\text{O}_2\text{NO}]^{\text{BuBu}}\}_2$ (**2.2**) as shown in Scheme 2.2. Lithium complexes of **L1** were not isolated and characterized due to solubility issues; the small Me group containing phenol did not give the sufficient lipophilicity needed for these compounds to dissolve in non-polar solvents. Reactions of the ligand precursors $\text{H}_2[\text{O}_2\text{NN}^{\text{MeMe}}]$, $\text{H}_2[\text{O}_2\text{NN}^{\text{BuMe}}]$ and $\text{H}_2[\text{O}_2\text{NN}^{\text{BuBu}}]$ (**L4-L6**) with $n\text{BuLi}$ in THF were generated *in situ* for the synthesis of chromium complexes, which are discussed in Chapter 4. Attempts were made to isolate single crystals of lithium complexes supported by ligands **L4** and **L6**, but these were unsuccessful to date. The synthesis and characterization of the lithium complex (**1.47**) possessing **L5** was previously reported by Chen and co-workers.⁷



Scheme 2.2. Synthesis of lithium complexes **2.1** and **2.2**.

2.2.2 Structural Characterization

Single crystals of **2.1** were isolated from a 1:1 toluene-hexane mixture and crystals of **2.2** were grown from benzene. Isolated crystals of **2.1** and **2.2** were subjected to X-ray diffraction studies for structural analysis. Solid state structures of **2.1** and **2.2** were found to produce tetralithium species (Figure 2.3). These complexes were also shown to have a ladder-like motif similar to the structures described by O'Hara² and Chen⁷ (Figure 2.1).

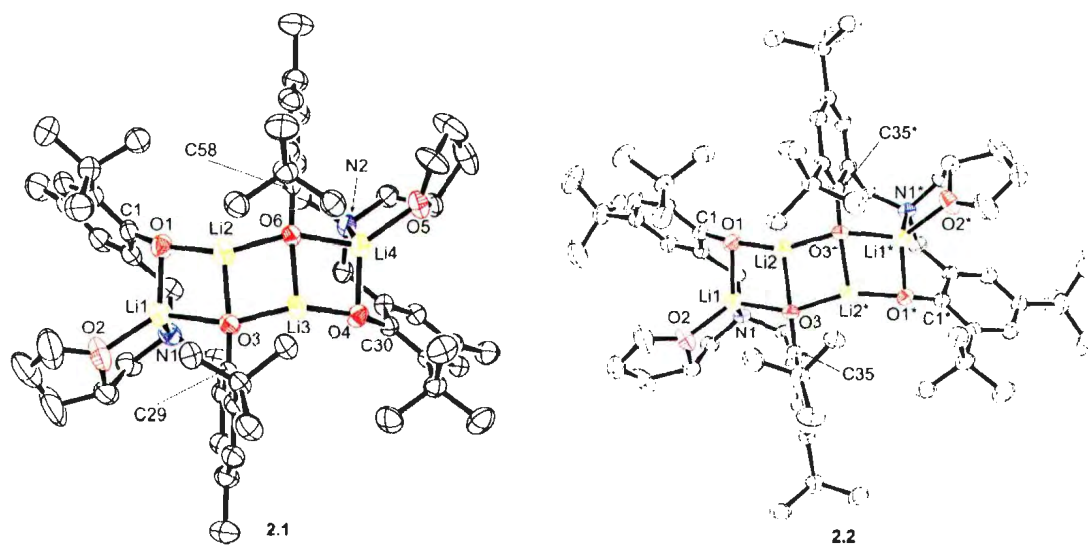


Figure 2.3. ORTEP diagrams of the molecular structures and partial numbering schemes of **2.1** (left) and **2.2** (right). Ellipsoids are shown at 50% probability. Hydrogen atoms were omitted for clarity. Symmetry operation used to generate equivalent atoms for **2.2**: $1-x, y, \frac{1}{2}-z$.

The tetralithium complexes each possess two $[\text{O}_2\text{NO}]^{\text{RR}'}$ ligands at each end of the complex. Two of the lithium ions (Li(1) and Li(4) in **2.1** and Li(1) and Li(1)* in **2.2**) are four-coordinate, possessing distorted tetrahedral geometries. The other two Li ions (Li(2) and Li(3) in **2.1** and Li(2) and Li(2)* in **2.2**) adopt three-coordinate, distorted trigonal planar geometries. Structurally, complexes **2.1** and **2.2** do not exhibit any interaction between the four-coordinate lithiums and the *ipso*-carbon on the phenolates. The interatomic distances for both **2.1** and **2.2** is greater than 2.5 Å, unlike O'Hara and co-workers² where they observed a Li...C distance of 2.437(5) Å for their base-free dimer structure (**2.0**), as shown in Figure 2.1. Complexes **2.1** and **2.2** possess interatomic distances more closely related to the tetralithium complexes of Chen⁷ (**1.46**, **1.47** and **1.48**) shown in Figure 2.1.

Selected bond angles for **2.1** and **2.2** are given in Table 2.1 and bond lengths in Table 2.2. The distorted tetrahedral bond angles observed for **2.1** are 125.0(3), 87.3(2), 98.5(2) and 87.12(18)° for O(1)-Li(1)-O(2), O(2)-Li(1)-N(1), O(4)-Li(4)-O(6) and O(5)-Li(4)-N(2), respectively. Complex **2.2** contains two unique Li environments due to the presence of an internal rotation axis. Similar to **2.1** the distorted tetrahedral bond angles for **2.2** are 100.7(2) and 87.57(19)° for O(1)-Li(1)-O(3) and O(2)-Li(1)-N(1), respectively. The bond angles for the three-coordinate Li atoms in **2.1** are 102.5(2), 99.5(2), 98.8(2) and 103.6(2)° for O(1)-Li(2)-O(3), O(3)-Li(2)-O(6), O(3)-Li(3)-O(6) and O(4)-Li(3)-O(6), respectively. The bond angles for the three-coordinate Li atoms in **2.2** are 155.8(3)° for O(1)-Li(2)-O(3) and 99.4(2)° for O(3)-Li(2)-O(3)*. The average O-Li-N bond angles of each ligand in **2.1** are experimentally identical at 94.6° for O-Li(1)-N(1) and O-Li(4)-N(2). Complex **2.2** has an average O-Li(1)-N(1) angle of 95.4°.

The Li-O bond lengths for **2.1** range from 1.786(5) Å for Li(3)-O(4) to 1.976(4) Å for Li(4)-O(6). For **2.2** they range from 1.791(5) Å for Li(2)-O(1) to 1.955(4) Å for Li(2)-O(3). As expected, the Li-O bond distances for the μ_3 -O atoms are the longest, as well as the O donor atoms from the pendant tetrahydrofuranyl group. The Li-N bond distances for both **2.1** and **2.2** are experimentally identical, whereby Li(1)-N(1) is 2.029(5) Å and Li(4)-N(2) is 2.030(5) Å for **2.1**, and Li(1)-N(1) is 2.025(5) Å for **2.2**. These bond distances are similar to other related Li amine-bis(phenolate) complexes.^{2,3,7}

An essentially planar Li₂O₂ core exists for both **2.1** and **2.2**. Corresponding dihedral angles for **2.1** are 3.5(3)°, 9.8(2)° and 2.84(19)°, observed for Li(1)-O(1)-Li(2)-O(3), Li(2)-O(3)-Li(3)-O(6) and Li(3)-O(6)-Li(4)-O(4), respectively. Complex **2.2** possesses two Li₂O₂ dihedral angles; 5.0(2)° for Li(1)-O(1)-Li(2)-O(3) and 11.2(2)° for Li(2)-O(3)-Li(2)*-O(3)*.

Table 2.1. Selected bond angles (°) for **2.1** and **2.2**

2.1		2.2	
O(1)-Li(1)-O(2)	125.0(3)	O(1)-Li(1)-O(2)	126.0(2)
O(1)-Li(1)-O(3)	96.8(2)	O(1)-Li(1)-O(3)	100.7(2)
O(2)-Li(1)-O(3)	136.9(3)	O(2)-Li(1)-O(3)	131.1(2)
O(1)-Li(2)-O(3)	102.5(2)	O(1)-Li(2)-O(3)	155.8(3)
O(1)-Li(2)-O(6)	155.8(3)	O(1)-Li(2)-O(3)*	103.4(2)
O(3)-Li(2)-O(6)	99.5(2)	O(3)-Li(2)-O(3)*	99.4(2)
O(3)-Li(3)-O(6)	98.8(2)	O(1)-Li(1)-N(1)	100.0(2)
O(3)-Li(3)-O(4)	152.5(3)	O(2)-Li(1)-N(1)	87.57(19)
O(4)-Li(3)-O(6)	103.6(2)	O(3)-Li(1)-N(1)	98.7(2)
O(4)-Li(4)-O(5)	126.4(2)	Li(1)-O(1)-Li(2)	80.20(19)
O(4)-Li(4)-O(6)	98.5(2)	Li(1)-O(3)-Li(2)	151.0(2)
O(5)-Li(4)-O(6)	133.7(3)	Li(1)-O(3)-Li(2)*	75.26(19)
O(1)-Li(1)-N(1)	99.8(2)	Li(2)-O(3)-Li(2)*	79.5(2)
O(2)-Li(1)-N(1)	87.3(2)	Li(1)-O(1)-C(1)	105.90(19)
O(3)-Li(1)-N(1)	96.7(2)	Li(1)-O(3)-C(35)	100.18(18)
O(4)-Li(4)-N(2)	100.3(2)	Li(2)-O(1)-C(1)	164.2(2)
O(5)-Li(4)-N(2)	87.12(18)	Li(2)-O(3)-C(35)	168.4(2)

O(6)-Li(4)-N(2)	96.42(19)	Li(2)-O(3)*-C(35)*	101.70(18)
Li(1)-O(1)-Li(2)	82.9(2)		
Li(1)-O(3)-Li(2)	77.6(2)		
Li(1)-O(3)-Li(3)	152.6(2)		
Li(2)-O(3)-Li(3)	80.7(2)		
Li(3)-O(4)-Li(4)	81.8(2)		
Li(2)-O(6)-Li(3)	79.4(2)		
Li(2)-O(6)-Li(4)	146.4(2)		
Li(3)-O(6)-Li(4)	75.89(19)		
Li(1)-O(1)-C(1)	109.8(2)		
Li(2)-O(1)-C(1)	153.3(2)		
Li(1)-O(3)-C(29)	95.45(19)		
Li(2)-O(3)-C(29)	170.6(2)		
Li(3)-O(3)-C(29)	104.0(2)		
Li(3)-O(4)-C(30)	154.4(2)		
Li(4)-O(4)-C(30)	107.78(19)		
Li(2)-O(6)-C(58)	105.6(2)		
Li(3)-O(6)-C(58)	169.6(2)		
Li(4)-O(6)-C(58)	95.80(18)		

Table 2.2. Selected bond lengths (Å) for 2.1 and 2.2

	2.1		2.2
Li(1)-O(1)	1.877(5)	Li(1)-O(1)	1.889(5)
Li(1)-O(2)	1.948(5)	Li(1)-O(2)	1.918(5)
Li(1)-O(3)	1.973(5)	Li(1)-O(3)	1.929(4)
Li(2)-O(1)	1.790(5)	Li(2)-O(1)	1.791(5)
Li(2)-O(3)	1.899(5)	Li(2)-O(3)	1.955(4)
Li(2)-O(6)	1.900(5)	Li(2)-O(3)*	1.905(5)
Li(3)-O(3)	1.884(5)	Li(1)-N(1)	2.025(5)
Li(3)-O(4)	1.786(5)	O(1)-C(1)	1.332(3)
Li(3)-O(6)	1.935(5)	O(3)-C(35)	1.359(3)
Li(4)-O(4)	1.885(5)	Li(1)···Li(2)	2.371(6)
Li(4)-O(5)	1.950(5)	Li(2)···Li(2)*	2.469(9)
Li(4)-O(6)	1.976(4)		
Li(1)-N(1)	2.029(5)		
Li(4)-N(2)	2.030(5)		
O(1)-C(1)	1.330(3)		
O(3)-C(29)	1.360(3)		
O(4)-C(30)	1.326(3)		
O(6)-C(58)	1.358(3)		
Li(1)···Li(2)	2.428(7)		
Li(2)···Li(3)	2.449(6)		
Li(3)···Li(4)	2.406(6)		

Additionally, a dilithium complex, $(py)_2Li_2[O_2NO]^{BuMe}$ (**2.3**), could be isolated upon crystallization of **2.1** from pyridine. The solid state structure of **2.3** was found to be dimetallic, where 1 equivalent of **L2** is coordinated to Li(1) and Li(2) and 2 equivalents of pyridine were found to be coordinated to Li(2), as shown in Figure 2.4.

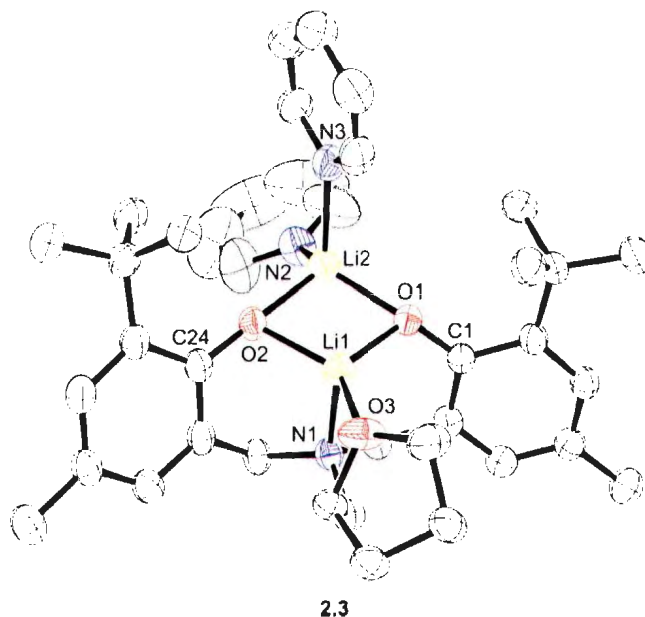


Figure 2.4. ORTEP diagram of the molecular structure and partial numbering scheme of **2.3**. Ellipsoids are shown at 50% probability. Hydrogen atoms were omitted for clarity.

Both lithium ions in **2.3** are shown to be four-coordinate. Selected bond lengths and angles for **2.3** are given in Table 2.3. The Li(1) atom is observed to be very distorted and although four-coordinate, the angles suggest the geometry is actually trigonal monopyramidal. The bond angles for O(1)-Li(1)-O(2) and O(3)-Li(1)-N(1) are 103.77(17) and 89.11(16)°, respectively. The bond angles for Li(2) are also distorted but are closer to the ideal tetrahedral geometry. Angles were shown to be 100.65(18),

101.73(19), 109.4 (2) and 108.59 (19)°, respectively for O(1)-Li(2)-O(2), N(2)-Li(2)-N(3), O(1)-Li(2)-N(2) and O(2)-Li(2)-N(2). A similar result was observed by Kerton and Kozak, where the Li bonded to the phenoxide oxygens and amine nitrogen donors of the ligand was found to be trigonal pyramidal, while the Li bonded to the phenoxide oxygen atoms of the ligand and two ether oxygen atoms from the bridging dioxane molecules exhibited a distorted tetrahedral geometry (**2.0b**, Figure 2.2).³

The Li(1)-O(1) and Li(1)-O(2) bond lengths from the phenoxide oxygens are similar at 1.896(4) and 1.874(4) Å, respectively. Longer bonds are observed for Li(2)-O, where Li(2)-O(1) is 1.912(4) Å and Li(2)-O(2) is 1.941(4) Å. The Li(1)-O(3) distance corresponding to the pendant oxygen donor on the ligand is 1.944(4) Å. Similar to that of complexes **2.1** and **2.2**, the longest Li-O bond distance in **2.3** is observed to be from the neutral O donor of the pendant arm. The Li-N bond lengths in **2.3** are 2.019(4) Å for Li(1)-N(1), 2.143(5) Å for Li(2)-N(2) and 2.059(4) Å for Li(2)-N(3). The two pyridine molecules show slightly weaker coordination to the Li than the amine nitrogen atom of the ligand. The Li₂O₂ core exhibited a nearly planar, dihedral angle of 3.61(16)°, similar to those shown by complexes **2.1** and **2.2**.

Table 2.3 Selected bond lengths (Å) and angles (°) for **2.3**

Li(1)-O(1)	1.896(4)	O(1)-Li(1)-O(2)	103.77(17)
Li(1)-O(2)	1.874(4)	O(1)-Li(1)-O(3)	132.7(2)
Li(1)-O(3)	1.944(4)	O(2)-Li(1)-O(3)	120.9(2)
Li(2)-O(1)	1.912(4)	O(1)-Li(2)-O(2)	100.65(18)
Li(2)-O(2)	1.941(4)	O(1)-Li(1)-N(1)	98.19(17)
Li(1)-N(1)	2.019(4)	O(2)-Li(1)-N(1)	100.22(17)
Li(2)-N(2)	2.143(5)	O(3)-Li(1)-N(1)	89.11(16)
Li(2)-N(3)	2.059(4)	O(1)-Li(2)-N(2)	109.4(2)
O(1)-C(1)	1.330(2)	O(2)-Li(2)-N(2)	108.59(19)
O(2)-C(24)	1.325(2)	O(1)-Li(2)-N(3)	111.4(2)
Li(1)···Li(2)	2.391(5)	O(2)-Li(2)-N(3)	124.7(2)
		N(2)-Li(2)-N(3)	101.73(19)
		Li(1)-O(1)-Li(2)	77.77(16)
		Li(1)-O(2)-Li(2)	77.59(16)
		Li(1)-O(1)-C(1)	107.04(16)
		Li(1)-O(2)-C(24)	113.58(16)
		Li(2)-O(1)-C(1)	167.59(19)
		Li(2)-O(2)-C(24)	149.99(18)

2.2.3 NMR Spectroscopy

Nuclear Magnetic Resonance (NMR) studies were performed on compounds **2.1** and **2.2** both in solution and the solid state. Solution experiments included ^1H , ^{13}C and ^7Li NMR. Four deuterated solvents (Chloroform- d (CDCl_3), Benzene- d_6 (C_6D_6), Toluene- d_8 ($\text{D}_8\text{-Tol}$) and Pyridine- d_5 ($\text{D}_5\text{-Py}$)) were used for both **2.1** and **2.2**. The solid state structures of **2.1** and **2.2** were both found to be base-free adducts, however, in their $\text{D}_8\text{-Tol}$ ^1H NMR spectra residual THF from the amorphous powders was observed. Similarly, the elemental analysis indicated 2.0 and 1.8 equivalents of THF should be included for **2.1** and **2.2**, respectively. However, upon recrystallization from a non-coordinating solvent this residual THF is lost.

¹H NMR of **2.1** and **2.2** in CDCl₃ was performed; see Appendix A1.13 and A1.14, respectively. Previous reports of amine-bis(phenolate) lithium salts, with pendant methoxyethyl donors, showed sharp peaks at room temperature in CDCl₃ solutions.⁷ However, for complexes **2.1** and **2.2** broad peaks were observed making assignment difficult and suggested the presence of fluxional behaviour. Spectra in C₆D₆ solutions have also been performed, but broad resonances were found again (Figure 2.5 for **2.1**). This led us to pursue variable temperature (VT) experiments in Toluene-d₈. Room temperature experiments were first explored, as a linear lithium diamine-bis(phenolate) was reported to show sharp peaks and observable coupling constants at room temperature measurements.² Although sharper peaks (than CDCl₃ or C₆D₆) were observed, broad resonances still caused peak assignment to be inconclusive (Figure 2.6). Interestingly, both the increase and decrease of temperatures in D₈-Tol caused broadening of the peaks, which can be attributed to fluxionality of the molecule at these temperatures (Figure 2.7). However, sharper peaks were attainable at 298 K when D₅-Py was employed as the solvent (Figure 2.8).

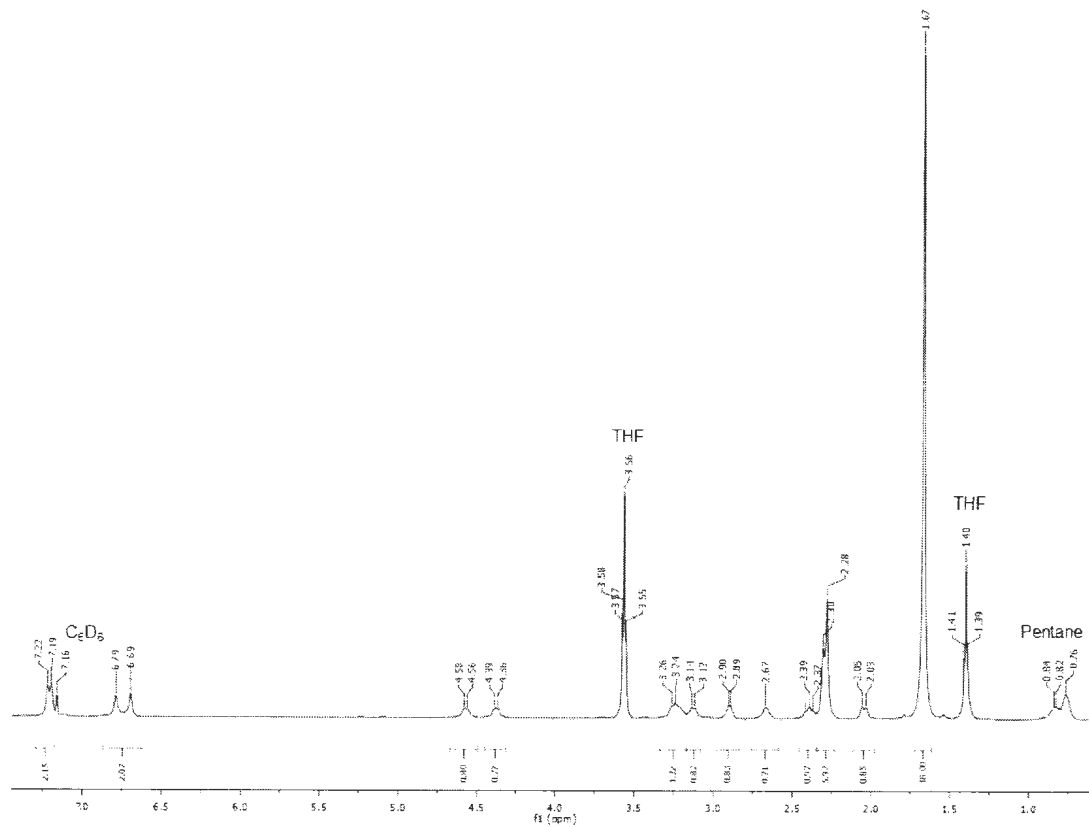


Figure 2.5. ^1H NMR spectrum of **2.1** in C_6D_6 at 298 K (500 MHz).

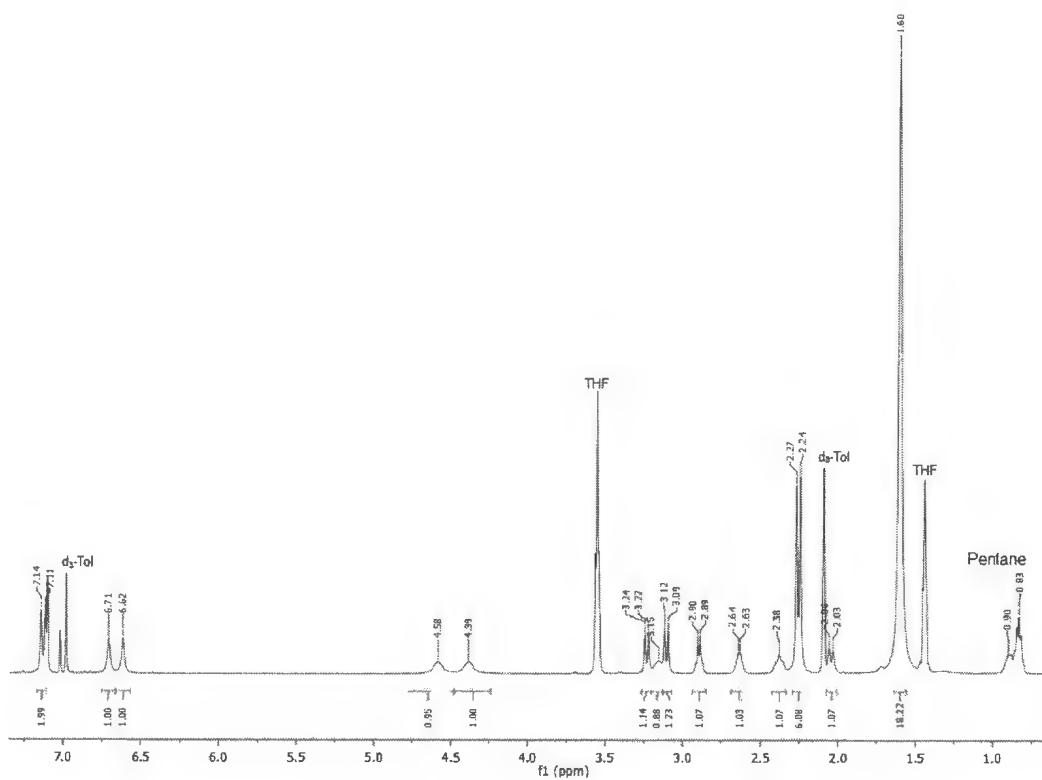


Figure 2.6. ^1H NMR spectrum of 2.1 in $\text{D}_8\text{-Tol}$ at 298 K (500 MHz).

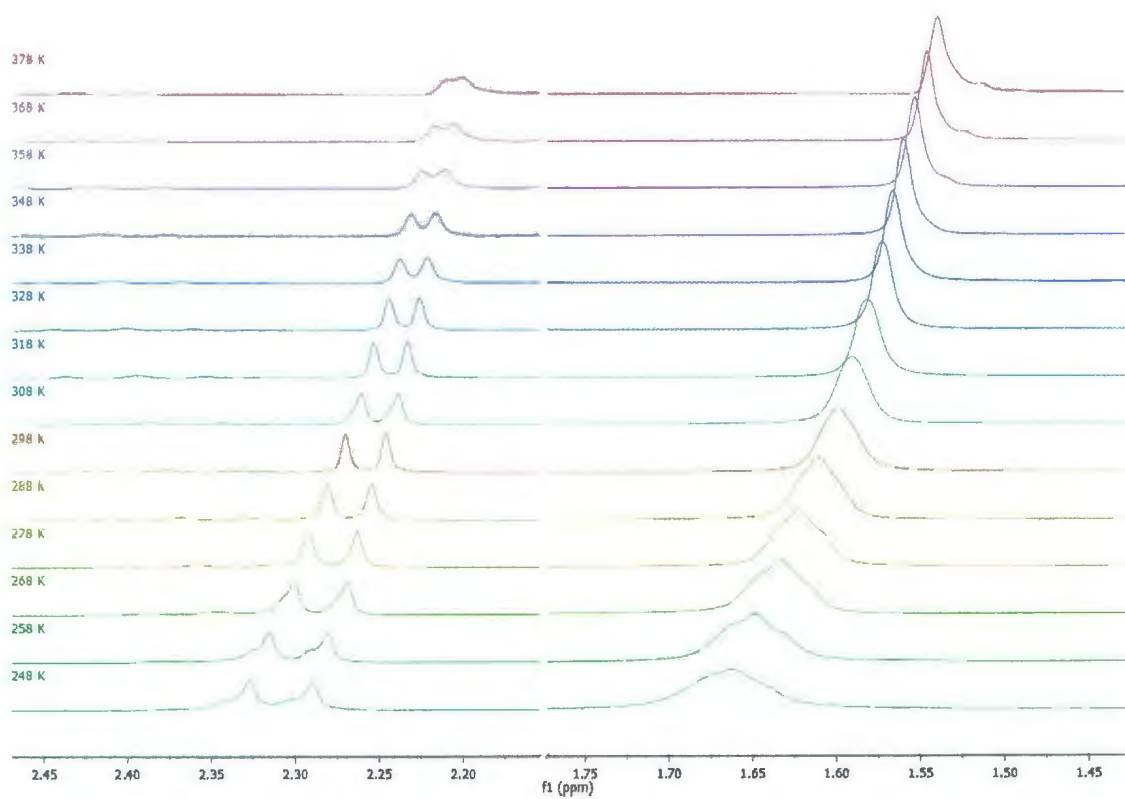


Figure 2.7. Portion of the VT ¹H NMR spectrum of **2.1** in D₈-Tol from 248 – 378 K, corresponding to methyl and *tert*-butyl peaks (300 MHz).

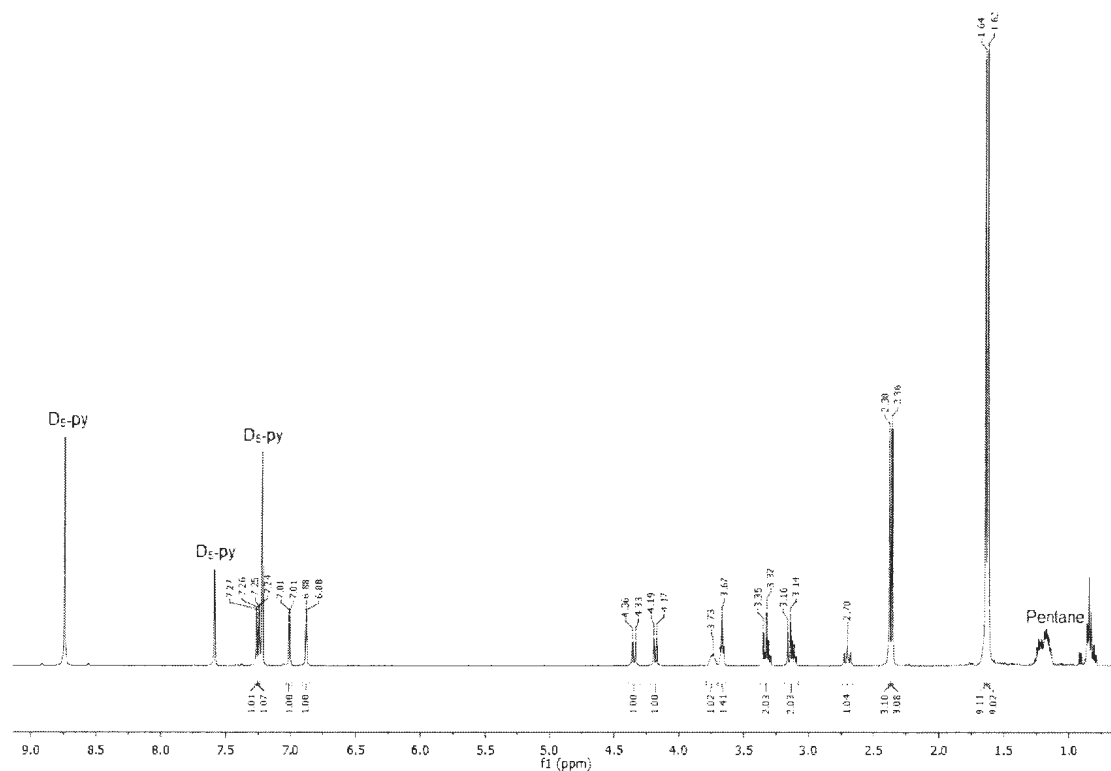


Figure 2.8. ^1H NMR spectrum of **2.1** in $\text{D}_5\text{-Py}$ at 298 K (500 MHz).

The loss of the residual THF in the $\text{D}_5\text{-Py}$ spectrum is likely a result of complexes **2.1** and **2.2** drying over time in the glove box. Additional ^1H and ^{13}C NMR spectra of the ligands, complexes **2.1** and **2.2** can be found in Appendix A.

The solid state structures of **2.1** and **2.2**, shown in Figure 2.3, show that two different bridging modes exist; $\mu_2\text{-O}$ and $\mu_3\text{-O}$. These should be evident in the ^1H NMR if the solid state structure is maintained in solution. It is possible that the coordinating pyridine may cause fragmentation of the tetralithium structure producing a similar structure to the dioxane adduct (**2.0b**) previously reported by the Kerton and Kozak

group.³ This synthesis of a pyridine coordinated adduct, **2.3**, provided evidence that the tetralithium dimer does in fact fragment when exposed to excess coordinating solvent such as pyridine. The ¹H NMR spectra in D₅-Py show two different phenolate environments for each of **2.1** and **2.2**, where four aromatic *H* resonances are observed in their spectra along with two *CH*₃ and two *t*-butyl resonances for **2.1** and four *t*-butyl resonances for **2.2**. This is likely due to the symmetry of the pyridine adduct being disrupted by a chiral center on the pendant tetrahydrofuranyl donor. Free rotation of the pendant donor, tetrahydrofuranyl, is possible in the protonated ligand form, generating equivalent phenolate groups in CDCl₃ solution as previously shown by Kozak¹⁵ and Kol¹⁸ in NMR spectroscopy studies. However, when this ligand is coordinated to Li, the tetrahydrofuranyl pendant arm is held in place, causing inequivalence in the phenolate groups.

Solution ⁷Li (spin 3/2) NMR was also carried out on compounds **2.1** and **2.2** in C₆D₆, D₈-Tol and D₅-Py solvent systems. In the presence of non-coordinating deuterated benzene or toluene, two overlapping asymmetric peaks at low δ are observed. Two different ⁷Li environments would be expected resulting from the three- and four-coordinate lithium ions observed in the solid state structures (Figure 2.9). VT ⁷Li NMR studies were also performed to determine whether similar Li environments were observed at increased and decreased temperatures. Interestingly, it was found that complex **2.1** did in fact keep the same structure with only a small change in the chemical shift ~0.2 ppm being observed from 248 - 378 K (Figure 2.10). As the peaks were shown to overlap, deconvolution of the resonances was performed (Table 2.4). In a coordinating solvent such as D₅-Py, two distinct ⁷Li environments are observed at higher δ. The two symmetric

^7Li environments here are likely due to the presence of two four-coordinate Li centers, which is consistent with the solid state structure observed in 2.3.

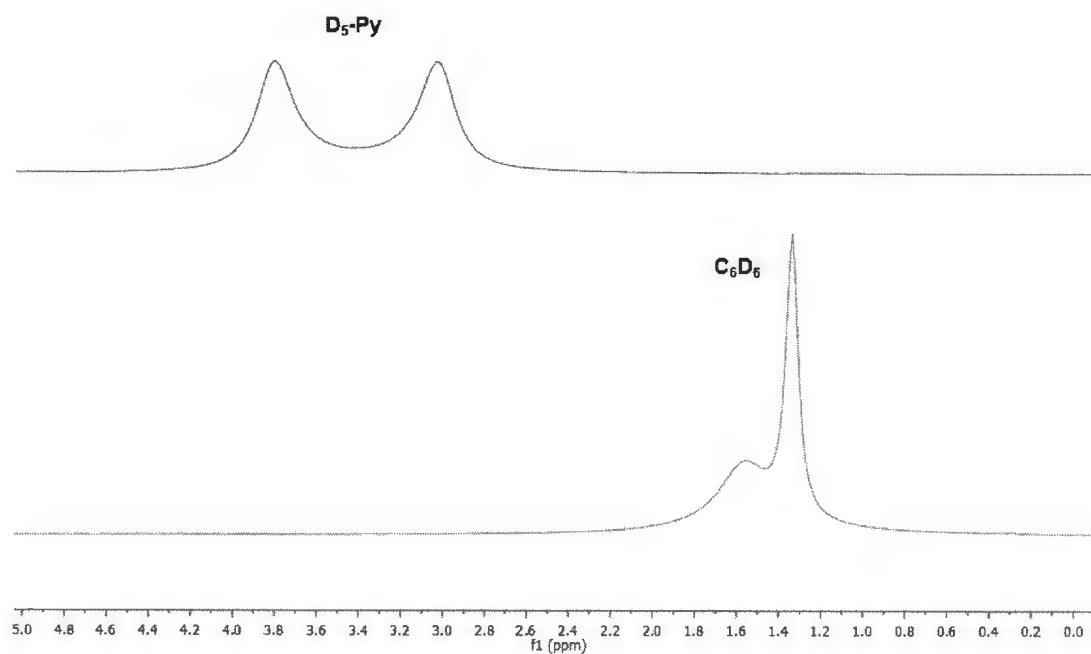


Figure 2.9. ^7Li NMR spectra at 7.04 T for complex 2.2 in $\text{D}_5\text{-Py}$ (top) and C_6D_6 (bottom).

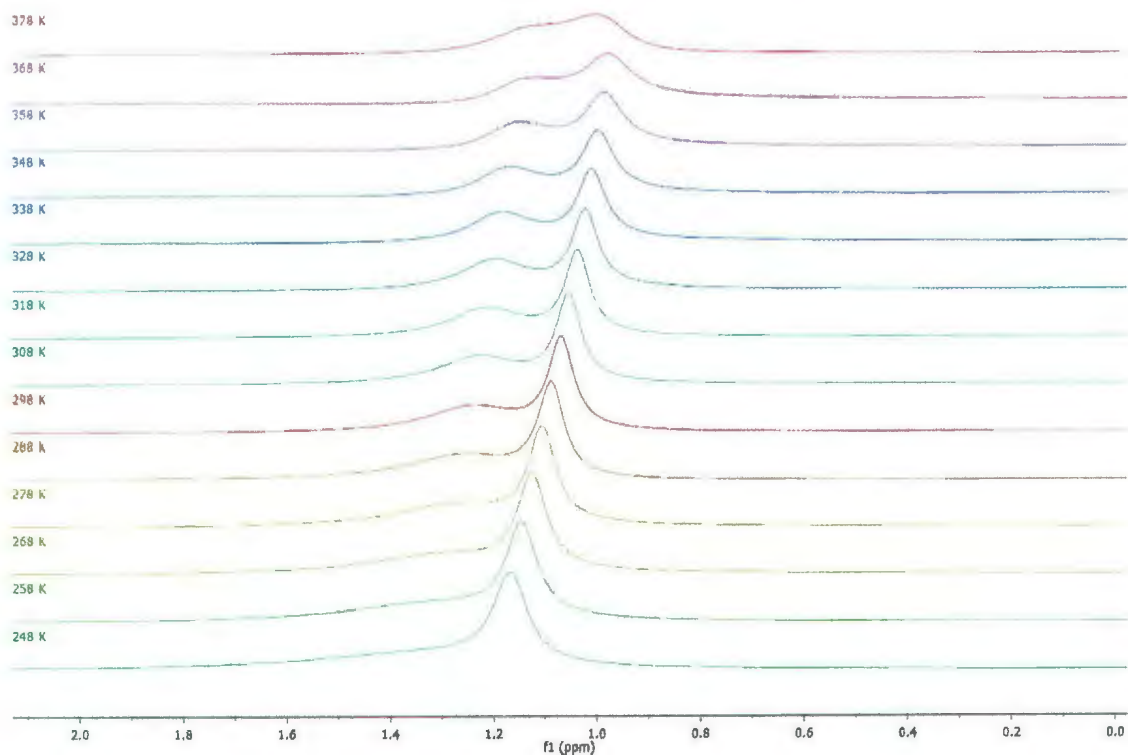


Figure 2.10. VT ^7Li NMR spectra at 7.04 T for complex **2.1** in $\text{D}_8\text{-Tol}$.

Table 2.4 Chemical shifts δ (ppm), peak width at half height (Hz) and peak areas for complexes **2.1** and **2.2** in solution (^7Li)^a and solid state ($^{6,7}\text{Li}$) NMR

	δ ^7Li ^b			δ ^6Li MAS ^c		δ ^7Li MAS ^d				
	C_6D_6			$\text{D}_5\text{-Py}$			ppm	$\text{LW}_{1/2}$ (Hz)	ppm	$\text{LW}_{1/2}$ (Hz)
	ppm	$\text{LW}_{1/2}$ (Hz)	Peak Area ($\times 10^5$)	ppm	$\text{LW}_{1/2}$ (Hz)	Peak Area ($\times 10^5$)				
2.1	1.34	9.6	1.19	3.40	24.0	3.36	0.77	65.75	0.56	528.55
	1.52	31.3	1.08	4.13	20.8	3.04	(1.08) ^e	(58.68) ^e		
2.2	1.34	7.8	1.06	3.03	23.2	2.50	0.70	45.04	0.79	425.44
	1.56	39.9	1.33	3.80	24.8	2.59				

^aT = 298 K for amorphous powders (100 mg/mL). ^bCalculated from line fitting program in MestReNova. ^c 15 kHz. ^d 20 kHz. ^eCrystalline.

The chemical shifts for both **2.1** and **2.2** were also observed to change depending on the solvent system used (Table 2.4). In C_6D_6 the resonances were observed to range between 1.34-1.56 ppm, compared to 3.03-4.13 ppm in D_5 -Py. The differences observed for the resonances are likely due to the change in structure as well as the change in polarity of the solvent, where complexes **2.1** and **2.2** coordinate pyridine to one of the lithium atoms, as found in complex (**2.3**), shifting to higher δ . Two peaks of comparable chemical shifts, 2.91 and 3.68 ppm (measured in D_8 -Tol), to **2.1** and **2.2** in D_5 -Py were observed for the 7Li NMR spectrum of Chen's lithium amine-bis(phenolate) complex (**1.47**).⁷

Solid state $^{6,7}Li$ NMR was also explored for **2.1** and **2.2**. However, broad peaks were observed for both complexes (45.04 – 65.75 Hz for 6Li and 425.44 – 528.55 Hz for 7Li) as shown in Table 2.4. Shoulders were also evident on the peaks but were not well defined, making it difficult to model the spectra. The 7Li (20 kHz) MAS spectrum for **2.2**, as well as the 6Li (15 kHz) MAS spectrum is shown in Figure 2.11. Various spinning rates were tested ranging from static (0 kHz) to 20 kHz. Spinning side bands are observed for **2.1** and **2.2** in their 7Li MAS NMR spectra suggesting chemical shift anisotropy, but a small difference in the chemical shifts of 6Li and 7Li MAS suggests an insignificant quadrupolar interaction.⁴ Evidence from the 6Li solid state spectra for more than one lithium environment does exist, but attempts to model the peaks to calculate quadrupolar coupling parameters were unsuccessful. Confirmation of multiple lithium peaks was shown in solution 7Li NMR, as previous mentioned, giving sharper resonances resulting in two distinct lithium environments. The Li chemical shifts presented in Table 2.4 were all found to be in the range of similar Li aggregates observed in the literature.^{4,21}

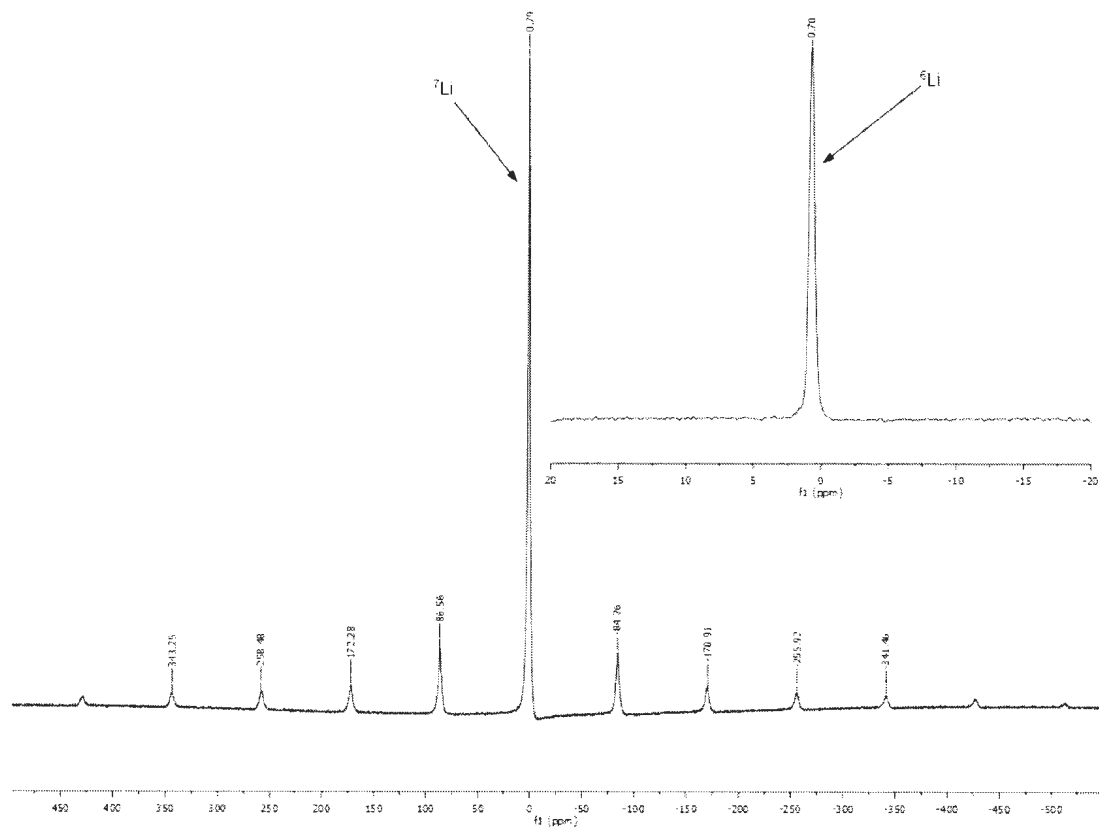


Figure 2.11. ^7Li MAS (20 kHz) and ^6Li MAS (15 kHz) spectra of complex **2.2** at 14 T.

2.2.4 Mass Spectrometry

The use of NMR spectroscopy played an essential role in the characterization of these complexes, but mass spectrometry (MS) has also become an important characterization method for metal compounds. Soft ionization, which results in minimal fragmentation of the compound, make electrospray ionization (ESI) and matrix-assisted laser desorption/ionization time-of-flight (MALDI-TOF) MS ideal methods to analyze complex mixtures.²² Specifically, MALDI-TOF MS has provided an additional way for

coordination compounds to be analyzed. The TOF detector allows ions to be detected based on their mass-to-charge ratio.

The MALDI-TOF MS spectra of **2.1** and **2.2** were both found to possess the expected characteristic peaks. For compound **2.1** the mass spectrum shows peaks corresponding to the monomer $[\text{Li}_2[\mathbf{L2}]]^+$ at m/z 465.3 and ligand fragments, as well as a very weak ion corresponding to the dimeric species $[\{\text{Li}_2[\mathbf{L2}]\}_2]^+$ at m/z 930.6 (Figure 2.12). Comparison of the experimental with the theoretical isotope pattern was found to agree with the assignments found, as shown in Figure 2.13. A similar result was observed for compound **2.2**, the mass spectrum and isotope patterns are included in Appendix B, Figures B1.1 and B1.2, respectively.

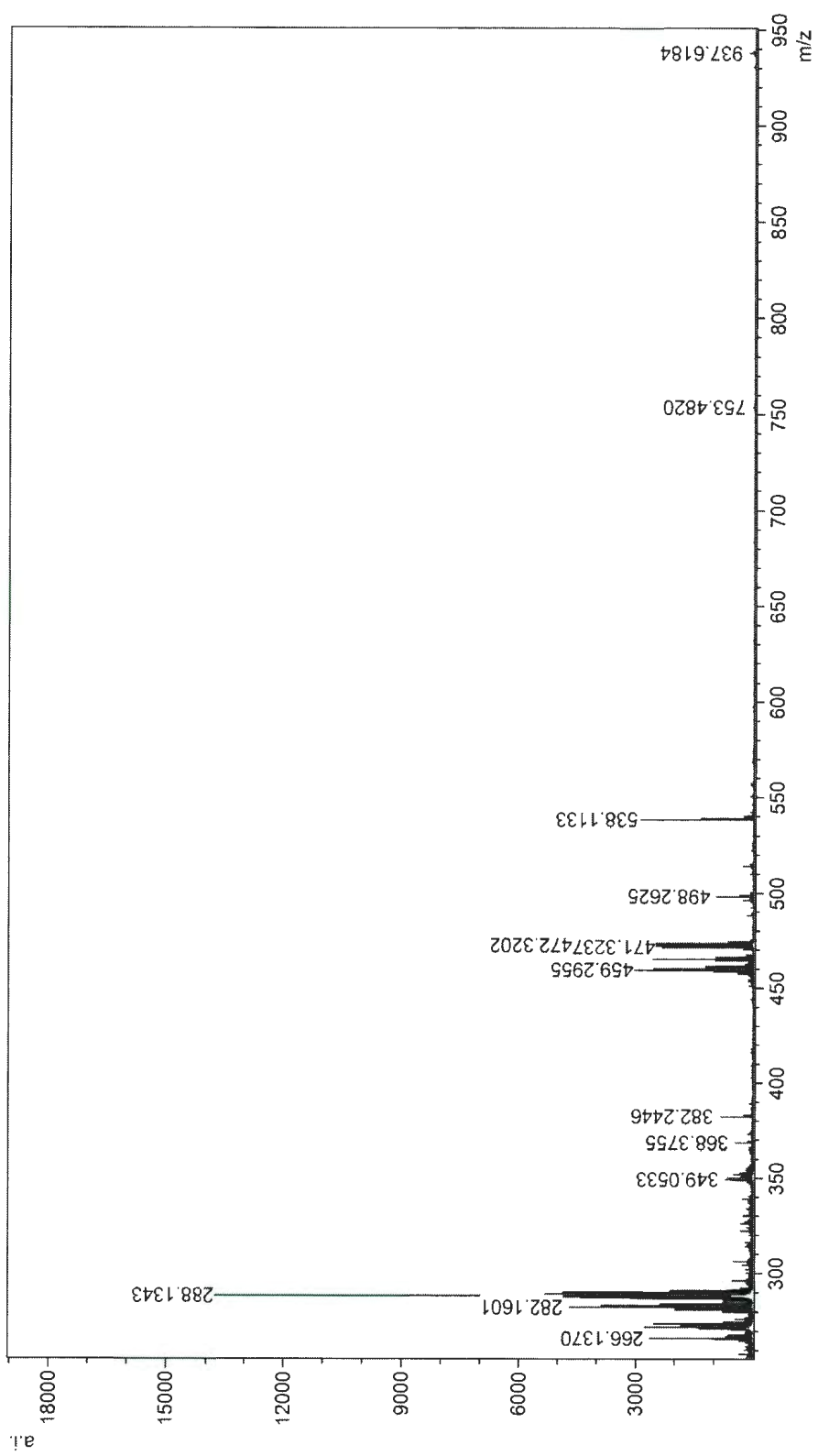


Figure 2.12. MALDI-TOF mass spectrum of $\{\text{Li}_2[\text{O}_2\text{NO}]^{\text{BuMe}}\}_2$ (2.1).

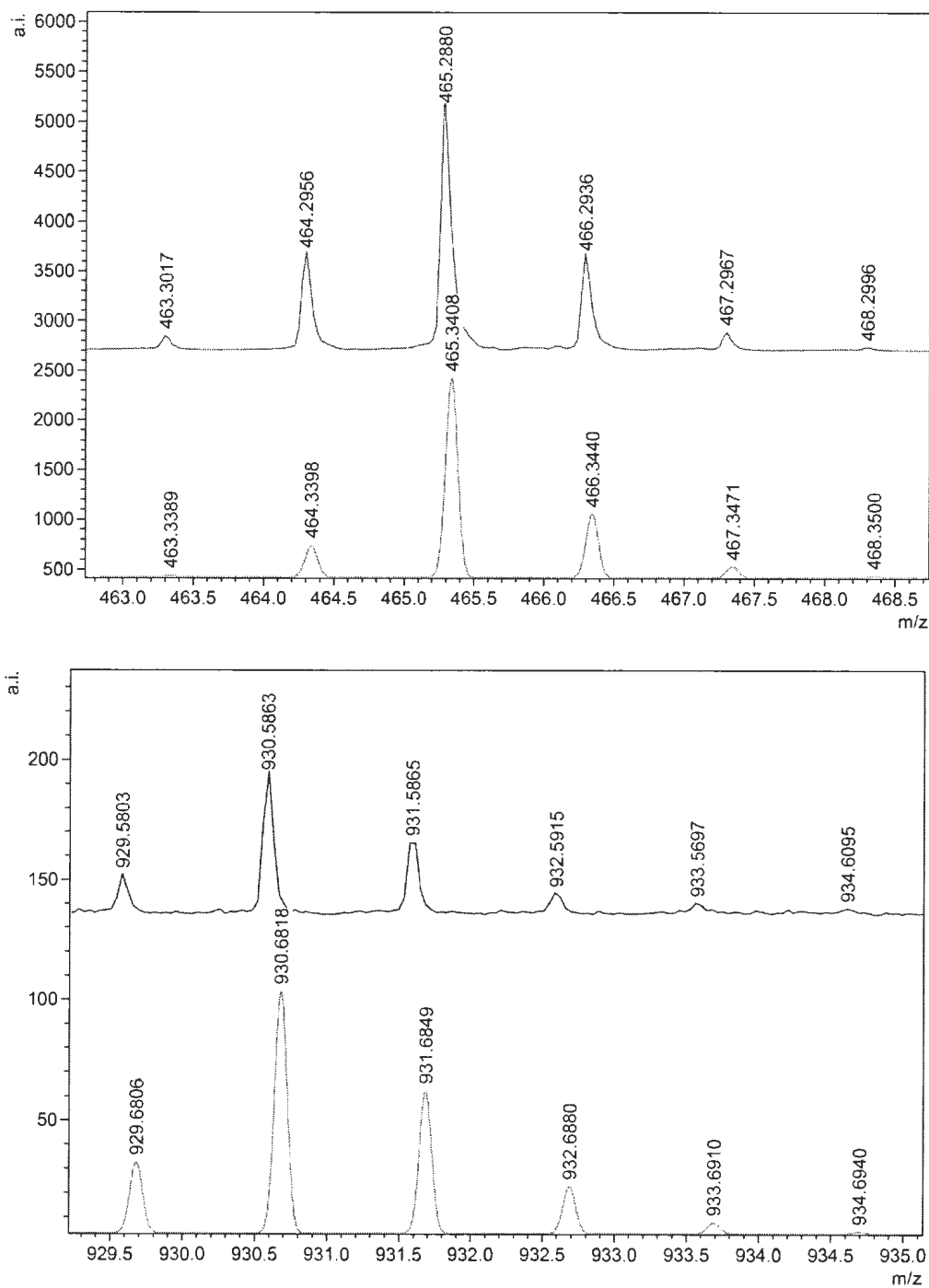


Figure 2.13. Experimental and theoretical MALDI-TOF MS isotopic distribution pattern for **2.1** (top = monomer, bottom = dimer).

2.3 Experimental

2.3.1 General Experimental Conditions

Unless otherwise stated, all manipulations were performed under an atmosphere of dry, oxygen-free nitrogen by means of standard Schlenk techniques or using an MBraun Labmaster glove box. Anhydrous THF, toluene, pentane, hexanes and benzene were distilled from sodium benzophenone ketyl under nitrogen. Reagents were purchased either from Aldrich or Alfa Aesar and used without further purification. MALDI-TOF MS was performed using an Applied Biosystems 4800 MALDI TOF/TOF Analyzer equipped with a reflectron, delayed ion extraction and high performance nitrogen laser (200 Hz operating at 355 nm). Samples were prepared in the glove box and sealed under nitrogen in a Ziploc[®] bag for transport to the instrument. Anthracene was used as the matrix. Elemental analyses were performed at Canadian Microanalytical Service, Ltd. Delta, BC, Canada.

Solution NMR: ¹H and ¹³C NMR spectra were recorded on either a 11.7 T Bruker AVANCE (500 MHz) or a 7.04 T Bruker AVANCE III (300 MHz and 75.5 MHz) spectrometers. ⁷Li NMR spectra were recorded on a 7.04 T Bruker AVANCE III spectrometer at 166.7 MHz. Both solution and solid state Li spectra were referenced externally to a saturated solution of LiCl in D₂O. CDCl₃, C₆D₆ and D₈-Tol were purchased from Cambridge Isotope Laboratories and D₅-Py from Aldrich. All deuterated solvents used in the analysis of the lithium complexes were dried over calcium hydride (CDCl₃ and D₅-Py) or sodium/potassium alloy (C₆D₆ and D₈-Tol), vacuum transferred

and stored under nitrogen in ampules fitted with Teflon valves. NMR solutions of complexes **2.1** and **2.2** were prepared under nitrogen and sealed in J-Young NMR tubes.

Solid state NMR: $^{6,7}\text{Li}$ NMR spectra were performed on a 14 T Bruker AVANCE II 600 MHz spectrometer (at frequencies of 233.3 MHz for ^7Li , and 88.3 MHz for ^6Li) equipped with a 4 mm double-tuned MAS probe. Typical 90° pulse lengths were 3.5 μs for ^6Li and 3 μs for ^7Li . Dipolar coupling to protons was removed by continuous-wave ^1H high-power decoupling during acquisition. All experiments were measured at room temperature. Samples were packed in 4 mm ZrO_2 rotors, sealed with KEL-F caps under nitrogen in a glove box.

2.3.2 Synthesis of Ligands and Lithium Compounds

The synthesis and spectroscopic characterization, including ^1H and ^{13}C NMR of amine-bis(phenol) ligands used through out this thesis are presented here. The ligands $\text{H}_2[\text{O}_2\text{NO}]^{\text{MeMe}}$ (**L1**),²³ $\text{H}_2[\text{O}_2\text{NO}]^{\text{BuMe}}$ (**L2**),¹⁵ $\text{H}_2[\text{O}_2\text{NO}]^{\text{BuBu}}$ (**L3**),¹⁸ $\text{H}_2[\text{O}_2\text{NN}]^{\text{MeMe}}$ (**L4**),¹⁹ $\text{H}_2[\text{O}_2\text{NN}]^{\text{BuMe}}$ (**L5**),¹⁶ $\text{H}_2[\text{O}_2\text{NN}]^{\text{BuBu}}$ (**L6**)²⁰ were prepared according to previously reported procedures.

$\text{H}_2[\text{O}_2\text{NO}]^{\text{MeMe}}$ (**L1**). A solution of 2,4-dimethylphenol (15.03 g, 0.123 mol), tetrahydrofurfurylamine (6.22 g, 0.0615 mol), and 37% aqueous formaldehyde (10 mL, 0.123 mol) in water (100 mL) was stirred and refluxed overnight. Upon cooling, a large quantity of beige product formed. The solvents were decanted, and the remaining solid residue was washed with cold methanol to give a pure, white powder (16.13 g, 71% yield). ^1H NMR (500 MHz, 298 K, CDCl_3 , δ): 8.75 (br s, *OH*, 2H); 6.85 (s, *ArH*, 2H);

6.66 (s, ArH, 2H); 4.20 (m, CH, 1H); 4.02 (m, CHHO, 1H); 3.92 (m, CHHO, 1H); 3.87 (d, $^2J_{\text{HH}} = 13.6$ Hz, ArCH₂N, 2H); 3.65 (d, $^2J_{\text{HH}} = 13.6$ Hz, ArCH₂N, 2H); 2.64 (dd, $^2J_{\text{HH}} = 3.2$ Hz, $^2J_{\text{HH}} = 3.2$ Hz, CHHN, 1H); 2.51 (dd, $^2J_{\text{HH}} = 9.9$ Hz, $^2J_{\text{HH}} = 9.9$ Hz, CHHN, 1H); 2.20 (s, CH₃, 6H); 2.19 (s, CH₃, 6H); 1.90 (m, CH₂CH₂, 4H). ¹³C {¹H} NMR (75.49 MHz, 298 K, CDCl₃, δ): 152.59 (ArCOH); 131.27 (ArC(CH₃)₃); 128.54 (ArCCH₃); 127.81 (ArCH); 125.31 (ArCH); 121.24 (ArCCH₂N); 78.53 (CHO); 68.49 (CH₂); 57.20 (CH₂); 56.30 (CH₂); 29.66 (CH₂); 25.34 (CH₂); 20.50 (CH₃); 16.20 (CH₃).

H₂[O₂NO]^{BuMe} (L2). A solution of 2-*tert*-butyl-4-methylphenol (20.26 g, 0.123 mol), tetrahydrofurfurylamine (6.26 g, 0.0616 mol), and 37% aqueous formaldehyde (10 mL, 0.123 mol) in water (91 mL) was stirred and refluxed overnight. Upon cooling, a large quantity of beige solid formed. The solvents were decanted, and the remaining solid residue was washed with cold methanol to give a pure, white powder (24.23 g, 87% yield). Crystalline product was obtained by slow cooling from chloroform. ¹H NMR (500 MHz, 298 K, CDCl₃, δ): 8.74 (s, OH, 2H); 6.98 (d, $^2J_{\text{HH}} = 1.7$ Hz, ArH, 2H); 6.70 (d, $^2J_{\text{HH}} = 1.6$ Hz, ArH, 2H); 4.21 (m, CH, 1H); 4.00 (m, CHHO, 1H); 3.89 (m, CHHO, 1H); 3.72 (m, ArCH₂N, 4H); 2.60 (dd, $^2J_{\text{HH}} = 3.4$ Hz, $^2J_{\text{HH}} = 3.4$ Hz, CHHN, 1H); 2.52 (dd, $^2J_{\text{HH}} = 9.5$ Hz, $^2J_{\text{HH}} = 9.5$ Hz, CHHN, 1H); 2.22 (s, CH₃, 6H); 1.88 (m, CH₂CH₂, 4H); 1.39 (s, C(CH₃)₃, 18H). ¹³C {¹H} NMR (75.49 MHz, 298 K, CDCl₃, δ): 153.17 (ArCOH); 136.79 (ArC(CH₃)₃); 128.82 (ArCCH₃); 127.21 (ArCH); 127.13 (ArCH); 122.25 (ArCCH₂N); 77.58 (CHO); 68.34 (CH₂); 57.06 (CH₂); 55.81 (CH₂); 34.71 (CMe₃); 29.57 (CH₃)₃; 29.53 (CH₂); 25.20 (CH₂); 20.77 (CH₃).

H₂[O₂NO]^{BuBu} (L3). A solution of 2,4-di-*tert*-butylphenol (25.41 g, 0.123 mol), tetrahydrofurfurylamine (6.26 g, 0.0619 mol), and 37% aqueous formaldehyde (10 mL,

0.123 mol) in water (100 mL) was stirred and refluxed overnight. Upon cooling, a large quantity of white solid formed. The solvents were decanted, and the remaining solid residue was washed with cold methanol to give a pure, white powder (24.23 g, 87% yield). Crystalline product was obtained by slow cooling from chloroform. ^1H NMR (500 MHz, 298 K, CDCl_3 , δ): 8.83 (s, OH, 2H); 7.20 (d, $^2J_{\text{HH}} = 2.4$ Hz, ArH, 2H); 6.88 (d, $^2J_{\text{HH}} = 2.4$ Hz, ArH, 2H); 4.27 (m, CH, 1H); 4.02 (m, CHHO, 1H); 3.90 (m, CHHO, 1H); 3.77 (m, ArCH₂N, 4H); 2.62 (dd, $^2J_{\text{HH}} = 3.5$ Hz, $^2J_{\text{HH}} = 3.5$ Hz, CHHN, 1H); 2.54 (dd, $^2J_{\text{HH}} = 9.6$ Hz, $^2J_{\text{HH}} = 9.6$ Hz, CHHN, 1H); 1.90 (m, CH₂CH₂, 4H); 1.40 (s, C(CH₃)₃, 18H); 1.27 (s, C(CH₃)₃, 18H). $^{13}\text{C}\{^1\text{H}\}$ NMR (75.49 MHz, 298 K, CDCl_3 , δ): 153.18 (ArCOH); 140.76 (ArC(CH₃)₃); 136.19 (ArCCH₃); 125.08 (ArCH); 123.52 (ArCH); 121.58 (ArCCH₂N); 77.70 (CHO); 68.42 (CH₂); 57.68 (CH₂); 56.09 (CH₂); 35.13 (CMe₃); 34.25(CMe₃); 31.84 (CH₃)₃; 29.75 (CH₃)₃; 29.68 (CH₂); 25.38 (CH₂).

$\text{H}_2[\text{O}_2\text{NN}']^{\text{MeMe}}$ (**L4**). A solution of 2,4-methylphenol (15.04 g, 0.123 mol), aminomethylpyridine (6.65 g, 0.0615 mol) and 37% aqueous formaldehyde (10.0 mL, 0.123 mol) in water (90 mL) was stirred and refluxed for 24 h. Upon cooling, a large quantity of yellow oil/solid formed. The solvents were decanted, and the remaining solid residue was washed with cold ethanol and sonicated. Crystalline product was obtained by slow cooling from chloroform to give a pure, white powder (12.1 g, 52% yield). ^1H NMR (300 MHz, 298 K, CDCl_3 , δ): 10.43 (s, OH, 2H); 8.71 (dd, $^3J_{\text{HH}} = 5.1$ Hz, $^4J_{\text{HH}} = 0.9$ Hz, PyH, 1H); 7.70 (td, $^3J_{\text{HH}} = 7.7$ Hz, $^4J_{\text{HH}} = 1.8$ Hz, PyH, 1H); 7.29 (d, $^4J_{\text{HH}} = 1.3$ Hz, PyH, 1H); 7.12 (d, $^3J_{\text{HH}} = 7.9$ Hz, PyH, 1H); 6.87 (d, $^4J_{\text{HH}} = 2.1$ Hz, ArH, 2H); 6.71 (d, $^4J_{\text{HH}} = 2.2$ Hz, ArH, 2H); 3.83 (s, CH₂, 2H); 3.75 (s, CH₂, 4H); 2.21 (s, CH₃, 12H). $^{13}\text{C}\{^1\text{H}\}$

NMR (75.48 MHz, 298 K, CDCl₃, δ): 156.31 (Py); 153.22 (ArCOH); 148.40 (Py); 137.58 (Py); 131.33 (ArCH); 128.60 (ArCH); 127.66 (Ar); 125.64 (Ar); 123.85 (Py); 122.63 (Py); 120.89 (ArCCH₂N); 56.54 (ArCH₂N); 55.58 (NCH₂Py); 20.52 (CH₃); 16.36 (CH₃).

H₂[O₂NN]^{BuMe} (**L5**). A solution of 2-*tert*-butyl-4-methylphenol (20.24 g, 0.123 mol), aminomethylpyridine (6.68 g, 0.062 mol) and 37% aqueous formaldehyde (10.0 mL, 0.123 mol) in water (100 mL) was stirred and refluxed for 24 h. Upon cooling, a large quantity of yellow solid formed. The solvents were decanted, and the remaining solid residue was washed with cold methanol to give a pure, white powder (22.5 g, 80% yield). Crystalline product was obtained by slow cooling from dichloromethane to give pure white crystals. ¹H NMR (300 MHz, 298 K, CDCl₃, δ): 10.48 (s, OH, 2H); 8.69 (dd, ³J_{HH} = 5 Hz, ⁴J_{HH} = 0.8 Hz, PyH, 1H); 7.69 (td, ³J_{HH} = 7.7 Hz, ⁴J_{HH} = 1.8 Hz, PyH, 1H); 7.27 (d, ⁴J_{HH} = 1.4 Hz, PyH, 1H); 7.12 (d, ³J_{HH} = 7.8 Hz, PyH, 1H); 7.00 (d, ⁴J_{HH} = 1.8 Hz, ArH, 2H); 6.74 (d, ⁴J_{HH} = 1.6 Hz, ArH, 2H); 3.81 (s, CH₂, 2H); 3.75 (s, CH₂, 4H); 2.23 (s, CH₃, 6H); 1.39 (s, C(CH₃)₃, 18H). ¹³C {¹H} NMR (75.48 MHz, 298 K, CDCl₃, δ): 156.09 (Py); 153.93 (ArCOH); 148.16 (Py); 137.38 (Py); 137.12 (Ar); 128.99 (Ar); 127.17 (Ar); 127.05 (Ar); 123.71 (Py); 122.52 (Py); 122.11 (Ar); 56.20 (CH₂); 55.28 (CH₂); 34.80 (CMe₃); 29.60 (CH₃)₃; 20.77 (CH₃).

H₂[O₂NN]^{BuBu} (**L6**). A solution of 2,4-di-*tert*-butylphenol (25.58 g, 0.124 mol), aminomethylpyridine (6.65 g, 0.0615 mol) and 37% aqueous formaldehyde (10.0 mL, 0.123 mol) in water (90 mL) was stirred and refluxed for 24 h. Upon cooling, a large quantity of white/grey solid formed. The solvents were decanted, and the remaining solid residue was washed with cold methanol to give a white powder (28.7 g, 85% yield).

Crystalline product was obtained by slow cooling from chloroform to give pure white crystals. ^1H NMR (300 MHz, 298 K, CDCl_3 , δ): 10.54 (s, *OH*, 2H); 8.68 (d, $^3J_{\text{HH}} = 4.4$ Hz, *PyH*, 1H); 7.69 (d, $^3J_{\text{HH}} = 5.5$ Hz, *PyH*, 1H); 7.27 (d, $^3J_{\text{HH}} = 5.5$ Hz, *PyH*, 1H); 7.22 (d, $^4J_{\text{HH}} = 2.2$ Hz, *PyH*, 2H); 7.10 (d, $^3J_{\text{HH}} = 7.8$ Hz, *PyH*, 1H); 6.93 (d, $^4J_{\text{HH}} = 2.1$ Hz, *ArH*, 2H); 3.84 (s, *CH*₂, 2H); 3.80 (s, *CH*₂, 4H); 1.40 (s, $\text{C}(\text{CH}_3)_3$, 18H); 1.28 (s, $\text{C}(\text{CH}_3)_3$, 18H). $^{13}\text{C}\{^1\text{H}\}$ NMR (75.48 MHz, 298 K, CDCl_3 , δ): 156.43 (*Py*); 153.93 (*ArCOH*); 148.29 (*Py*); 140.56 (*Py*); 137.38 (*ArCH*); 136.46 (*ArCH*); 125.23 (*Ar*); 123.80 (*Ar*); 123.54 (*Py*); 122.55 (*Py*); 121.42 (*Ar*); 56.98 (*ArCH*₂*N*); 55.50 (*NCH*₂*Py*); 35.22 (*CMe*₃); 34.26 (*CMe*₃); 31.86 (*CH*₃)₃; 29.77 (*CH*₃)₃.

$\{\text{Li}_2[\text{O}_2\text{NO}]^{\text{BuMe}}\}_2$ (**2.1**) and $(\text{py})_2\text{Li}_2[\text{O}_2\text{NO}]^{\text{BuMe}}$ (**2.3**). $\text{H}_2[\text{O}_2\text{NO}]^{\text{BuMe}}$ (**L2**) (5.01 g, 11.04 mmol) was dissolved in THF (100 mL) and cooled to -78 °C. *n*-Butyllithium (1.6 M, 14 mL, 22.40 mmol) was slowly added resulting in a clear, yellow solution, which was warmed to room temperature and stirred for 2 h. Solvent was removed under vacuum and the product was washed with pentane. Removal of volatiles under vacuum yielded 6.08 g of beige product, which upon combustion analysis was shown to contain two equivalents of THF per dilithium salt (90% yield). Single crystals were obtained by slow evaporation of **2.1** in toluene and single crystals of **2.3** were obtained by slow evaporation of a solution of **2.1** in $\text{D}_5\text{-Py}$. Anal. calcd for $\text{C}_{29}\text{H}_{41}\text{Li}_2\text{NO}_3 \cdot (\text{C}_4\text{H}_8\text{O})_2$: C, 72.88; H, 9.42; N, 2.30. Found: C, 73.13; H, 9.02; N, 2.62%. ^1H NMR (500 MHz, 295K, $\text{D}_5\text{-Py}$, δ): 7.25 (d, $^4J_{\text{HH}} = 2.5$ Hz, *ArH*, 1H); 7.24 (d, $^4J_{\text{HH}} = 2.5$ Hz, *ArH*, 1H); 7.00 (d, $^4J_{\text{HH}} = 2.5$ Hz, *ArH*, 1H); 6.88 (d, $^4J_{\text{HH}} = 2.5$ Hz, *ArH*, 1H); 4.34 (d, $^2J_{\text{HH}} = 12.0$ Hz, *ArCHHN*, 1H); 4.18 (d, $^2J_{\text{HH}} = 12.0$ Hz, *ArCHHN*, 1H); 3.74 (m,

$\text{CH}_2\text{CH}(\text{O})\text{CH}_2$, 1H); 3.67 (m, CHH , 1H); 3.33 (d, $^2J_{\text{HH}} = 12.0$ Hz, ArCHHN , 1H); 3.31 (m, CHH , 1H); 3.20 (d, $^2J_{\text{HH}} = 12.0$ Hz, ArCHHN , 1H); 3.14 (m, CHH , 1H); 2.70 (m, CH_2 , 2H); 2.38 (s, CH_3 , 3H); 2.36 (s, CH_3 , 3H); 1.64 (s, $\text{C}(\text{CH}_3)_3$, 9H); 1.62 (s, $\text{C}(\text{CH}_3)_3$, 9H). $^{13}\text{C}\{^1\text{H}\}$ NMR (75.48 MHz, $\text{D}_5\text{-Py}$, 298 K, δ): 166.82 (ArCO); 138.66 ($\text{ArC}(\text{CH}_3)_3$); 130.58 (ArCCH_3); 129.38 (ArCH); 129.17 (ArCH); 128.18 (CHN); 127.74 (CHN); 119.17 (ArCCH_2N); 79.01 (CHO); 67.34 (CH_2); 64.25 (CHN); 63.04 (CH_2); 57.82 (CH_2); 35.68 (CMe_3); 30.39 ($\text{C}(\text{CH}_3)_3$); 29.12 (CH_2); 25.51 (CH_2); 21.71 (CH_3). ^1H NMR (500 MHz, 298 K, $\text{D}_8\text{-Tol}$, δ): 7.14 (d, $^2J_{\text{HH}} = 13.7$ Hz, ArH , 2H); 6.71 (s, ArH , 1H); 6.62 (s, ArH , 1H); 4.58 (s, ArCHHN , 1H); 4.39 (s, ArCHHN , 1H); 3.24 (d, $^2J_{\text{HH}} = 11.9$ Hz, CHH , 1H); 3.15 (br s, $\text{CH}_2\text{CH}(\text{O})\text{CH}_2$, 1H); 3.12 (d, $^2J_{\text{HH}} = 11.7$ Hz, CHH , 1H); 2.90 (m, CH_2 , 2H); 2.64 (d, $^3J_{\text{HH}} = 5.9$ Hz, CH_2 , 2H); 2.38 (m, CHH , 1H); 2.27 (d, $^2J_{\text{HH}} = 12.3$ Hz, CH_3 , 6H); 2.06 (m, CHH , 1H); 1.60 (s, $\text{C}(\text{CH}_3)_3$, 18H). ^7Li NMR (166.66 MHz, 298 K, $\text{D}_5\text{-Py}$, δ): 4.13; 3.40. ^7Li NMR (166.66 MHz, 298 K, C_6D_6 , δ): 1.52; 1.34. ^7Li NMR (166.66 MHz, 298 K, $\text{D}_8\text{-Tol}$, δ): 1.24; 1.07. ^7Li MAS NMR (233.31 MHz, 298 K, δ): 0.56. ^6Li MAS NMR (88.35 MHz, 298 K, δ): 0.77. MS (MALDI-TOF) m/z (% ion): 937.7 (2, $\{\text{Li}_2[\text{L2}]\}_2^+$), 465.3 (23, $\text{Li}_2[\text{L2}]^+$).

$\{\text{Li}_2[\text{O}_2\text{NO}]^{\text{BuBu}}\}_2$ (**2.2**). $\text{H}_2[\text{O}_2\text{NO}]^{\text{BuBu}}$ (**L3**) (5.01 g, 9.31 mmol) was dissolved in THF (100 mL) and cooled to -78 °C. *n*-Butyllithium (1.6 M, 12 mL, 19.20 mmol) was slowly added resulting in a clear, yellow solution, which was warmed to room temperature and stirred for 2 h. Solvent was removed under vacuum; the product was then washed with pentane. Removal of volatiles under vacuum yielded 6.11 g of beige product (95% yield). Single crystals were obtained by slow evaporation of **2.2** in benzene. Anal. calcd for $\text{C}_{35}\text{H}_{53}\text{Li}_2\text{NO}_3 \cdot (\text{C}_4\text{H}_8\text{O})_{1.8}$: C, 74.59; H, 10.00; N, 2.06. Found: C, 74.13; H,

9.82; N, 1.74%. ^1H NMR (500 MHz, 295K, $\text{D}_5\text{-Py}$, δ): 7.52 (d, $^4J_{\text{HH}} = 2.5$ Hz, ArH, 1H); 7.49 (d, $^4J_{\text{HH}} = 2.5$ Hz, ArH, 1H); 7.28 (d, $^4J_{\text{HH}} = 2.5$ Hz, ArH, 1H); 7.10 (d, $^4J_{\text{HH}} = 2.5$ Hz, ArH, 1H); 4.41 (d, $^2J_{\text{HH}} = 12.0$ Hz, ArCHHN, 1H); 4.26 (d, $^2J_{\text{HH}} = 12.0$ Hz, ArCHHN, 1H); 3.78 (m, $\text{CH}_2\text{CH}(\text{O})\text{CH}_2$, 1H); 3.47 (d, $^2J_{\text{HH}} = 12.0$ Hz, ArCHHN, 1H); 3.32 (m, CHH, 1H); 3.27 (d, $^2J_{\text{HH}} = 12.0$ Hz, ArCHHN, 1H); 3.05 (m, CHH, 1H); 2.73 (m, CHH, 1H); 2.43 (m, CHH, 1H); 1.67 (d, $^4J_{\text{HH}} = 4.58$ Hz, $\text{C}(\text{CH}_3)_3$, 18H); 1.43 (s, $\text{C}(\text{CH}_3)_3$, 9H); 1.40 (s, $\text{C}(\text{CH}_3)_3$, 9H). $^{13}\text{C}\{^1\text{H}\}$ NMR (75.48 MHz, 298 K, $\text{D}_5\text{-Py}$, δ): 166.70 (ArCO); 137.79 (ArCHN); 133.22 (ArCH); 128.70 (ArCH); 127.73 (ArCH); 126.73 (ArCH); 125.58 (ArCH); 123.27 (ArCHN); 78.59 (CHO); 67.38 (CH_2); 63.98 (ArCHN); 62.84 (CH_2); 57.22 (CH_2); 36.00 (CMe_3); 34.54 (CMe_3); 32.92 ($\text{C}(\text{CH}_3)_3$); 30.47 ($\text{C}(\text{CH}_3)_3$); 29.12 (CH_2); 25.51 (CH_2). ^1H NMR (500 MHz, 298 K, $\text{D}_8\text{-Tol}$, δ): 7.37 (s, ArH, 1H); 7.33 (s, ArH, 1H); 6.90 (s, ArH, 1H); 6.80 (s, ArH, 1H); 4.66 (s, ArCHHN, 1H); 4.44 (s, ArCHHN, 1H); 3.27 (d, $^2J_{\text{HH}} = 11.3$ Hz, CHH, 1H); 3.12 (d, $^2J_{\text{HH}} = 11.4$ Hz, CHH, 1H); 3.01 (br s, $\text{CH}_2\text{CH}(\text{O})\text{CH}_2$, 1H); 2.85 (m, CH_2 , 2H); 2.46 (d, $^3J_{\text{HH}} = 5.9$ Hz, CH_2 , 2H); 2.34 (m, CHH, 1H); 1.99 (m, CHH, 1H); 1.59 (s, $\text{C}(\text{CH}_3)_3$, 18H); 1.32 (s, $\text{C}(\text{CH}_3)_3$, 9H); 1.30 (s, $\text{C}(\text{CH}_3)_3$, 9H). ^7Li NMR (166.66 MHz, 298 K, $\text{D}_5\text{-Py}$, δ): 3.80; 3.03. ^7Li NMR (166.66 MHz, 298 K, C_6D_6 , δ): 1.56; 1.34. ^7Li MAS NMR (233.31 MHz, 298 K, δ): 0.79. ^6Li MAS NMR (88.35 MHz, 298 K, δ): 0.70. MS (MALDI-TOF) m/z (% ion): 1098.9 (2, $\{\text{Li}_2[\text{L3}]\}_2^+$), 549.4 (25, $\text{Li}_2[\text{L3}]^+$).

2.3.3 X-ray Crystallography

Crystallographic and structure refinement data are given in Table 2.5. Single crystals of **2.1**, **2.2** and **2.3** were mounted on glass fibers using Paratone-N oil. All measurements were made on a Rigaku Saturn CCD area detector with graphite monochromated Mo-K α radiation solved on an AFC8-Saturn 70 single crystal X-ray diffractometer from Rigaku, equipped with an X-stream 2000 low temperature system. The data were processed²⁴ and corrected for Lorentz and polarization effects and absorption.²⁵ Neutral atom scattering factors for all non-hydrogen atoms were taken from the *International Tables for X-ray Crystallography*.²⁶ All structures were solved by direct methods using SIR92²⁷ and expanded using Fourier techniques (DIRDIF99).²⁸ All non-hydrogen atoms were refined anisotropically. Hydrogen atoms were refined using the riding model. Anomalous dispersion effects were included in Fcalc;²⁹ the values for $\Delta f'$ and $\Delta f''$ were those of Creagh and McAuley.³⁰ The values for the mass attenuation coefficients are those of Creagh and Hubbell.³¹ All calculations were performed using the CrystalStructure³² crystallographic software package except for refinement, which was performed using SHELXL-97.³³ Molecular structures were generated using ORTEP-III (v. 2.02) for Windows.³⁴ For **2.1**, the asymmetric unit contains one toluene solvent molecule modelled at 60% occupancy. Two disordered pendant tetrahydrofuranlyl groups were modelled using partial occupancy carbons. One tetrahydrofuranlyl ring was modelled over two sites with 75%/25% occupancy; the other is modelled similarly but with 60%/40% occupancy. All but two hydrogen atoms on the two disordered groups were omitted and three carbon atoms were refined isotropically. For **2.2**, the pendant

tetrahydrofuranyl group was disordered, with C(17 and 19) and H(25, 27 and 28) at 60% occupancy and C(17A and 19A) and H(25A, 27A and 28A) at 40% occupancy. For **2.3**, the pendant tetrahydrofuranyl was disordered over two positions; C(26 and 29) at 82% occupancy and C(30 and C33) at 18% occupancy and their corresponding protons. A similarity restraint (SIMU; same U_{ij} components) was applied to the coordinated pyridine N3, C(39 and 43), and a distance restraint (DFIX) was applied to the C(32-33) bond.

Table 2.5 Crystallographic and structure refinement data for **2.1**, **2.2** and **2.3**

Compound	2.1	2.2	2.3
Chemical formula	$C_{58}H_{66}Li_4N_2O_6(C_7H_8)_{0.6}$	$C_{70}H_{106}Li_4N_2O_6$	$C_{39}H_{51}Li_2N_3O_3$
Formula weight	983.59	1099.38	623.73
<i>T</i> /K	138	123	153
Colour, habit	Colorless, block	Colorless, prism	Colorless, prism
Crystal dimensions/mm	0.52 × 0.23 × 0.12	0.14 × 0.13 × 0.07	0.36 × 0.24 × 0.23
Crystal system	Triclinic	Monoclinic	Monoclinic
Space group	$P\bar{1}$ (#2)	$C2/c$ (#15)	$P2_1/c$ (#14)
<i>a</i> /Å	10.6033(17)	16.331(4)	13.499(2)
<i>b</i> /Å	14.459(3)	14.455(4)	14.9155(19)
<i>c</i> /Å	20.660(4)	28.696(7)	19.625(3)
α /°	106.382(4)	90	90
β /°	93.500(4)	92.989(5)	111.490(3)
γ /°	91.895(4)	90	90
<i>V</i> /Å ³	3029.1(9)	6765(3)	3676.8(10)
<i>Z</i>	2	4	4
<i>D_c</i> /g cm ⁻³	1.081	1.079	1.127
μ (MoK α)/cm ⁻¹	0.668	0.66	0.70
<i>F</i> (000)	1068.00	2400	1344
θ Range for collection /°	1.5 to 30.8	2.8 to 30.6	2.1 to 30.9
Reflections collected	25664	44372	48100
Independent reflections	12432	6994	7616
<i>R</i> (int)	0.025	0.0711	0.0386
<i>R</i> , <i>wR</i> ₂ (all)	0.1216, 0.3379	0.0992, 0.1952	0.0773, 0.1948
<i>R</i> , <i>wR</i> ₂ [<i>I</i> > 2 σ (<i>I</i>)]	0.1083, 0.3215	0.0905, 0.1894	0.0759, 0.1934
GOF on <i>F</i> ²	1.094	1.217	1.148

2.4 Conclusion

Amine-bis(phenolate) ligands with a tetrahydrofuranyl and pyridyl pendant arm have been synthesized *via* a modified Mannich condensation reaction. Lithium salts of the tetrahydrofuranyl donor have been synthesized and characterized. Two tetra- and one dilithium complex were isolated and structurally characterized by single crystal X-ray diffraction. Multinuclear solution and solid state NMR studies have been performed providing further structural evidence for these species. The use of these complexes as polymerization initiators will be presented in the following chapter.

2.5 References

- (1) Wichmann, O.; Sillanpää, R.; Lehtonen, A. *Coord. Chem. Rev.* **2012**, *256*, 371-392.
- (2) Clegg, W.; Davidson, M. G.; Graham, D. V.; Griffen, G.; Jones, M. D.; Kennedy, A. R.; O'Hara, C. T.; Russo, L.; Thomson, C. M. *Dalton Trans.* **2008**, 1295-1301.
- (3) Kerton, F. M.; Kozak, C. M.; Lüttgen, K.; Willans, C. E.; Webster, R. J.; Whitwood, A. C. *Inorg. Chim. Acta* **2006**, *359*, 2819-2825.
- (4) Boyle, T. J.; Pedrotty, D. M.; Alam, T. M.; Vick, S. C.; Rodriguez, M. A. *Inorg. Chem.* **2000**, *39*, 5133-5146.
- (5) Jackman, L. M.; Cizmeciyan, D.; Williard, P. G.; Nichols, M. A. *J. Am. Chem. Soc.* **1993**, *115*, 6262-6267.
- (6) MacDougall, D. J.; Noll, B. C.; Kennedy, A. R.; Henderson, K. W. *Dalton Trans.* **2006**, 1875-1884.
- (7) Huang, C.; Chen, C. *Dalton Trans.* **2007**, 5561-5566.
- (8) Mulvey, R. E. *Chem. Soc. Rev.* **1991**, *20*, 167-209.
- (9) Downard, A.; Chivers, T. *Eur. J. Inorg. Chem.* **2001**, 2193-2201.
- (10) Bond, A. D. *Chem. Eur. J.* **2004**, *10*, 1885-1898.
- (11) Carmichael, C. D.; Fryzuk, M. D. *Dalton Trans.* **2008**, 800-806.
- (12) Huang, B.; Ko, B.; Athar, T.; Lin, C. *Inorg. Chem.* **2006**, *45*, 7348-7356.
- (13) Hsu, Y.; Liang, L. *Organometallics* **2010**, *29*, 6201-6208.
- (14) Kerton, F. M.; Holloway, S.; Power, A.; Soper, R. G.; Sheridan, K.; Lynam, J. M.; Whitwood, A. C.; Willans, C. E. *Can. J. Chem.* **2008**, *86*, 435-443.
- (15) Chowdhury, R. R.; Crane, A. K.; Fowler, C.; Kwong, P.; Kozak, C. M. *Chem. Commun.* **2008**, 94-96.
- (16) Hasan, K.; Fowler, C.; Kwong, P.; Crane, A. K.; Collins, J. L.; Kozak, C. M. *Dalton Trans.* **2008**, 2991-2998.
- (17) Collins, K. L.; Corbett, L. J.; Butt, S. M.; Madhurambal, G.; Kerton, F. M. *Green Chem. Lett. Rev.* **2007**, *1*, 31-35.

- (18) Groysman, S.; Goldberg, I.; Kol, M.; Genizi, E.; Goldschmidt, Z. *Inorg. Chim. Acta* **2003**, *345*, 137-144.
- (19) Toupance, T.; Dubberley, S. R.; Rees, N. H.; Tyrrell, B. R.; Mountford, P. *Organometallics* **2002**, *21*, 1367-1382.
- (20) Shimazaki, Y.; Huth, S.; Odani, A.; Yamauchi, O. *Angew. Chem. Int. Ed.* **2000**, *39*, 1666-1669.
- (21) Hartung, M.; Günther, H.; Amoureux, J.; Fernández, C. *Magn. Reson. Chem.* **1998**, *36*, S61-S70.
- (22) Henderson, W.; McIndoe, J. S. In *Mass Spectrometry of Inorganic, Coordination and Organometallic Compounds*; John Wiley & Sons Ltd.: Chichester, England, **2005**.
- (23) Chowdhury, R. R. *Masters thesis*, **2007**, Memorial University of Newfoundland, St. John's, NL.
- (24) Pflugrath, J. W. *Acta Crystallogr., Sect. D: Biol. Crystallogr.* **1999**, *55*, 1718-1725.
- (25) Larson, A. C. In *Crystallographic Computing*; Ahmed, F. R., Ed.; Munksgaard, Copenhagen, 1970, p. 291.
- (26) Cromer, D. T.; Waber, J. T. In *International Tables for X-ray Crystallography*; The Kynoch Press: Birmingham, UK, **1974**.
- (27) Altomare, A.; Cascarano, G.; Giacovazzo, C.; Guagliardi, A.; Burla, M.; Polidori, G.; Camalli, M. *J. Appl. Crystallogr.* **1994**, *27*, 435.
- (28) Beurskens, P. T.; Admiraal, G.; Beurskens, G.; Bosman, W. P.; de Gelder, R.; Israel, R.; Smits, J. M. M. In *DIRDIF99*, University of Nijmegen, Netherlands, **1999**.
- (29) Ibers, J. A.; Hamilton, W. C. *Acta Crystallogr.* **1964**, *17*, 781-782.
- (30) Creagh, D. C.; McAuley, W. J. In *International Tables for Crystallography (A.J.C. Wilson, ed.)*; Kluwer Academic Publishers: Boston, **1992**; Vol. C, Table 4.2.6.8, pages 219-222.
- (31) Creagh, D. C.; Hubbell, J. H. In *International Tables for Crystallography (A.J.C. Wilson, ed.)*; Kluwer Academic Publishers: Boston, **1992**; Vol. C, Table 4.2.4.3, pages 200-206.

- (32) Watkin, D. J.; Prout, C. K.; Carruthers, J. R.; Betteridge, P. W. *CRYSTALS Issue 10*, Chemical Crystallography Laboratory, Oxford, UK, **1996**; *CrystalStructure 3.7.0: Crystal Structure Analysis Package*, Rigaku and Rigaku/MSO, The Woodlands, Texas, 2000-2005.
- (33) Sheldrick, G. M. *SHELXL-97, Program for refinement of crystal structures*, University of Göttingen, Germany, **1997**.
- (34) Farrugia, L. J. *J. Appl. Crystallogr.* **1997**, 30, 565.

Chapter 3

Ring-opening Polymerization of Cyclic Esters with Lithium Amine-bis(phenolate) Complexes

3.1 Introduction

The mass production of plastic dates back to the Second World War when little thought was placed on oil reserves ever being depleted. A predicted 300 million tonnes of plastic was produced worldwide in 2010.¹ Higher oil prices due to depleting oil stocks and current environmental problems as a result of fossil fuels have challenged society to explore alternative sources for the production of plastics, particularly from renewable resources. Research on aliphatic polyesters such as poly(lactide) and poly(ϵ -caprolactone) within the past couple of decades has shown promise towards the development of biodegradable and non-toxic materials.²⁻⁵

The ring-opening polymerization (ROP) of lactides and lactones has been gaining attention in polymer research for good reason. The monomers used come from renewable resources and are often not petroleum based, and their biodegradable and biocompatible properties allow for a truly 100% renewable polymer. Although these are important advantages, there are some existing limitations. Specifically for poly(lactide), physical properties such as its low glass transition temperature (~ 55 °C) and brittleness hinder its applications.⁶ It is also noteworthy that the monomer lactic acid can be derived from cornstarch, a renewable feedstock. However, it has a potentially negative environmental

and social impact as a food source, corn, is used to produce it. Additionally, the most widely known and used metal catalyst in the ROP process is tin(II) 2-ethylhexanoate, or stannous octoate ($\text{Sn}(\text{Oct})_2$). The use of tin complexes in ROP because of their potential toxicity, particularly for polymers aimed at medical applications, is still questionable.^{7,8}

The main disadvantages of metal-based catalyst systems are their toxicity, their often complex synthesis and the expense of the materials. A metal such as lithium could possibly circumvent these issues. Lithium compounds are already utilized in the pharmaceutical industry today, providing a non-toxic and cheap alternative for metal catalysts.⁹ Lithium complexes have shown activity for the ROP of cyclic esters as presented in Chapter 1. However, despite their commercial importance, a limited number of examples with lithium as the active catalyst exist. Continued investigation of lithium initiators for this purpose is important.

In this chapter, lithium amine-bis(phenolate) complexes were explored for their potential use as initiators in the ROP of cyclic esters. Various parameters for the ROP of DL-lactide were explored including catalyst loading, amount of co-initiator, temperature and reaction time in order to gain insight into the reactivity of these lithium initiators.

3.2 Results and Discussion

3.2.1 Synthesis

Synthesis and characterization of lithium amine-bis(phenolate) complexes **2.1** and **2.2** were presented in Chapter 2. These complexes were investigated as potential initiators for the ring-opening polymerization (ROP) of ϵ -caprolactone (CL), β -butyrolactone (β -

BL) and DL-lactide (LA). It is important to note that initiators **2.1**, **2.2**, **3.1** and **3.2** were found to be tetralithium compounds in the solid state, however, in solution they are presumed to dissociate, where each Li cation results in an initiation site. Therefore, the amount of complex used in the reactions was calculated per Li centre through out this chapter. Additionally, complexes **3.1** and **3.2** bearing tridentate ligands were also examined for their ROP ability with LA in order to allow a comparison between differing ligand frameworks (Figure 3.1). The synthesis and structural characterization of complexes **3.1** and **3.2** were previously reported in a former undergraduate student's thesis from the Kozak group.¹⁰

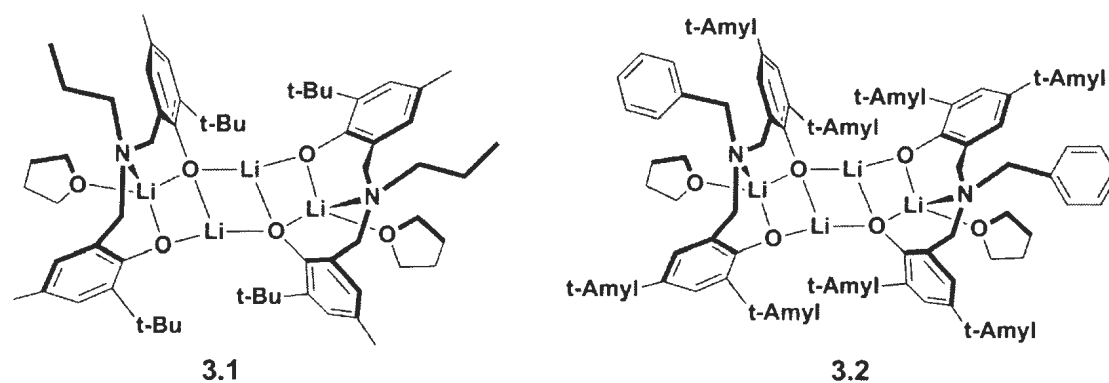
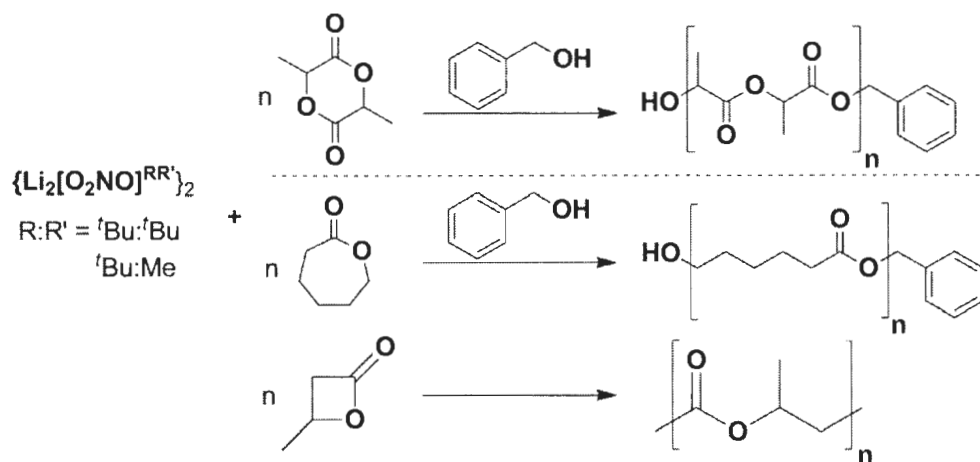


Figure 3.1. Lithium amine-bis(phenolate) complexes **3.1** and **3.2**.

The procedure used for the synthesis of these polymers varied slightly depending on the monomer used (Scheme 3.1). A stock solution including benzyl alcohol (BnOH), used as a co-initiator where appropriate, and the suitable lithium complex, acting as the initiator, was prepared to a known concentration and added to the required amount of monomer. The reaction was stirred vigorously for the allotted time and the

polymerization reaction was stopped by quenching the reaction with methanol. Benzyl alcohol has been shown to be important in the activation of many initiators where the active species, a metal alkoxide bond forms allowing the ROP process to occur.



Scheme 3.1. Synthetic procedure for the ROP of LA, CL and β -BL.

3.2.2 Structural Characterization of Polymers

In order to allow analysis of the growing polymer in real time, a 0.5 mL aliquot was taken from the reaction mixture at timed intervals and followed via 1H NMR. Complexes **2.1** and **2.2** showed no activity towards the ROP of ϵ -caprolactone, at ambient temperature over 2 hours, and only limited activity for β -butyrolactone. As shown in Figure 3.2 a large amount of monomer, β -BL, remained unreacted after 24 hours. Further investigations of the ROP with β -BL were not pursued due to the poor conversions obtained and the high cost of the monomer.

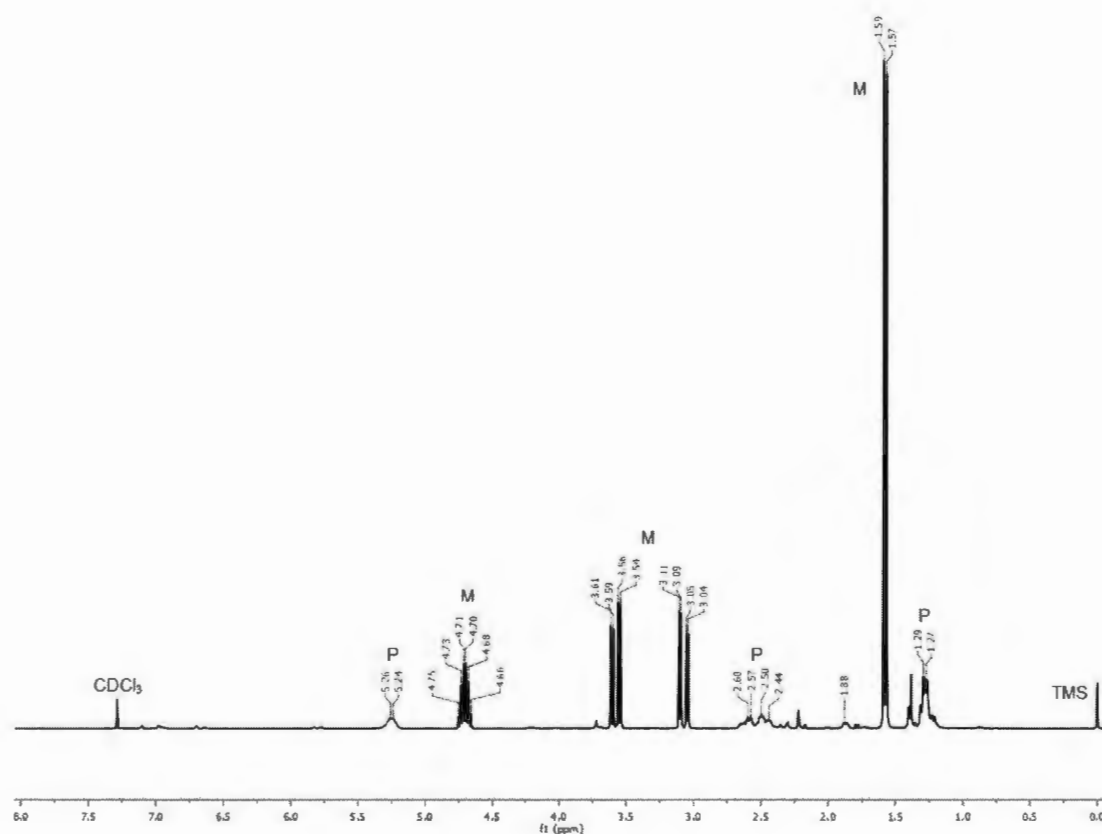


Figure 3.2. ^1H NMR spectrum for an attempted ROP reaction of β -BL, where M = monomer and P = polymer (in CDCl_3).

The ring-opening polymerization of DL-lactide (also known as *rac*-lactide) with complexes **2.1** and **2.2** in toluene, in the presence or absence of BnOH, was also examined (Table 3.1). For comparison purposes, complexes **3.1** and **3.2** were included in this study. The activity of this system was found to have a moderate dependence on the sterics of the substituents on the phenolates, where complex **2.1** gave slightly higher conversions than the more sterically demanding complex **2.2** (entries 1 and 6). Interestingly, PLA could be produced in the presence or absence of BnOH, while not

having a significant effect on the activity of conversion. However, the calculated number-averaged molecular weights (M_n), $M_n(\text{calcd})$, for theoretical, and $M_n(\text{obsd})$, for experimental, were observed to vary significantly, along with the polydispersity indices (PDIs) (entries 2, 3 for **2.1** and 7, 8 for **2.2**). In the absence of BnOH lower molecular weights and very broad PDIs were observed. The polymerization of *rac*-lactide was observed to reach completion within 120 minutes at 26 °C with a monomer-to-initiator ratio of 100:1. Analogous tetradentate lithium compounds (**1.46**, **1.47** and **1.48**) reported by Chen were found to polymerize L-lactide in the presence of BnOH and CH₂Cl₂ at 26.5 °C within 20 min having a monomer-to-initiator ratio of 100:1 with conversions above 90%.¹¹

In the case of complexes **3.1** and **3.2**, the polymerizations were found to be near completion within 30 min at ambient temperature when 2 equivalents of BnOH were employed (entries 12 and 16). Similar to what was observed with initiators **2.1** and **2.2**, the sterically bulkier complex **3.2** gave somewhat lower conversions than **3.1**. This trend has been reported in other ROP studies involving lithium.¹² The difference between $M_n(\text{calcd})$ and $M_n(\text{obsd})$ were also found to vary significantly for the reactions initiated with complexes **3.1** and **3.2**. The polydispersity indices (PDIs) were generally observed to be broad, greater than 1.5, suggestive that the polymerization is occurring in an uncontrolled manner and that transesterification took place. An increase in the PDIs was also observed for increasing [LA]:[Li] ratios and in the absence of BnOH. These higher PDIs are uncharacteristic of bi-, tri- and tetradentate lithium bis(phenolate) complexes previously reported in the literature for the ROP of L-lactide, where generally well controlled systems produced low PDIs.¹¹⁻¹⁴ Interestingly, the addition of 2 equivalents of

BnOH to the reactions involving **3.1** and **3.2** was shown to lower the PDIs to 1.3 and 1.2, respectively (Table 3.1, entries 12 and 16). As well, longer reaction times were observed to increase the PDIs moderately from 1.3 to 1.5 (entries 12 and 11 for **3.1**) and 1.2 to 1.3 (entries 16 and 15 for **3.2**), respectively.

No immortal character was observed for these systems, based on entries 10, 12 and 13 for **3.1**; and entries 14, 16 and 17 for **3.2**, as the increase in the ratio of BnOH was found to produce an increase in the M_n , rather than a decrease.¹¹ The resumption experiment for initiator **2.1** (entry 5) does exhibit some living character for the polymerization process, as an additional 100 equivalents of LA continued to generate PLA after 2 hours, albeit at a slower rate than the initial 2 hours. Unfortunately, broad PDIs are obtained for these reactions, indicating that the polymerization behaves in an uncontrolled manner. Furthermore, the gel permeation chromatography (GPC) traces were in general not well defined, at times possessing shoulders and tended to elute as broad peaks, making analysis difficult.

Table 3.1 ROP of *rac*-LA initiated by complexes **2.1**, **2.2**, **3.1** and **3.2**^a

Entry	Initiator	[Li]:[LA]: [BnOH]	<i>t</i> (min)	Conv. (%) ^b	<i>M</i> _n (calcd) ^c	<i>M</i> _n (NMR) ^b	<i>M</i> _n (obsd) ^d	PDI ^d
1	2.1	1:50:0.25	120	98	28 400	42 800	2100	4.1
2	2.1	1:50:1	120	99	7240	7300	5811	1.6
3	2.1	1:50:0	60	86	6200	15 300	3280	4.1
4	2.1	1:100:1	120	99	14 400	14 400	5951	1.7
5 ^e	2.1	1:100(100):1	120(120)	96(78)	13 900	20 400	5577	1.7
6	2.2	1:50:0.25	120	96	27 800	10 800	2793	1.8
7	2.2	1:50:1	120	99	7200	6700	5208	1.5
8	2.2	1:50:0	120	91	6300	8400	2187	2.5
9	2.2	1:100:1	120	99	14 400	14 800	5473	1.8
10	3.1	1:50:0.5	120	94	13 700	8800	1651	2.4
11	3.1	1:50:2	120	98	3600	3400	2273	1.5
12	3.1	1:50:2	30	98	3600	3000	4016	1.3
13	3.1	1:50:1	30	89	6500	7000	1610	2.4
14	3.2	1:50:0.5	120	92	13 400	11 000	1509	2.3
15	3.2	1:50:2	120	98	3600	3300	1987	1.3
16	3.2	1:50:2	30	95	3500	2800	3870	1.2
17	3.2	1:50:1	30	88	6450	4900	1624	2.3

^a Reaction conditions: T = 26 °C, toluene (10 mL). ^b Calculated from ¹H NMR analysis. ^c Calculated from $(\frac{[LA]}{[Li]} \times \text{conv. \%}/100 \times 144.13/[BnOH]) + 108.14$. ^d Determined by gel permeation chromatography in CHCl₃, calculated by including the correction factor of 0.58,¹⁵ calibrated with polystyrene standards.

^e Values in brackets represent the resumption experiment.

Reactions performed at increased temperatures were also explored for complexes **2.1** and **2.2** conducted in toluene with BnOH. Aliquots were taken of the reaction mixture at specific time intervals and measured by ¹H NMR. All plots of % conversion versus time for the various temperatures followed a similar trend to what is shown in Figure 3.3. The remaining plots can be found in Appendix C. Significantly shorter reaction times were needed for the polymerizations to go to completion upon increasing the temperature to 40, 60 and 80 °C (Table 3.2). Conversions were nearly complete after only 6 min at 80 °C (entries 4 for **2.1** and 8 for **2.2**). It should be noted that at 60 °C and above the product did not precipitate upon addition of cold methanol, rather a thick, viscous solution was

obtained. This suggests that the product formed at these higher temperatures may be oligomers rather than long chain polymers and therefore, M_n and PDI analysis could not be performed on these products.

A similar trend between **2.1** and **2.2** is observed for reactions carried out at elevated temperatures as with room temperature, where the 'Bu, Me analogue (**2.1**) produces slightly higher conversions than **2.2** (Table 3.2). Overall the M_n values of the polymer samples generated from heating the reactions were found to be higher than at room temperature (entries 1, 2 and 5, 6). PDIs were still observed to be high at increased temperatures indicating the polymerizations were still proceeding in an uncontrolled fashion.

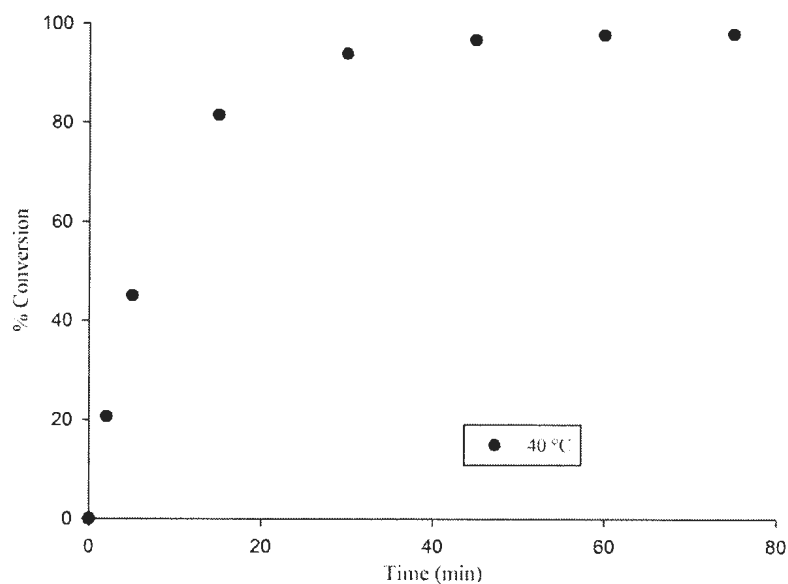


Figure 3.3. % conversion vs. time for the ROP of LA at 40 °C initiated by **2.1**.

Table 3.2 ROP of *rac*-LA initiated by complexes **2.1** and **2.2**^a

Entry	Initiator	[Li]:[LA]: [BnOH]	<i>t</i> (min)	T (°C)	Conv. (%) ^b	<i>M_n</i> (calcd) ^c	<i>M_n</i> (NMR) ^b	<i>M_n</i> (obsd) ^d	PDI ^d
1	2.1	1:100:1	60	26	76	11 100	12 800	5851	1.6
2	2.1	1:100:1	30	40	94	13 700	13 700	8765	1.7
3	2.1	1:100:1	15	60	97	14 100	15 700	-	-
4	2.1	1:100:1	6	80	96	13 900	16 000	-	-
5	2.2	1:100:1	60	26	67	10 000	11 000	5409	1.5
6	2.2	1:100:1	30	40	92	13 500	15 700	7688	1.5
7	2.2	1:100:1	15	60	96	13 900	15 700	-	-
8	2.2	1:100:1	6	80	95	13 800	14 200	-	-

^a Reaction conditions: toluene (10 mL). ^b Calculated from ¹H NMR analysis. ^c Calculated from $(\frac{[LA]}{[Li]} \times \text{conv. \%}/100 \times 144.13)/[BnOH] + 108.14$. ^d Determined by gel permeation chromatography in CHCl₃, calculated by including the correction factor of 0.58,¹⁵ calibrated with polystyrene standards.

Plots of the ROP of *rac*-lactide were generated for the temperature dependent studies in order to gain insight into the reaction kinetics of these systems (Figure 3.4 for **2.1** and Figure 3.5 for **2.2**). In order to determine the appropriate rate constant for the system, plots of zero-order, first-order and second-order rate laws were generated. Based on the line obtained from the plots, the appropriate rate law could be determined. To test for a zero-order rate law the integrated zero-order equation was used (Equation 3.1).

$$[LA]_t = -kt + [LA]_0 \quad (3.1)$$

where $[LA]_t$ represents the concentration of the monomer at a particular time, and $[LA]_0$ represents the initial concentration. A plot of $[LA]_t$ versus time did not produce a straight line for any of the temperatures examined. The first-order reaction equation of the integrated rate law is shown in Equation 3.2.

$$\ln[LA]_t = -kt + \ln[LA]_0 \quad (3.2)$$

A plot of $\ln[LA]_0/\ln[LA]_t$ versus time was found to produce straight lines for the majority of the reactions. For second-order reactions the integrated rate law is given in Equation 3.3.

$$1/[LA]_t = 1/[LA]_0 + kt \quad (3.3)$$

A plot of $1/[LA]_t$ versus time was found to give straight lines for only the highest temperatures used, and indicate transesterification.¹⁶

Preliminary studies indicate a first-order dependence on the monomer concentration for 26 and 40 °C and second-order dependence for 60 and 80 °C for **2.1** (Figure 3.4). Because the LA is effectively consumed within 10 minutes, at these temperatures, only 3 data points could be obtained at 60 and 80 °C, therefore the rates obtained are crude, but do support second-order reactions. A similar trend was found for **2.2** as shown in Figure 3.5. A noticeable change occurred at higher temperatures, where the rate law is observed to follow a second-order reaction, suggesting transesterification side-reactions now dominate, and short-chain polymers are obtained. The uncontrolled nature of the polymerization, as well as initiator decomposition at increased temperatures could also affect the polymerization. Both **2.1** and **2.2** appear to possess an induction period for the reactions performed at ambient temperature. Induction periods have been shown to occur in ROP of lactide when the monomer is slow to coordinate to the initiator, which may be a result of the dimer dissociating to form the active species.¹⁷

Polymerization was observed to occur without the addition of BnOH. Although, rate constants were found to be the same within experimental error in the absence of BnOH compared to when it is added to **2.1** and **2.2**. This reaction proceeds due to the presence of metal-phenoxy bonds on these complexes, which can undergo nucleophilic attack at the LA carbonyl carbon.

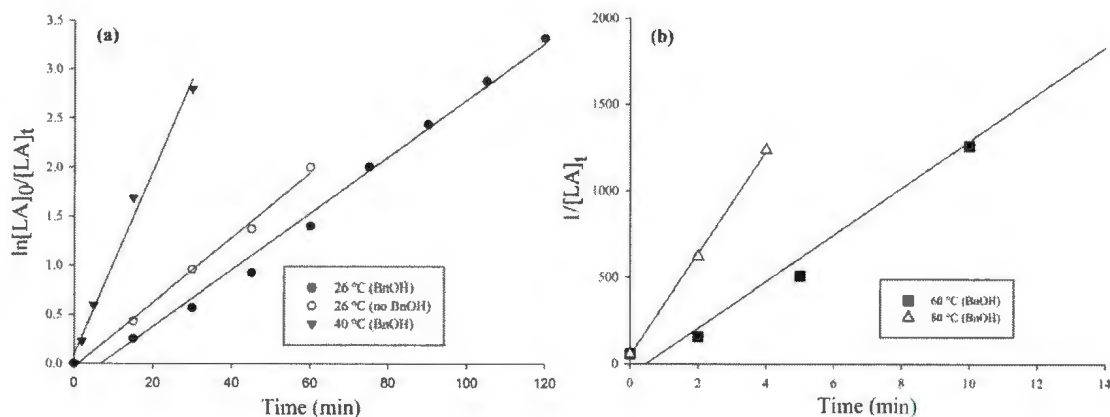


Figure 3.4. Plots of $\ln[LA]_0/[LA]_t$ vs. time and $1/[LA]_t$ vs. time, $[LA]_0/[2.1]_0 = 100$, $[Li] = 17.2$ mM; (a) ● = 26 °C (BnOH) ($R^2 = 0.97_6$), ○ = 26 °C (no BnOH) ($R^2 = 0.98_2$), ▼ = 40 °C (BnOH) ($R^2 = 0.98_9$), and (b) ■ = 60 °C (BnOH) ($R^2 = 0.98_5$), △ = 80 °C (BnOH) ($R^2 = 0.99_9$).

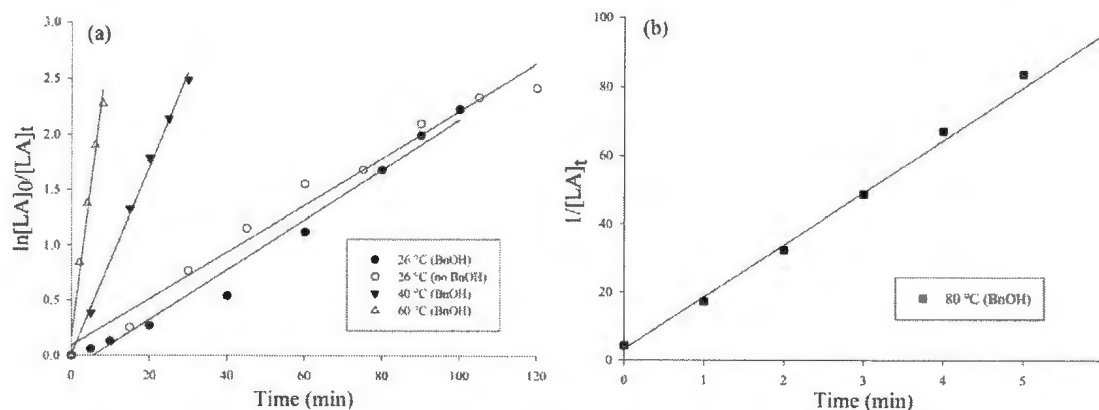


Figure 3.5. Plots of $\ln[LA]_0/[LA]_t$ vs. time and $1/[LA]_t$ vs. time, $[LA]_0/[2.2]_0 = 100$, $[Li] = 14.7$ mM; (a) ● = 26 °C (BnOH) ($R^2 = 0.97_4$), ○ = 26 °C (no BnOH) ($R^2 = 0.97_4$), ▼ = 40 °C (BnOH) ($R^2 = 0.99_7$), △ = 60 °C (BnOH) ($R^2 = 0.96_7$), and (b) ■ = 80 °C (BnOH) ($R^2 = 0.99_4$).

Rate constants determined for **2.1** and **2.2** are presented in Table 3.3. Increasing temperatures produced higher rate constants for both **2.1** and **2.2** (entries 1, 3 and 6, 8, respectively). As previously mentioned, a small increase in activity is observed for initiator **2.1** over **2.2** (entries 1, 2, 3, 4 and 5). The absence of BnOH at 26 °C was shown to give similar reaction rates to that with BnOH (entries 6 and 7 for **2.2**). The rate constants obtained at 60 and 80 °C for **2.1** and at 80 °C for **2.2** were calculated using a second-order dependence on monomer (entries 4, 5 and 10). Unfortunately, these rate constants cannot be directly compared to other lithium bis(phenolate) initiators as no prior kinetics data for *rac*-lactide have been presented in the literature. However, comparison of these rate constants to other initiators employing bis(phenolate) ligands was possible. It should be noted that the ligands used in the literature vary from the system employed here. The ROP reactions from the literature were performed at 70 °C in toluene with a monomer-to-initiator ratio of 100:1, unless otherwise stated. An aluminium alkyl bis(phenolate) complex, having a bis(thioether) backbone (AlMe[OSSO]) was found to have a first-order k_{obs} of $5.74 \times 10^{-3} \text{ min}^{-1}$.¹⁸ Further studies by Okuda's group showed a similar Al complex, (*rac*-Al[OSSO]) giving a slightly higher, but still slow rate constant $k_{\text{obs}} = 1.02 \times 10^{-2} \text{ min}^{-1}$.¹⁹ Both **2.1** and **2.2** are found to possess slightly faster rates than these Al systems. An indium amine-bis(phenolate) complex, $\text{In}[\text{O}_2\text{NN}^{\text{MeMe}}(\text{CH}_2\text{SiMe}_3)]$, was found to have a $k_{\text{obs}} = 1.27 \times 10^{-2} \text{ min}^{-1}$,²⁰ possessing a slower rate than what was observed for initiator **2.2** at 60 °C. Miller and Lin⁷ have also reported a sodium bis(phenolate) complex, (EDBPH)Na(MeOH)₂(THF)₂, similar to their previous reported lithium analogues (**1.38**, **1.39**, **1.40**, **1.43**, **1.44** and **1.45** as previously shown in Chapter 1),^{21,22} where a $k_{\text{obs}} = 8.4 \times 10^{-3} \text{ min}^{-1}$ was determined from their kinetic study performed

in THF at 20 °C with a monomer-to-initiator ratio of 63:1. Lithium complexes **2.1** and **2.2** are found to have faster rate constants than the sodium complex presented above.

A recent report of related Li complexes (lithium piperazinyl-aminephenolates) studied for the ROP of ϵ -caprolactone at 40 °C in toluene was found to have similar rate constants (0.019 – 0.273 min⁻¹) to complexes **2.1** and **2.2**.²³

Although the majority of rate laws presented in the literature are first-order with respect to lactide, second-order dependence on lactide concentration has been observed. Comparison of the k_{obs} obtained for **2.1** and **2.2** to those in the literature for L-lactide found these catalysts to be superior. The ROP of L-lactide at room temperature afforded rates of 0.0375 to 0.0938 and 1.98 M⁻¹min⁻¹ for lanthanide phenolate²⁴ and zinc-BDI²⁵ catalysts, respectively. Furthermore, a recent study by Williams and co-workers²⁶ employing a phosphasalen-yttrium complex (200:1) was found to have a similar k_{obs} (15.1 M⁻¹min⁻¹) to that of complex **2.2** at 80 °C.

Table 3.3 Rate constants for the ROP of LA initiated by **2.1** and **2.2**.^a

Entry	Initiator	T (°C)	k_{obs}
1	2.1	26	0.026 min ⁻¹
2 ^b	2.1	26	0.032 min ⁻¹
3	2.1	40	0.093 min ⁻¹
4 ^c	2.1	60	$1.3 \times 10^2 \text{ M}^{-1} \text{ min}^{-1}$
5 ^c	2.1	80	$2.9 \times 10^2 \text{ M}^{-1} \text{ min}^{-1}$
6	2.2	26	0.021 min ⁻¹
7 ^b	2.2	26	0.022 min ⁻¹
8	2.2	40	0.086 min ⁻¹
9	2.2	60	0.31 min ⁻¹
10 ^c	2.2	80	$1.5 \times 10^1 \text{ M}^{-1} \text{ min}^{-1}$

^a Polymerization conditions: [LA]₀/[Li]₀ = 100, solvent = Toluene (10 mL). ^b Reaction done without BnOH.

^c Second-order rate constant.

3.2.2.1 NMR Spectroscopy

Nuclear Magnetic Resonance (NMR) spectroscopy is a powerful method used in the analysis of polymers. Specifically, the reaction can be monitored by taking aliquots of the polymer solution at desired time intervals through out the polymerization, as shown in Figure 3.6. Through ^1H NMR, the % conversion and yield were calculated by integrating the methine region of the PLA at 5.17 ppm and normalizing the CH proton from LA to 1 at 5.02 ppm. Comparison of these two peaks allowed the determination of the theoretical yield and hence calculation of the actual yield and conversion.

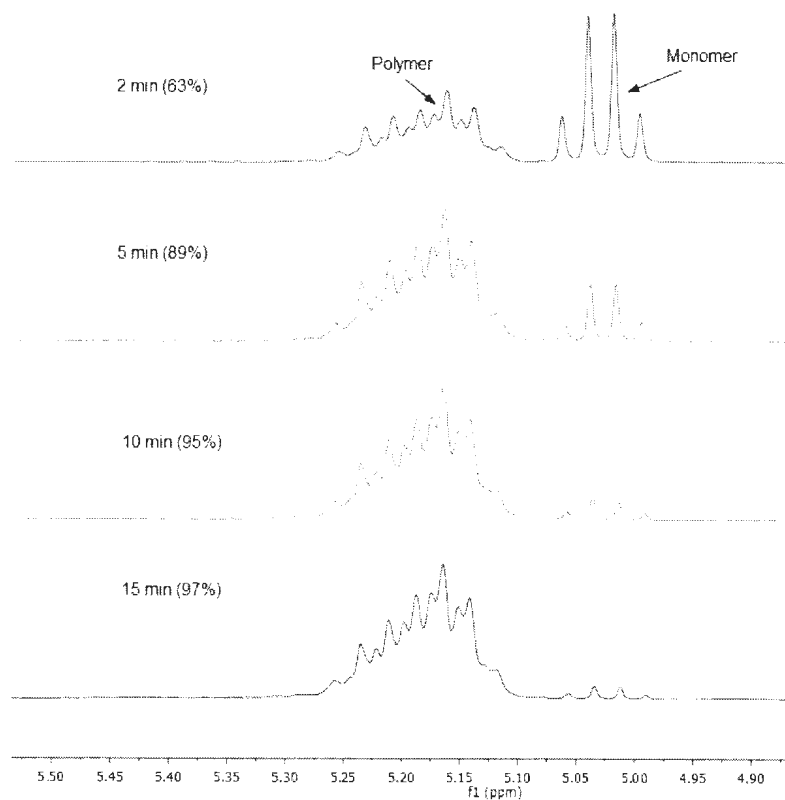


Figure 3.6. ^1H NMR spectra of the methine region for aliquots taken from ROP of LA initiated by complex **2.1** at 60 °C (300 MHz, CDCl_3).

Typical ^1H NMR spectra of the resulting polymers were found to show the corresponding peaks of PLA as labelled in Figure 3.7. End group analysis of the polymers was also made possible through ^1H NMR spectroscopy. Reactions performed in the presence of BnOH exhibited the distinctive chemical shifts for the benzyl ester group (OCH_2Ph), (e) at 7.35 ppm; methylene group (CH_2Ph), (d) and the methine group (OCHMe), (b) at 5.17 ppm; a hydroxymethine group (HOCH-), (c) at 4.38 ppm; a hydroxyl group (HOCH-), (g) at 2.70 ppm; and the methyl group (CHCH_3), (a) at 1.57 ppm and (f) at 1.48 ppm as shown in Figure 3.7.²⁷⁻²⁹ This suggests that the polymer chains likely formed through a coordination-insertion mechanism. The ^{13}C NMR also provided evidence towards these end-groups mentioned above. Chemical shifts appeared at 128.82 and 69.20-69.62 ppm correspond to the (OCH_2Ph) and (HOCH-) regions respectively (Figure 3.8). Additionally, the average chain length (n) and the number average molecular weight (M_n) of the polymers could be estimated from the ^1H NMR spectra by integration and comparison of the methyl (a) and phenyl (e) peaks. It was found that the $M_n(\text{NMR})$ values were generally similar to the $M_n(\text{calcd})$. However, values were found to differ when less than 1 equivalent of BnOH was used (Table 3.1). A significant difference is observed between the $M_n(\text{NMR})$ values and the M_n observed by GPC. The low molecular weight for the values determined by GPC is uncharacteristic and suggests that the polymer may be breaking apart into smaller chains while in solution.

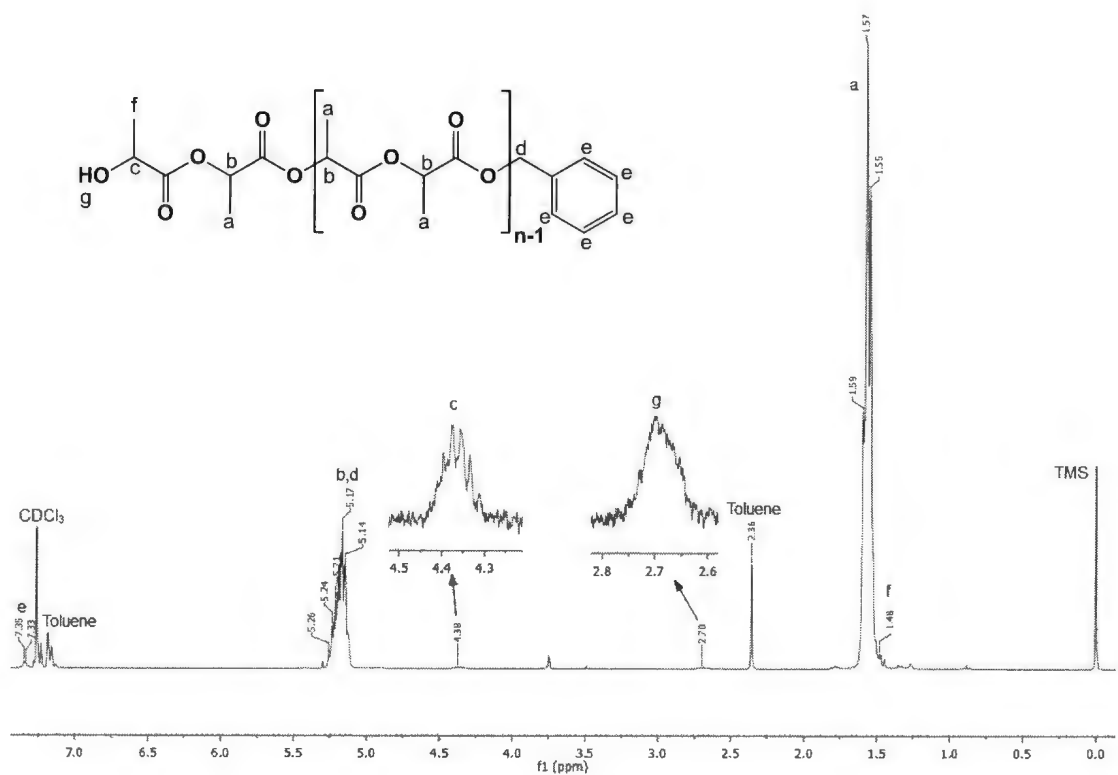


Figure 3.7. Typical ¹H NMR spectrum of [LA]:[Li]:[BnOH] = 1:100:1 in CDCl₃, 300 MHz (entry 9, Table 3.1).

chain transfer may be occurring through a contaminant in the reaction mixture, producing shorter than expected polymer chains.

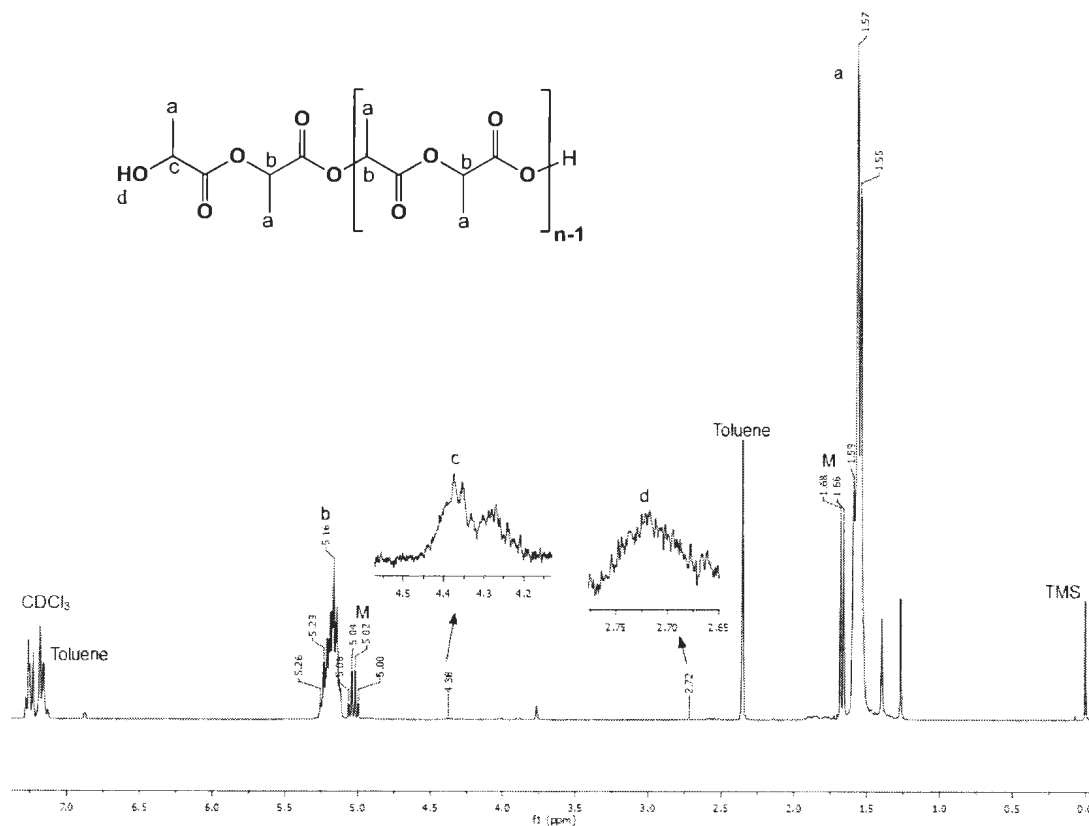


Figure 3.9. Typical ^1H NMR spectrum of $[\text{LA}]:[\text{Li}]:[\text{BnOH}] = 1:50:0$ in CDCl_3 , 300 MHz (entry 8, Table 3.1), where M = monomer.

Additionally, the tacticity of the PLA produced could also be determined by NMR, via ^{13}C and homodecoupled ^1H NMR experiments. The resonances representing the methine region in the ^{13}C NMR spectrum, 69.20-69.62 ppm (left image in Figure 3.10), were found to be attributed to tetrads as previously described in the literature.³⁰⁻³² The weaker resonances observed at 69.62, 69.50 and 69.28 ppm are an indication that

some transesterification or racemisation has occurred, which changes a normally atactic polymer to appear more isotactic.³³ This apparent change in tacticity is due to an inversion of the stereocentres.³⁴ Additionally, the P_r values (probability of racemic enchainment of the monomer unit) for complexes **2.1** and **2.2** were found to range between 0.50-0.59. The apparent increase in P_r values is typical when transesterification has occurred, signifying that the synthesized polymers actually possess a heterotactic bias.^{35,36} Therefore, the methine region of the homodecoupled ^1H NMR spectrum (right image in Figure 3.10), provided further evidence towards this perceived change in tacticity. Decoupling of the methyl protons provides a significant improvement in the resolution of the methine resonance.³⁴ The $^1\text{H}\{^1\text{H}\}$ spectrum was also shown to be in agreement with the observed ^{13}C spectrum (Figure 3.10). Interestingly, the tridentate lithium complexes **3.1** and **3.2** were observed to have P_r values of 0.38 and 0.39, respectively, leading to a more isotactic polymer being produced from these initiators. This result indicates a more stereocontrolled reaction may be occurring in the presence of the tridentate lithium complexes.

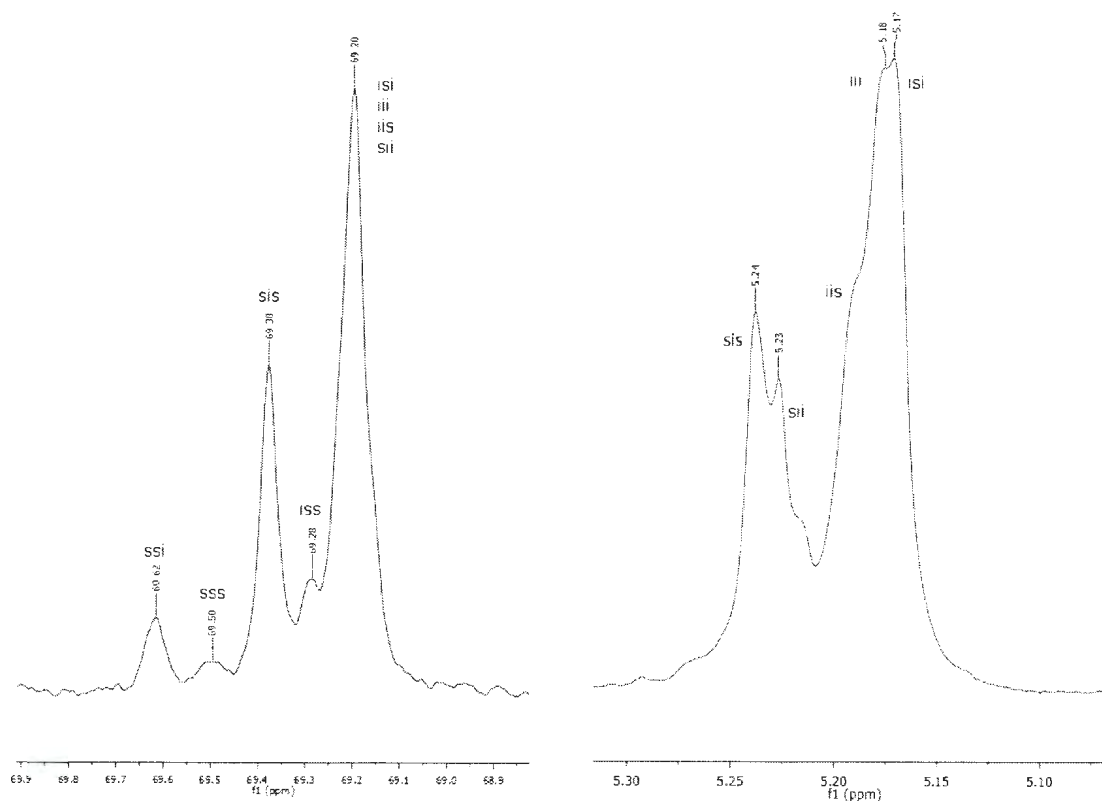


Figure 3.10. (Left) ^{13}C NMR spectrum (75.49 MHz, CDCl_3) and (Right) $^1\text{H}\{^1\text{H}\}$ NMR spectrum (500 MHz, CDCl_3) of the methine region of PLA produced by $[\text{LA}]_0:[\mathbf{2.1}]_0:[\text{BnOH}]_0 = 100:1:1$ in toluene.

3.2.2.2 Mass Spectrometry

Mass spectrometry (MS) experiments involving matrix assisted laser desorption ionization time-of-flight (MALDI-TOF) MS provide important analysis of the polymer composition and can offer further mechanistic insight. The MALDI-TOF mass spectrum, shown in Figure 3.11, on the isolated polymer reveals that the main repetition pattern, starting at m/z 1098.5, has a repeating unit of 72 Da. This mass corresponds to a half

monomer unit (-OCHMeC(O)-), labelled $(LA/2)_n$. The major repeating series corresponds to the cyclic species $(LA/2)_n$ where the peaks are sodiated.³⁷ The next minor series are cycles of $(LA/2)_n + K^+$, and chains of $H-(LA/2)_n-OH + K^+$ or $H-(LA/2)_n-OH + Na^+$, just detectable in the MALDI spectrum. In each series the repeating unit differs by 72 Da. Intramolecular transesterification is known to produce an even- or odd-number of half-lactide units, as was observed here.³⁷ The results of the MALDI-TOF MS provide additional support for the low molecular weights found from GPC analysis. This also offers a reason as to why the M_n values calculated from the 1H NMR spectra was found to be significantly higher than the GPC values. In transesterification reactions the formation of cyclic polymers are known to produce end group resonances that are less intense. This leads to an increase in the M_n values as calculated by 1H NMR.³⁸

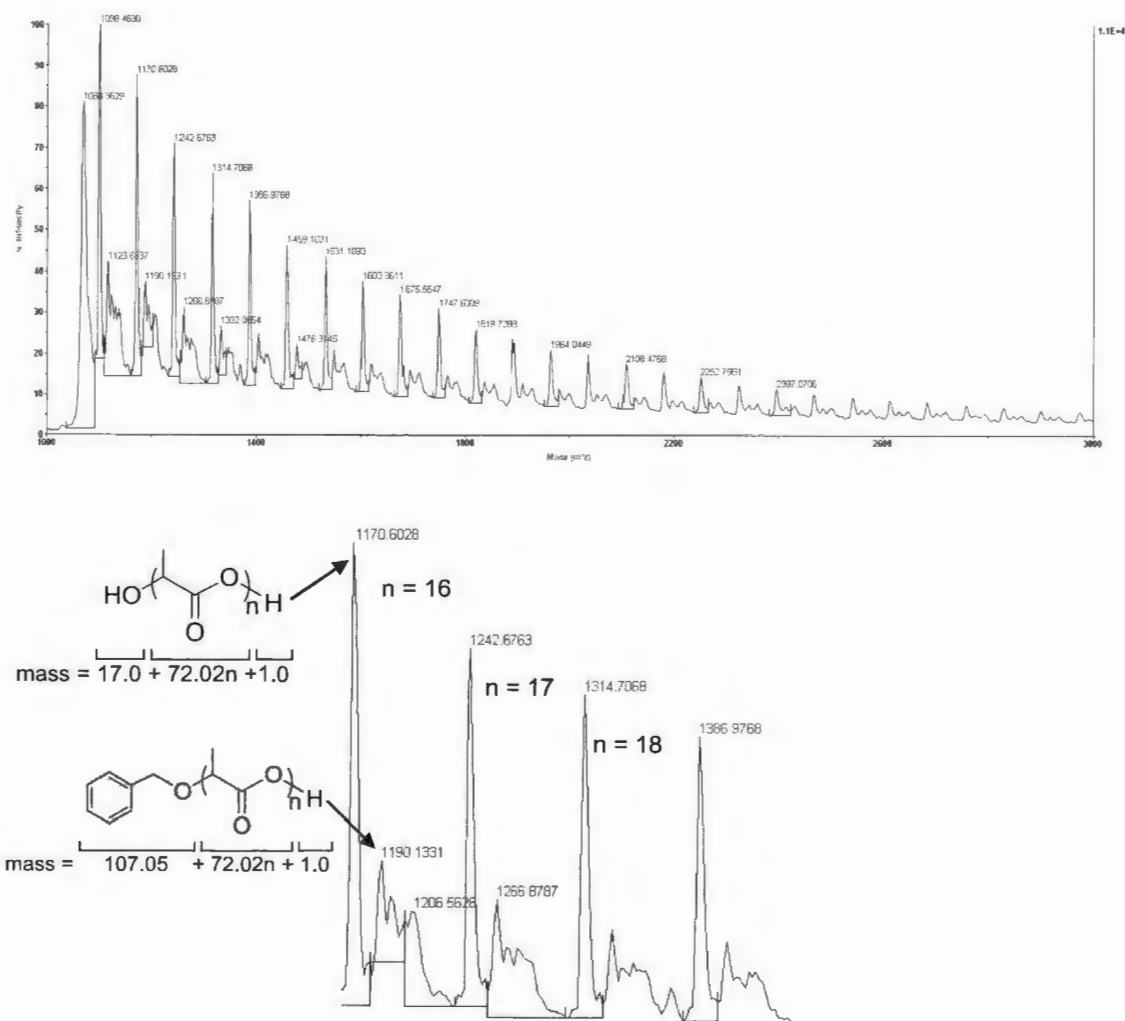


Figure 3.11. Typical MALDI-TOF mass spectrum of PLA (entry 9, Table 3.1).

3.2.2.3 Gel Permeation Chromatography

Gel permeation chromatography (GPC), also known as size exclusion chromatography (SEC), separates compounds based on their size rather than their chemical interactions with the column. Generally, in GPC the chromatogram obtained is

the plot of the differential weight fraction ($dw/d \log M$) versus the logarithm of the molar mass ($\log M$), representing the average molecular weight distribution.³⁹ It is widely accepted that a significant overestimation of M_n values occurs for polyesters when using polystyrene standards. For this reason methods have been developed to determine an appropriate correction factor from the Mark-Houwink parameter of the polymer, where a correction of 0.58 is employed for calculating the absolute average molar mass of PLA.^{15,40}

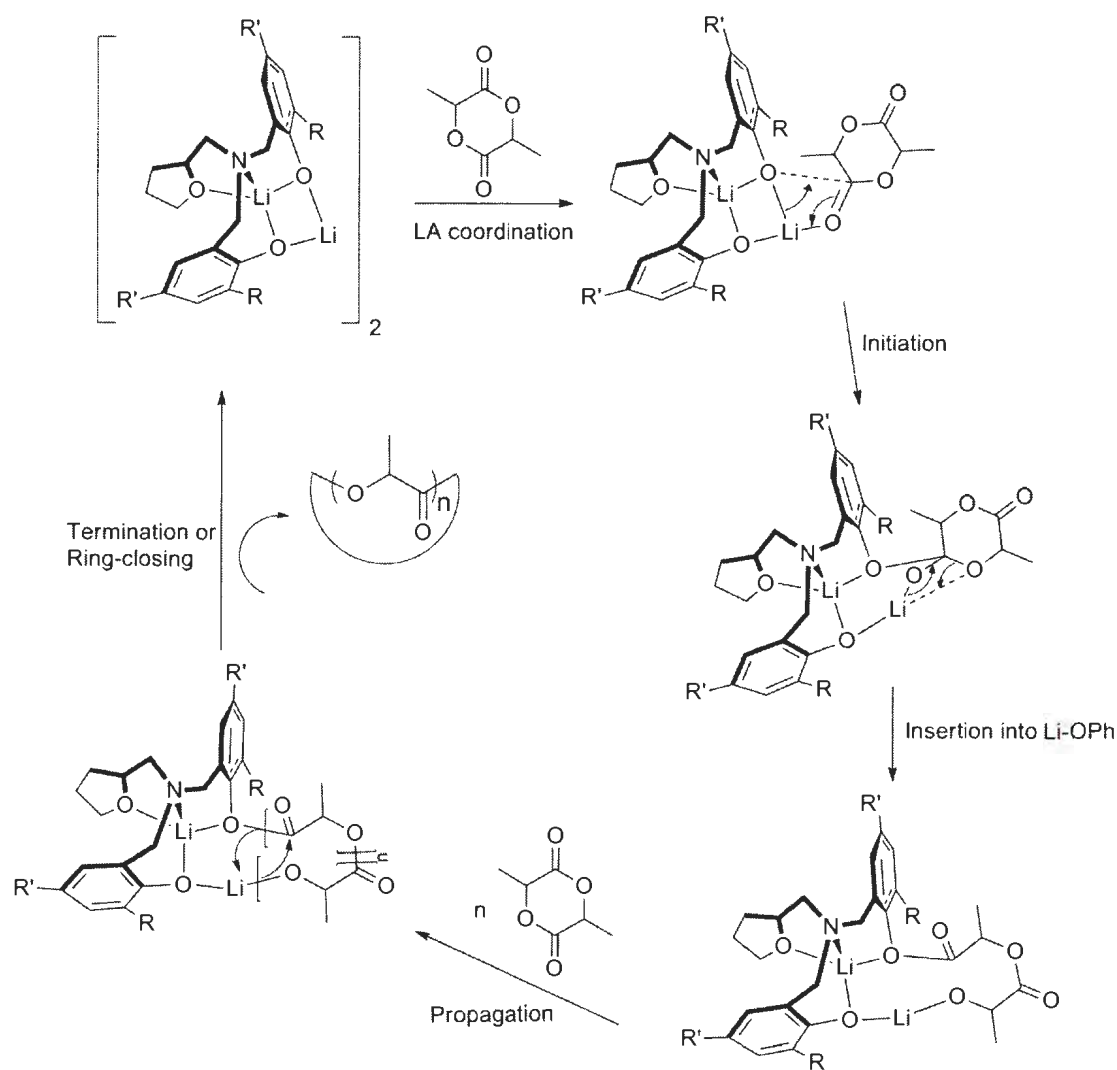
GPC traces of polymers from complexes **2.1** and **2.2** yielded M_n values ranging from 2000 to 9000 g/mol. Molecular weight distributions were generally found to be broad (PDI = 1.3-4.1). Observed M_n values were found to be quite different to calculated M_n values, with the exception of the reactions with a ratio of $\{[LA]:[Li]\}:[BnOH] = 50:1$ (entries 2 and 7, Table 3.1). Interestingly, the M_w/M_n values for these reactions were the lowest for complexes **2.1** and **2.2**. The broadening of the polydispersities and the low M_n values compared to those expected can be most likely linked to the resulting transesterification taking place. Additionally, the reactions performed in a reduced amount or the absence of BnOH gave some of the highest polydispersities, suggesting the polymerization may be occurring in a more uncontrolled manner. Increasing the temperature and reaction time was shown to have an adverse effect on the PDIs. GPC data for 60 and 80 °C could not be obtained due to the lack of precipitation of the polymer. This was most likely due to the highly uncontrolled nature of the polymerizations when performed with these reaction conditions, resulting in short oligomer chains.⁴¹

A similar trend was observed for complexes **3.1** and **3.2**, where molecular weights in the range of 1000-4000 g/mol were observed. Broad PDI values were also characteristic for these polymers with the exception of reactions performed with 2 equivalents of BnOH, where narrower PDIs were observed (entries 11, 12, 15 and 16, Table 3.1). Unlike the reactions initiated by **2.1** and **2.2**, initiators **3.1** and **3.2** showed significantly higher PDI values and deviations from the expected M_n for the 50:1 reaction ratio. This indicates that transesterification may be more dominant in the tridentate systems. Reactions were not performed at elevated temperatures for initiators **3.1** and **3.2**.

3.2.3 Mechanistic Proposal

Through the results obtained in the kinetic studies, NMR, MALDI-TOF MS and GPC it can be proposed that ring-opening polymerization for this system could be proceeding via insertion of the monomer into the metal-phenoxide bond, as previously proposed in the literature.^{42,43} This polymerization process is likely hindered through 'back-biting' or transesterification or hydrolysis by reaction contaminants from the initiator (i.e. water). In the ¹H NMR spectra of reactions including and excluding BnOH, terminal -CHOH peaks are present, supporting this hypothesis. Although end-groups are present in the ¹H NMR, MALDI-TOF analyses of the polymer samples show cyclic polymer formation as the dominant peaks observed. The presence of these cyclic species is also confirmed by the lower than expected molecular weights found in the GPC traces. These cycles are likely forming through a coordination-insertion mechanism into the Li-phenolate bond, followed by propagation and finally termination or ring-closing to

produce the cyclic polymers (Scheme 3.2). This result is not surprising as alkali metal initiators, such as lithium have been known to suffer from undesirable side reactions like back-biting and transesterification, producing cyclic esters, broad or bimodal polydispersities and catalyst inhomogeneity.^{7,9,21,41}



Scheme 3.2. Proposed mechanism of the ROP of *rac*-LA initiated by $\{Li_2[O_2NO]^{RR'}\}_2$.

3.3 Experimental

3.3.1. General Experimental Conditions

Unless otherwise stated, all manipulations were performed under an atmosphere of dry, oxygen-free nitrogen by means of standard Schlenk techniques or using an MBraun Labmaster glove box. Anhydrous toluene was purified by an MBraun Manual Solvent Purification System. THF was distilled from sodium benzophenone ketyl under nitrogen. ϵ -CL and β -BL were purchased from Aldrich and freshly distilled over calcium hydride (CaH_2), vacuum transferred and stored under nitrogen in ampules fitted with Teflon valves. DL-lactide (*rac*-lactide) was purchased from Alfa Aesar and dried over magnesium sulfate in THF and stored under an inert atmosphere. BnOH was purchased from Alfa Aesar and dried over activated 4 Å molecular sieves, distilled under reduced pressure and stored under nitrogen in an ampule prior to use. ^1H NMR spectra were recorded on either a Bruker AVANCE 500 MHz or a Bruker AVANCE III 300 MHz spectrometer. ^{13}C NMR spectra were obtained on a Bruker AVANCE III 300 MHz spectrometer at 75.487 MHz. CDCl_3 was purchased from Cambridge Isotope Laboratories. Chemical shifts are given in ppm relative to TMS. Homonuclear decoupled ^1H NMR (CDCl_3) was used to determine the P_r from the methine region of the spectra. Equations previously reported by Coates⁴⁴ were used to calculate the amount of racemic enchainment.

3.3.2. Polymerization Procedure

For all polymerization calculations ratios were calculated per Li center.

ϵ -Caprolactone: All attempted reactions were performed in the glove box at 26 °C. A vial with the appropriate amount of initiator (0.047 mmol) and BnOH (0.047 mmol) in toluene (10 mL) was added to another vial containing a stir bar and the monomer (2.5 mmol). The reaction mixture was stirred for the appropriate time. An aliquot of the reaction mixture was taken for ^1H NMR analysis, followed by quenching the reaction with methanol. An additional 10 mL of cold methanol was added to the product and left in the freezer to precipitate. Unfortunately no precipitation occurred. All attempts at purification and separation of the product were unsuccessful. ^1H NMR for ϵ -CL (500 MHz, 298 K, CDCl_3 , δ): 4.21 (t, $J_{\text{HH}} = 4.6$ Hz, OCCH_2CH_2 , 2H); 2.64 (t, $J_{\text{HH}} = 4.6$ Hz, OCH_2CH_2 , 2H); 1.85 (m, $\text{CH}_2\text{CH}_2\text{CH}_2$, 2H); 1.76 (m, $\text{CH}_2\text{CH}_2\text{CH}_2$, 4H).

β -Butyrolactone: All attempted reactions were performed neat in the glove box. A vial containing the initiator (0.047 mmol) and monomer (2.5 mmol, 100 equiv.) was immediately stirred with a magnetic stir bar at 26 °C for 24 hr. An aliquot was removed for ^1H NMR analysis, followed by quenching the reaction with methanol. ^1H NMR for β -BL (300 MHz, 298 K, CDCl_3 , δ): 4.71 (m, OCHCH_3 , 1H); 3.61 (d, $J_{\text{HH}} = 5.7$ Hz, CH_2 , 1H); 3.11 (d, $J_{\text{HH}} = 4.2$ Hz, CH_2 , 1H); 1.59 (d, $J_{\text{HH}} = 6.1$ Hz, CH_3 , 3H). ^1H NMR for PHB (300 MHz, 298 K, CDCl_3 , δ): 5.26 (br, m, OCHCH_3 , 1H); 2.60 (br, m, CH_2 , 1H); 2.50 (br, m, CH_2 , 1H); 1.29 (br, m, CH_3 , 3H).

***rac*-Lactide: Method A):** Solution polymerizations of LA with and without BnOH were prepared and performed in the glove box for room temperature experiments. The

appropriate monomer:initiator ratio was employed. A typical reaction (Table 3.1, entry 9) included a vial of a stock solution containing the initiator (0.0129 g, 0.0472 mmol) and BnOH (0.00510 g, 0.0472 mmol, where appropriate) in toluene (10 mL) was added to another vial containing a stir bar and the monomer (0.680 g, 4.72 mmol). The reaction mixture was stirred for the appropriate time. An aliquot of the reaction mixture was taken for ^1H NMR analysis, followed by quenching the reaction with methanol. An additional 10 mL of cold methanol was added to the product precipitating the polymer. Separation and removal of the solvent was followed by drying the polymer *in vacuo* to yield a white crystalline solid.

Method B): Solutions for the heated reactions were prepared in the glove box while the polymerization was performed via standard Schlenk techniques. A monomer:initiator ratio of 100:1 was employed. A typical stock solution of the initiator and BnOH consisted of (0.0999 g, 0.364 mmol) and (0.0393 g, 0.364 mmol) respectively, prepared in toluene (14.7 mM), (Table 3.2, for complex 2.2 entries). A 2.50 mL portion of this stock solution was placed in an ampule fitted with a Teflon valve. A second ampule containing a stir bar and the required amount of monomer and toluene (7.50 mL) was heated to the desired temperature. The initiator solution was added to the monomer ampule after being heated to the same temperature as the monomer solution. The mixture was then stirred for the appropriate time. An aliquot of the reaction mixture was taken for ^1H NMR analysis, followed by quenching the reaction with methanol. The product was then precipitated with cold methanol. After removal of the solvent the polymer was dried *in vacuo* to yield a white crystalline solid. ^1H NMR for LA (500 MHz, 298 K, CDCl_3 , δ): 5.05 (m, OCCCH_3 , 2H); 1.64 (d, $J_{\text{HH}} = 6.7$ Hz, CHCH_3O , 6H). ^1H NMR for PLA with

BnOH (300 MHz, 298 K, CDCl₃, δ): 7.35 (m, ArH, 5H); 5.17 (m, CHCH₃, 2H); 5.17 (m, CH₂Ar, 2H); 4.38 (br, m, HOCHCH₃, 1H); 1.54 (m, CHCH₃, 6H). ¹H NMR for PLA without BnOH (300 MHz, 298 K, CDCl₃, δ): 5.16 (m, CHCH₃, 2H); 4.38 (br, m, HOCHCH₃, 1H); 1.57 (m, CHCH₃, 6H).

3.3.3. MALDI-TOF Mass Spectrometry

MALDI measurements were performed on an Applied Biosystems 4800 MALDI TOF/TOF Analyzer equipped with a reflectron, delayed ion extraction and high performance nitrogen laser (200 Hz operating at 355 nm). 2,5-dihydroxybenzoic acid (DHBA) was used as the matrix. The matrix was dissolved in THF at a concentration of 10 mg/mL. Polymer was dissolved in THF at approximately 1 mg/mL. The matrix and polymer solutions were mixed together at a ratio of 5 to 1, respectively; 1 μ L of this was spotted on the MALDI plate and left to dry.

3.3.4. Gel Permeation Chromatography

GPC analysis was performed on a Viscotek VE 2001 GPCMax at 35 °C equipped with a Viscotek VE 3580 Refractive Index Detector, and two phenogel 5 μ Linear Mixed Bed columns purchased from Phenomenex (300 x 4.60 mm column in series with a 100 Å, 300 x 4.60 mm column). Samples were prepared at a concentration of 2 mg/mL and left to equilibrate for ~ 2 h. The samples were filtered through syringe filters before analysis. The GPC columns were eluted with chloroform (HPLC grade) at a flow rate of 0.35 mL/min with a 100 μ L injection volume. Six polystyrene standards (Viscotek) were

used in making the calibration curve, bracketing molecular ranges from 1050 to 3 800 000 Da. A correction factor of 0.58 was used to calculate the M_n value.

3.4 Conclusions

Lithium amine-bis(phenolate) complexes **2.1**, **2.2**, **3.1** and **3.2** were all found to initiate the ROP of *rac*-lactide in toluene solutions. Kinetic studies indicated that a first-order dependence on monomer concentration was achieved for 26 and 40 °C when initiated by **2.1** and 26, 40 and 60 °C for **2.2**. Second-order dependence was observed for 60 and 80 °C polymerization reactions of **2.1** and 80 °C for **2.2**. All rate constants obtained with initiators **2.1** and **2.2** have relatively fast kinetics, but control of the system still remains problematic. Similar activities were observed in the presence and absence of BnOH, indicating that complexes **2.1** and **2.2** were able to initiate the polymerization process through the metal-phenoxy bond. The polymers produced do show evidence of end-groups in their ^1H NMR spectra, although analysis through MALDI-TOF MS was dominated by the presence of cyclic polymers. This is most likely due to the presence of transesterification. Supporting evidence for such back-biting was also established from the molecular weights determined by GPC, where short-chain polymers or oligomers were obtained, differing drastically from the expected M_n values, and broad polydispersities were common.

3.5 References

- (1) Thompson, R. C.; Swan, S. H.; Moore, C. J.; vom Saal, F. S. *Phil. Trans. R. Soc. B* **2009**, *364*, 1973-1976.
- (2) Lunt, J. *Polym. Degrad. Stab.* **1998**, *59*, 145-152.
- (3) Auras, R.; Harte, B.; Selke, S. *Macromol. Biosci.* **2004**, *4*, 835-864.
- (4) Platel, R. H.; Hodgson, L. M.; Williams, C. K. *Polym. Rev.* **2008**, *48*, 11-63.
- (5) Labet, M.; Thielemans, W. *Chem. Soc. Rev.* **2009**, *38*, 3484-3504.
- (6) Baker, G. L.; Vogel, E. B.; Smith III, M. R. *Polym. Rev.* **2008**, *48*, 64-84.
- (7) Chen, H.; Zhang, J.; Lin, C.; Reibenspies, J. H.; Miller, S. A. *Green Chem.* **2007**, *9*, 1038-1040.
- (8) Blakey, I.; Yu, A.; Howdle, S. M.; Whittaker, A. K.; Thurecht, K. J. *Green Chem.* **2011**, *13*, 2032-2037.
- (9) Sutar, A. K.; Maharana, T.; Dutta, S.; Chen, C.; Lin, C. *Chem. Soc. Rev.* **2010**, *39*, 1724-1746.
- (10) Reckling, A. M. *Honours thesis*, **2010**, Memorial University of Newfoundland, St. John's, NL.
- (11) Huang, C.; Chen, C. *Dalton Trans.* **2007**, 5561-5566.
- (12) Huang, Y.; Tsai, Y.; Hung, W.; Lin, C.; Wang, W.; Huang, J.; Dutta, S.; Lin, C. *Inorg. Chem.* **2010**, *49*, 9416-9425.
- (13) Chisholm, M. H.; Lin, C.; Gallucci, J. C.; Ko, B. *Dalton Trans.* **2003**, 406-412.
- (14) Huang, C.; Ho, C.; Chen, C. *Dalton Trans.* **2008**, 3502-3510.
- (15) Save, M.; Schappacher, M.; Soum, A. *Macromol. Chem. Phys.* **2002**, *203*, 889-899.
- (16) Börner, J.; dos Santos Vieira, I.; Pawlis, A.; Döring, A.; Kuckling, D.; Herres-Pawlis, S. *Chem. Eur. J.* **2011**, *17*, 4507-4512.
- (17) Ropson, N.; Dubois, P.; Jerome, R.; Teyssie, P. *Macromolecules* **1995**, *28*, 7589-7598.

- (18) Ma, H.; Melillo, G.; Oliva, L.; Spaniol, T. P.; Englert, U.; Okuda, J. *Dalton Trans.* **2005**, 721-727.
- (19) Lian, B.; Ma, H.; Spaniol, T. P.; Okuda, J. *Dalton Trans.* **2009**, 9033-9042.
- (20) Blake, M. P.; Schwarz, A. D.; Mountford, P. *Organometallics* **2011**, *30*, 1202-1214.
- (21) Ko, B.; Lin, C. *J. Am. Chem. Soc.* **2001**, *123*, 7973-7977.
- (22) Hsueh, M.; Huang, B.; Wu, J.; Lin, C. *Macromolecules* **2005**, *38*, 9482-9487.
- (23) Ikpo, N.; Hoffmann, C.; Dawe L. N.; Kerton, F. M. *Dalton Trans.* **2012**, *41*, 6651-6660.
- (24) Binda, P. I.; Delbridge, E. E. *Dalton Trans.* **2007**, 4685-4692.
- (25) Chen, H.; Huang, B.; Lin, C. *Macromolecules* **2005**, *38*, 5400-5405.
- (26) Cao, T.; Buchard, A.; Le Goff, X. F.; Auffrant, A.; Williams, C. K. *Inorg. Chem.* **2012**, *51*, 2157-2169.
- (27) Ma, H.; Okuda, J. *Macromolecules* **2005**, *38*, 2665-2673.
- (28) Zhang, Z.; Xu, X.; Li, W.; Yao, Y.; Zhang, Y.; Shen, Q.; Luo, Y. *Inorg. Chem.* **2009**, *48*, 5715-5724.
- (29) Lu, M.; Yao, Y.; Zhang, Y.; Shen, Q. *Dalton Trans.* **2010**, *39*, 9530-9537.
- (30) Kasperczyk, J.; Bero, M. *Polymer* **2000**, *41*, 391-395.
- (31) Zell, M. T.; Padden, B. E.; Paterick, A. J.; Thakur, K. A. M.; Kean, R. T.; Hillmyer, M. A.; Munson, E. J. *Macromolecules* **2002**, *35*, 7700-7707.
- (32) Stanford, M. J.; Dove, A. P. *Chem. Soc. Rev.* **2010**, *39*, 486-494.
- (33) Thibault, M.-H.; Fontaine, F.-G. *Dalton Trans.* **2010**, *39*, 5688-5697.
- (34) Thakur, K. A. M.; Kean, R. T.; Hall, E. S.; Kolstad, J. J.; Lindgren, T. A.; Doscotch, M. A.; Siepmann, J. I.; Munson, E. J. *Macromolecules* **1997**, *30*, 2422-2428.
- (35) Drouin, F.; Oguadinma, P. O.; Whitehorne, T. J. J.; Prud'homme, R. E.; Schaper, F. *Organometallics* **2010**, *29*, 2139-2147.
- (36) Drouin, F.; Whitehorne, T. J. J.; Schaper, F. *Dalton Trans.* **2011**, *40*, 1396-1400.

- (37) Chisholm, M. H.; Delbridge, E. E. *New J. Chem.* **2003**, *27*, 1177-1183.
- (38) Ikpo, N.; Saunders, L. N.; Walsh, J. L.; Smith, J. M. B.; Dawe, L. N.; Kerton, F. M. *Eur. J. Inorg. Chem.* **2011**, 5347-5359.
- (39) *Characterization analysis of polymers*; Wiley-Interscience: Hoboken, N.J, **2008**; pp 230-251.
- (40) Baran, J.; Duda, A.; Kowalski, A.; Szymanski, R.; Penczek, S. *Macromol. Rapid Commun.* **1997**, *18*, 325-333.
- (41) O'Keefe, B. J.; Hillmyer, M. A.; Tolman, W. B. *J. Chem. Soc., Dalton Trans.* **2001**, 2215-2224.
- (42) Willans, C. E.; Sinenkov, M. A.; Fukin, G. K.; Sheridan, K.; Lynam, J. M.; Trifonov, A. A.; Kerton, F. M. *Dalton Trans.* **2008**, 3592-3598.
- (43) Sinenkov, M. A.; Fukin, G. K.; Cherkasov, A. V.; Ajellal, N.; Roisnel, T.; Kerton, F. M.; Carpentier, J.; Trifonov, A. A. *New J. Chem.* **2011**, *35*, 204-212.
- (44) Chamberlain, B. M.; Cheng, M.; Moore, D. R.; Ovitt, T. M.; Lobkovsky, E. B.; Coates, G. W. *J. Am. Chem. Soc.* **2001**, *123*, 3229-3238.

Chapter 4

Synthesis and Structure of Chromium(III) Amine-bis(phenolate)

Complexes

Parts of this chapter have been published: Rebecca K. Dean, Stephanie L. Granville, Louise N. Dawe, Andreas Decken, Karen M. Hattenhauer and Christopher M. Kozak, *Dalton Trans.*, **2010**, 39, 548-559.

4.1 Introduction

A large number of transition metal complexes possessing β -diketiminato and diimine-bis(phenolate) or 'salen' ligands have been reported in the literature. Chromium complexes in particular have been important in the development of catalysts in organic, inorganic and organometallic chemistry. Gilheany, Jacobsen, Theopold, Gibson and Darensbourg, to name a few, played instrumental roles in the development of novel chromium complexes. Some examples of these Cr complexes and their specific applications were presented in Chapter 1.

A more recent but growing area of transition-metal catalyst design involves the amine-bis(phenolate) ligand class.¹ Early transition-metals were most commonly used as they provided an alternative to cyclopentadienyl-based systems, which were typically used in olefin polymerization processes. Research in mid-to-late first row transition metals with this ligand class has provided interesting structural and physical properties.²⁻⁸

Complexes bearing ligands with greater donor ability, such as

tetramethyltetraazaannulene (tmtaa), salan and amine-bis(phenolate) have been shown to exhibit different structural and chemical behaviours than those of the corresponding salen complexes.^{9,10} With amine-phenolate ligands, this is likely due to an increased flexibility of the ligand framework, whereby modification of the pendant donor can provide sp^3 hybridized N-donor atoms, allowing non-planar geometries to be produced. Additionally, the change in ligand field strength for these ligands could be important for the design of new catalysts.

Specifically, group 6 complexes of this ligand class have not been studied in detail. Only dioxomolybdenum(VI) and -tungsten(VI),¹¹ and a homoleptic anionic chromium(III) tridentate complex (**1.6**)¹² were previously reported before this work. Interest in homogeneous polymerization catalysis and the success of chromium as a catalyst in such areas of ethylene, α -olefin and CO_2 /epoxide copolymerization sparked the interest of the Kozak group to explore new chromium amine-bis(phenolate) complexes.^{10,13-17}

This chapter describes the synthesis, structural, spectroscopic and magnetic properties of chromium(III) complexes possessing amine-bis(phenolate)-ether and amine-bis(phenolate)-pyridyl ligands.

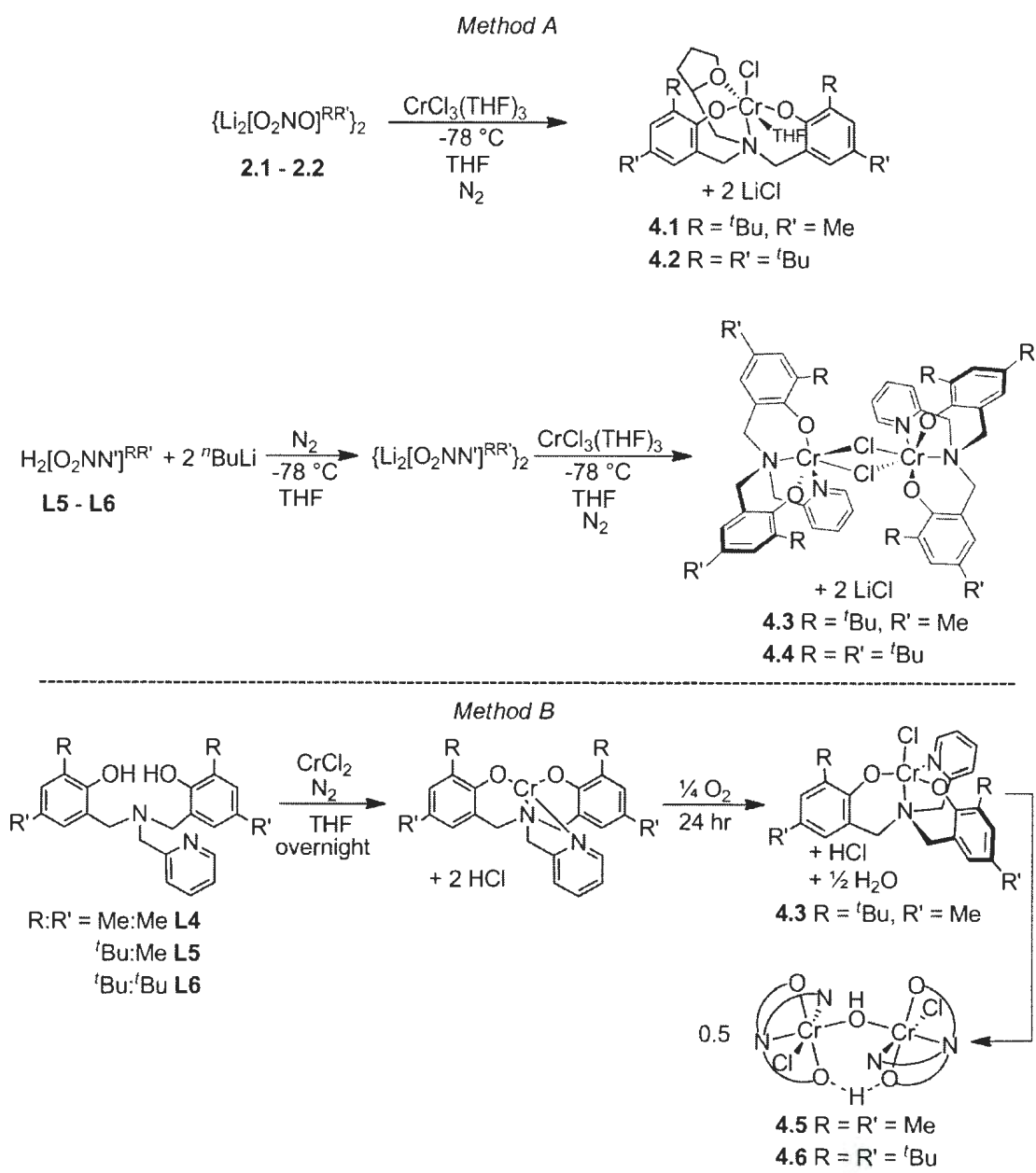
4.2 Results and Discussion

4.2.1 Synthesis of Cr(III) Complexes

Two methods were used in the synthesis of the chromium(III) complexes, a salt metathesis route and a protonolysis/oxidation by air of Cr(II) to Cr(III) as shown in

Scheme 4.1. In *Method A*, the appropriate dilithio diamine-bis(phenolate) ligands, $\text{Li}_2[\text{O}_2\text{NL}']^{\text{RR}'}$, where $\text{L}' = \text{N}$ or O , were reacted with $\text{CrCl}_3(\text{THF})_3$ in THF at -78°C , resulting in the isolation of purple powders when using the amine-bis(phenolate)-ether ligands, **L1-L3**. The synthesis of $\text{CrCl}[\text{O}_2\text{NO}]^{\text{MeMe}}$ was performed, however, poor yields and solubility of the complex led to the decision to focus only on the $\text{CrCl}[\text{O}_2\text{NO}]^{\text{RR}'}$ ($\text{R} = \text{'Bu}$, $\text{R}' = \text{Me}$ and $\text{R} = \text{R}' = \text{'Bu}$) analogues. The lithiated amine-bis(phenolate) ligands presented in Chapter 2 were used in the preparation of Cr(III) complexes, **4.1** and **4.2**. Purification of the crude product by recrystallization produces pink, paramagnetic $\text{CrCl}(\text{THF})[\text{O}_2\text{NO}]^{\text{BuMe}}$ (**4.1**) and $\text{CrCl}(\text{THF})[\text{O}_2\text{NO}]^{\text{BuBu}}$ (**4.2**) complexes in good yields. In the presence of the pyridyl ligands, **L5-L6**, green powders were observed, giving $\text{CrCl}[\text{O}_2\text{NN}']^{\text{BuMe}}$ (**4.3**) and $\text{CrCl}[\text{O}_2\text{NN}']^{\text{BuBu}}$ (**4.4**). Purification of crude **4.4** by recrystallization from benzene produced a green, paramagnetic chloride-bridged dimer, $\{\text{CrCl}[\text{O}_2\text{NN}']^{\text{BuBu}}\}_2$ (**4.4**), which was obtained in good yield.

Method B involved stirring a mixture of $\text{H}_2[\text{O}_2\text{NN}']^{\text{RR}'}$ (**L4-L6**) and anhydrous CrCl_2 under nitrogen for 12 h followed by stirring in air for 4 h. A colour change from grey-green to brown occurred, producing $\text{CrCl}[\text{O}_2\text{NN}']^{\text{RR}'}$ complexes (**4.3-4.6**). By this method, $\{\text{CrCl}[\text{O}_2\text{NN}']^{\text{MeMe}}\}(\mu\text{-HO})\{\text{CrCl}[\text{HO}_2\text{NN}']^{\text{MeMe}}\}$ (**4.5**) and $\{\text{CrCl}[\text{O}_2\text{NN}']^{\text{BuBu}}\}(\mu\text{-HO})\{\text{CrCl}[\text{HO}_2\text{NN}']^{\text{BuBu}}\}$ (**4.6**) were obtained in good yield after recrystallization. Attempts were made to isolate single crystals of the $\text{CrCl}[\text{O}_2\text{NN}']^{\text{BuMe}}$ complex (**4.3**) but were unsuccessful to date.



Scheme 4.1. Synthetic routes to Cr(III) complexes, *Method A*: salt metathesis and *Method B*: protonolysis/oxidation by air.

4.2.2 Structural Characterization

4.2.2.1 MALDI-TOF Mass Spectrometry

Structural characterization of paramagnetic complexes by NMR is often more difficult due to a decrease in the longitudinal relaxation time (T_2) resulting in line broadening of the ^1H NMR spectrum. Therefore, MALDI-TOF MS has become an important tool in the characterization of paramagnetic coordination complexes.¹⁸ This soft ionization technique by charge transfer in the presence of a neutral UV-absorbent matrix, such as anthracene affords minimal compound fragmentation. In addition, amine-bis(phenolate) ligands already possess a chromophore (from the phenol groups) which can be suitable for the absorption of laser energy providing enhanced ionization of the sample.¹⁹

The mass spectra generated for these Cr(III) complexes show molecular ion peaks and characteristic fragment ions. The mass spectra of both **4.1** and **4.2** using anthracene as the matrix show parent ions (without the coordinated THF) and a fragment corresponding to the loss of the chloride ligand, $[\text{M} - \text{Cl}]^+$. The parent ion for complex (**4.1**) occurs at m/z 538.2, correlating well to the theoretically calculated molecular weight 538.2 (Figure 4.1). The isotopic distribution pattern of the experimental $[\text{M}]^+$ ion agrees well with the theoretical peaks for **4.1**, as shown in Figure 4.2, providing strong evidence for the observed molecular structure. Additional peaks at lower masses of the spectrum correspond to ligand fragments, while peaks with masses higher than the molecular ion still remain unidentified, but could be possible bimetallic fragments.

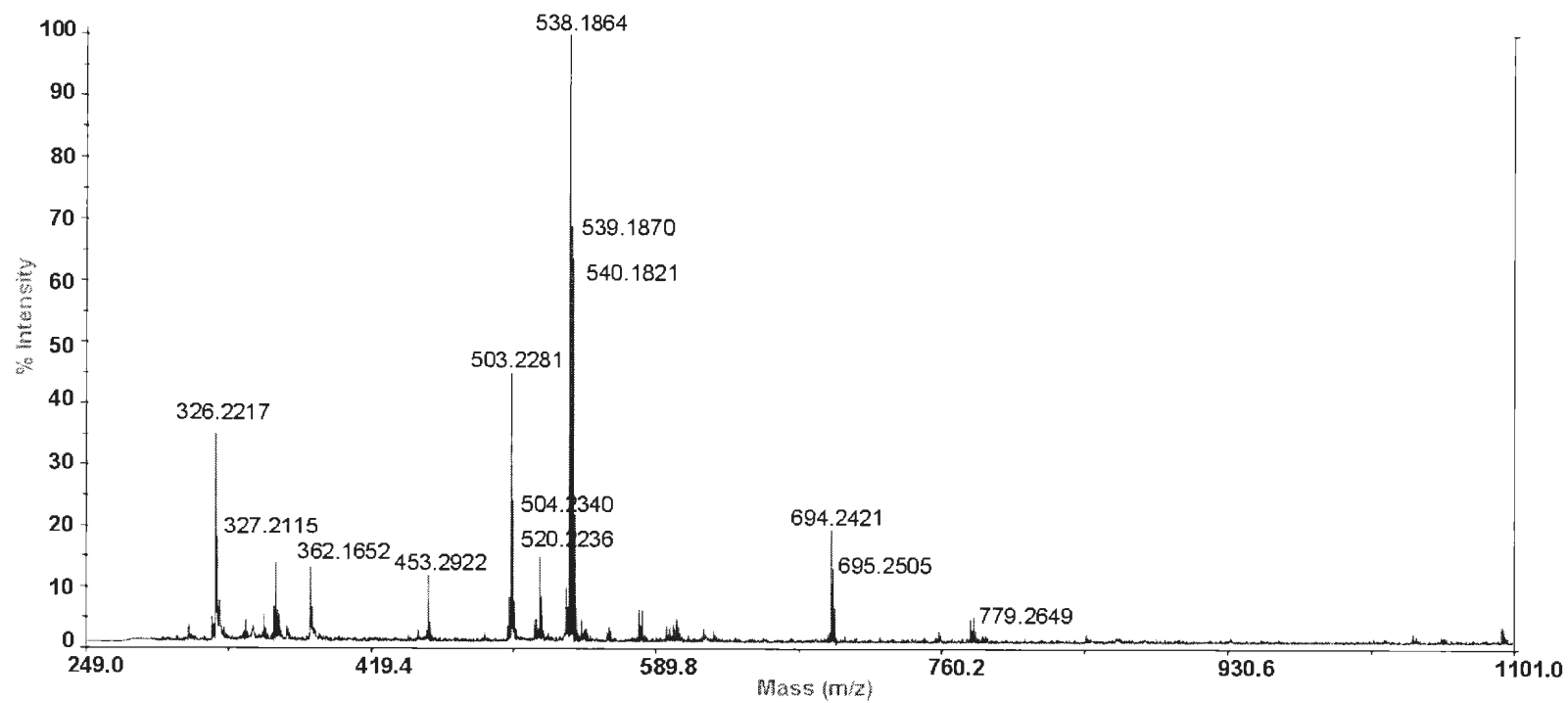


Figure 4.1. MALDI-TOF mass spectrum of $\text{CrCl}(\text{THF})[\text{O}_2\text{NO}]^{\text{BuMe}}$ (**4.1**).

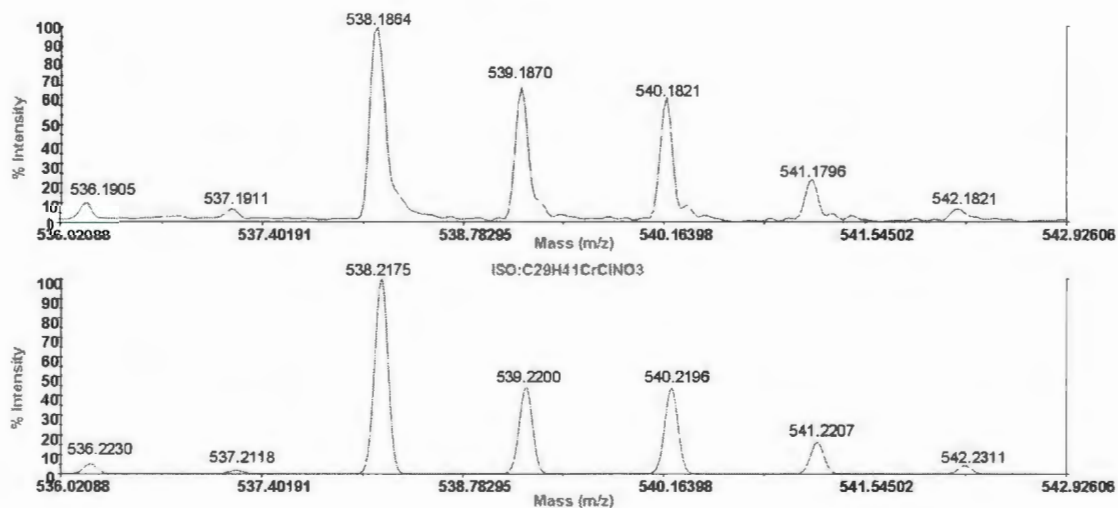


Figure 4.2. Experimental and theoretical MALDI-TOF MS isotopic distribution pattern for **4.1**.

Similarly, compounds **4.3**, **4.5** and **4.6** show loss of the chloride ligand from the parent ion in their mass spectrum. The most intense peak for **4.6** at m/z of 629.0 corresponds to the fragment $[\text{CrCl}[\text{O}_2\text{NN}']]^+$. In addition, the loss of chloride could be observed at 544.2 corresponding to $[\text{Cr}[\text{O}_2\text{NN}']]^+$ (Figure 4.3). Compound **4.6** exhibits an isotopic distribution pattern for the $[\text{CrCl}[\text{O}_2\text{NN}']]^+$ ion which closely resembles its theoretical spectrum, as shown in Figure 4.4. In addition to the monomeric peaks, evidence of bimetallic fragments in both **4.5** and **4.6** exist, corresponding to $[\{\text{Cr}[\text{O}_2\text{NN}']^{\text{MeMe}}\}_2\text{Cl}]^+$ at 887.1 (Appendix B, Figure B1.8) and $[\{\text{Cr}[\text{O}_2\text{NN}']^{\text{BuBu}}\}_2\text{Cl}]^+$ at 1223.6 (Appendix B, Figure B1.10), respectively.

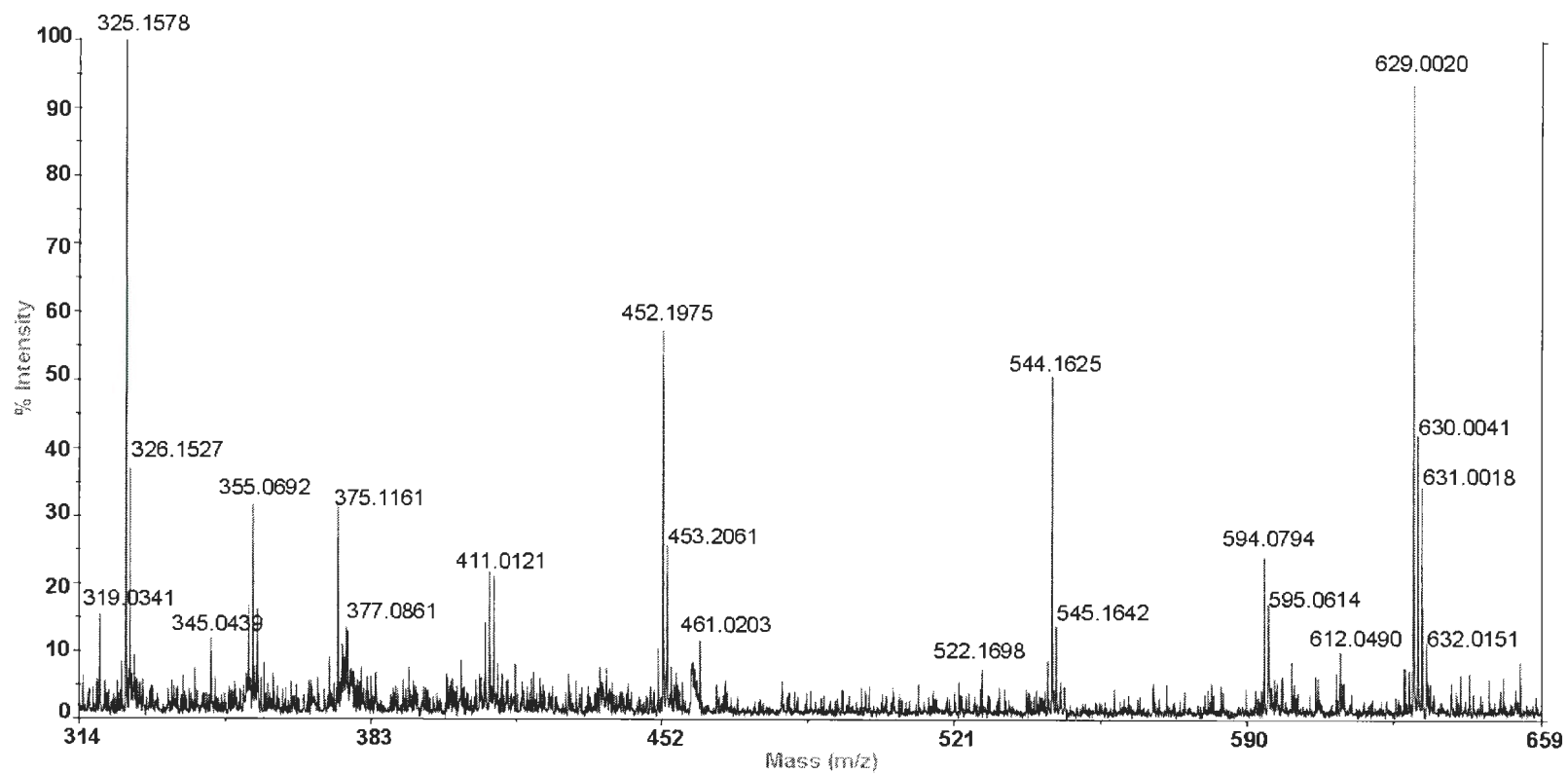


Figure 4.3. Lower mass region of the MALDI-TOF mass spectrum of $\{\text{CrCl}[\text{O}_2\text{NN}^{\text{tBuBu}}]\}(\mu\text{-HO})\{\text{CrCl}[\text{HO}_2\text{NN}^{\text{tBuBu}}]\}$ (4.6).

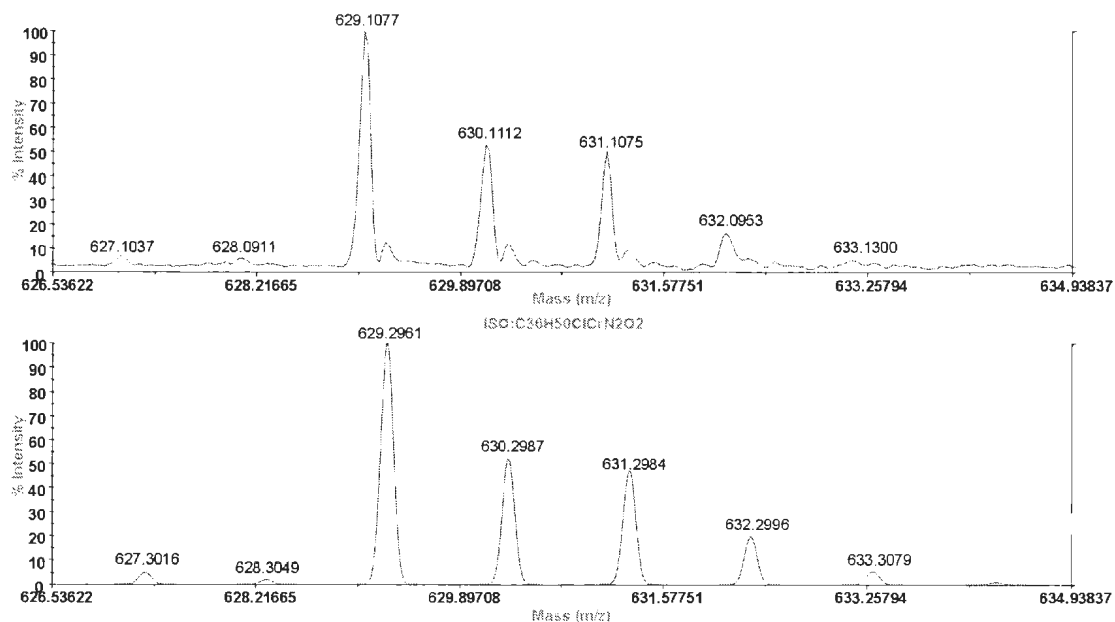


Figure 4.4. Experimental and theoretical MALDI-TOF MS isotopic distribution pattern for $\text{CrCl}[\text{O}_2\text{NN}']^{\text{BuBu}}$ fragment in **4.6**.

Compound **4.4** was also found to give peaks arising from monomer and dimer fragments present in the MALDI-TOF mass spectrum (Figure 4.5). The monomeric parent ion at 629.4 is found to be the most intense peak observed, with the characteristic $[\text{M} - \text{Cl}]^+$ peak found at 594.3. The dimer parent ion shown at 1259.7 is significantly less intense than the monomer peak, but this does show the bonding was strong enough to withstand fragmentation in the mass spectrometer. The isotopic distribution pattern for the monomer, Figure 4.6 closely resembles the theoretical spectra. Additional MALDI-TOF mass spectra for complexes **4.2-4.6** along with their isotopic patterns are given in Appendix B, Figures B1.3-1.10.

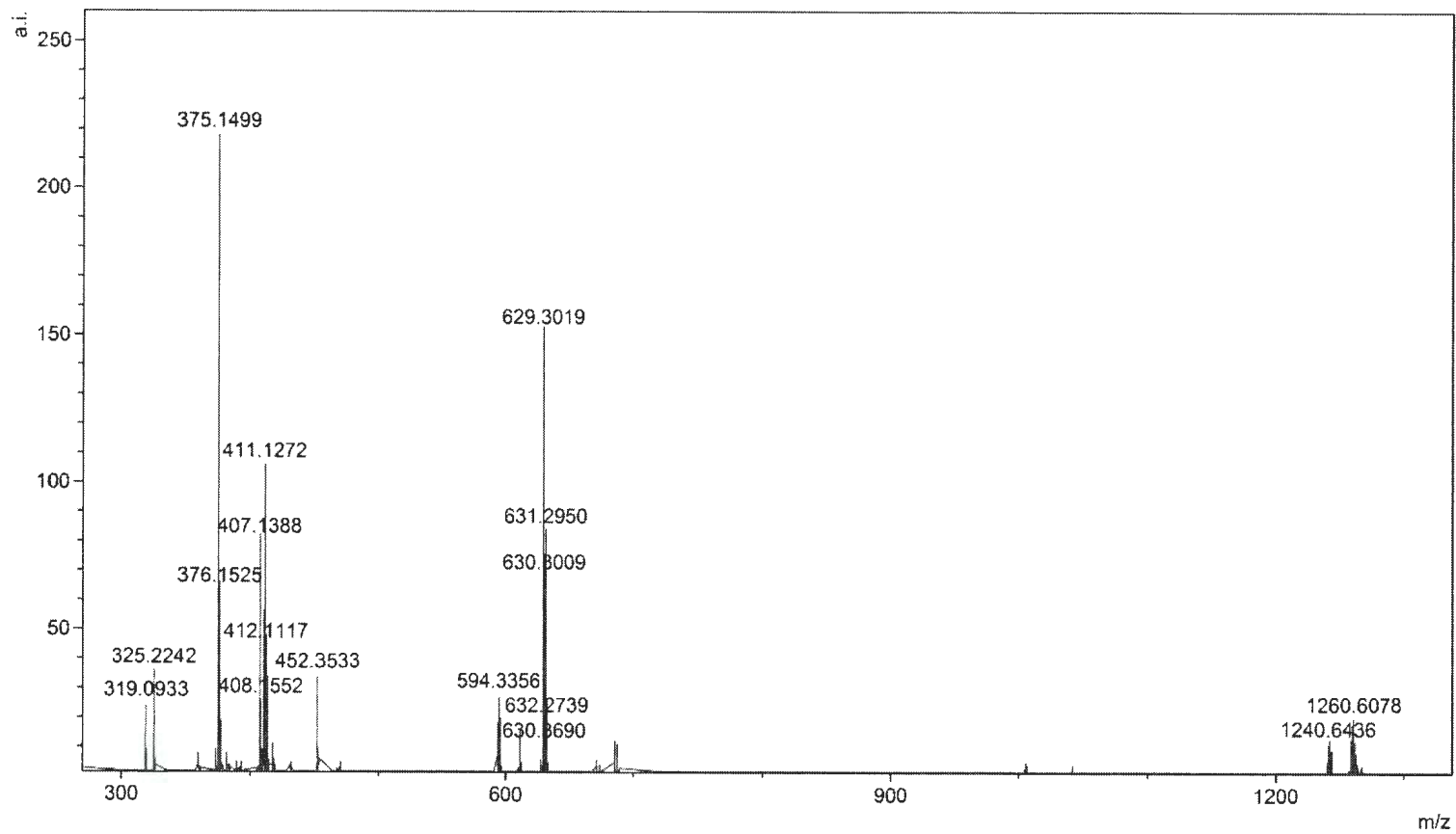


Figure 4.5. MALDI-TOF mass spectrum of $\{\text{CrCl}[\text{O}_2\text{NN}^t\text{BuBu}]\}_2$ (**4.4**).

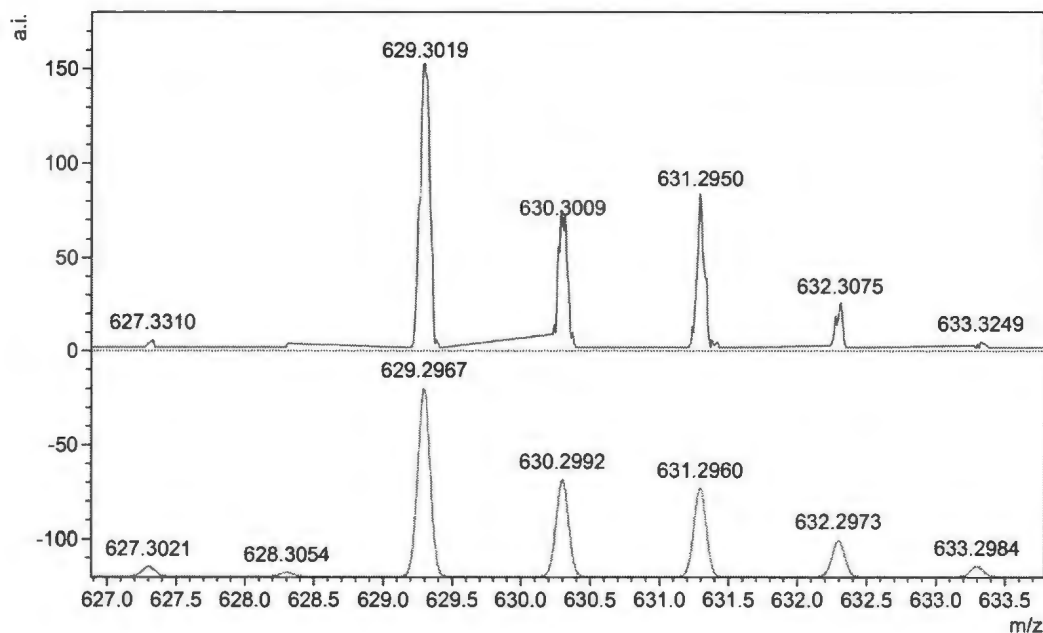


Figure 4.6. Experimental and theoretical MALDI-TOF MS isotopic distribution pattern for monomer fragment in 4.4.

4.2.2.2 Single Crystal X-ray Diffraction

Single crystals of **4.1** and **4.2** suitable for X-ray diffraction analysis were isolated via slow evaporation in toluene under a N_2 atmosphere in a glove box. Structures of $CrCl(THF)[O_2NO]^{BuMe}$ (**4.1**) and $CrCl(THF)[O_2NO]^{BuBu}$ (**4.2**) are shown in Figure 4.7, important bond distances and angles are listed in Table 4.1. Both complexes contain Cr in distorted octahedral geometries with the chloride ligand residing *trans* to the amino donor. The amine-bis(phenolate) ligands are both observed to adopt tetradentate bonding with the two phenolate groups coordinating in a mutually *trans* orientation at the

chromium centre. The six-coordinate geometry is completed by a THF ligand *trans* to the pendant tetrahydrofurfuryl group of the [O₂NO] ligand. The *cis* bond angles range from 81.0(4)°, O(2)-Cr(1)-N(1), at the most acute angle found from the five-membered chelate ring to 94.32 (14)°, O(4)-Cr(1)-N(1) for compound **4.1**. Compound **4.2** is shown to have similar angles ranging from 80.33(9)°, O(2)-Cr(1)-N(1), to 95.78(9)°, O(4)-Cr(1)-N(1). As expected, bond lengths for complexes **4.1** and **4.2** were observed to follow similar trends. The Cr(1)-O(1) and Cr(1)-O(3) bond distances were 1.916(4), 1.899(4), 1.911(2) and 1.937(2) Å for **4.1** and **4.2**, respectively. The bond distances for the ether-donor ligands coordinated to chromium, Cr(1)-O(2) and Cr(1)-O(4), were observed to be 2.009(13), 2.043(3), 2.020(2) and 2.048(2) Å in complexes **4.1** and **4.2**. These bond distances lie within the typical ranges for Cr complexes possessing chelating ligands with amine-nitrogen and phenolate-oxygen donors.^{12,20-23}

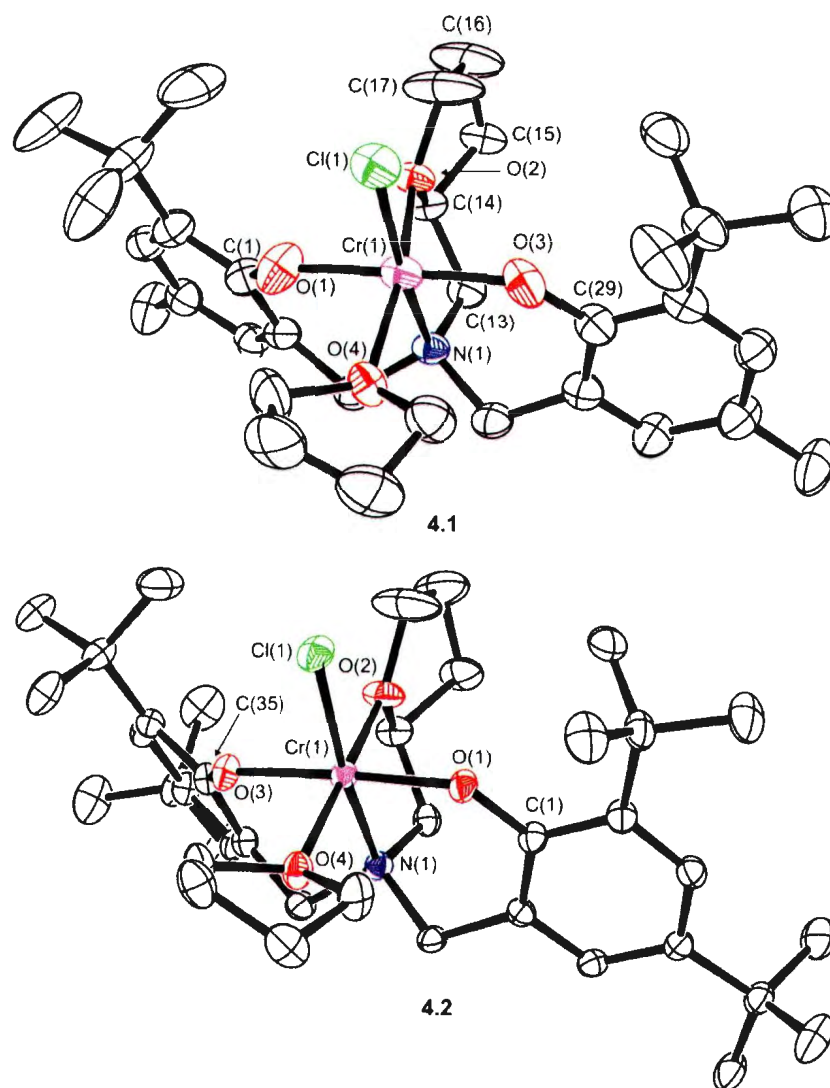


Figure 4.7. Molecular structures (ORTEP) and partially labelled numbering scheme of **4.1** (top) and **4.2** (bottom). Ellipsoids are shown at 30% and 50% probability, respectively. Hydrogen atoms are omitted for clarity.

Table 4.1 Selected bond lengths (Å) and angles (°) for **4.1** and **4.2**

4.1		4.2	
Cr(1)-O(1)	1.916(4)	Cr(1)-O(1)	1.911(2)
Cr(1)-O(2)	2.009(13)	Cr(1)-O(2)	2.020(2)
Cr(1)-O(3)	1.899(4)	Cr(1)-O(3)	1.937(2)
Cr(1)-O(4)	2.043(3)	Cr(1)-O(4)	2.048(2)
Cr(1)-N(1)	2.109(4)	Cr(1)-N(1)	2.124(3)
Cr(1)-Cl(1)	2.3329(14)	Cr(1)-Cl(1)	2.3394(9)
O(1)-C(1)	1.337(6)	O(1)-C(1)	1.334(3)
O(3)-C(29)	1.332(6)	O(3)-C(35)	1.335(3)
O(3)-Cr(1)-O(1)	177.29(17)	O(1)-Cr(1)-O(3)	176.39(10)
O(3)-Cr(1)-O(2)	99.4(3)	O(1)-Cr(1)-O(2)	92.19(11)
O(1)-Cr(1)-O(2)	83.3(3)	O(3)-Cr(1)-O(2)	90.99(10)
O(3)-Cr(1)-O(4)	90.24(15)	O(1)-Cr(1)-O(4)	89.90(9)
O(1)-Cr(1)-O(4)	87.06(15)	O(3)-Cr(1)-O(4)	86.81(9)
O(2)-Cr(1)-O(4)	169.2(3)	O(2)-Cr(1)-O(4)	175.51(9)
O(3)-Cr(1)-N(1)	89.03(14)	O(1)-Cr(1)-N(1)	88.14(9)
O(1)-Cr(1)-N(1)	91.32(14)	O(3)-Cr(1)-N(1)	90.70(9)
O(2)-Cr(1)-N(1)	81.0(4)	O(2)-Cr(1)-N(1)	80.33(9)
O(4)-Cr(1)-N(1)	94.32(14)	O(4)-Cr(1)-N(1)	95.78(9)
O(3)-Cr(1)-Cl(1)	88.95(11)	O(1)-Cr(1)-Cl(1)	88.88(7)
O(1)-Cr(1)-Cl(1)	91.00(11)	O(3)-Cr(1)-Cl(1)	92.65(7)
O(2)-Cr(1)-Cl(1)	93.1(3)	O(2)-Cr(1)-Cl(1)	93.22(7)
O(4)-Cr(1)-Cl(1)	92.09(10)	O(4)-Cr(1)-Cl(1)	90.79(7)
N(1)-Cr(1)-Cl(1)	173.29(11)	N(1)-Cr(1)-Cl(1)	172.78(7)
C(1)-O(1)-Cr(1)	130.4(3)	C(1)-O(1)-Cr(1)	135.19(18)
		C(35)-O(3)-Cr(1)	125.33(18)

These amine-bis(phenolate) chromium complexes are mildly hygroscopic and proceed to react with adventitious moisture present in air or solvent. When recrystallization of the $\text{CrCl}[\text{O}_2\text{NN}]^{\text{RR}'}$ compounds was performed in air, single crystals of **4.5** and **4.6** were each obtained via slow evaporation in toluene. The X-ray structures of **4.5** and **4.6** are shown in Figure 4.8. Selected bond lengths and angles for complexes **4.5** and **4.6** are given in Table 4.2. The structures of both complexes are bimetallic and possess a bridging oxygen-containing ligand. It is important to note that identical

structures were obtained whether the complexes were prepared via the salt metathesis or by the protonolysis/oxidation route, when recrystallizations were performed in air. Both complexes **4.5** and **4.6** exhibit “butterfly-like” structures where each amine-bis(phenolate) ligand is shown to push towards the other. Each Cr(III) ion adopts distorted octahedral geometries, where the phenolate oxygen atoms are *trans* to one another. In addition, the chloride atoms are observed to be *trans* to the central nitrogen donor of the ligands as well as the O-bridging ligand to the nitrogen from the pendant pyridyl donor. The bridging Cr-O-Cr angle is found to be 143.5(3)° for **4.5** and 147.40(10)° for **4.6**. These angles are typical of Cr complexes possessing bridging oxygen-containing ligands (water or hydroxide).²⁴⁻²⁹

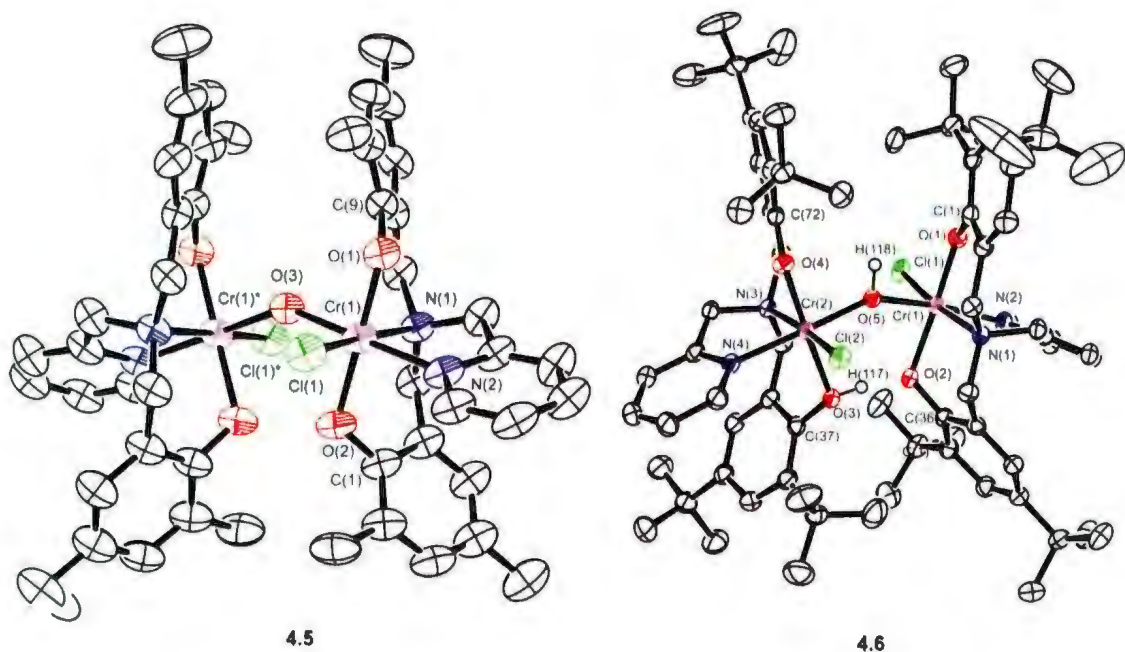


Figure 4.8. Molecular structures (ORTEP) and partially labelled numbering scheme of **4.5** (left) and **4.6** (right). Ellipsoids are shown at 50% probability and hydrogen atoms are omitted for clarity, except for H(117) and H(118) on **4.6**. Symmetry operation used to generate equivalent atoms in **4.5**: $\frac{1}{2}-x, y, \frac{1}{2}-z$.

In order to determine what the most likely species was for the bridging O-ligand various scenarios were examined. For example, if it was an oxide (O^{2-}) bridge, typical bond angles of 180° are commonly observed for Cr(III)/Cr(III) compounds with only a single bridging ligand.²⁷⁻²⁹ The Cr-O bond lengths do suggest some ionic interactions, where the Cr(1)-O(3) distance is 1.9745(16) Å in **4.5**, and in **4.6** the Cr(1)-O(5) and Cr(2)-O(5) lengths are 1.9750(17) Å and 1.9730(17) Å, respectively. Typical bond distances for Cr(III), O^{2-} bridged species are usually much shorter, between 1.767 and

1.82 Å. However, dimeric Cr(III) complexes with only one (μ -O) ligand (H_2O , OH^- or O^{2-}) are rare.²⁴⁻²⁹ Additionally, if one assumes a (μ - H_2O) or a (μ - OH^-) ligand, the Cr(III)-O-Cr(III) bond angles should be closer to 145° , which is the case for the angles observed in **4.5** and **4.6**. Bond lengths of Cr-O for bridging- OH^- Cr(III) compounds generally lie between 1.941 and 1.989 Å. The vast majority of bridged species, however, contain more than one bridging group making direct comparison of bond angles unreliable.³⁰⁻³⁴ The bond lengths for the OH^- bridged compounds found in the literature lie between 1.918 and 1.981 Å and are therefore more consistent with those found in **4.5** and **4.6**.

As previously described, an apparent pinching-in of the phenolate groups on either side of the complexes causes asymmetry between the bond distances of the Cr(III) centres and the oxygen donors of the phenolate groups in **4.5** and **4.6**. Bond distances in **4.5** are 1.905(3) and 2.004(4) Å for Cr(1)-O(1) and Cr(1)-O(2), respectively. In the sterically more hindered complex, **4.6**, bond lengths of 1.8931(18), 2.0364(18), 1.8878(18) and 2.0493(17) Å are found for Cr(1)-O(1), Cr(1)-O(2), Cr(2)-O(4) and Cr(2)-O(3), respectively. The longer distances originate from the sides of the ligand that are forced into close quarters of the ligand on the opposite side of the bimetallic unit. Typically Cr-O bond distances greater than 2.0 Å indicate a more coordinate-covalent interaction is at play as opposed to an anionic one.^{35,36} A potential explanation for the lengthening of the Cr-O bond distances in addition to the “butterfly-like” structure could be the result of one of the phenolate oxygen atoms being protonated, where a hydrogen-bonding interaction between the phenolate oxygens of the ligands would be observed. Further examination of the crystallographic data from the residual electron density (Q-peaks) in the final difference map supported this proposal. The structure of **4.6** was then refined according to

this model. Hydrogens H(117) bonded to O(3) and H(118) bonded to O(5) were introduced in difference map positions and initially refined positionally (on x, y, z) with fixed thermal parameters, and finally on the riding model, with isotropic thermal parameters set twenty percent greater than those of their bonding partners. This refinement generated an improved solution, resulting in an R -factor of 6.82% (compared to 6.87% for the initial solution where these H-atoms were not included in the model). Other structural characterization, such as infrared did show a broad O-H band at 3200 cm^{-1} , but does not confirm whether the bridging ligand is H_2O or OH^- (see Appendix E). Elemental analysis for each of **4.5** and **4.6** favourably supports the presence of between one and two formula units of “ H_2O ” per two molecules of $\text{CrCl}[\text{O}_2\text{NN}']^{\text{RR}'}$. Therefore, as a result of the analysis conducted on these complexes, strong evidence suggests that the bridging ligand for **4.5** and **4.6** is a hydroxide. The protonated phenol on one of the ligands provides the additional hydrogen from the water. This implies both Cr centres have a +3 oxidation state, which is supported by spectroscopy and magnetic measurement data presented in the following sections.

Table 4.2 Selected bond lengths (\AA) and angles ($^\circ$) for **4.5** and **4.6**

	4.5		4.6
Cr(1)-O(1)	1.905(3)	Cr(1)-O(1)	1.8931(18)
Cr(1)-O(2)	2.004(4)	Cr(1)-O(2)	2.0364(18)
Cr(1)-O(3)	1.9745(16)	Cr(1)-O(5)	1.9750(17)
Cr(1)-N(1)	2.098(4)	Cr(1)-N(1)	2.115(2)
Cr(1)-N(2)	2.080(4)	Cr(1)-N(2)	2.095(2)
Cr(1)-Cl(1)	2.3526(14)	Cr(1)-Cl(1)	2.3457(7)
O(1)-C(9)	1.337(5)	Cr(2)-O(3)	2.0493(17)
O(2)-C(1)	1.383(6)	Cr(2)-O(4)	1.8878(18)
		Cr(2)-O(5)	1.9730(17)
O(1)-Cr(1)-O(2)	176.38(13)	Cr(2)-N(3)	2.116(2)

4.5		4.6	
O(1)-Cr(1)-O(3)	89.77(16)	Cr(2)-N(4)	2.099(2)
O(3)-Cr(1)-O(2)	88.00(17)	Cr(2)-Cl(2)	2.3357(7)
O(1)-Cr(1)-N(1)	86.27(15)	O(1)-C(1)	1.339(3)
O(2)-Cr(1)-N(1)	91.00(15)	O(2)-C(36)	1.381(3)
O(3)-Cr(1)-N(1)	93.00(11)	O(3)-C(37)	1.386(3)
O(1)-Cr(1)-N(2)	91.14(16)	O(4)-C(72)	1.332(3)
O(2)-Cr(1)-N(2)	90.71(16)		
O(3)-Cr(1)-N(2)	172.72(11)	O(1)-Cr(1)-O(2)	175.36(7)
N(2)-Cr(1)-N(1)	79.85(15)	O(1)-Cr(1)-O(5)	89.21(8)
O(1)-Cr(1)-Cl(1)	91.67(10)	O(5)-Cr(1)-O(2)	86.85(7)
O(2)-Cr(1)-Cl(1)	91.40(10)	O(1)-Cr(1)-N(1)	87.45(8)
O(3)-Cr(1)-Cl(1)	96.11(5)	O(2)-Cr(1)-N(1)	90.32(7)
N(1)-Cr(1)-Cl(1)	170.65(12)	O(5)-Cr(1)-N(1)	93.10(8)
N(2)-Cr(1)-Cl(1)	91.08(12)	O(1)-Cr(1)-N(2)	94.60(8)
C(9)-O(1)-Cr(1)	126.2(3)	O(2)-Cr(1)-N(2)	89.02(8)
C(1)-O(2)-Cr(1)	120.5(3)	O(5)-Cr(1)-N(2)	172.21(8)
Cr(1)*-O(3)-Cr(1)	143.5(3)	N(2)-Cr(1)-N(1)	80.31(8)
		O(1)-Cr(1)-Cl(1)	90.09(6)
		O(2)-Cr(1)-Cl(1)	92.77(5)
		O(5)-Cr(1)-Cl(1)	96.13(5)
		N(1)-Cr(1)-Cl(1)	170.42(6)
		N(2)-Cr(1)-Cl(1)	90.66(6)
		O(4)-Cr(2)-O(3)	177.12(7)
		O(4)-Cr(2)-O(5)	90.52(8)
		O(5)-Cr(2)-O(3)	87.15(7)
		O(3)-Cr(2)-N(3)	91.25(7)
		O(4)-Cr(2)-N(3)	87.13(8)
		O(5)-Cr(2)-N(3)	91.93(7)
		O(3)-Cr(2)-N(4)	91.12(8)
		O(4)-Cr(2)-N(4)	90.96(8)
		O(5)-Cr(2)-N(4)	172.05(8)
		N(4)-Cr(2)-N(3)	80.34(8)
		O(3)-Cr(2)-Cl(2)	90.54(5)
		O(4)-Cr(2)-Cl(2)	91.36(6)
		O(5)-Cr(2)-Cl(2)	94.96(5)
		N(3)-Cr(2)-Cl(2)	172.96(6)
		N(4)-Cr(2)-Cl(2)	92.82(6)
		C(1)-O(1)-Cr(1)	132.82(16)
		C(36)-O(2)-Cr(1)	119.60(14)
		C(37)-O(3)-Cr(2)	118.52(14)
		C(72)-O(4)-Cr(2)	132.63(16)
		Cr(2)-O(5)-Cr(1)	147.40(10)

Single crystals of **4.4** suitable for X-ray diffraction were grown from a benzene solution under N₂. The solid-state structure of **4.4** was found to be a chloride-bridged dimer, as shown in Figure 4.9. Selected bond lengths and angles for **4.4** are given in Table 4.3. The complex lies on an inversion centre located within the Cr₂Cl₂ rhomboid and the Cr(III) centres exhibit distorted octahedral geometries. Although six coordinate chromium(III) complexes are common, non-Cp compounds bearing two bridging chlorides (Cr(μ-Cl)₂Cr) are not. These complexes often possess phosphine, bis(phosphino)amine²⁰ or phosphinimines,²¹ sulfanylamines,²² or κ²-nacnac ligands.²³ The majority of the Cr(μ-Cl)₂Cr structures reported are five-coordinate and possess κ²-nacnac³⁷⁻³⁹ or diamidosilylether ligands.⁴⁰ The Cr(1)-Cl(1)-Cr(1)* angle was observed to be 95.66(3)° for **4.4**, and the chlorides are orientated *cis* to the nitrogen on the pendant pyridyl group. This angle is observed to be slightly more acute than what is reported in the literature for other Cl-bridged Cr(III) dimers.³⁷⁻⁴⁰ The Cr(μ-Cl) bond distances are asymmetric at 2.4050(8) and 2.4431(8) Å. These distances encompass the range typical for five or six-coordinate chromium(III) chloride-bridged species.^{37,39} Theopold and co-workers observed similar Cr(μ-Cl) distances of 2.4217(6) and 2.4127(6) Å for an octahedral dimeric, chromium(III) chloride-bridged monoalkyl β-diketimate complex.³⁷ The Cr(1)···Cr(1)* interatomic distance in **4.4** is 3.5935(2) Å and lies within the typical reported range of 3.23-3.64 Å.^{39,23-24}

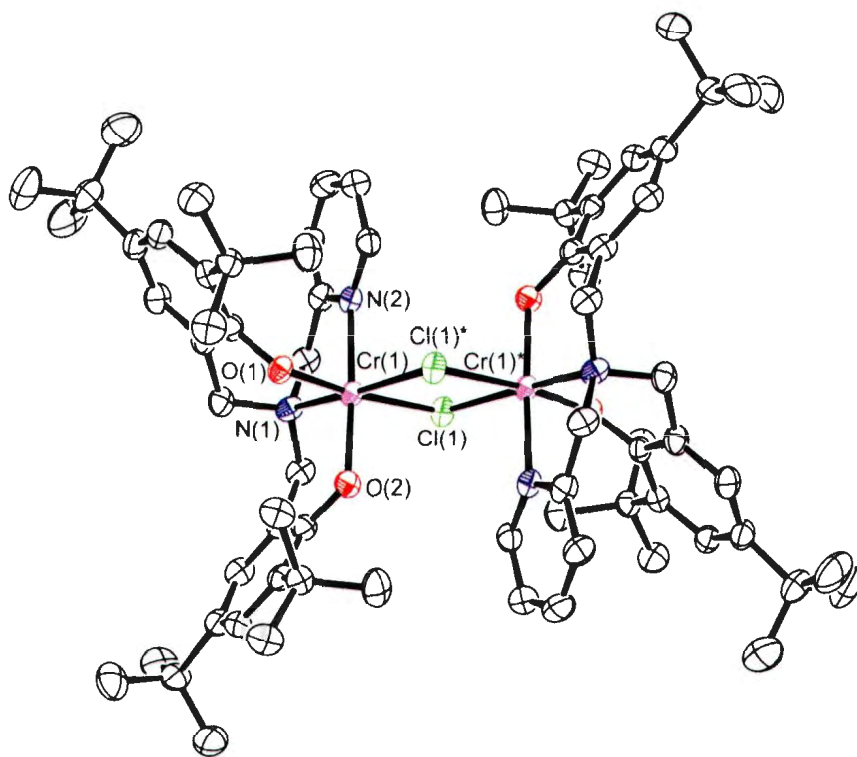


Figure 4.9. Molecular structure (ORTEP) and partial numbering scheme of $\{\text{CrCl}[\text{O}_2\text{NN}^{\text{tBuBu}}]\}_2$ (**4.4**). Ellipsoids are drawn at 50% probability and hydrogen atoms are omitted for clarity. Symmetry operation used to generate equivalent atoms: $1-x, -y, 1-z$.

Table 4.3 Selected bond lengths (Å) and angles (°) for **4.4**

Cr(1)-O(1)	1.9110(18)
Cr(1)-O(2)	1.9050(18)
Cr(1)-N(1)	2.080(2)
Cr(1)-N(2)	2.103(2)
Cr(1)-Cl(1)	2.4050(8)
Cr(1)-Cl(1)*	2.4431(8)
Cr(1)···Cr(1)*	3.5935(2)
O(2)-Cr(1)-O(1)	93.33(8)
O(2)-Cr(1)-N(1)	91.15(8)
O(2)-Cr(1)-N(2)	171.78(8)
N(1)-Cr(1)-N(2)	80.96(8)
N(1)-Cr(1)-Cl(1)	173.80(7)
N(2)-Cr(1)-Cl(1)	94.74(6)
O(1)-Cr(1)-Cl(1)	173.93(6)
O(2)-Cr(1)-Cl(1)	91.89(6)
Cl(1)-Cr(1)-Cl(1)*	84.34(3)
Cr(1)-Cl(1)-Cr(1)*	95.66(3)

4.2.3 UV-Visible Spectroscopy

Electronic absorption spectra of complexes **4.1-4.6** show multiple intense bands in the UV and visible regions. Solvents employed in this study varied depending on the complexes solubility. Solvents investigated for these complexes included THF, toluene, CH₂Cl₂ and CH₃CN. The absorption maxima observed in the near-UV regions (below 300 nm) are caused by $\pi \rightarrow \pi^*$ transitions involving the phenolate units. Intense, high energy bands are also observed in the region between 330 and 450 nm, which are assigned to charge transfer transitions from the p_π orbital (HOMO) of the phenolate oxygen to the empty $d_{x^2-y^2}/d_{z^2}$ and the half-filled d_{π^*} orbital of Cr(III). A shift of these LMCT bands is observed on changing the solvent used. In order to observe the weaker, very broad d-d transitions ($\epsilon \approx 200 \text{ L mol}^{-1} \text{ cm}^{-1}$) observed between 450 and 700 nm, a higher concentration of $1 \times 10^{-3} \text{ mol L}^{-1}$ was required. The intense LMCT bands obscure

the low energy visible region making assignment of the metal-centred transitions more difficult.

Solvent dependence is observed in the ${}^4T_2 \leftarrow {}^4A_2 (O_h)$ band at 508 nm (19 700 cm^{-1}) in THF, and at 552 nm (18 100 cm^{-1}) in CH_3CN for **4.1** and **4.2**, respectively, as shown in Figure 4.10. This change in absorbance suggests that the THF ligand present in the solid state structure is sufficiently labile and undergoes exchange with other donor solvents. In the presence of acetonitrile a distinct colour change occurs suggesting that CH_3CN adducts may form and are found to shift to lower energy at this transition, consistent with the decrease in ligand field strength when going from THF to CH_3CN . The ${}^4T_1 \leftarrow {}^4A_2 (O_h)$ band is obscured by the CT bands and exist as poorly-resolved shoulders. Estimates place this transition at 390 nm (25 600 cm^{-1}) and 410 nm (24 400 cm^{-1}) in THF for complexes **4.1** and **4.2**, respectively. This band appears at 429 nm (23 300 cm^{-1}) and 440 nm (22 700 cm^{-1}) for **4.1** and **4.2**, respectively, in CH_3CN . These data provide ligand field strengths, $10Dq (\Delta_o)$, of the two amine-bis(phenolate)-THF ligands of 19 700 cm^{-1} , or slightly lower than that of the ammonia ligand in the spectrochemical series. Since the ${}^4T_1 \leftarrow {}^4A_2$ band is obscured by the LMCT bands, only an approximate value for the Racah parameter, B , of 450 cm^{-1} can be calculated. For the A_2 ground term for the Cr(III) ion, the mixing of terms with the same spin multiplicity is expressed by the formula $g = 2.0023 - (8\lambda/10Dq)$ where λ is the spin-orbit coupling constant ($\lambda \approx 92 \text{ cm}^{-1}$ for Cr(III)) and $10Dq$ is the energy of the lowest excited state (4T_2). For **4.1** and **4.2**, $10Dq$ is 19 700 cm^{-1} , giving $g = 1.96$.

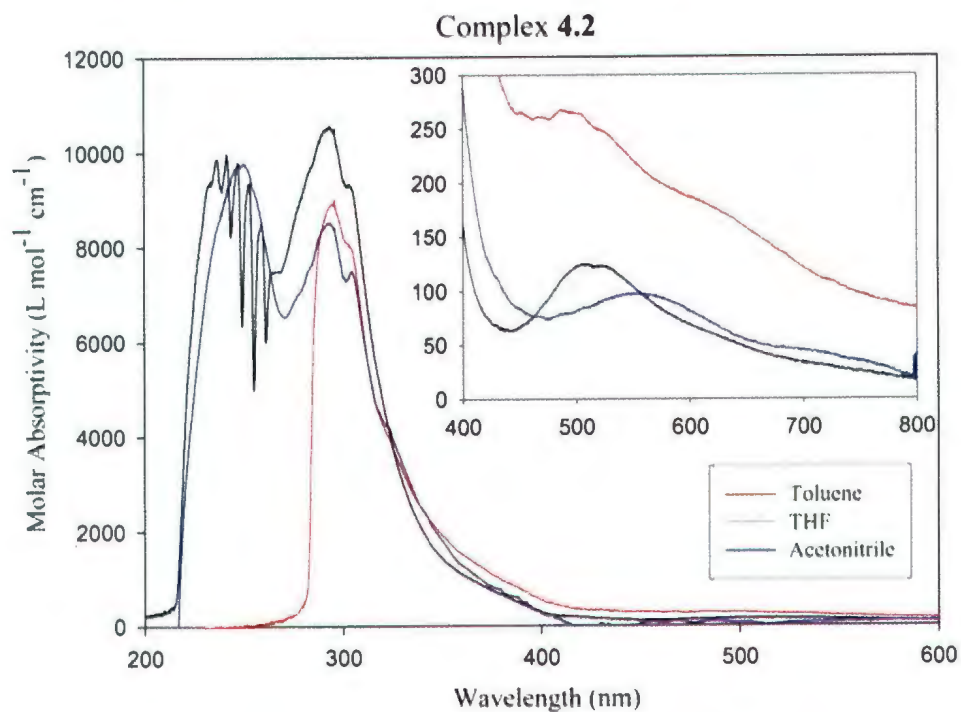
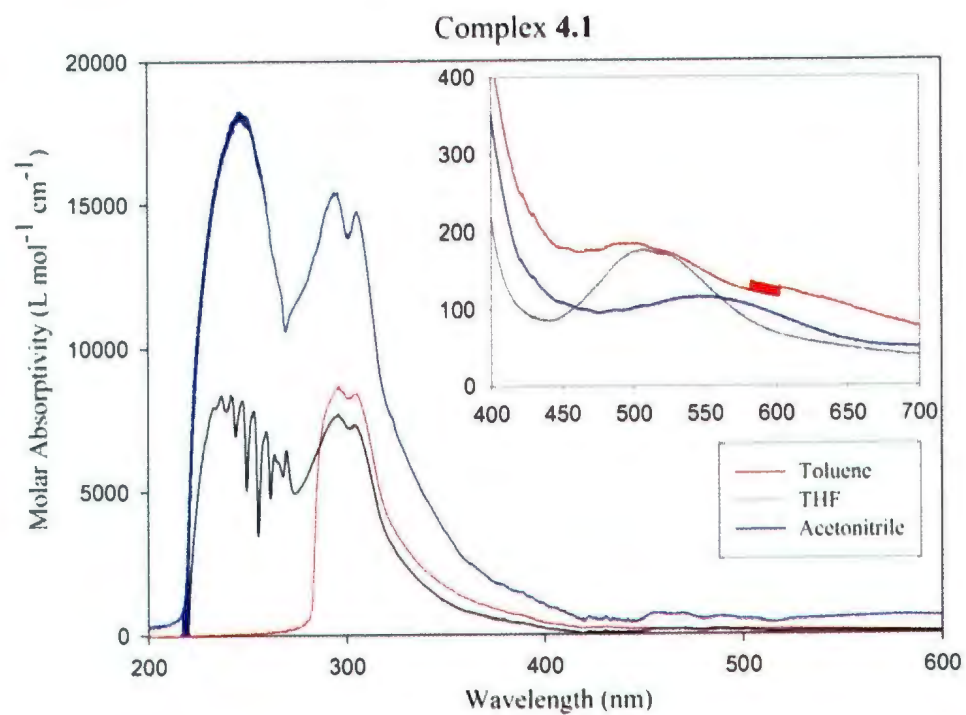


Figure 4.10. UV-Vis absorption spectra of **4.1** (top) and **4.2** (bottom).

The UV-vis spectra of complexes **4.3**, **4.5** and **4.6** also show changes to the energies of their d-d transitions in different solvents. Compound **4.3** was examined in dichloromethane as it was found to be insoluble in acetonitrile. The ${}^4T_2 \leftarrow {}^4A_2$ band for compound **4.3** in CH_2Cl_2 is observed at 598 nm ($16\,700\text{ cm}^{-1}$) and shoulders at approximately 402 nm ($24\,900\text{ cm}^{-1}$) are observed for the ${}^4T_1 \leftarrow {}^4A_2$ band. In THF, the ${}^4T_2 \leftarrow {}^4A_2$ band appears at 495 nm ($20\,200\text{ cm}^{-1}$) and ${}^4T_1 \leftarrow {}^4A_2$ appears at 400 nm ($25\,000\text{ cm}^{-1}$) as shown in Figure 4.11. Compound **4.4** was also examined in dichloromethane. The ${}^4T_2 \leftarrow {}^4A_2$ band for compound **4.4** in CH_2Cl_2 is observed at 606 nm ($16\,500\text{ cm}^{-1}$) and shoulders at approximately 386 nm ($25\,900\text{ cm}^{-1}$) are observed for the ${}^4T_1 \leftarrow {}^4A_2$ band as shown in Appendix D, Figure D1.1. Compound **4.5** shows the ${}^4T_2 \leftarrow {}^4A_2$ band at 598 nm ($16\,700\text{ cm}^{-1}$) and shoulders at approximately 416 nm ($24\,000\text{ cm}^{-1}$) for the ${}^4T_1 \leftarrow {}^4A_2$ band in CH_3CN . In THF, the ${}^4T_2 \leftarrow {}^4A_2$ band appears at 605 nm ($16\,500\text{ cm}^{-1}$) and ${}^4T_1 \leftarrow {}^4A_2$ appears at 400 nm ($25\,000\text{ cm}^{-1}$) as observed in Appendix D, Figure D1.2. Compound **4.6** shows the ${}^4T_2 \leftarrow {}^4A_2$ band at 492 nm ($20\,300\text{ cm}^{-1}$) in CH_3CN and ${}^4T_1 \leftarrow {}^4A_2$ appears at 385 nm ($26\,000\text{ cm}^{-1}$). In THF these bands appear at 494 nm ($20\,200\text{ cm}^{-1}$) and 386 nm ($25\,900\text{ cm}^{-1}$) as shown in Figure 4.11. The resulting ligand field strength of the amine-bis(phenolate)-pyridyl ligands gives $10Dq$ (Δ_o) of $20\,200\text{ cm}^{-1}$, which is larger than that of the tetrahydrofurfurylcontaining ligand. This is consistent with the stronger ligand field strength of pyridine compared to THF. Estimates of the Racah parameter give $B = 454\text{ cm}^{-1}$. These values yield an estimate for $g = 1.97$, which is close to the value obtained from magnetic data of **4.6** (see Section 4.2.4) when the Heisenberg dimer model is employed and using a Curie-Weiss term for the paramagnetic impurity.

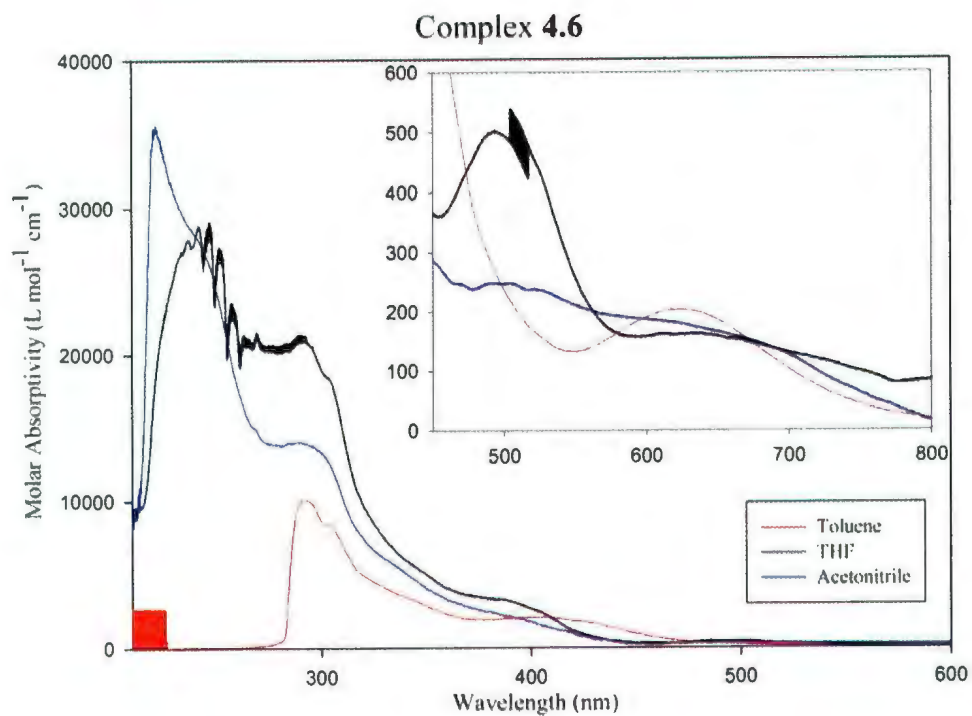
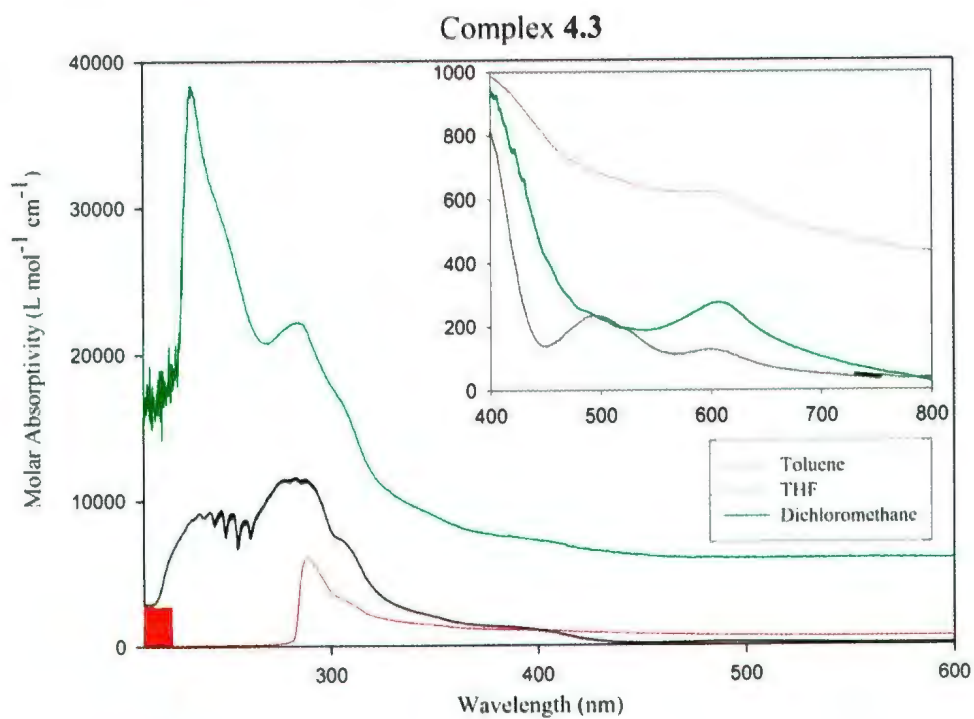


Figure 4.11. UV-Vis absorption spectra of **4.3** (top) and **4.6** (bottom).

4.2.4 Magnetometry

Solution magnetic moments for **4.1** and **4.2** were obtained by Evans' method. Both complexes exhibited moments of $3.8\mu_B$, consistent with $S = 3/2$ spin states of Cr(III) d^3 centres. The room temperature magnetic moments of **4.5** and **4.6** are identical with $\mu_{\text{eff}} = 5.3\mu_B$ per bimetallic unit. These values are only slightly lower than expected for two isolated Cr(III) ions (the spin-only moment for two $S = 3/2$ ions exhibiting no magnetic exchange would be $\approx 5.48\mu_B$). The temperature (T) dependence of the magnetic susceptibility (χ_m) of **4.6** was measured from 2–300 K. The plots of χ_m vs. T and μ_{eff} vs. T per chromium dimer are shown in Figure 4.12. Complex **4.6** shows a significant decrease in μ_{eff} as T decreases as well as a broad maximum in the plot of χ_m vs. T indicative of antiferromagnetic coupling between the metal atoms. Data were first modeled using the spin Hamiltonian $H = -2JS_1 \cdot S_2$, considering a pair of exchange coupled centres where $S_1 = S_2 = 3/2$ according to the Heisenberg dimer model:⁴¹

$$\chi = \frac{2Ng^2\mu_B^2}{kT} \left\{ \frac{e^{(2J/kT)} + 5e^{(6J/kT)} + 14e^{(12J/kT)}}{1 + 3e^{(2J/kT)} + 5e^{(6J/kT)} + 7e^{(12J/kT)}} \right\}$$

To account for the presence of a small amount of paramagnetic impurity the expression was combined with the Curie law term, $\chi_{\text{para}} = C/T$, according to $\chi_m = [1-P]\chi + P\chi_{\text{para}}$, where P represents the fraction of paramagnetic $S = 3/2$ impurity, likely $\text{CrCl}_3(\text{H}_2\text{O})_x$. The resulting analysis of the data yielded $J = -16.5 \text{ cm}^{-1}$, $g = 1.92$ and $P = 0.0079$. The presence of temperature independent paramagnetism (*TIP*) was also included in the model, where $TIP = 23.0 \times 10^{-4} \text{ cm}^3 \text{ mol}^{-1}$. While the calculated g is slightly lower than

typically predicted for Cr(III) (where values nearer to 1.98 are commonly observed),⁴² and the *TIP* can be considered high for this ion, these values are in agreement with those reported for [(MeCN)₅Cr(OH)Cr(MeCN)₅]⁵⁺, where $g = 1.966(4)$ and $TIP = 89(3) \times 10^{-4} \text{ cm}^3$.²⁵ In addition, the Cr-O-Cr' bond angle of 147.5(2)° in this compound is very similar to the bond angles of 143.5(3)° and 147.40(10)° observed in complexes **4.5** and **4.6**, respectively.

An alternate model was examined where the paramagnetic impurity was considered to obey the Curie-Weiss law, hence $\chi_{\text{para}} = C/(T - \theta)$ was included in the calculation of χ_{m} . This model gave similar values of $J = -16.6 \text{ cm}^{-1}$ and $g = 1.95$ compared to the model employed above. Other terms obtained were $\theta = -0.4$, $P = 0.0095$ and $TIP = 20.0 \times 10^{-4} \text{ cm}^3$. The calculated Curie-Weiss term θ is slightly larger than expected for Cr(III),⁴² but only moderately decreases the amount of *TIP*. Fixing the *TIP* to values of $6.0 \times 10^{-4} \text{ cm}^3$ or lower only raises the percentage of paramagnetic impurity and gives unrealistic g values.

The magnetic properties of some Cr(III) dimers^{25,26,31-33,43-47} have been modelled by including biquadratic exchange interactions according to the general exchange Hamiltonian $\mathbf{H} = -2J\mathbf{S}_1 \cdot \mathbf{S}_2 - j(\mathbf{S}_1 \cdot \mathbf{S}_2)^2$, where j is the biquadratic exchange constant.⁴² This leads to the following expression:

$$\chi = \frac{2Ng^2\mu_B^2}{kT} \left\{ \frac{e^{(2J-6.5j)/kT} + 5e^{(6J-13.5j)/kT} + 14e^{(12J-9j)/kT}}{1 + 3e^{(2J-6.5j)/kT} + 5e^{(6J-13.5j)/kT} + 7e^{(12J-9j)/kT}} \right\}$$

Using this model, $J = -18.2 \text{ cm}^{-1}$, $j = -0.69 \text{ cm}^{-1}$, $g = 2.10$ and $P = 0.011$. The exchange coupling constants, J for both models are similar in magnitude and suggest

antiferromagnetic coupling between two Cr(III) centres. The biquadratic exchange constant j is of much lower amplitude with a $j/2J$ ratio equal to 0.02.⁴² This model, however, employs a larger g value which is unreasonable for a d^3 ion. A larger paramagnetic impurity contribution is also required, but as shown in Figure 4.12, the model provides a good fit of the experimental data, particularly at lower temperature. The magnetic properties of **4.6** are similar to other hydroxide-bridged compounds, particularly when compared to systems possessing similar Cr-O-Cr bond angles.²⁵

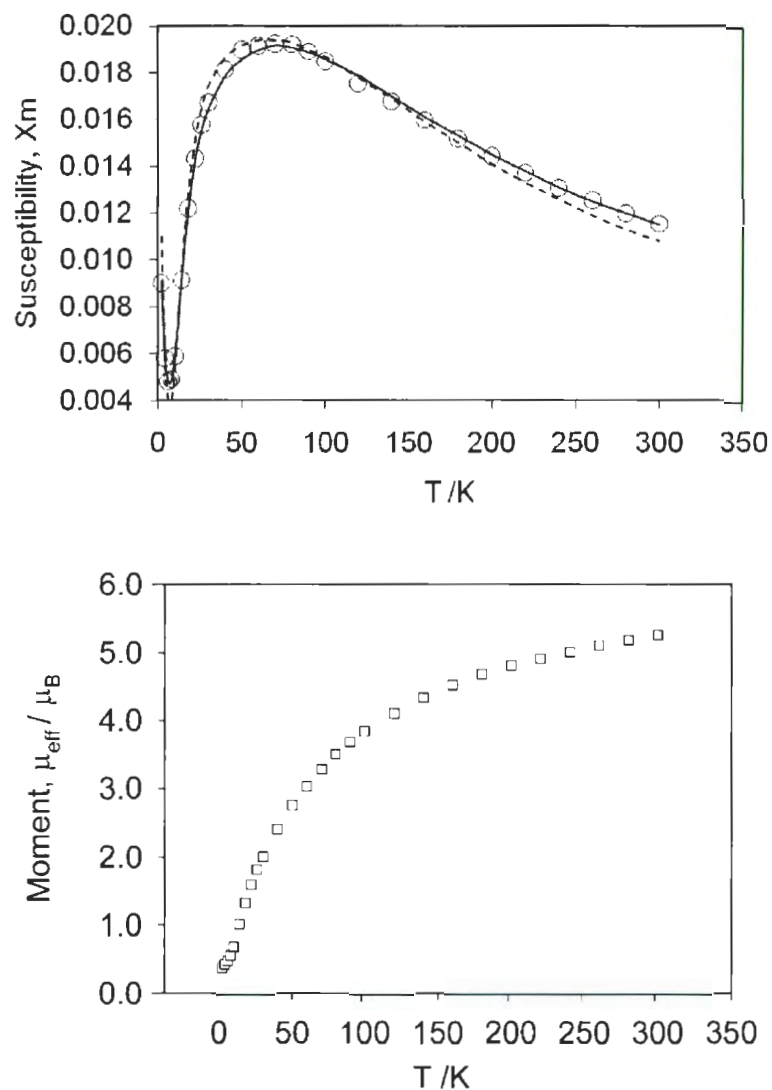


Figure 4.12. Magnetic susceptibility (per mole of bimetallic complex) vs. temperature plot (top) and magnetic moment vs. temperature plot (bottom) for **4.6**. The solid line (—) was generated using the Heisenberg dimer model with $J = -16.5 \text{ cm}^{-1}$, $g = 1.92$ and $P = 0.0079$. Experimental data were corrected for $TIP = 23.0 \times 10^{-4} \text{ cm}^3 \text{ mol}^{-1}$. The dashed line (--) was generated using a biquadratic function with $J = -18.2 \text{ cm}^{-1}$, $j = -0.69 \text{ cm}^{-1}$, $g = 2.10$ and $P = 0.011$.

The room temperature effective magnetic moment of **4.4** in the solid state was observed to be $3.5\mu_B$ per mol of Cr(III), which is slightly lower than expected for a magnetically dilute $S = 3/2$ Cr(III) centre.⁴² Variable temperature magnetic measurements show the magnetic moment is virtually constant over the temperature range studied (2 to 300 K) and no evidence of exchange between the Cr(III) centres is observed (Figure 4.13).

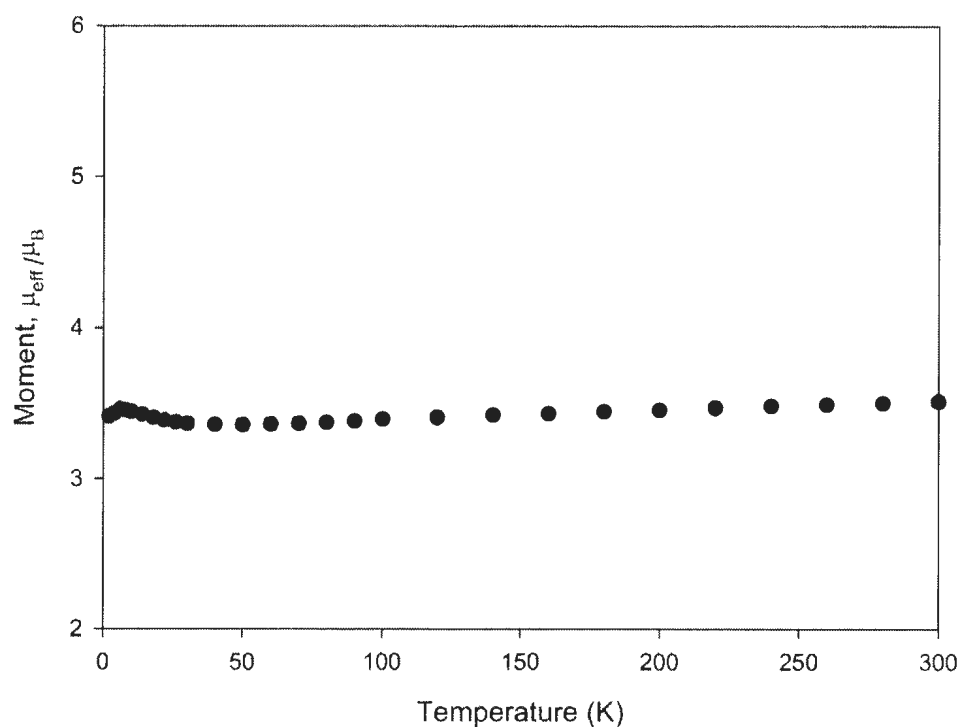


Figure 4.13. Magnetic moment vs. temperature plot for **4.4**.

4.2.5 Cyclic Voltammetry

All electrochemistry experiments were carried out using a three-compartment electrochemical cell, consisting of a platinum counter electrode, saturated calomel electrode (SCE) as a reference and a glassy carbon working electrode. Compounds **4.1**,

4.2 and **4.6** along with the ligand **L3** were investigated by cyclic voltammetry (CV) in CH_2Cl_2 solutions containing 0.1 M $[(n\text{Bu})_4\text{N}]\text{PF}_6$ electrolyte solution. Solutions were prepared in the glove box, under nitrogen and sealed with Parafilm[®]. Nitrogen was immediately bubbled through the solution once out of the glove box. All experiments were performed at a scan rate of 200 mV s^{-1} . Negative scans were performed, but no electrochemical activity was observed. All half wave potentials are very similar between each of the compounds **4.1**, **4.2** and **4.6** as was expected (Table 4.4). Compounds **4.3** and **4.5** have no electrochemical data due to insufficient quantities of available pure material. Voltammograms are shown in Figure 4.14. The CVs of the Cr(III) complexes are virtually identical and display two reversible oxidations. Related Cr(III) complexes bearing three aminophenolato⁴⁸ and two amine-bis(phenolate)¹² ligands, each display three and four oxidation waves, respectively. These oxidations were assigned as ligand centred since Cr(III) is expected to be redox-inert.⁴⁸ These ligand oxidations are attributed to the oxidation of the phenolate form of the ligand to the phenoxy radical, hence the presence of two phenolate groups per metal in complexes **4.1** and **4.2** results in the two observed potentials. Compound **4.6** was also shown to exhibit two reversible oxidation waves, suggesting that the solid state bimetallic species may undergo dissociation to form a monochromium species in solution, at least under the conditions employed during this electrochemical study. The CV of the ligand, **L3** as shown in Figure 4.15 was found to only exhibit a quasi-reversible oxidation wave.

Table 4.4 Half wave potentials for oxidation of complexes **4.1**, **4.2**, **4.6** and **L3**

	$E_2^{\text{ox}} / \text{V}$	$E_1^{\text{ox}} / \text{V}$
4.1	1.14 ^a	0.75 ^a
4.2	1.14 ^a	0.69 ^{a,c}
4.6	1.16 ^a	0.68 ^a
L3	-	0.86 ^b

^a Reversible reaction. ^b Irreversible reaction, $E_{1/2}$ value estimated.

^c Oxidation and reduction waves possess a slight shoulder.

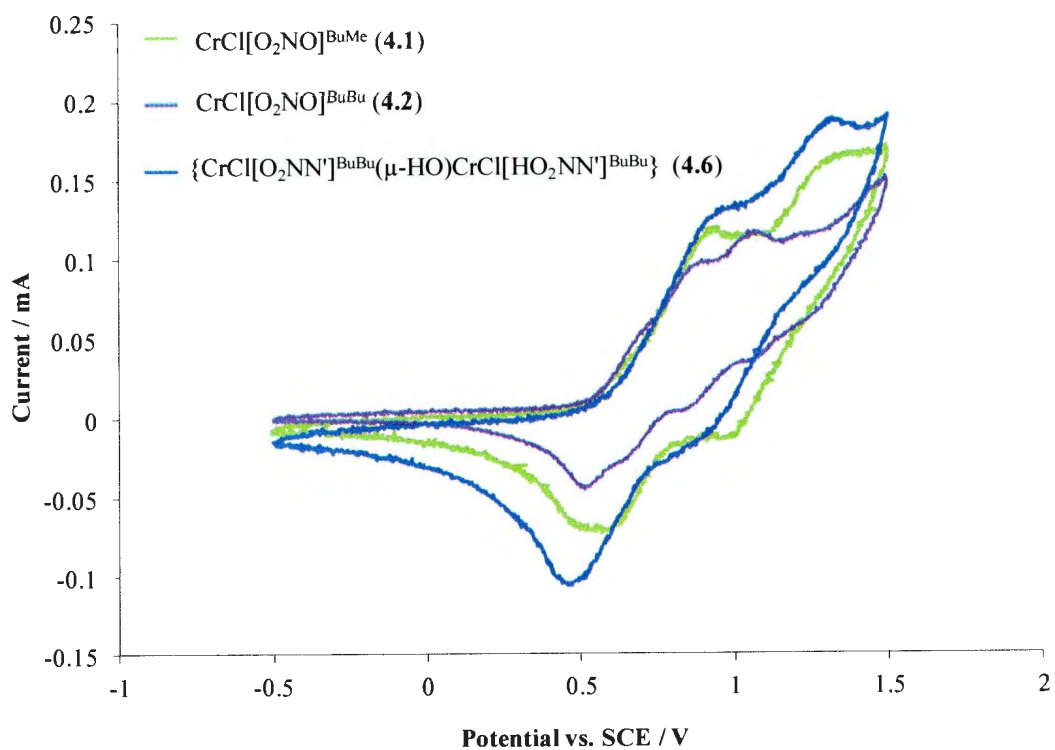


Figure 4.14. Cyclic voltammograms of **4.1**, **4.2** and **4.6** [$(n\text{-Bu})_4\text{N}]\text{PF}_6$] at 20 °C and a scan rate of 200 mV s⁻¹.

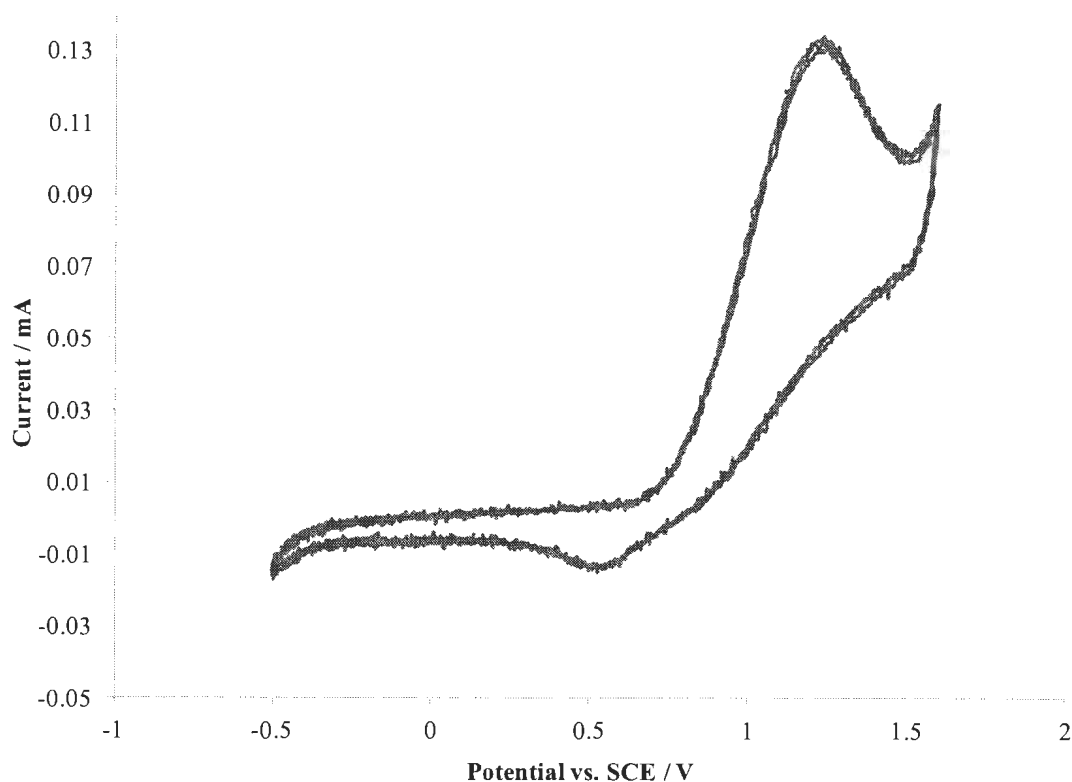
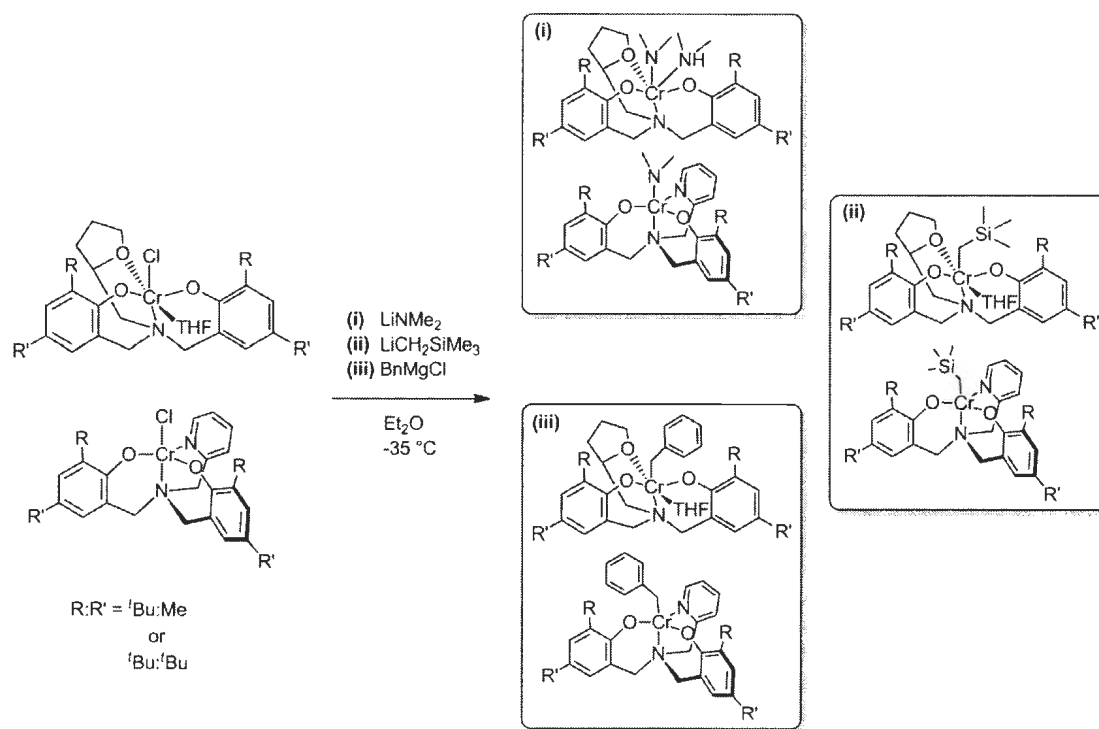


Figure 4.15. Cyclic voltammogram of L3 in CH₂Cl₂ (0.1 M [(*n*-Bu)₄N]PF₆) at 20 °C and a scan rate of 200 mV s⁻¹.

4.2.6 Attempted Synthesis of Cr Amide and Alkyl Complexes

The preparation of a series of chromium amide and alkyl derivatives was attempted. The synthesis involved the addition of the appropriate CrCl[O₂NL]^{RR'} complex (4.1, 4.2, 4.3 and 4.4) to lithium dimethylamide, trimethylsilylmethyl lithium or benzylmagnesium chloride in diethyl ether at -35 °C (Scheme 4.2). A change in colour was observed upon warming to room temperature under an inert atmosphere to either dark black (LiNMe₂), dark navy blue (LiCH₂SiMe₃) or dark green (BnMgCl). The colour

changes observed implies that a reaction took place. However, these complexes when exposed to air immediately changed colour, suggesting decomposition. Attempted recrystallizations afforded a $\text{CrNMe}_2(\text{NHMe}_2)$ hydrolysis product in the case of the dimethylamide derivative (4.7) or a $\text{Cr}_2\text{Li}_2\text{O}$ cluster (4.8) when $\text{LiCH}_2\text{SiMe}_3$ was used.



Scheme 4.2. Attempted synthesis of Cr(III) amide and alkyl complexes.

Attempts to keep complex 4.7 cold until the crystal could be mounted for XRD failed to stop the decomposition. The complex was observed to be dark black/purple under a nitrogen atmosphere changing to dark brown once exposed to air. The isolated single crystals were obtained from a 1:1 benzene-hexamethyldisiloxane mixture (Figure 4.16). Selected bond angles and distances obtained for 4.7 are given in Table 4.5.

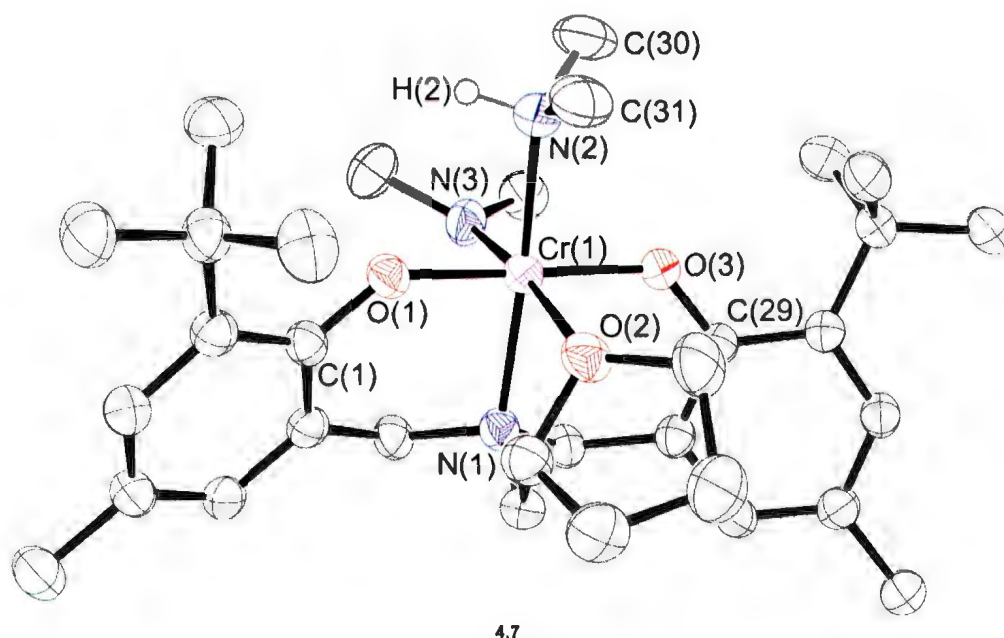


Figure 4.16. Molecular structure (ORTEP) and partially labelled numbering scheme of $\text{Cr}(\text{NMe}_2)\text{NHMe}_2[\text{O}_2\text{NO}]^{\text{BuMe}}$ complex **4.7**. Ellipsoids are shown at 50% probability and hydrogen atoms other than H(2) are omitted for clarity.

Table 4.5 Selected bond lengths (Å) and angles (°) for **4.7**

Cr(1)-O(1)	1.943(2)	O(3)-Cr(1)-O(1)	171.68(8)
Cr(1)-O(3)	1.934(2)	O(3)-Cr(1)-O(2)	88.90(8)
Cr(1)-O(2)	2.181(2)	O(1)-Cr(1)-O(2)	84.28(8)
Cr(1)-N(1)	2.118(2)	N(1)-Cr(1)-O(2)	78.01(8)
Cr(1)-N(2)	2.134(3)	N(2)-Cr(1)-O(2)	94.74(9)
Cr(1)-N(3)	1.952(3)	N(3)-Cr(1)-O(2)	172.34(9)
O(1)-C(1)	1.330(3)	O(1)-Cr(1)-N(1)	88.70(8)
O(3)-C(29)	1.336(3)	O(3)-Cr(1)-N(1)	94.54(8)
N(2)-H(2)	0.9300	N(3)-Cr(1)-N(1)	94.43(10)
		O(1)-Cr(1)-N(2)	83.66(9)
		O(3)-Cr(1)-N(2)	92.19(9)
		N(1)-Cr(1)-N(2)	169.99(10)
		N(3)-Cr(1)-N(2)	92.61(11)
		O(1)-Cr(1)-N(3)	94.43(10)
		O(3)-Cr(1)-N(3)	92.95(10)
		C(1)-O(1)-Cr(1)	133.30(18)
		C(29)-O(3)-Cr(1)	128.84(17)
		Cr(1)-N(2)-H(2)	103.6
		C(30)-N(2)-H(2)	103.6
		C(31)-N(2)-H(2)	103.6

Slow evaporation of complex **4.8** in a benzene/hexamethyldisiloxane (1:1) solution under a N₂ atmosphere in a glove box provided single crystals of $[\{\text{CrCl}[\text{O}_2\text{NO}]^{\text{BuBu}}\}_2(\mu_4\text{-O})-(\mu_3\text{-Li})_2]$, not the Cr alkyl complex as expected (Figure 4.17). The structure obtained contains two crystallographically distinct molecules within the asymmetric unit. One of these molecules is shown in the figure. Complex **4.8** consists of a dichromium species containing two amine-bis(phenolate) ligands, as well as an oxo-bridged dilithium core. The origin of the bridging oxo ligand is unknown but may be due to the presence of water in the reaction.

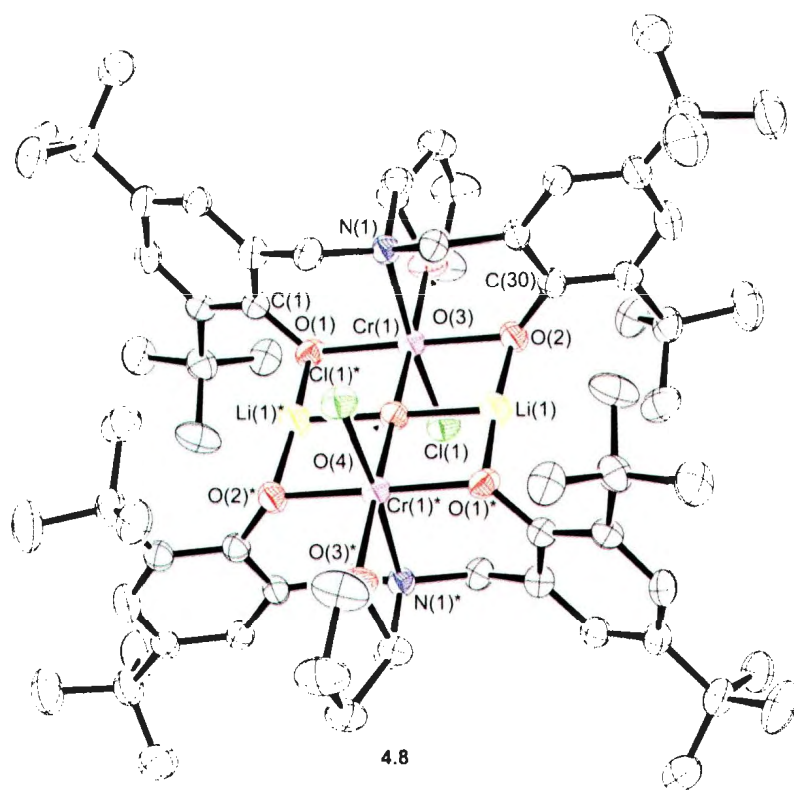


Figure 4.17. Molecular structure (ORTEP) and partially labelled numbering scheme of a single $\text{Cr}_2\text{Li}_2\text{O}_5$ moiety of complex **4.8**. Ellipsoids are shown at 50% probability and hydrogen atoms were omitted for clarity. Symmetry operation used to generate equivalent atoms: $-x, -y, -z$.

The “window pane-like” $\text{Cr}_2\text{Li}_2\text{O}_5$ core, as shown in Figure 4.18 is unusual for Cr(III) compounds. Typically lanthanides have been shown to possess this kind of coordination framework.⁴⁹⁻⁵¹ The slightly distorted octahedral geometry of complex **4.8** shows similar bond lengths and angles to the monomeric chromium chloride complex **4.2** described in Section 4.2.2.2. As expected, the bridging $\mu_4\text{-O}$ bond length is found to be

longer, 1.885(13) Å, than the μ_3 -O bond lengths involving the ligand, 1.840(14) and 1.851(14) Å. The Li_2O bridged dimer core was found to possess nearly complete planarity. Angles of $89.10(15)^\circ$ and $179.999(2)^\circ$ are obtained for $\text{O}(2)\text{-Cr}(1)\text{-O}(4)$ and $\text{Cr}(1)\text{-O}(4)\text{-Cr}(1)^*$, respectively. Selected bond lengths and angles for **4.8** are given in Table 4.6. No further characterization was performed on this complex.

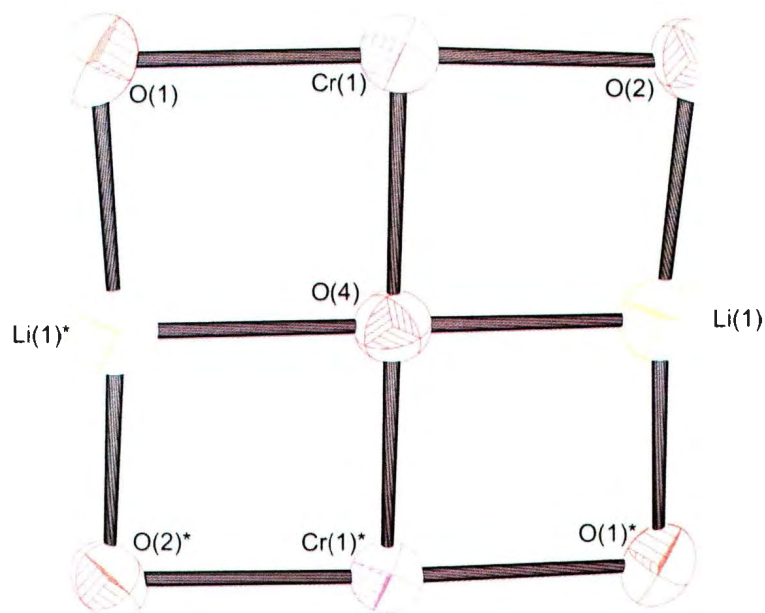


Figure 4.18. Molecular structure (ORTEP) and partially labelled numbering scheme of the “window pane-like” $\text{Cr}_2\text{Li}_2\text{O}_5$ core of complex **4.8**. Ellipsoids are shown at 50% probability and hydrogen atoms were omitted for clarity.

Table 4.6 Selected bond lengths (Å) and angles (°) for **4.8**

Cr(1)-O(1)	1.970(5)	O(1)-Cr(1)-O(2)	176.8(2)
Cr(1)-O(2)	1.972(5)	O(1)-Cr(1)-O(3)	92.1(2)
Cr(1)-O(3)	2.057(5)	O(1)-Cr(1)-O(4)	88.09(14)
Cr(1)-O(4)	1.8915(11)	O(1)-Cr(1)-N(1)	90.4(2)
Cr(1)-N(1)	2.130(5)	O(1)-Cr(1)-Cl(1)	91.05(14)
Cr(1)-Cl(1)	2.3525(19)	O(2)-Cr(1)-O(3)	90.6(2)
O(1)-C(1)	1.353(8)	O(2)-Cr(1)-O(4)	89.10(15)
O(2)-C(30)	1.353(8)	O(2)-Cr(1)-N(1)	88.4(2)
O(1)-Li(1)	1.840(14)	O(2)-Cr(1)-Cl(1)	90.71(14)
O(2)-Li(1)	1.851(14)	O(3)-Cr(1)-O(4)	176.13(14)
O(4)-Li(1)	1.885(13)	O(3)-Cr(1)-N(1)	79.6(2)
		O(3)-Cr(1)-Cl(1)	89.71(14)
		O(4)-Cr(1)-N(1)	96.52(15)
		O(4)-Cr(1)-Cl(1)	94.16(6)
		N(1)-Cr(1)-Cl(1)	169.26(16)
		O(4)-Li(1)-O(2)	93.0(6)
		O(2)-Li(1)-O(1)*	174.1(9)
		Li(1)*-O(4)-Li(1)	180.0(7)
		Li(1)*-O(1)-Cr(1)	89.3(4)
		Li(1)-O(2)-Cr(1)	88.2(4)
		Li(1)-O(4)-Cr(1)	89.6(4)
		Li(1)*-O(4)-Cr(1)	90.4(4)
		Cr(1)-O(4)-Cr(1)*	179.999(2)
		C(1)-O(1)-Cr(1)	131.0(4)
		C(1)-O(1)-Li(1)*	107.4(6)
		C(30)-O(2)-Li(1)	106.0(6)
		C(30)-O(2)-Cr(1)	132.8(4)

4.3 Experimental

4.3.1 General Experimental Conditions

Unless otherwise stated, all manipulations were performed under an atmosphere of dry oxygen-free nitrogen by means of standard Schlenk techniques or using an MBraun Labmaster glove box. Anhydrous THF was stored over sieves and distilled from sodium benzophenone ketyl under nitrogen. Reagents were purchased either from Aldrich, Alfa

Aesar or Strem and used without further purification. $\text{CrCl}_3(\text{THF})_3$ was prepared by the standard method,⁵² ligands **L1-L6** were prepared as mentioned in Chapter 2. *n*-Butyllithium was purchased as a 1.6 M solution in hexanes and used as received. Trimethylsilylmethylithium and lithium dimethylamide were purchased as solutions in pentane and hexanes, respectively. Solid reagents were obtained by careful removal of the solvents under vacuum. Benzylmagnesium chloride was purchased as a 1.0 M solution in diethyl ether and used as received. MALDI-TOF MS was performed using one of two instruments. An Applied Biosystems Voyager DE-PRO equipped with a reflectron, delayed ion extraction and high performance nitrogen laser (337 nm) was used for complexes **4.1**, **4.2**, **4.3** (prepared by *Method B*), **4.5** and **4.6**. MALDI-TOF MS for complexes **4.3** (prepared by *Method A*) and **4.4** were carried out on a QSTAR XL hybrid quadrupole/time-of-flight MS equipped with an *o*-MALDI ion source. Samples were prepared in the glove box and sealed under nitrogen in a Ziploc[®] bag for transport to the spectrometer. Anthracene was used as the matrix. Variable temperature magnetic moments were measured on powdered samples at 1000 G using a Quantum Design MPMS-5S SQUID Magnetometer. The data were corrected for background and for the diamagnetism of all atoms. UV-Vis spectra were recorded on an Ocean Optics USB4000+ fiber optic spectrophotometer. IR spectra were prepared as KBr pellets and recorded on a Bruker Tensor 27 FT-IR spectrometer. Elemental analyses were performed at Canadian Microanalytical Service, Ltd. Delta, BC, Canada or Guelph Chemical Laboratories, Guelph, ON, Canada.

4.3.2 Synthesis of Cr(III) Compounds

$\text{CrCl}(\text{THF})[\text{O}_2\text{NO}]^{\text{BuMe}}$ (**4.1**). $\text{H}_2[\text{O}_2\text{NO}]^{\text{BuMe}}$ (2.00 g, 4.41 mmol) was dissolved in THF (50 mL) and cooled to $-78\text{ }^\circ\text{C}$. *n*-Butyllithium (4.7 mL, 7.5 mmol) was slowly added to give a clear, yellow solution of $\text{Li}_2[\text{O}_2\text{NO}]^{\text{BuMe}}$, which was warmed to room temperature and further stirred for 2 h. This mixture was transferred via cannula to a solution of $\text{CrCl}_3(\text{THF})_3$ (1.64 g, 4.41 mmol) in THF (50 mL) cooled to $-78\text{ }^\circ\text{C}$ to give a bright purple suspension. Warming to room temperature and stirring for 16 h produced a dark purple solution. The solvent was removed *in vacuo* and the residue was extracted into toluene. The mixture was filtered through Celite and the solvent was removed under vacuum. The product was washed with pentane and dried to yield 2.45 g (91% yield) of purple-brown powder. Crystals suitable for X-ray diffraction were obtained by slow evaporation of a solution of **4.1** in toluene at room temperature under inert atmosphere. Anal. Calcd for $\text{C}_{33}\text{H}_{49}\text{ClCrNO}_4$: C, 64.85; H, 8.08; N, 2.29. Found: C, 64.35; H, 7.95; N, 2.16. MS (MALDI-TOF) *m/z* (% ion): 538.2 (100, $[\text{CrCl}[\text{L}]^+]$), 503.2 (45, $[\text{Cr}[\text{L}]^+]$). UV-vis (THF) λ_{max} , nm (ϵ): 237 (8360), 295 (7682), 304 (7332), 508 (176); (Toluene) λ_{max} , nm (ϵ): 296 (8682), 304 (8450), 496 (186); (Acetonitrile) λ_{max} , nm (ϵ): 246 (18 238), 291 (15 060), 303 (14 460), 552 (116). μ_{eff} (solution in benzene, $25\text{ }^\circ\text{C}$) $3.8\mu_{\text{B}}$.

$\text{CrCl}(\text{THF})[\text{O}_2\text{NO}]^{\text{BuBu}}$ (**4.2**). $\text{H}_2[\text{O}_2\text{NO}]^{\text{BuBu}}$ (2.00 g, 3.72 mmol) was dissolved in THF (50 mL) and cooled to $-78\text{ }^\circ\text{C}$. *n*-Butyllithium (4.7 mL, 7.5 mmol) was slowly added to give a clear, yellow solution of $\text{Li}_2[\text{O}_2\text{NO}]^{\text{BuBu}}$, which was warmed to room temperature and further stirred for 2 h. This mixture was transferred via cannula to a

solution of $\text{CrCl}_3(\text{THF})_3$ (1.38 g, 3.72 mmol) in THF (20 mL) cooled to $-78\text{ }^\circ\text{C}$ to give a bright purple suspension. Warming to room temperature and stirring for 16 h produced a dark purple solution. The solvent was removed *in vacuo* and the residue was extracted into toluene. The mixture was filtered through Celite and the solvent was removed under vacuum. The product was washed with pentane and dried to yield 2.17 g (84% yield) of dark purple powder. Crystals suitable for X-ray diffraction were obtained by slow evaporation of a solution of **4.2** in toluene at room temperature under inert atmosphere. Anal. Calcd for $\text{C}_{39}\text{H}_{61}\text{ClCrNO}_4$: C, 67.36; H, 8.84; N, 2.01. Found: C, 66.59; H, 8.80; N, 1.89. MS (MALDI-TOF) m/z (% ion): 622.2 (60, $[\text{CrCl}[\text{L}]^+]$), 587.2 (100, $[\text{Cr}[\text{L}]^+]$). UV-vis (THF) λ_{max} , nm (ϵ): 242 (9840), 293 (8511), 304 (7505), 512 (125); (Toluene) λ_{max} , nm (ϵ): 295 (8914), 303 sh (8068), 490 (267), 622 sh (178); (Acetonitrile) λ_{max} , nm (ϵ): 246 (9610), 290 (10 420), 300 (9420), 553 (98), 712 sh (43). μ_{eff} (solution in benzene, $25\text{ }^\circ\text{C}$) $3.8\mu_{\text{B}}$.

$\text{CrCl}[\text{O}_2\text{NN}']^{\text{BuMe}}$ (**4.3**). *Method A:* A 1.6 M solution of *n*-butyllithium in hexanes (11.7 mL, 18.7 mmol) was added via syringe to a stirring solution of $\text{H}_2[\text{O}_2\text{NN}']^{\text{BuMe}}$ (3.92 g, 8.50 mmol) in THF (50 mL) at $-78\text{ }^\circ\text{C}$. The reaction mixture was warmed to room temperature and stirred for 2 h to give a clear orange solution. This mixture was transferred via cannula to a solution of $\text{CrCl}_3(\text{THF})_3$ (3.29 g, 8.86 mmol) in THF (50 mL) at $-78\text{ }^\circ\text{C}$ to give a purple suspension. Upon warming to room temperature under nitrogen a dark purple mixture remained. The solvent was removed *in vacuo* and the residue was extracted into toluene. The mixture was filtered through Celite and the solvent was removed under vacuum. The product was washed with pentane and dried to

yield 2.37 g (49% yield) of green powder. Anal. Calcd for $C_{30}H_{38}ClCrN_2O_2 \cdot (CrCl_3(THF)_3)$: C, 54.97; H, 6.48; N, 3.05. Found: C, 53.43; H, 7.40; N, 3.24. MS (MALDI-TOF) m/z (% ion): 1090.4 (12, $[(CrCl[L])_2]^+$), 545.2 (96, $[CrCl[L]]^+$), 510.2 (25, $[Cr[L]]^+$).

Method B: Anhydrous $CrCl_2$ (0.27 g, 2.2 mmol) and $H_2[O_2NN]^BuMe$ (1.0 g, 2.2 mmol) in THF (50 mL) was stirred for 12 h under nitrogen to give a cloudy dark brown solution. The reaction flask was opened to air and the reaction mixture was stirred for 4 h. Removing the solvent *in vacuo* yielded 1.11 g of brown powder (83% yield). MS (MALDI-TOF) m/z (% ion): 1090.9 (4, $[(CrCl[L])_2]^+$), 1072.9 (10, $[(Cr[L])_2Cl(OH)]^+$), 545.2 (45, $[CrCl[L]]^+$), 510.1 (40, $[Cr[L]]^+$), 460.2 (60, $[L]^+$). UV-vis (THF) λ_{max} , nm (ϵ): 238 (8930), 278 (11 310), 303 (7410), 495 (234), 594 (126); (Toluene) λ_{max} , nm (ϵ): 286 (5650), 303 sh (3460), 599 (626); (Dichloromethane) λ_{max} , nm (ϵ): 232 (37 667), 279 (21 867), 305 sh (16 567), 598 (267). IR (cm^{-1}): 3216 (OH); 2947 (C-H); 1583 (C=C, phenyl ring); 1500 (m); 1244 (m); 862 (w).

$\{CrCl[O_2NN]^BuBu\}_2$ (**4.4**). $H_2[O_2NN]^BuBu$ (4.00 g, 7.42 mmol) was dissolved in THF (50 mL) and cooled to -78 °C. *n*-Butyllithium (9.2 mL, 15 mmol) was slowly added to give a dark orange solution of $Li_2[O_2NN]^BuBu$, which was warmed to room temperature and further stirred for 2 h. This mixture was transferred via cannula to a suspension of $CrCl_3(THF)_3$ (2.75 g, 7.39 mmol) in THF (50 mL) cooled to -78 °C to give a dark brown mixture. Upon warming to room temperature and stirring for 16 h the solids dissolved giving a dark brown solution. The solvent was removed *in vacuo* and the residue was extracted into toluene. The mixture was filtered through Celite and the solvent was

removed under vacuum. The product was washed with pentane and dried to yield 4.62 g (98% yield) of dark brown powder. Crystals suitable for X-ray diffraction were obtained by slow evaporation of a solution of **4.4** in benzene at room temperature under inert atmosphere. Anal. Calcd for $C_{36}H_{50}ClCrN_2O_2$: C, 67.47; H, 7.86; N, 4.37. Found: C, 67.12; H, 8.36; N, 4.38. MS (MALDI-TOF) m/z (% ion): 1259.6 (20, $[(CrCl[L])_2]^+$), 629.3 (100, $[CrCl[L]]^+$), 593.3 (40, $[Cr[L]]^+$). UV-vis (CH_2Cl_2) λ_{max} , nm (ϵ): 235 (46 500), 280 sh (23 000), 386 sh (3134), 606 (450). μ_{eff} (solid, 25 °C) $3.5\mu_B$.

$\{CrCl[O_2NN']^{MeMe}\}(\mu-HO)\{CrCl[HO_2NN']^{MeMe}\}$ (**4.5**). *Method A:* A 1.6 M hexanes solution of *n*-butyllithium (5.6 mL, 9.0 mmol) was added via syringe to a stirring solution of $H_2[O_2NN']^{MeMe}$ (2.00 g, 4.44 mmol) in THF (50 mL) at -78 °C. The reaction mixture was warmed to room temperature and stirred for 2 h to give a clear pale yellow solution. This mixture was transferred via cannula to a solution of $CrCl_3(THF)_3$ (1.65 g, 4.44 mmol) in THF (25 mL) at -78 °C to give a cloudy orange/brown solution. Upon warming to room temperature and stirring overnight the mixture darkened. The solvent was removed *in vacuo* and the product was extracted into dichloromethane. The mixture was filtered through Celite and the solvent was removed under vacuum. The product was then washed with pentane and dried to yield 1.64 g (80% yield) of a dark olive green powder.

Method B: Anhydrous $CrCl_2$ (0.33 g, 2.7 mmol) and $H_2[O_2NN']^{MeMe}$ (1.0 g, 2.7 mmol) in THF (50 mL) was stirred for 12 h to give a cloudy teal blue solution with teal blue solid residue. The reaction flask was opened to air and the reaction mixture was stirred for 4 h to give a dark green/black solution with a green precipitate. Removing the

solvent under vacuum yielded an olive green powder. The crude product was recrystallized from toluene in air to give analytically pure **4.5** (65% yield). Anal. Calcd for C₄₈H₅₄Cl₂Cr₂N₄O₅: C, 61.21; H, 5.78; N, 5.95. Found: C, 60.27; H, 5.74; N, 5.90. MS (MALDI-TOF) *m/z* (% ion): 887.1 (100, [(Cr[L])₂Cl]⁺), 461.1 (40, [CrCl[L]]⁺). UV-vis (THF) λ_{max}, nm (ε): 251 (855), 307 (1248), 605 sh (211); (Toluene) λ_{max}, nm (ε): 321 (1215), 630 sh (209); (Acetonitrile) λ_{max}, nm (ε): 245 (1186), 288 (1179), 385 (1621), 598 (262). IR (cm⁻¹): 3407 (OH); 2917 (C-H); 1611 (C=C, phenyl ring); 1477 (s); 1261 (m); 856 (w); 809 (w). μ_{eff} (solid, 25 °C) 5.3μ_B.



A 1.6 M hexanes solution of *n*-butyllithium (6.0 mL, 8.1 mmol) was added via syringe to a stirring solution of H₂[O₂NN']^{BuBu} (2.00 g, 3.67 mmol) in THF (50 mL) at -78 °C. The reaction mixture was warmed to room temperature and stirred for 2 h to give a clear pale yellow solution. This mixture was transferred via cannula to a solution of CrCl₃(THF)₃ (1.36 g, 3.67 mmol) in THF (25 mL) at -78 °C to give a cloudy orange/brown solution. Upon warming to room temperature and stirring overnight the mixture darkened. The solvent was removed *in vacuo* and the residue was extracted into toluene. The mixture was filtered through Celite and the solvent was removed under vacuum. The product was washed with pentane and dried to yield 2.47 g (53% yield) of dark olive green powder.

Method B: Anhydrous CrCl₂ (0.23 g, 1.9 mmol) and H₂[O₂NN']^{BuBu} (1.0 g, 1.9 mmol) in THF (50 mL) was stirred for 12 h under nitrogen to give a cloudy dark brown solution. The reaction flask was opened to air and the reaction mixture was stirred for 4 h. Removing the solvent *in vacuo* yielded 1.20 g of dark brown powder. The crude product

was recrystallized from toluene in air to give analytically pure **4.6** (70% yield). Anal. Calcd for $C_{72}H_{102}Cl_2Cr_2N_4O_5$: C, 67.64; H, 8.04; N, 4.38. Found: C, 66.53; H, 8.05; N, 4.11. MS (MALDI-TOF) m/z (% ion): 1223.6 (18, $[(Cr[L])_2Cl]^+$), 629.1 (95, $[CrCl[L]]^+$), 594.2 (25, $[Cr[L]]^+$). UV-vis (THF) λ_{max} , nm (ϵ): 245 (28 500), 287 (21 067), 301 sh (18 767), 386 (3267), 634 (163); (Toluene) λ_{max} , nm (ϵ): 289 (9660), 301 sh (8550), 409 (2120), 621 (204); (Acetonitrile) λ_{max} , nm (ϵ): 220 (35 433), 241 (28 033), 288 (13 967), 385 sh (2300), 612 (184). IR (cm^{-1}): 3422 (OH); 2955 (C-H); 1612 (C=C, phenyl ring); 1500 (m); 1240 (m); 850 (w). μ_{eff} (solid, 25 °C) $5.3\mu_B$.

4.3.2.1 Reaction of CrCl complexes with salt metathesis reagents

*Attempted synthesis of $Cr(NMe_2)[O_2NL]^RR'$. $CrCl(THF)[O_2NO]^{BuMe}$ (**4.1**) (1.0180 g, 1.6656 mmol) was dissolved in ~12 mL of Et_2O and cooled to -35 °C. $LiNMe_2$ (0.0838 g, 1.64 mmol) was added to the cold solution containing **4.1**. The brown mixture was warmed to room temperature and held at this temperature while stirring for ~12 h, giving a dark black solution. The solution was filtered through Celite and dried *in vacuo*. Crystals were obtained by slow evaporation in a 1:1 benzene/hexamethyldisiloxane solution at -35 °C under inert atmosphere. Crystals suitable for X-ray diffraction revealed the structure to be **4.7**.*

*Attempted synthesis of $Cr(CH_2Si(CH_3)_3)[O_2NL]^RR'$. $CrCl(THF)[O_2NO]^{BuBu}$ (**4.2**) (0.3001 g, 0.4316 mmol) was dissolved in ~5 mL of Et_2O and cooled to -35 °C. $LiCH_2Si(CH_3)_3$ (0.0409 g, 0.434 mmol) was added to the cold solution containing **4.2**. The dark pink mixture was warmed to room temperature and held at this temperature*

while stirring for ~30 min, giving a dark navy solution. The solution was filtered through Celite and dried *in vacuo*. Crystals were obtained by slow evaporation of **4.8** in a 1:1 benzene/hexamethyldisiloxane solution at -35 °C under inert atmosphere. Crystals suitable for X-ray diffraction revealed the structure to be **4.8**.

*Attempted synthesis of Cr(CH₂Ph)[O₂NL]^{RR'}. {CrCl[O₂NNⁱBuBu]}₂ (**4.4**)* (0.3012 g, 0.2389 mmol) was dissolved in ~5 mL of Et₂O and cooled to -35 °C. BnMgCl (0.48 mL, 0.48 mmol) in Et₂O was added dropwise to the cold solution containing **4.4**. The green mixture was warmed to room temperature and held at this temperature while stirring for ~2 h, giving a dark green solution. The solution was filtered through Celite and dried *in vacuo*. All attempts to grow crystals failed and no further characterization was attempted.

4.3.3 X-ray Crystallography

Crystallographic and structure refinement data are given in Table 4.7 for complexes **4.1**, **4.2**, **4.4**, **4.5** and **4.6** and Table 4.8 for complexes **4.7** and **4.8**. Diffraction data were collected on a Rigaku Saturn CCD area detector with a SHINE optic and Mo-K α radiation solved on an AFC8-Saturn 70 single crystal X-ray diffractometer from Rigaku, equipped with an X-stream 2000 low temperature system. The data were processed using CrystalClear⁵³ software and corrected for Lorentz and polarization effects and absorption.⁵⁴ Neutral atom scattering factors for all non-hydrogen atoms were taken from the *International Tables for X-ray Crystallography*.⁵⁵ The structure was solved by direct methods using SIR92⁵⁶ and expanded using Fourier techniques (DIRDIF99).⁵⁷ All non-hydrogen atoms were refined anisotropically. Hydrogen atoms were refined using the

riding model. Anomalous dispersion effects were included in Fcalc;⁵⁸ the values for $\Delta f'$ and $\Delta f''$ were those of Creagh and McAuley.⁵⁹ The values for the mass attenuation coefficients are those of Creagh and Hubbell.⁶⁰ All calculations were performed using the CrystalStructure⁶¹ crystallographic software package except for refinement, which was performed using SHELXL-97.⁶² For **4.1**, one 3/5-occupancy toluene molecule is present as lattice solvent. A pendant ligand tetrahydrofuran group is disordered over two positions, each with 50% occupancy. For **4.2**, one disordered 1/2-occupancy toluene molecule is present as lattice solvent. A pendant ligand tetrahydrofurfuryl group is disordered over two positions (65%/35%). Disordered solvent lattice for **4.4** was removed through applying Platon's Squeeze⁶³ procedure. For **4.6**, H(117 and 118) were introduced in difference map positions, and initially refined positionally (on x,y,z) with fixed thermal parameters, and finally on the riding model, with isotropic thermal parameters set twenty percent greater than those of their bonding partners. For **4.7**, H(2) was located in its difference map position, but introduced in a calculated position and refined on a riding model with isotropic thermal parameters 1.2 times that of their bonding partners. For **4.8**, the asymmetric unit contains two "half-molecules"; upon symmetry expansion, two Cr₂Li₂O₅ grids result. The ligands in each moiety both contain a disordered THF group. In one case a single atom is disordered over two sites, each with 50% occupancy. In the second case, the disorder involves two atoms, each disordered over two sites, one with 70% occupancy, and the other with 30% occupancy. The asymmetric unit also contains two badly disordered lattice solvent benzene rings. The rings were modeled as disordered over two positions, with 50%/50% occupancy. Distance, angle, plane and rigid bond restraints were applied to both disorder groups.

Single crystals of **4.5** were coated with Paratone-N oil, mounted using a polyimide MicroMount and frozen in the cold nitrogen stream of the goniometer. A hemisphere of data was collected on a Bruker AXS P4/SMART 1000 diffractometer using ω and θ scans with a scan width of 0.3° and 40 s exposure times. The detector distance was 5 cm. The data were reduced (SAINT)⁶⁴ and corrected for absorption (SADABS).⁶⁵ The structure was solved by direct methods and refined by full-matrix least squares on F^2 (SHELXTL)⁶². A toluene molecule was disordered over two sites and refined with equal site occupancy factors. Structural illustrations were created using ORTEP-III (v. 2.02) for Windows.⁶⁶

Table 4.7 Crystallographic and structure refinement data for **4.1**, **4.2**, **4.4**, **4.5** and **4.6**

Compound	4.1	4.2	4.4	4.5	4.6
Chemical formula	C ₃₃ H ₅₀ NO ₄ CrCl (C ₇ H ₈) _{0.6}	C ₃₉ H ₆₁ NO ₄ CrCl (C ₇ H ₈) _{0.5}	[(C ₃₆ H ₅₀ N ₂ O ₂)ClCr] ₂ (C ₆ H ₆) _{2.5}	[(C ₂₄ H ₂₆ N ₂ O ₂)CrCl] ₂ (HO)(H)(C ₇ H ₈)	[(C ₃₆ H ₅₀ O ₂ N ₂)CrCl] ₂ (HO)(H)(C ₇ H ₈) ₂
Formula weight	667.50	741.43	1455.79	1033.99	1462.80
<i>T</i> /K	118	123	153	198	118
Colour, habit	Pink, irregular	Pink, prism	Blue, prism	Green, plate	Green, prism
Crystal dimensions/mm	0.12 × 0.12 × 0.06	0.32 × 0.06 × 0.05	0.21 × 0.14 × 0.08	0.40 × 0.20 × 0.05	0.31 × 0.26 × 0.25
Crystal system	Monoclinic	Monoclinic	Monoclinic	Monoclinic	Triclinic
Space group	<i>P</i> 2 ₁ / <i>c</i> (#14)	<i>P</i> 2 ₁ / <i>c</i> (#14)	<i>P</i> 2 ₁ / <i>c</i> (#14)	<i>P</i> 2/ <i>n</i> (#13)	<i>P</i> $\bar{1}$ (#2)
<i>a</i> /Å	16.182(4)	12.816(2)	15.3979(12)	14.222(3)	15.8636(18)
<i>b</i> /Å	16.300(3)	20.060(4)	13.4522(10)	13.867(3)	16.1865(16)
<i>c</i> /Å	16.266(4)	16.455(3)	21.3183(17)	14.612(3)	18.334(2)
α /°	90	90	90	90	71.836(7)
β /°	118.046(4)	94.055(4)	109.020(2)	108.533(3)	78.206(9)
γ /°	90	90	90	90	67.999(7)
<i>V</i> /Å ³	3786.7(15)	4219.6(13)	4174.7(6)	2732.2(9)	4126.9(8)
<i>Z</i>	4	4	2	2	2
<i>D</i> _c /g cm ⁻³	1.171	1.167	1.158	1.257	1.177
μ (MoK α)/cm ⁻¹	4.09	3.73	3.73	5.44	3.79
<i>F</i> (000)	1432	1600	1558	1084	1568.00
θ Range for collection /°	2.4391 to 30.6011	2.1975 to 30.8114	3.03 to 26.50	1.47 to 27.50	2.56 to 26.50
Reflections collected	25 913	37 202	53 858	18 165	71 780
Independent reflections	7833	8726	8 649	6028	17 081
<i>R</i> (int)	0.0609	0.0532	0.0640	0.0573	0.0281
<i>R</i> , <i>wR</i> ₂ (all)	0.1246, 0.2911	0.0807, 0.1964	0.0847, 0.1668	0.1339, 0.2609	0.0699, 0.1924
<i>R</i> , <i>wR</i> ₂ [<i>I</i> > 2 σ (<i>I</i>)]	0.1049, 0.2758	0.0744, 0.1906	0.0640, 0.1548	0.0701, 0.2174	0.0682, 0.1905
GOF on <i>F</i> ²	1.148	1.101	1.077	1.046	1.080

Table 4.8 Crystallographic and structure refinement data for **4.7** and **4.8**

Compound	4.7	4.8
Chemical formula	C ₃₃ H ₅₄ CrN ₃ O ₃	[(C ₃₅ H ₅₃ NO ₃) ₂ Cr ₂ Li ₂ Cl ₂ O] (C ₆ H ₆) ₂
Formula weight	592.80	1432.62
<i>T</i> /K	153	153
Colour, habit	Brown, prism	Green, prism
Crystal dimensions/mm	0.15 × 0.12 × 0.10	0.36 × 0.35 × 0.19
Crystal system	Monoclinic	Triclinic
Space group	<i>P</i> 2 ₁ / <i>c</i> (#14)	<i>P</i> $\bar{1}$ (#2)
<i>a</i> /Å	12.9786(18)	15.6451(13)
<i>b</i> /Å	16.844(2)	15.9918(11)
<i>c</i> /Å	18.392(3)	19.5927(19)
α /°	90	68.284(9)
β /°	124.224(4)	72.270(9)
γ /°	90	61.797(8)
<i>V</i> /Å ³	3324.5(8)	3962.8(6)
<i>Z</i>	4	2
<i>D</i> _c /g cm ⁻³	1.184	1.201
μ (MoK α)/cm ⁻¹	3.79	3.94
<i>F</i> (000)	1284	1536
θ Range for collection /°	2.2490 to 30.6546	2.2123 to 30.7083
Reflections collected	43 049	32 435
Independent reflections	6891	16 066
<i>R</i> (int)	0.0668	0.0393
<i>R</i> , <i>wR</i> ₂ (all)	0.0777, 0.1822	0.1122, 0.3379
<i>R</i> , <i>wR</i> ₂ [<i>I</i> > 2 σ (<i>I</i>)]	0.0745, 0.1798	0.1052, 0.3347
GOF on <i>F</i> ²	1.211	1.074

4.4 Conclusion

A series of chromium complexes stabilized by a family of dianionic amine-bis(phenolate) ligands was synthesized and characterized. In the solid state, chromium tetrahydrofurfuryl complexes made through the salt metathesis method generated monometallic, THF coordinated compounds when handled under strictly anhydrous conditions. Interestingly, related chromium pyridyl complexes form bimetallic dichromium complexes in air or under a N₂ atmosphere. These chromium complexes are hygroscopic and react with water to generate a HO⁻ bridging group, found through a closer investigation of the crystallographic data. Cleavage of a water H-O bond results in protonation of one of the ligand phenolate groups and incorporation of the resulting hydroxide bridge into the molecule. All complexes reported contained six-coordinate chromium in an octahedral geometry. Two additional compounds were structurally characterized by single crystal X-ray diffraction. The attempted synthesis of Cr amide and alkyl compounds led to the production of Cr(NMe₂)NHMe₂[O₂NO]^{BuMe} and [$\{\text{CrCl}[\text{O}_2\text{NO}]^{\text{BuBu}}\}_2(\mu_4\text{-O})-(\mu_3\text{-Li})_2$], respectively. The following chapter will introduce the use of the Cr diamine-bis(phenolate) complex **4.4** for the copolymerization of epoxides with carbon dioxide.

4.5 References

- (1) Wichmann, O.; Sillanpää, R.; Lehtonen, A. *Coord. Chem. Rev.* **2012**, *256*, 371-392.
- (2) Rodríguez, L.; Labisbal, E.; Sousa-Pedrares, A.; García-Vázquez, J. A.; Romero, J.; Durán, M. L.; Real, J. A.; Sousa, A. *Inorg. Chem.* **2006**, *45*, 7903-7914.
- (3) Velusamy, M.; Palaniandavar, M.; Gopalan, R. S.; Kulkarni, G. U. *Inorg. Chem.* **2003**, *42*, 8283-8293.
- (4) Safaei, E.; Weyhermüller, T.; Bothe, E.; Wieghardt, K.; Chaudhuri, P. *Eur. J. Inorg. Chem.* **2007**, 2334-2344.
- (5) Chowdhury, R. R.; Crane, A. K.; Fowler, C.; Kwong, P.; Kozak, C. M. *Chem. Commun.* **2008**, 94-96.
- (6) Hasan, K.; Fowler, C.; Kwong, P.; Crane, A. K.; Collins, J. L.; Kozak, C. M. *Dalton Trans.* **2008**, 2991-2998.
- (7) Reckling, A. M.; Martin, D.; Dawe, L. N.; Decken, A.; Kozak, C. M. *J. Organomet. Chem.* **2011**, *696*, 787-794.
- (8) Das, U. K.; Bobak, J.; Fowler, C.; Hann, S. E.; Petten, C. F.; Dawe, L. N.; Decken, A.; Kerton, F. M.; Kozak, C. M. *Dalton Trans.* **2010**, *39*, 5462-5477.
- (9) Darensbourg, D. J.; Fitch, S. B. *Inorg. Chem.* **2007**, *46*, 5474-5476.
- (10) Darensbourg, D. J.; Ulusoy, M.; Karroonnirum, O.; Poland, R. R.; Reibenspies, J. H.; Çetinkaya, B. *Macromolecules* **2009**, *42*, 6992-6998.
- (11) Lehtonen, A.; Wasberg, M.; Sillanpää, R. *Polyhedron* **2006**, *25*, 767-775.
- (12) Weyhermüller, T.; Paine, T. K.; Bothe, E.; Bill, E.; Chaudhuri, P. *Inorg. Chim. Acta* **2002**, *337*, 344-356.
- (13) Gibson, V.; Newton, C.; Redshaw, C.; Solan, G.; White, A. P.; Williams, D.; Maddox, P. *Chem. Commun.* **1998**, 1651-1652.
- (14) MacAdams, L. A.; Buffone, G. P.; Incarvito, C. D.; Rheingold, A. L.; Theopold, K. *H. J. Am. Chem. Soc.* **2005**, *127*, 1082-1083.
- (15) Smith, K. M. *Curr. Org. Chem.* **2006**, *10*, 955-963.

- (16) Darensbourg, D. J.; Phelps, A. L. *Inorg. Chem.* **2005**, *44*, 4622-4629.
- (17) Darensbourg, D. J.; Frantz, E. B.; Andreatta, J. R. *Inorg. Chim. Acta* **2007**, *360*, 523-528.
- (18) Eelman, M.; Blacquiere, J.; Moriarty, M.; Fogg, D. *Angew. Chem. Int. Ed.* **2008**, *47*, 303-306.
- (19) Ikpo, N.; Butt, S. M.; Collins, K. L.; Kerton, F. M. *Organometallics* **2009**, *28*, 837-842.
- (20) Böttcher, A.; Elias, H.; Glerup, J.; Neuburger, M.; Olsen, C.,E.; Springborg, J.; Weihe, H.; Zehnder, M. *Acta Chem. Scand.* **1994**, *48*, 981-988.
- (21) Böttcher, A.; Elias, H.; Glerup, J.; Neuburger, M.; Olsen, C.,Erik; Paulus, H.; Springborg, J.; Zehnder, M. *Acta Chem. Scand.* **1994**, *48*, 967-980.
- (22) Sanzenbacher, R.; Böttcher, A.; Elias, H.; Hüber, M.; Haase, W.; Glerup, J.; Jensen, T. B.; Neuburger, M.; Zehnder, M.; Springborg, J.; Olsen, C. E. *Inorg. Chem.* **1996**, *35*, 7493-7499.
- (23) Cox, A. R. F.; Gibson, V. C.; Marshall, E. L.; White, A. J. P.; Yeldon, D. *Dalton Trans.* **2006**, 5014-5023.
- (24) Dossetter, A. G.; Jamison, T. F.; Jacobsen, E. N. *Angew. Chem. Int. Ed.* **1999**, *38*, 2398-2400.
- (25) Andersen, N. H.; Døssing, A.; Mølgaard, A. *Inorg. Chem.* **2003**, *42*, 6050-6055.
- (26) Cline, S. J.; Glerup, J.; Hodgson, D. J.; Jensen, G. S.; Pedersen, E. *Inorg. Chem.* **1981**, *20*, 2229-2233.
- (27) Rупpa, K.,B.P.; Feghali, K.; Kovacs, I.; Aparna, K.; Gambarotta, S.; Yap, G.,P.A.; Bensimon, C. *J. Chem. Soc., Dalton Trans.* **1998**, 1595-1606.
- (28) Gafford, B. G.; Holwerda, R. A.; Schugar, H. J.; Potenza, J. A. *Inorg. Chem.* **1988**, *27*, 1126-1128.
- (29) Di Vaira, M.; Mani, F. *Inorg. Chem.* **1984**, *23*, 409-412.
- (30) Wieghardt, K.; Schmidt, W.; Van Eldik, R.; Nuber, B.; Weiss, J. *Inorg. Chem.* **1980**, *19*, 2922-2926.

- (31) Heinrichs, M. A.; Hodgson, D. J.; Michelsen, K.; Pedersen, E. *Inorg. Chem.* **1984**, *23*, 3174-3180.
- (32) Chen, X.; Xia, J.; Zhao, B.; Cheng, P.; Yan, S.; Liao, D.; Jiang, Z.; Song, H.; Wang, H. *J. Coord. Chem.* **2004**, *57*, 231-237.
- (33) Novitchi, G.; Costes, J.; Ciornea, V.; Shova, S.; Filippova, I.; Simonov, Y. A.; Gulea, A. *Eur. J. Inorg. Chem.* **2005**, 929-937.
- (34) Zhang, L.; Wang, Y.; Gu, W.; Liu, X.; Liao, D. *Inorg. Chem. Commun.* **2006**, *9*, 46-49.
- (35) Hesschenbrouck, J.; Solari, E.; Floriani, C.; Re, N.; Rizzoli, C.; Chiesi-Villa, A. *J. Chem. Soc., Dalton Trans.* **2000**, 191-198.
- (36) Agapie, T.; Schofer, S. J.; Labinger, J. A.; Bercaw, J. E. *J. Am. Chem. Soc.* **2004**, *126*, 1304-1305.
- (37) MacAdams, L. A.; Kim, W.; Liable-Sands, L.; Guzei, I. A.; Rheingold, A. L.; Theopold, K. H. *Organometallics* **2002**, *21*, 952-960.
- (38) Gibson, V. C.; Newton, C.; Redshaw, C.; Solan, G. A.; White, A. J. P.; Williams, D. J.; Maddox, P. J. *Chem. Commun.* **1998**, 1651-1652.
- (39) Gibson, V. C.; Newton, C.; Redshaw, C.; Solan, G. A.; White, A. J. P.; Williams, D. *J. Eur. J. Inorg. Chem.* **2001**, 1895-1903.
- (40) Wong, E. W. Y.; Das, A. K.; Katz, M. J.; Nishimura, Y.; Batchelor, R. J.; Onishi, M.; Leznoff, D. B. *Inorg. Chim. Acta* **2006**, *359*, 2826-2834.
- (41) O'Connor, C. J. *Prog. Inorg. Chem.* **1982**, *29*, 203.
- (42) Carlin, R. L. In *Magnetochemistry*; Springer-Verlag: Heidelberg, **1986**.
- (43) Hodgson, D. J.; Pedersen, E. *Inorg. Chem.* **1980**, *19*, 3116-3121.
- (44) Veal, J. T.; Jeter, D. Y.; Hempel, J. C.; Eckberg, R. P.; Hatfield, W. E.; Hodgson, D. *J. Inorg. Chem.* **1973**, *12*, 2928-2931.
- (45) Cline, S. J.; Kallesoe, S.; Pedersen, E.; Hodgson, D. J. *Inorg. Chem.* **1979**, *18*, 796-801.
- (46) Scaringe, R. P.; Singh, P.; Eckberg, R. P.; Hatfield, W. E.; Hodgson, D. J. *Inorg. Chem.* **1975**, *14*, 1127-1133.

- (47) Veal, J. T.; Hatfield, W. E.; Jeter, D. Y.; Hempel, J. C.; Hodgson, D. J. *Inorg. Chem.* **1973**, *12*, 342-346.
- (48) Chun, H.; Verani, C. N.; Chaudhuri, P.; Bothe, E.; Bill, E.; Weyhermüller, T.; Wieghardt, K. *Inorg. Chem.* **2001**, *40*, 4157-4166.
- (49) Aspinall, H. C.; Tillotson, M. R. *Inorg. Chem.* **1996**, *35*, 2163-2164.
- (50) Dube, T.; Gambarotta, S.; Yap, G. *Organometallics* **1998**, *17*, 3967-3973.
- (51) Barroso, S.; Cui, J.; Carretas, J. M.; Cruz, A.; Santos, I. C.; Duarte, M. T.; Telo, J. P.; Marques, N.; Martins, A. M. *Organometallics* **2009**, *28*, 3449-3458.
- (52) So, J. H.; Boudjouk, P. *Inorg. Chem.* **1990**, *29*, 1592-1593.
- (53) Pflugrath, J. W. *Acta Crystallogr., Sect. D: Biol. Crystallogr.* **1999**, *55*, 1718-1725.
- (54) Larson, A. C. In *Crystallographic Computing*; Ahmed, F. R., Ed.; Munksgaard, Copenhagen, 1970, p. 291.
- (55) Cromer, D. T.; Waber, J. T. In *International Tables for X-ray Crystallography*; The Kynoch Press: Birmingham, UK, **1974**.
- (56) Altomare, A.; Cascarano, G.; Giacovazzo, C.; Guagliardi, A.; Burla, M.; Polidori, G.; Camalli, M. *J. Appl. Crystallogr.* **1994**, *27*, 435.
- (57) Beurskens, P. T.; Admiraal, G.; Beurskens, G.; Bosman, W. P.; de Gelder, R.; Israel, R.; Smits, J. M. M. In *DIRDIF99*, University of Nijmegen, Netherlands, **1999**.
- (58) Ibers, J. A.; Hamilton, W. C. *Acta Crystallogr.* **1964**, *17*, 781-782.
- (59) Creagh, D. C.; McAuley, W. J. In *International Tables for Crystallography (A.J.C. Wilson, ed.)*; Kluwer Academic Publishers: Boston, **1992**; Vol. C, Table 4.2.6.8, pages 219-222.
- (60) Creagh, D. C.; Hubbell, J. H. In *International Tables for Crystallography (A.J.C. Wilson, ed.)*; Kluwer Academic Publishers: Boston, **1992**; Vol. C, Table 4.2.4.3, pages 200-206.
- (61) Watkin, D. J.; Prout, C. K.; Carruthers, J. R.; Betteridge, P. W. *CRYSTALS Issue 10*, Chemical Crystallography Laboratory, Oxford, UK, **1996**; *CrystalStructure 3.7.0: Crystal Structure Analysis Package*, Rigaku and Rigaku/MSK, The Woodlands, Texas, 2000-2005.

- (62) Sheldrick, G. M. SHELXL-97, *Program for refinement of crystal structures*, University of Göttingen, Germany, **1997**.
- (63) Spek, A. L. *J. Appl. Cryst.* **2003**, 36, 7-13.
- (64) SAINT 7.23A, Bruker AXS Inc., Madison, Wisconsin **2006**.
- (65) Sheldrick, G. M. SADABS, *Program for area detector adsorption correction*, Bruker AXS Inc., Madison, Wisconsin, **2004**.
- (66) Farrugia, L. J. *J. Appl. Crystallogr.* **1997**, 30, 565.

Chapter 5

Chromium Amine-bis(phenolate) Complexes for the Copolymerization of Epoxides and Carbon Dioxide

5.1 Introduction

In recent years, the search towards a more reactive metal catalyst for the copolymerization of epoxides and carbon dioxide to yield polycarbonates has been actively pursued.¹⁻⁶ The use of carbon dioxide as a C1 feedstock is appealing due to its widespread availability, low cost and non-toxicity.³ Metals such as Al, Zn, Cr, Co and Fe have been examined for use in the copolymerization of carbon dioxide (CO₂) and epoxides.

Metal catalysts using Cr(III) as the active site have shown promising results.⁷⁻¹¹ Previous reports of homogeneous catalysis towards epoxide and CO₂ copolymerization include such ligand classes as the porphyrins, where both Cr¹²⁻¹⁴ and Al¹⁵ complexes have been used. Another established ligand system, introduced by Darensbourg and Holtcamp, used for epoxide/CO₂ copolymerization includes the phenoxides, where Zn is commonly the metal used.¹⁶⁻¹⁸ Although these Zn complexes did not produce high turnover frequencies (TOFs), they did provide a leap from the more traditional heterogeneous Zn catalysts to homogeneous systems. Further research towards a more active catalyst led Coates and co-workers to explore the use of β -diketiminato (BDI) ligand systems with Zn at lower pressures and temperatures than had previously been reported.¹⁹ The most widely

studied ligands for epoxide/CO₂ copolymerization have been the salen and, more recently, the salan ligands, which have been primarily used with Cr^{10,11,20-22} and Co.^{23,24} More recently, a ditopic derivative of these ligands that gives bimetallic Fe complexes has been investigated.²⁵ Due to their easily modifiable steric and electronic properties, these complexes exhibit some of the highest activities reported to date. For example, Cr-salan complexes show high TOFs and under certain conditions give better activities than the well-defined Cr-salen analogs. Darensbourg recently reported the use of a CrCl(salan) complex which had a TOF of 405 h⁻¹ using 1 equivalent of PPNN₃ as the co-catalyst at 60 °C and 34 bar CO₂ for 4 h.⁹ Other metals and ligands are also being studied for epoxide/CO₂ copolymerization. Recently, Nozaki and co-workers reported tetravalent group 4 (Ti and Zr) and 14 (Ge and Sn) metals supported by planar trianionic bis(phenolato) ligands, which showed activity towards epoxide and CO₂ copolymerization, although the activities were typically lower than for previously reported catalysts.²⁶

The tetradentate, tripodal amine-bis(phenolato) ligand class presented in this thesis had yet to be investigated for CO₂/epoxide copolymerization. Initial studies were performed with bulky *t*-butyl substituents on the phenolate groups, and a pyridyl pendant arm as the second neutral donor site due to favorable activity for the coupling reaction of CO₂ and propylene oxide shown by cobalt complexes of this ligand.

Because chromium(III) catalysts have shown excellent activity towards CO₂/epoxide copolymerization,⁷⁻¹¹ a study was undertaken to explore the potential of these Cr(III) amine-bis(phenolato) complexes for this reaction. This metal-ligand combination offers new avenues for development of highly active catalysts because of the

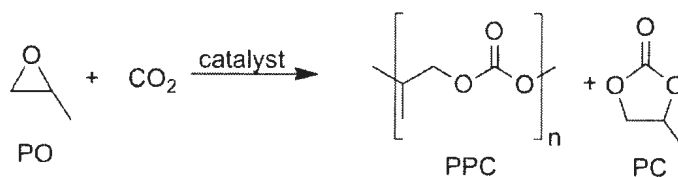
modifiable nature of the donor sites, their steric and electronic properties, and their geometry, which differs from those exhibited by the salen and salan-based systems. This chapter will focus on the activity of $\{\text{CrCl}[\text{O}_2\text{NN}^t\text{BuBu}]\}_2$ (**4.4**) for copolymerization of propylene oxide (PO), cyclohexene oxide (CHO) or styrene oxide (SO) with CO_2 .

5.2 Results and Discussion

5.2.1 Synthesis

5.2.2 Copolymerization of Propylene Oxide and CO_2

Initial studies were conducted on propylene oxide (PO) with CO_2 catalyzed by complex **4.4**. As outlined in Scheme 5.1, either the cyclic product, propylene carbonate (PC), and/or the polymer, poly(propylene carbonate) (PPC), were obtained for this process depending on the conditions used.



Scheme 5.1. Copolymerization of PO and CO_2 .

The copolymerization reactions investigated in this chapter utilized common co-catalysts previously reported in the literature to give high yields of copolymer.^{22,27} Neutral or ionic co-catalysts such as (4-dimethylamino)pyridine (DMAP), bis(triphenylphosphoranylidene)iminium chloride or azide (PPNCl or PPNN₃), and

tetrabutylammonium bromide (TBABr) have been shown to play an important role in the production of the desired product (Figure 5.1).

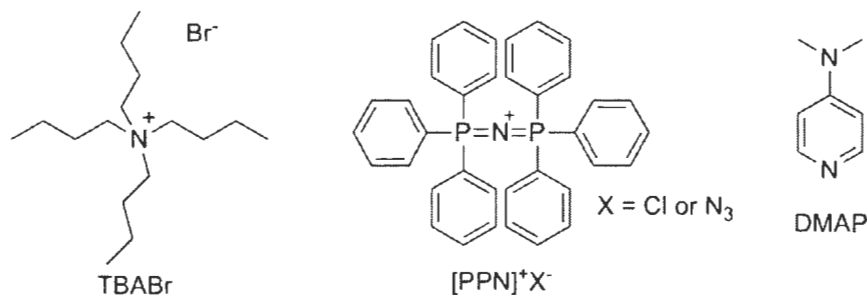


Figure 5.1. Common co-catalysts used in epoxide/CO₂ copolymerization reactions.

When no co-catalyst was used, 100% conversion of PO to PC was observed at relatively mild reaction conditions as shown in Table 5.1, entry 1. However, complex **4.4** combined with PPNN₃ co-catalyst gives high selectivity for polycarbonate at room temperature and moderate pressure of CO₂. The polymer obtained was of low molecular weight but also narrow polydispersity. Without the metal catalyst **4.4**, no PPC was produced, observing an 85% conversion to PC after 24 hours (entry 2). The amount of co-catalyst, 1 equivalent (entry 3) *versus* 0.5 equivalents (entry 4), did not prove to have a significant effect on the activity. However, a lower number average molecular weight (M_n) was observed when using a higher equivalent of PPNN₃. Generally, comparable results were obtained using PPNN₃ (entry 5) or PPNNCl (entry 11) as the co-catalyst. The catalyst loading also proved to be an important parameter. Using a 0.1% catalyst loading *versus* propylene oxide (entry 6) gave good selectivity for polycarbonate, but low yield. The polymer obtained was found to have a similar molecular weight to that obtained

when employing a 0.2% catalyst loading with PPNN₃ (entry 4), but was more polydisperse ($M_w/M_n = 1.40$). Increasing the catalyst loading to 0.2% (entry 7) gave a much higher yield of polycarbonate and maintained selectivity. Generally, using PPNCI as the co-catalyst (entries 7-11) gave good to excellent selectivity for polycarbonate, but required long reaction times. After 12 or 6 h (entries 9 and 10, respectively) modest yields of polymer were obtained. Since the PPNX salts are found to be sparingly soluble in epoxides at room temperature, a reaction was carried out where the autoclave was brought into the glove box in order to add complex **4.4** and the desired equivalents of co-catalyst and epoxide accurately. Such a procedure showed an improvement in the yield, while still maintaining good M_n and PDI (entry 11).

Mass transfer limitations inhibited the ability to increase yields. Therefore, a non-coordinating solvent, toluene was explored to try and overcome precipitation of the polymer in the autoclave during the reaction. Unfortunately, no copolymer or cyclic carbonate was produced in the presence of a co-solvent (entry 12). Heating the reaction to 80 °C for 4 h (entry 13) did not improve the yield of polymer. Under these conditions, quantitative conversion of propylene oxide to cyclic propylene carbonate was observed instead. This result was not surprising as Darensbourg and co-workers have shown that cyclic propylene carbonate preferentially forms at higher reaction temperatures.²¹

DMAP (entries 14 and 15) and TBABr (entries 16 and 17) were screened as Lewis basic co-catalysts. However, they were found to be inferior to PPNCI under the conditions investigated in entry 7. Using DMAP as the co-catalyst at room temperature and a CO₂ pressure of 39 bar gave 73% yield of polycarbonate in good selectivity after 24 h (entry 14). However, raising the temperature of the reaction to 61 °C lead to nearly

quantitative yield of propylene carbonate instead (entry 15). A similar trend was observed when TBABr was employed as the co-catalyst. Modest yield of polymer was obtained at room temperature (entry 16) but raising the temperature, again, gave quantitative yield of propylene carbonate and no polymer (entry 17). This temperature dependence is an intriguing feature of the reaction mechanism when this catalyst is used (i.e. the selectivity of the combination of catalyst and co-catalyst could be switched very easily by simply varying the temperature of the reaction). In short, performing the reaction at room temperature produces polycarbonate whereas raising the temperature produces propylene carbonate in high yield.

As a result of the success with complex **4.4** for the copolymerization of PO/CO₂, studies were also explored with **L6**, **4.2** and **4.3** (Table 5.2). However, preliminary results were shown to afford only cyclic propylene carbonate at 22 °C and 40 bar pressure over 24 h (entries 2, 3 and 4). In addition, the ligand of complex **4.4**, **L6** (entry 1) was observed to yield no polymer or cyclic carbonate indicating that the metal species, chromium, was important in the reaction. This was found to be in contradiction with salen and salan based systems, where the ligands alone were observed to yield cyclic carbonate with similar TONs as their metal complexes.²⁸ Although propylene carbonate was not the desired product in these reactions, the synthesis of organic carbonates from CO₂ has become increasingly important in industry due to their economic benefits in creating useful target molecules.^{29,30}

Table 5.1. Results of the Copolymerization of PO and CO₂ catalyzed by **4.4**.^a

Entry	[Cr]:[PO]:[Co-Cat.] (per Cr center)	Time (hr.)	Temp. (°C)	Pressure (bar)	% Yield ^b (PPC)	% Selectivity ^c	% Conversion ^b	TON	TOF ^d (h ⁻¹)	M _n ^c (kg/mol)	PDI ^c (M _w /M _n)
1 ^f	1:270:0	24	60	47	0	0	100	0	0	NA ^g	NA
2 ^f	0:500:1 (PPNN ₃)	24	23	45	0	0	85	0	0	NA	NA
3	1:500:1 (PPNN ₃)	24	23	38	83	88	94	414	17	5.5	1.14
4	1:500:0.5 (PPNN ₃)	24	25	45	83	93	89	422	18	21.1	1.15
5 ^h	1:500:0.5 (PPNN ₃)	6	25	40	59	96	61	280	47	12.4	1.19
6	1:1000:0.5 (PPNCl)	24	25	42	33	82	40	315	13	18.7	1.40
7	1:500:0.5 (PPNCl)	24	23	37	85	93	100	418	17	13.3	1.40
8	1:500:0.5 (PPNCl)	16	22	39	69	95	91	334	21	10.9	1.27
9	1:500:0.5 (PPNCl)	12	23	40	42	51	81	223	19	8.7	1.21
10	1:500:0.5 (PPNCl)	6	25	40	41	93	44	200	33	12.4	1.19
11 ^h	1:500:0.5 (PPNCl)	6	25	40	59	92	64	287	48	11.5	1.17
12 ⁱ	1:500:0.5 (PPNCl)	4	25	37	0	0	0	NA	NA	NA	NA
13 ^f	1:500:0.5 (PPNCl)	4	80	47	0	0	100	0	0	NA	NA
14	1:500:0.5 (DMAP)	24	24	39	73	73	100	386	16	12.7	1.32
15 ^f	1:500:0.5 (DMAP)	24	61	47	0	0	99	0	0	NA	NA
16	1:500:0.5 (TBABr)	24	25	40	42	46	65	212	9	ND ^g	ND
17 ^f	1:500:0.5 (TBABr)	24	60	48	0	0	100	0	0	NA	NA

^aPolymerization reactions were carried out in neat PO (2.8 mL). ^bYield calculated for PPC formation, conversion is % PO consumed by ¹H NMR. ^cSelectivity of polycarbonate over cyclic carbonate in units of % as determined by ¹H NMR spectroscopy of the crude product. ^dTurnover frequency is moles of PPC produced per mol of Cr per hour. ^eDetermined by gel permeation chromatography in CHCl₃, calibrated with polystyrene standards. ^fNo PPC formed only PC. ^gNA = not applicable (no polymer obtained), ND = not determined due to lack of polymer and/or work-up related issues. ^hLoaded reagents into autoclave in glove box. ⁱReaction performed in Toluene (16 mL).

Table 5.2. Coupling reaction of PO and CO₂ initiated by **L6** and complexes **4.2** and **4.3**.^a

Entry	Initiator	[Cr]:[PO]:[Co-Cat.]	Time (hr.)	Temp. (°C)	Pressure (bar)	% Yield ^b	TON	TOF ^c (h ⁻¹)
1	L6	1:500:1 (PPNCl)	24	22	39	0	NA ^d	NA
2	4.2	1:1000:1 (PPNCl)	24	22	40	84	823	34
3	4.3	1:250:1 (TBABr)	24	22	39	92	246	10
4	4.3	1:500:1 (TBABr)	24	22	37	100	501	21

^a Reactions were carried out in neat PO (2.8 mL). ^b Yield of PC calculated by ¹H NMR. No polymer obtained. ^c Turnover frequency is moles of PC produced per mol of Cr per hour. ^d NA = not applicable (no PC obtained).

Comparing to recent results in the literature, Darensbourg and co-workers⁹ reported an effective catalyst system using 1 equivalent of PPNN₃ in *rac*-PO with a CrCl(salan) derivative. Poly(propylene carbonate) was obtained at room temperature and under relatively low pressure (15 bar) yielding a polymer with a molecular weight of 8.0×10^3 kg/mol and a turnover frequency of 21. Comparing this to entries 5 and 11 in Table 5.1, using 0.5 equivalents of PPNN₃ and PPNCl, TOFs of 47 and 48 h⁻¹ were achieved, respectively. Lu, Zhang and co-workers have observed similar results with the use of a Cr(salan) complex. In the presence of 1 equivalent of DMAP, TOFs of 86 h⁻¹ at room temperature and 6 bar CO₂ pressure were observed.³¹

Although this new catalyst system shows similar catalytic activity as Cr salen and salan systems for PO/CO₂ copolymerization, Co(salen) catalysts are observed to have the highest activities, best stereochemical control and highest molecular weights reported in the literature.³²⁻³⁴

5.2.2.1 NMR Spectroscopy

^1H and ^{13}C NMR are essential techniques used in the analysis of the resulting polymers. ^1H NMR was used in the initial analysis of the product formed, whereby an aliquot of the crude reaction mixture was analyzed immediately after the reaction was terminated, in order to determine the conversion/yield and selectivity of the products produced. Integration of the methine protons in the ^1H NMR spectra allowed quantitative determination of the amount of cyclic carbonate produced relative to polycarbonate formation (Figure 5.2). Interestingly, it was also noticed that if the catalyst was not totally removed from a solution of the polymer in CDCl_3 (aliquot samples for NMR analysis), depolymerization occurred causing propylene carbonate formation to increase with time (Figure 5.3).

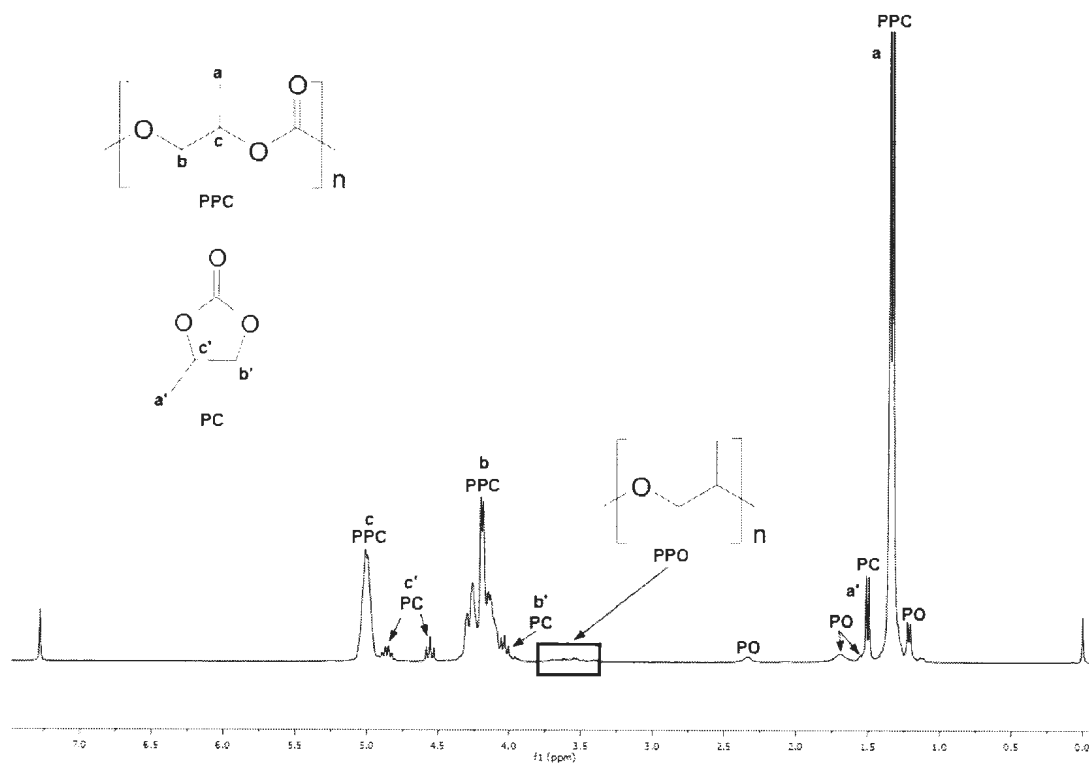


Figure 5.2. ^1H NMR of the copolymerization of PO and CO_2 (Table 5.1, entry 3, 300 MHz, CDCl_3).

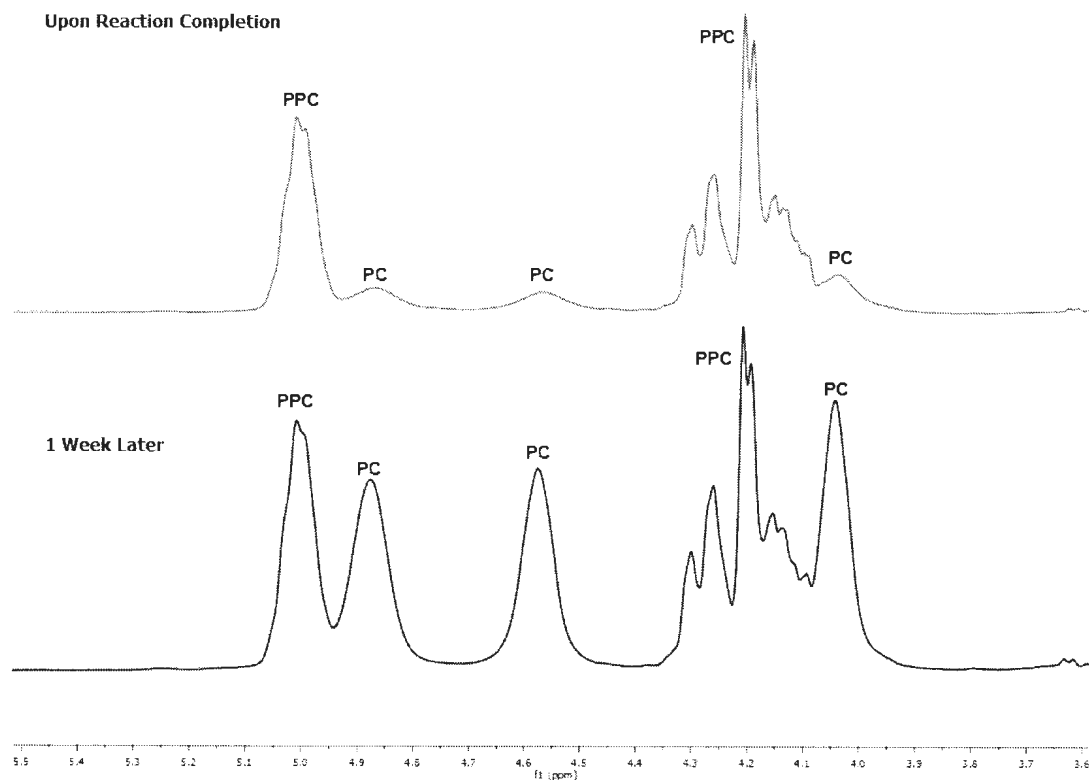


Figure 5.3. ^1H NMR of the depolymerization of PPC to PC with time (300 MHz, CDCl_3).

In addition, ^1H NMR allowed for the determination of the relative amount of ether linkages, poly(propylene oxide) produced, which in turn allows for the calculation of the percentage of CO_2 incorporation. The copolymerization of PO and CO_2 by complex **4.4** afforded >99% carbonate linkages. MALDI-TOF MS studies have also provided evidence towards a highly alternating copolymer.

Quantitative analysis of ^{13}C NMR of the carbonyl region allowed for the determination of regiochemistry in PPC (Figure 5.4). Similar to related catalysts^{9,35}

complex **4.4** is highly selective for head-to-tail (HT) linkages (Figure 5.5) showing 80-100% regioselectivity.

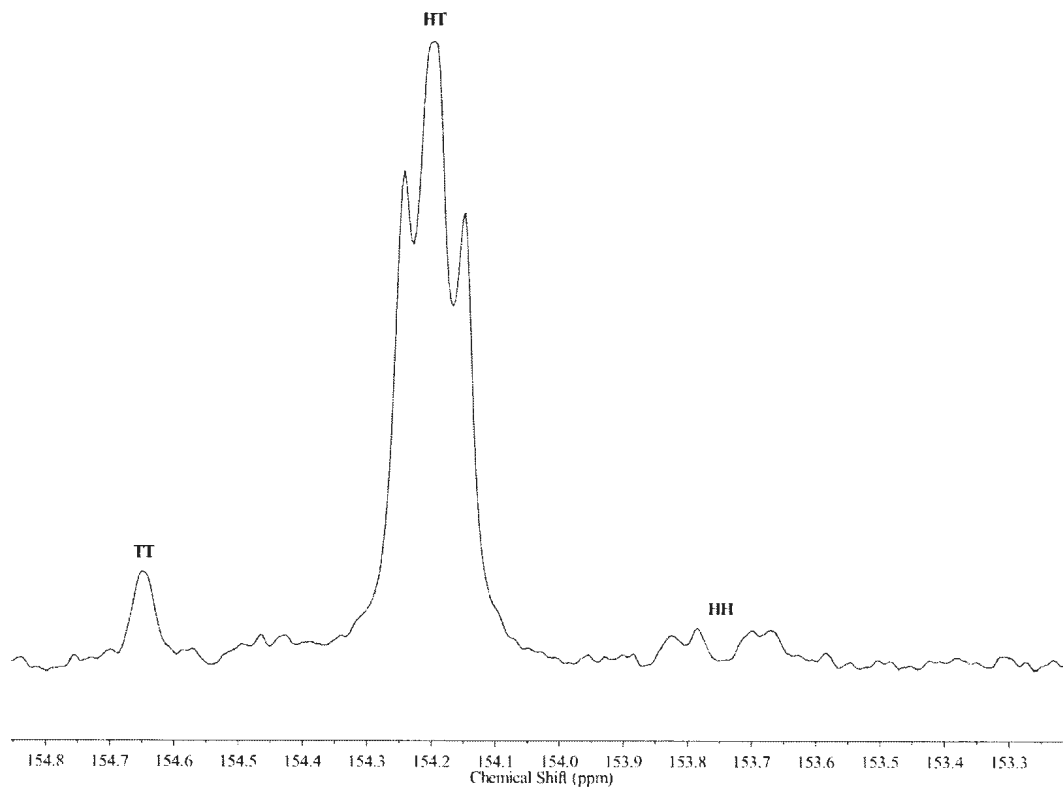


Figure 5.4. Carbonyl region of the ^{13}C NMR spectrum (75.5 MHz, CDCl_3) of PO/CO₂ copolymer prepared with PPNCI (Table 5.1, entry 7).

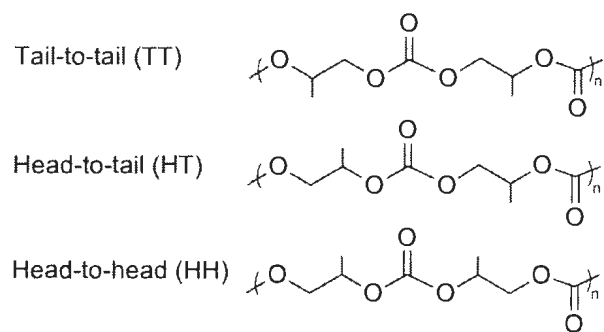


Figure 5.5. Possible regiochemistry of PPC.

5.2.2.2 Mass Spectrometry

Mass spectrometry (MS) has become an increasingly important tool in the analysis of polymeric materials. Methods such as Electrospray Ionization (ESI) MS and Matrix-Assisted Laser Desorption Ionization Time-of-Flight (MALDI-TOF) MS are commonly used as they are considered 'soft' ionization techniques. Minimal fragmentation of the polymer is required in order to obtain useful polymer data via MS analysis. MALDI-TOF MS was used for the majority of polymer chain end group analysis due to the ease of preparation, and analysis of the MS. Unlike ESI, no solvent is required for MALDI analysis and therefore less adducts and fragments were obtained.

A typical MALDI-TOF spectrum of poly(propylene carbonate) along with end group assignments is shown in Figure 5.6. The bimodal molecular weight distribution observed consists of three polymer chains. The lowest molecular weight corresponds to series (a), $[\text{Cl} (35) + 102n (\text{repeating unit}) + \text{C}_3\text{H}_7\text{O} (59)]$ where PPC is found to have chain ends with a chloride as the initiator and a hydroxyl group at the terminating end.

Series (b) was found to have both chain ends consisting of Cl, [Cl (35) + 102*n* (repeating unit) + C₃H₆Cl (77)]. The highest molecular weight series (c), [Cl (35) + 102*n* (repeating unit) + C₆H₁₂O (100) + Cl (35)] is modeled to have an ether-containing end group, likely resulting from double insertion of an epoxide unit during the reaction. Isotopic masses modeled for series a-c are found to agree well with the experimental peaks. In addition, all co-catalysts were observed to have the same three polymer chains in their MALDI-TOF spectra.

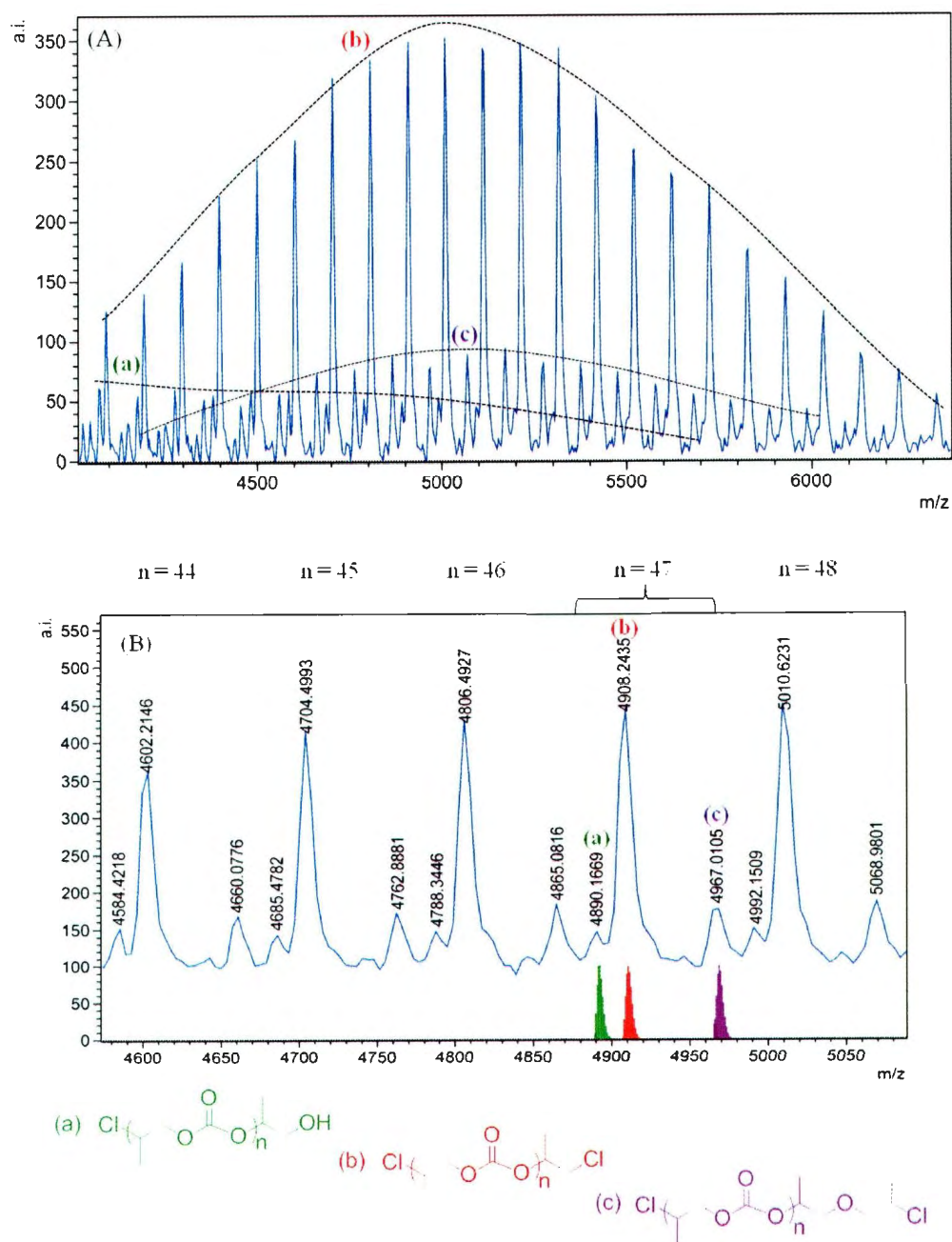


Figure 5.6. (A) MALDI-TOF MS of PPC produced by **4.4** (Table 5.1, entry 7). (B) Magnified region of the spectrum (n = 44-48). Modeled isotopic masses (when n = 47) and images for polymer chains with end groups (a-c).

5.2.2.3 Gel Permeation Chromatography

Gel permeation chromatography (GPC) was utilized in the determination of polymer molecular weights and polydispersity indices (PDIs). Resulting molecular weights listed in Table 5.1 were found to be dependent on time. Higher molecular weights were generally obtained over longer reaction times. PDIs were usually observed to be narrow, with most ranging between 1.1 and 1.3. Similar to the MALDI-TOF MS results, bimodal distributions were also observed in some GPC traces making accurate analysis of M_n values difficult.

5.2.2.4 Thermal Analysis (DSC & TGA)

Thermal analysis was also performed on the polymers obtained. Differential scanning calorimetry (DSC) measurements of the PPC afforded glass transition temperatures (T_g) ranging from 35 °C to 40 °C. The DSC trace and observable T_g for PPC produced by complex **4.4**, Table 5.1, entry 7 is given in Figure 5.7. The T_g values obtained are found to be within the ranges reported in the literature.^{24,36} Thermal gravimetric analysis (TGA) indicated 50% decomposition (T_{50}) at 146-187 °C. A representative TGA trace and derivative plot is shown in Figure 5.8. Darensbourg and co-workers have shown a similar TGA value where their onset of weight loss was 175 °C for PPC.⁹

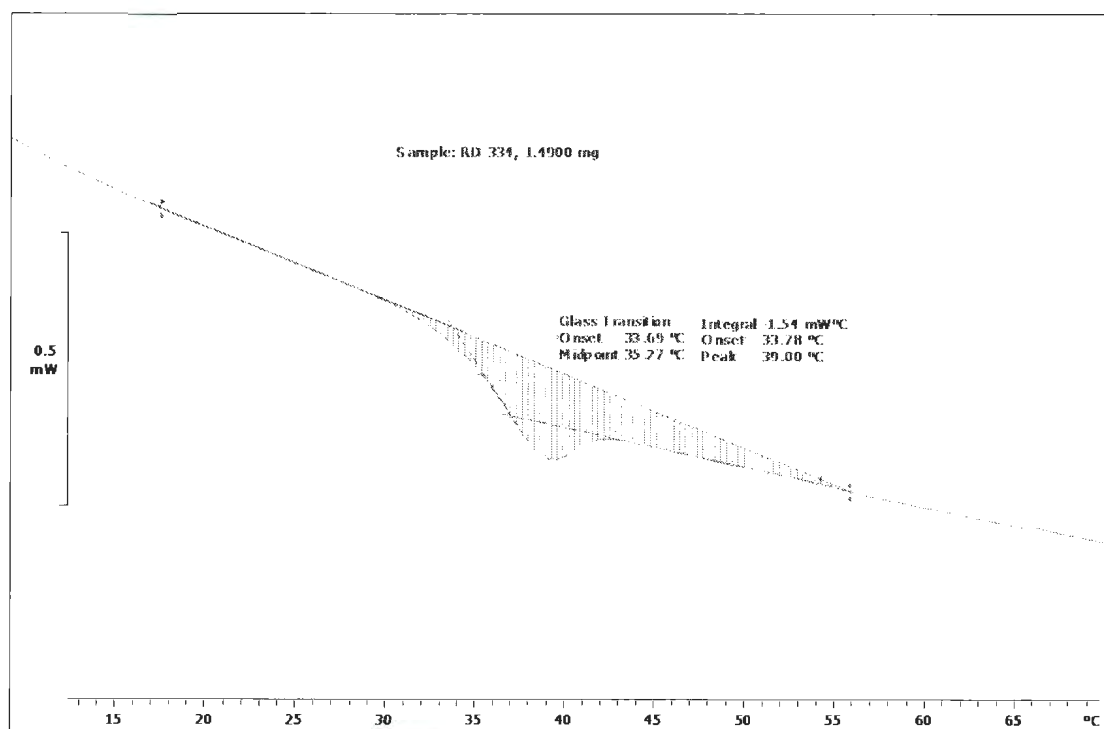


Figure 5.7. Representative DSC trace of PPC produced by 4.4, 2nd heat cycle (Table 5.1, entry 7).

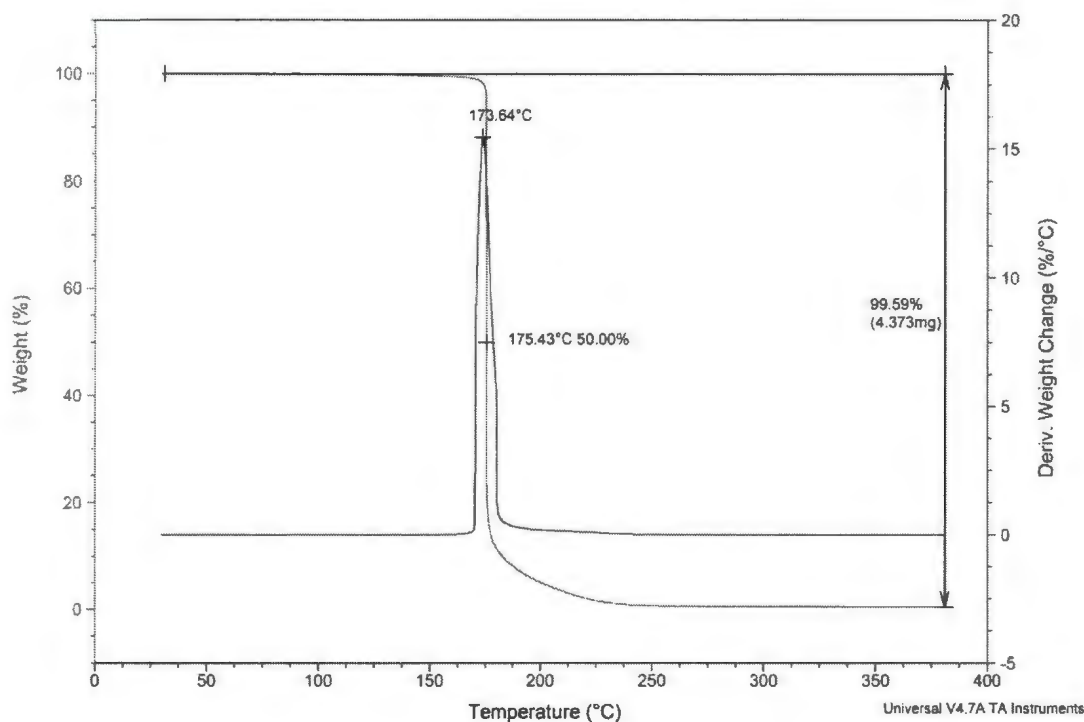
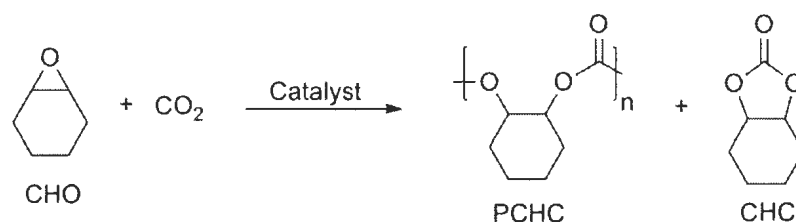


Figure 5.8. Representative TGA trace and derivative plot of PPC produced by **4.4** (Table 5.1, entry 7).

5.2.3 Copolymerization of Cyclohexene Oxide and CO₂

The copolymerization of CHO and CO₂ was also investigated using complex **4.4**. Neutral or ionic co-catalysts such as DMAP, PPNCI and PPNN₃ were employed in this study and were shown to be important for the formation of the desired product. When CHO, CO₂, complex **4.4** and a co-catalyst are combined, strictly poly(cyclohexene carbonate) (PCHC) is produced with no evidence of cyclohexene carbonate (CHC) formation (Scheme 5.2).



Scheme 5.2. Copolymerization of CHO and CO₂.

Initial reactions were performed employing ionic co-catalysts in neat epoxide due to the results observed in the PO/CO₂ copolymerization studies (Table 5.3). Reactions were first explored at room temperature over 24 h in the presence of PPNC1 and PPNN₃ (entries 1 and 7). In both cases the activities were found to be low. Therefore, reaction temperatures were elevated to 60 °C, entry 2 for PPNC1 and entry 9 for PPNN₃, giving increased TOFs while still maintaining pressures of 40 bar. In an effort to improve yields further a different procedure was employed when using PPN salts. The poor solubility of these co-catalysts in CHO required activating the catalyst and co-catalyst mixture first by dissolving them in dichloromethane, which is a protocol that has been employed when using these ionic co-catalysts with salen- or salan-based Cr(III) catalysts.^{9,37} Upon removal of the dichloromethane, the resulting catalyst mixture becomes soluble in CHO. As a result of a more homogeneous mixture, yields and activities were observed to increase (entry 9 *versus* entry 10 for PPNN₃). Additionally, the chloride salt gave lower yields of polycarbonate and was less active than the azide initiator, (entries 4 and 10, respectively). Reactions performed at 80 °C and 24 bar for 3 h gave the highest activities for these co-catalysts (entries 5 and 11). It is important to note that reactions with high

TOFs were repeated in order to ensure reproducibility of the result. For example, entry 6 is found to have a similar outcome to entry 5, within experimental error. Interestingly, increasing the amount of co-catalyst (PPNN₃) from 0.5 (entry 11) to 1 equivalent (entry 12) was not found to improve the yield or activity of the system. Such was also the case in PO/CO₂ copolymerization.

Molecular weights were found to range between 2.7 and 11.7 kg/mol, when employing ionic co-catalysts. The highest molecular weights were observed at longer reaction times (entries 2 and 7). However, at higher temperatures (80 °C) a decrease in M_n was observed (entries 5, 6, 11 and 12). The polydispersity (M_w/M_n) values generally fell within the range of 1.2 to 1.4, with the exception of entry 2 where a very broad PDI, 2.3 was observed.

Table 5.3. Results of the Copolymerization of CHO and CO₂ for catalyst **4.4** with PPNX salts.^a

Entry	[Cr]:[CHO]:[Co-Cat.]	Time (hr.)	Temp. (°C)	Pressure (bar)	% Yield ^b	TON	TOF ^c (h ⁻¹)	M _n ^d (kg/mol)	PDI ^d (M _w /M _n)
1	1:500:0.5 (PPNCl)	24	22	39	13	65	3	ND ^f	ND
2	1:500:0.5 (PPNCl)	24	60	45	72	359	15	11.7	2.27
3	1:500:0.5 (PPNCl)	6	60	23	53	265	44	10.6	1.18
4 ^e	1:500:0.5 (PPNCl)	4	60	44	60	295	74	6.6	1.27
5 ^e	1:500:0.5 (PPNCl)	3	80	24	45	233	78	3.9	1.40
6 ^e	1:500:0.5 (PPNCl)	3	80	24	45	218	73	3.6	1.37
7	1:500:0.5 (PPNN ₃)	24	25	38	59	292	12	9.5	1.44
8	1:500:0.5 (PPNN ₃)	4	25	38	11	54	13	ND	ND
9	1:500:0.5 (PPNN ₃)	4	60	43	52	256	64	7.2	1.35
10 ^e	1:500:0.5 (PPNN ₃)	4	60	40	71	356	89	7.1	1.24
11 ^e	1:500:0.5 (PPNN ₃)	3	80	24	58	296	99	3.8	1.27
12 ^e	1:500:1 (PPNN ₃)	3	80	23	55	274	91	2.7	1.41

^aAll polymerization reactions were carried out in neat CHO (4 mL). ^bCalculated by ¹H NMR. ^cTurnover frequency (TOF) is moles of repeating units produced per mol of Cr per hour. ^dDetermined by gel permeation chromatography in CHCl₃, calibrated with polystyrene standards. ^eActivated in 4 mL of dichloromethane prior to adding CHO. ^fND = not determined due to lack of polymer and/or work-up related issues.

The effect of changing the co-catalyst to DMAP, a neutral base was also explored for the copolymerization of CHO and CO₂ (Table 5.4). Initial reactions using DMAP were performed at low temperatures, over 24 h (entry 1). Comparison of the reactions carried out at 21 °C and 60 °C revealed a significant influence on the catalytic activities (entries 1 and 2, respectively), where both the yield and the molecular weight of the polymer obtained increased significantly at the higher temperature. In the case of the CHO monomer higher temperatures were required, but reaction times were generally much shorter than those required for the PO study. The effect of temperature on the rate of copolymerization was evident. When performed at 60 °C, a shorter reaction time was required to maintain good yields and activities compared to reactions carried out for 24 h (entries 3 to 5); after 2 h only moderate yields of polymer were obtained (entry 7). However, a significant increase in activity (almost 18-fold) was observed upon raising the reaction temperature from 21 °C for 24 h (entry 1) to 80 °C for 3 h (entry 8), giving a TOF of 89 mol epoxide consumed/mol Cr per h with DMAP as the co-catalyst. Co-catalysts PPNN₃ and DMAP were found to be very similar in inducing activity for poly(cyclohexene carbonate) formation using **4.4**. DMAP, however, is soluble in neat CHO thus simplifying the procedure; therefore this co-catalyst was used for optimizing further reactions.

As for PO, decreasing the catalyst loading to 0.1 mol% from 0.2 mol% had a detrimental effect on the activity as shown in entry 6. The resulting yields are also affected by mass transfer limitations due to the solidification of the polymer in the reaction vessel. In order to address the problem of mass transfer limitations on the overall yield of polymer, the reaction was performed in a 4:1 mixture of toluene and cyclohexene

oxide (entry 9). However, the dilution of the reactants resulted in a polymer yield half of that obtained in neat CHO at the same temperature, pressure and reaction time (entry 8).

Interestingly, decreasing the pressure from 47 to 24 bar did not significantly lower the yield (entry 10). However, decreasing the pressure to 12 bar while maintaining a temperature of 80 °C for 3 h did show a reduction in yield and TOF as well as giving lower polymer molecular weights (entry 11).

The amount of co-catalyst used is significant for the activity of this system. Increasing the ratio of DMAP to 1 equivalent per Cr center produced higher TOFs of 116 and 219 h⁻¹ (entries 12 and 13, respectively), but using 2 equivalents of DMAP per Cr center shuts down the polymerization entirely (entry 14).^{31,38}

Similar to PPNN₃ the presence of a lower catalyst loading caused a decrease in yield of polycarbonate (entry 15). Clearly, the chloride-bridged dimer (**4.4**) observed in the solid state is unlikely to persist in solution where potentially coordinating solvents (such as CHO) or Lewis basic co-catalysts are present. Therefore, the catalytically active species is most likely monomeric, similar to salen analogs. Interestingly, PCHC could be produced without the need of a co-catalyst, albeit only in very low yield and TOF. Temperature was shown to be an important factor, because performing the reaction at 25 °C showed no conversion of CHO (entry 16), whereas at 60 °C a 7% yield of polycarbonate was obtained (entry 17). In the absence of **4.4**, DMAP alone showed no conversion to PCHC or CHC (entry 18).

Table 5.4. Results of the Copolymerization of CHO and CO₂ for catalyst **4.4** with DMAP.^a

Entry	[Cr]:[CHO]:[Co-Cat.]	Time (hr.)	Temp. (°C)	Pressure (bar)	% Yield ^b	TON	TOF ^c (h ⁻¹)	M _n ^d (kg/mol)	PDI ^d (M _w /M _n)
1	1:500:0.5 (DMAP)	24	21	39	25	123	5	5.8	1.27
2	1:500:0.5 (DMAP)	24	60	44	81	400	17	13.1	1.37
3	1:500:0.5 (DMAP)	19	60	42	83	417	22	10.3	1.12
4	1:500:0.5 (DMAP)	12	60	40	77	382	32	9.4	1.11
5	1:500:0.5 (DMAP)	6	60	44	63	318	53	11.5	1.66
6	1:1000:0.5 (DMAP)	6	60	43	12	122	20	ND ^e	ND
7	1:500:0.5 (DMAP)	2	60	44	29	150	75	ND	ND
8	1:500:0.5 (DMAP)	3	80	47	59	266	89	10.4	1.37
9 ^f	1:500:0.5 (DMAP)	3	80	47	30	148	49	3.3	1.48
10	1:500:0.5 (DMAP)	3	80	24	58	288	96	9.2	1.21
11	1:500:0.5 (DMAP)	3	80	12	43	200	67	3.9	1.49
12	1:500:1 (DMAP)	3	80	22	69	349	116	8.0	1.13
13	1:500:1 (DMAP)	1	80	24	47	219	219	4.8	1.27
14	1:500:2 (DMAP)	1	80	24	0	NA	NA	NA ^e	NA
15	1:1000:1 (DMAP)	3	80	26	22	198	66	2.0	1.32
16	1:500:0	24	25	38	0	NA	NA	NA	NA
17	1:500:0	24	60	43	7	33	1	ND	ND
18	0:500:0.5 (DMAP)	24	60	45	0	NA	NA	NA	NA

^a All polymerization reactions were carried out in neat CHO (4 mL) except where noted otherwise. ^b Calculated by ¹H NMR. ^c Turnover frequency (TOF) is moles of repeating units produced per mol of Cr per hour. ^d Determined by gel permeation chromatography in CHCl₃, calibrated with polystyrene standards. ^e ND = not determined due to lack of polymer and/or work-up related issues, NA = not applicable (no polymer obtained). ^f Reaction performed in 4:1 Toluene:CHO mixture.

A preliminary investigation of the copolymerization of CHO/CO₂ with complexes **4.2** and **4.3** was also performed (Table 5.5). In the presence of DMAP under similar reaction conditions carried out for complex **4.4**, TOFs of 96 (entry 1) and 104 h⁻¹ (entry 2) were obtained for complexes **4.2** and **4.3**, respectively. These activities are slightly lower than that observed for complex **4.4** (entry 3). Importantly, these complexes were also found to only produce poly(cyclohexene carbonate) with no evidence of cyclic carbonate formation (see Appendix A, Figures A1.22 and A1.23 for ¹H NMR spectra). Complex **4.3** was also found to produce polymer with a low *M_n* value and a slightly broader PDI than complex **4.4**.

Table 5.5. Copolymerization of CHO and CO₂ initiated by complexes **4.2** and **4.3**.^a

Entry	Complex	[Cr]:[CHO]:[Co-Cat.]	Time (hr.)	Temp. (°C)	Pressure (bar)	% Yield ^b	TON	TOF ^c
1	4.2	1:500:1 (DMAP)	3	80	47	59	288	96
2	4.3 ^d	1:500:1 (DMAP)	3	80	46	63	311	104
3 ^e	4.4	1:500:1 (DMAP)	3	80	22	69	349	116

^a Polymerization reactions were carried out in neat CHO (4 mL). ^b Calculated by ¹H NMR. ^c Turnover frequency is moles of PCHC produced per mol of Cr per hour. ^d *M_n* = 5900, *M_w*/*M_n* = 1.26. ^e Result from Table 5.4, entry 12, shown here to facilitate comparison.

5.2.3.1 NMR Spectroscopy

The PCHC generated were shown to possess a small proportion of polyether linkages, poly(cyclohexene oxide) product (Figure 5.9), as was the case with PPC. The percentage of carbonate linkages was also found to be dependant on temperature. At ambient temperature ~13% of the copolymer consists of polyether linkages, while at higher temperatures only ~2% is found to contain ether linkages. It should be noted that

polyethers are not obtained when CHO solutions of **4.4** and DMAP are heated to 80 °C in the absence of CO₂. This observation suggests homopolymerization is not competitive to copolymer formation, unlike what is observed in related Cr(III) catalytic systems.

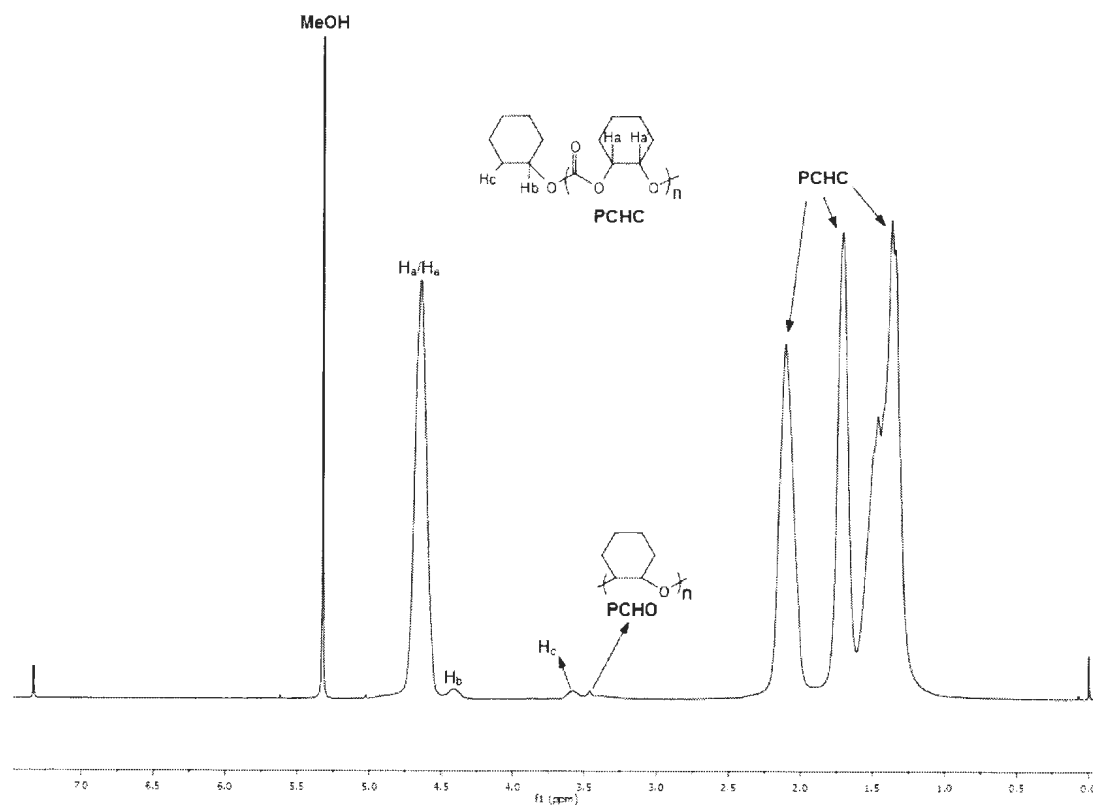


Figure 5.9. Typical ¹H NMR spectrum of PCHC in CDCl₃ (Table 5.4, entry 12).

The isolated poly(cyclohexene carbonate) stereochemistry was analyzed by ¹³C NMR, as shown in Figure 5.10. Through quantitative ¹³C NMR of the carbonyl region, equal amounts of isotactic and syndiotactic units were detected in the polymer obtained when employing DMAP as the co-catalyst, providing evidence that the dominant configuration of the polymer is atactic (Figure 5.11).^{23,39} In the presence of smaller

nucleophiles, such as the ionic co-catalysts (PPNCl and N_3) a more isotactic copolymer was observed (see Appendix A, Figures A1.24 for PPNCl and A1.25 for PPNN₃).

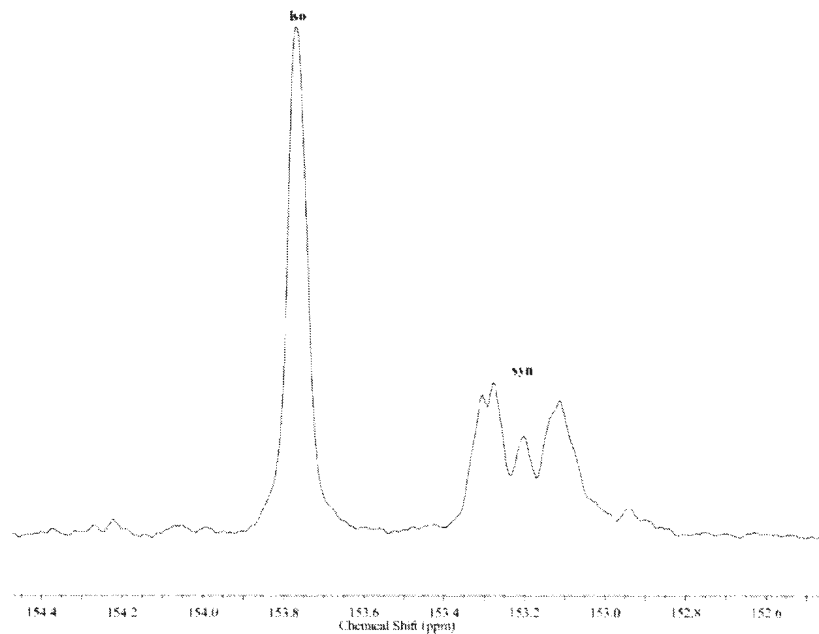


Figure 5.10. Carbonyl region of the ^{13}C NMR spectrum (75.5 MHz, $CDCl_3$) of CHO/ CO_2 copolymer prepared with DMAP (Table 5.4, entry 5).

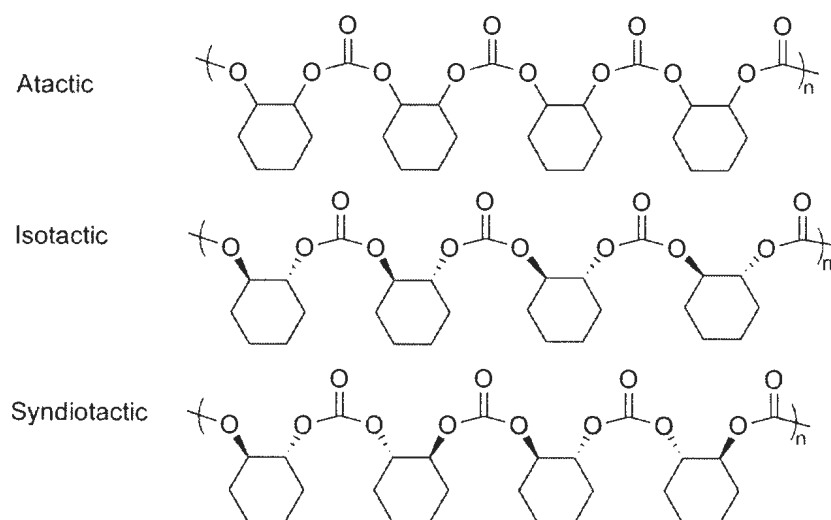


Figure 5.11. Stereochemistry of PCHC.

5.2.3.2 Mass Spectrometry

MALDI-TOF MS studies were performed in order to gain insight into the differences observed for theoretical and experimentally (GPC) calculated values of the number average molecular weights of the copolymers and possible end-groups providing mechanistic details for this system. In the MALDI-TOF mass spectra of these copolymers, multi-modal molecular weight distributions were observed showing multiple end group series, all separated with a repeating unit of 142 m/z . The differing end groups result from four polymer chains attributed to the various molecular weights (Figure 5.12). The lowest molecular weight series, (a), consists of two hydroxyl-end groups [17 (OH) + 142 n (repeating unit) + 82 (C₆H₁₀) + 17 (OH)] suggesting evidence of chain-transfer as a result of water contamination.^{11,40} Series (b), [35 (Cl) + 142 n (repeating unit) + 82 (C₆H₁₀) + 17 (OH)] would be expected if the polymerization was initiated by a chloride

and terminated by hydrolysis. Series (c) consists of both chain ends being chlorides [35 (Cl) + 142*n* (repeating unit) + 82 (C₆H₁₀) + 35 (Cl)], which could be the result of chain transfer between two separately growing polymer chains. The highest molecular weight polymer chain consists of an ether-containing end group, series (d) [17 (OH) + 142*n* (repeating unit) + 180 (C₁₂H₂₀O) + 17 (OH)], which may be a result of double epoxide insertion.⁴¹ Interestingly, it was also found that all co-catalysts, (DMAP, PPNCI or PPNN₃) gave the same polymer chains in their MALDI-TOF mass spectra suggesting the chloride from complex 4.4 is acting as the initiator, not the co-catalysts. Isotopic masses modeled for all four polymer chains are found to agree with the experimental spectra.

Additionally, two independently prepared polymer samples were analyzed by inductively coupled plasma (ICP) MS and were shown to contain 149 and 170 ppm of Cr. These concentrations are encouragingly low, given that the polymers obtained were simply purified from dichloromethane solutions by precipitation using methanol. For comparison, Darensbourg and co-workers⁴² observed low Cr leaching from their polyisobutylene supported Cr(III)salen catalyst, where 39 ppm Cr was found in their polycarbonate after one precipitation in heptane.

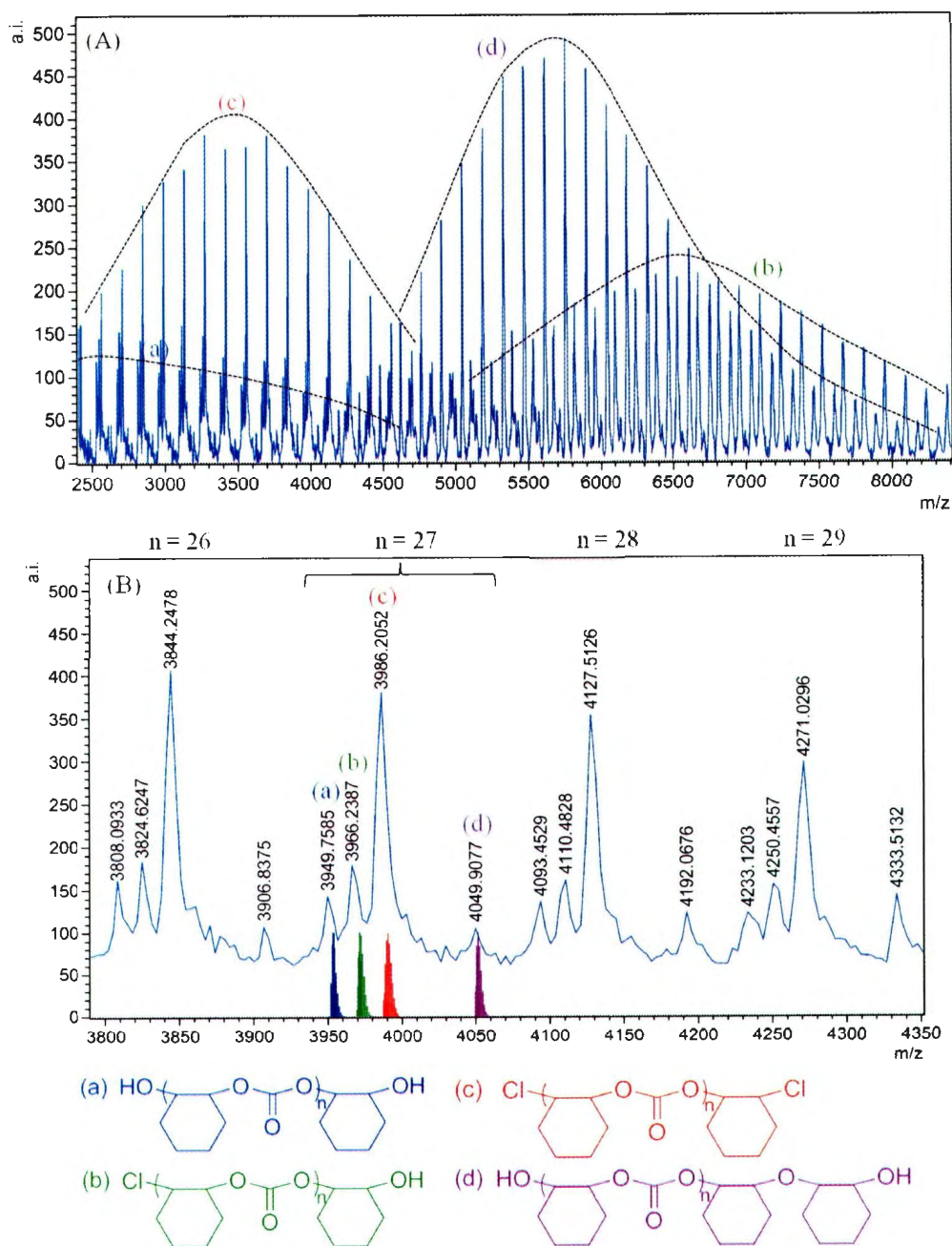
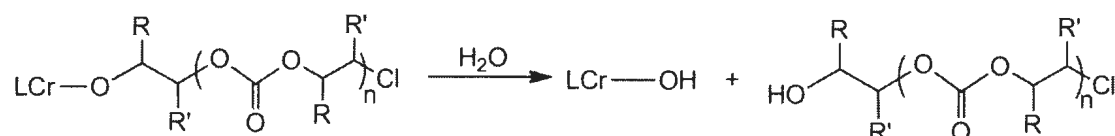


Figure 5.12. (A) MALDI-TOF MS of PCHC produced by **4.4** (Table 5.4, entry 13). (B) Magnified region of the spectrum ($n = 26-29$). Modeled isotopic masses (when $n = 27$) and images for polymer chains with end groups (a-d).

Although a chain-transfer reaction (Scheme 5.3) appears to be occurring, indication of any broadening of the molecular weights is not evident. A proposal by Nozaki and co-workers¹¹ alludes that the copolymerization is arising in an immortal fashion, which could likewise be occurring here. Furthermore, the lower than expected molecular weights could also be a result of this chain-transfer process. Support for this is shown by Williams and co-workers,⁴¹ where the addition of a 20-fold excess of water to their Zn catalyst still gave good activity towards PCHC formation. However, the M_n of the copolymer was substantially reduced. The presence of water in the reaction may originate from the CO_2 (despite using supercritical grade CO_2), CHO (even though it was dried over CaH_2), catalyst, glassware or the autoclave. From the results given above, it is not yet possible to determine whether chain transfer is occurring due to a change in catalyst structure as a result of hydrolysis, for example formation of a new chromium hydroxide species in solution, or if *in situ* hydrolysis of CHO by trace water is taking place.



Scheme 5.3. A proposed route to the chain transfer reaction.

5.2.3.3 Gel Permeation Chromatography

Similar to PO/ CO_2 copolymerization reactions, the number average molecular weights (M_n), determined by GPC for copolymer obtained with CHO were found to be

dependent on time. The highest molecular weight of 13.1 kg/mol was observed after 24 h. The M_n values reported are observed to be considerably smaller than the theoretical values. This likely suggests a chain-transfer process is happening due to a small amount of moisture in the reaction. Evidence towards bimodal molecular weights is apparent in some of the GPC traces. As well decreased CO₂ pressures gave lower M_n values. For all entries in Table 5.4 the PDIs are found to be generally narrow ranging from 1.1 to 1.7.

5.2.3.4 Thermal Analysis (DSC & TGA)

Thermal properties of poly(cyclohexene carbonate) were also investigated by TGA and DSC measurements. Representative traces for TGA and DSC of PCHC obtained in Table 5.4, entry 5 are shown in Figure 5.13 and Figure 5.14, respectively. The onset of weight loss for PCHC was observed to range between 214-235 °C. The T_g at the midpoint was found to range between 90-108 °C. Similar weight loss and T_g values have been reported by others.^{9,24}

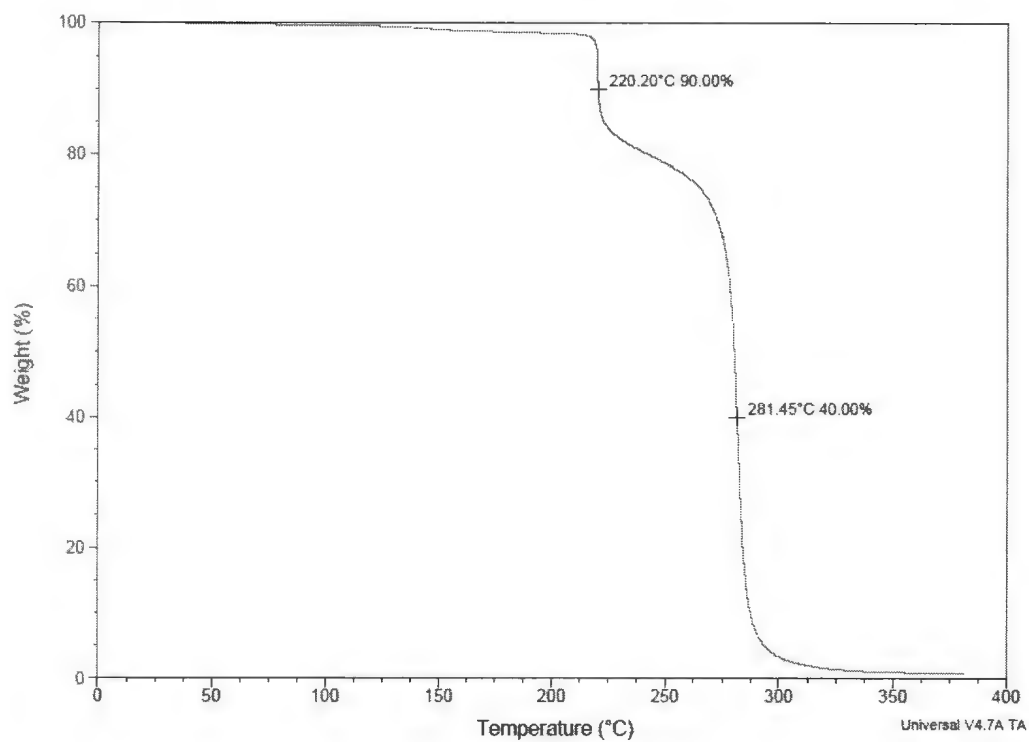


Figure 5.13. Representative TGA curve of PCHC produced by 4.4 (Table 5.4, entry 5).

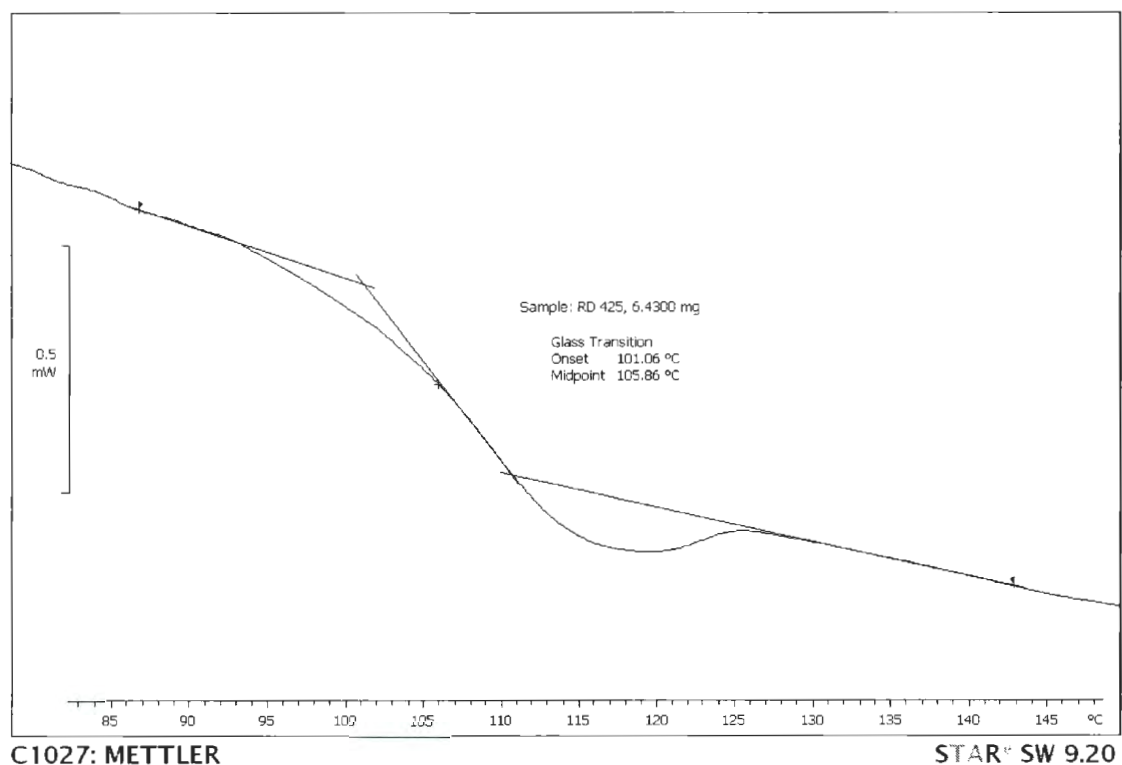
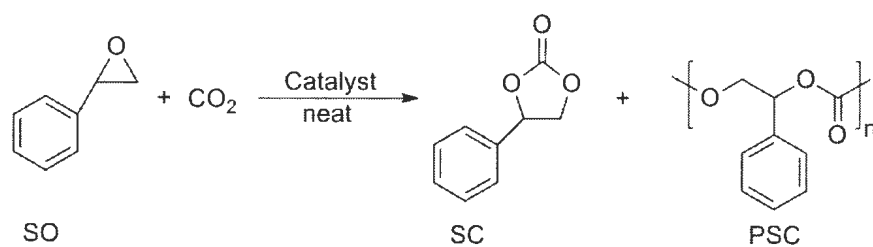


Figure 5.14. Representative DSC trace of PCHC produced by **4.4**, 2nd heat cycle (Table 5.4, entry 5).

5.2.4 Copolymerization of Styrene Oxide and CO₂

Preliminary studies were also conducted on the copolymerization of styrene oxide (SO) and carbon dioxide (Scheme 5.4). All reactions were performed in neat SO and initiated by complex **4.4**. In all cases, only the cyclic product, styrene carbonate (SC) was obtained. The ¹H NMR spectra of the products were found to be consistent with previously characterized SC (Figure 5.15).⁴³ Similar to PO and CHO an aliquot was taken from the reaction mixture in order to calculate the % yield.



Scheme 5.4. Copolymerization of SO and CO₂.

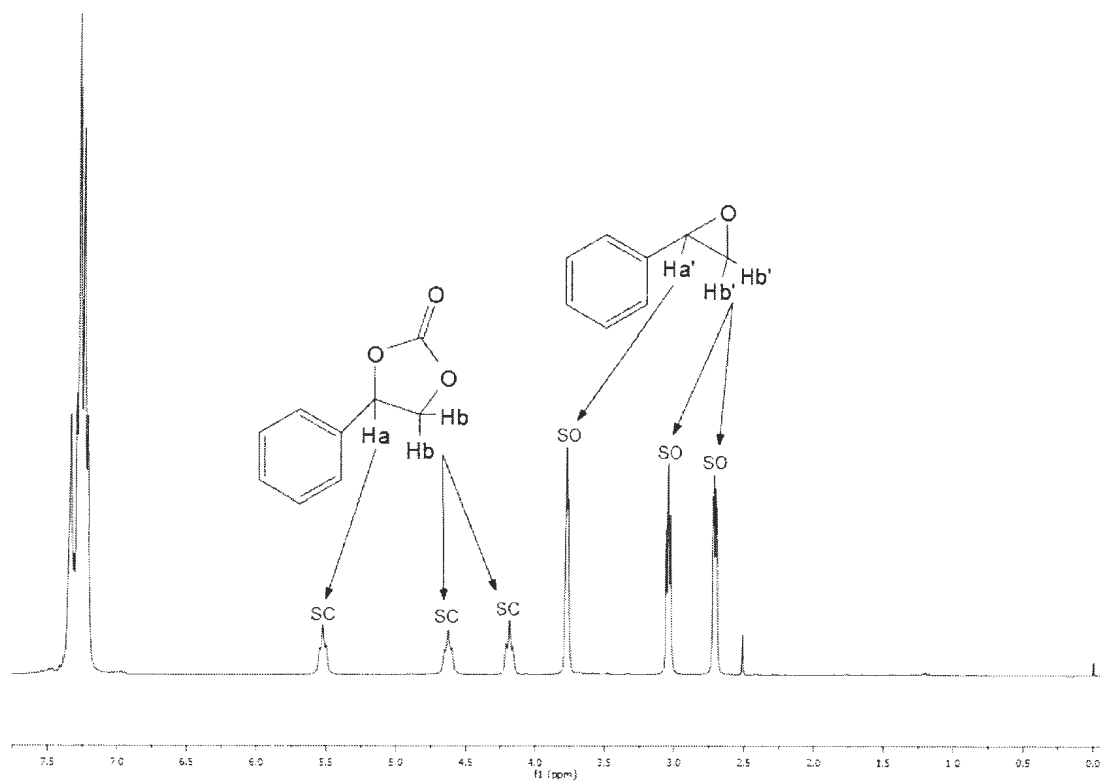


Figure 5.15. ¹H NMR spectrum of an aliquot from the reaction mixture of SO/CO₂ in CDCl₃ (Table 5.6, entry 3).

Complex **4.4** does exhibit some activity for the cyclic carbonate product, styrene carbonate at high temperatures and pressures (Table 5.6). Reactions performed at room temperature did not yield any product (entry 1). Optimal reaction conditions from CHO/CO₂ reactions were explored for SO yielding 16% SC after 3 hours (entry 2). Increasing the temperature to 100 °C (entry 3), gave an improved yield and TOF by almost double of entry 2. Additionally, PPnCl was explored at 80 °C and 45 bar (entry 4), yielding 65% SC over 18 h. Unfortunately, no copolymer was produced with this Cr initiator. This result was not surprising as the copolymerization of SO/CO₂ to form poly(styrene carbonate) is known to be very difficult to achieve due to the occurrence of ring-opening at the methine C_α-O bond. The electron-withdrawing nature of styrene oxide causes backbiting to occur through intramolecular cyclic elimination.⁴³ Recent advances with Co(salen) catalysts⁴³⁻⁴⁵ in conjunction with PPnX [X = acetate or 2,4-dinitrophenoxy] co-catalysts, has produced alternating poly(styrene carbonate) with an increase in thermal stability.⁴³

Table 5.6. Results of the coupling reaction of SO and CO₂ for complex **4.4**.^a

Entry	[Cr]:[SO]:[Co-Cat.]	Time (hr)	Temp. (°C)	Pressure (bar)	% Yield ^b	TON	TOF ^c (h ⁻¹)
1	1:500:0.5 (DMAP)	24	21	39	0	NA ^d	NA ^d
2	1:500:0.5 (DMAP)	3	80	48	16	79	26
3	1:500:0.5 (DMAP)	3	100	50	28	140	47
4	1:500:0.5 (PPnCl)	18	80	45	65	313	17

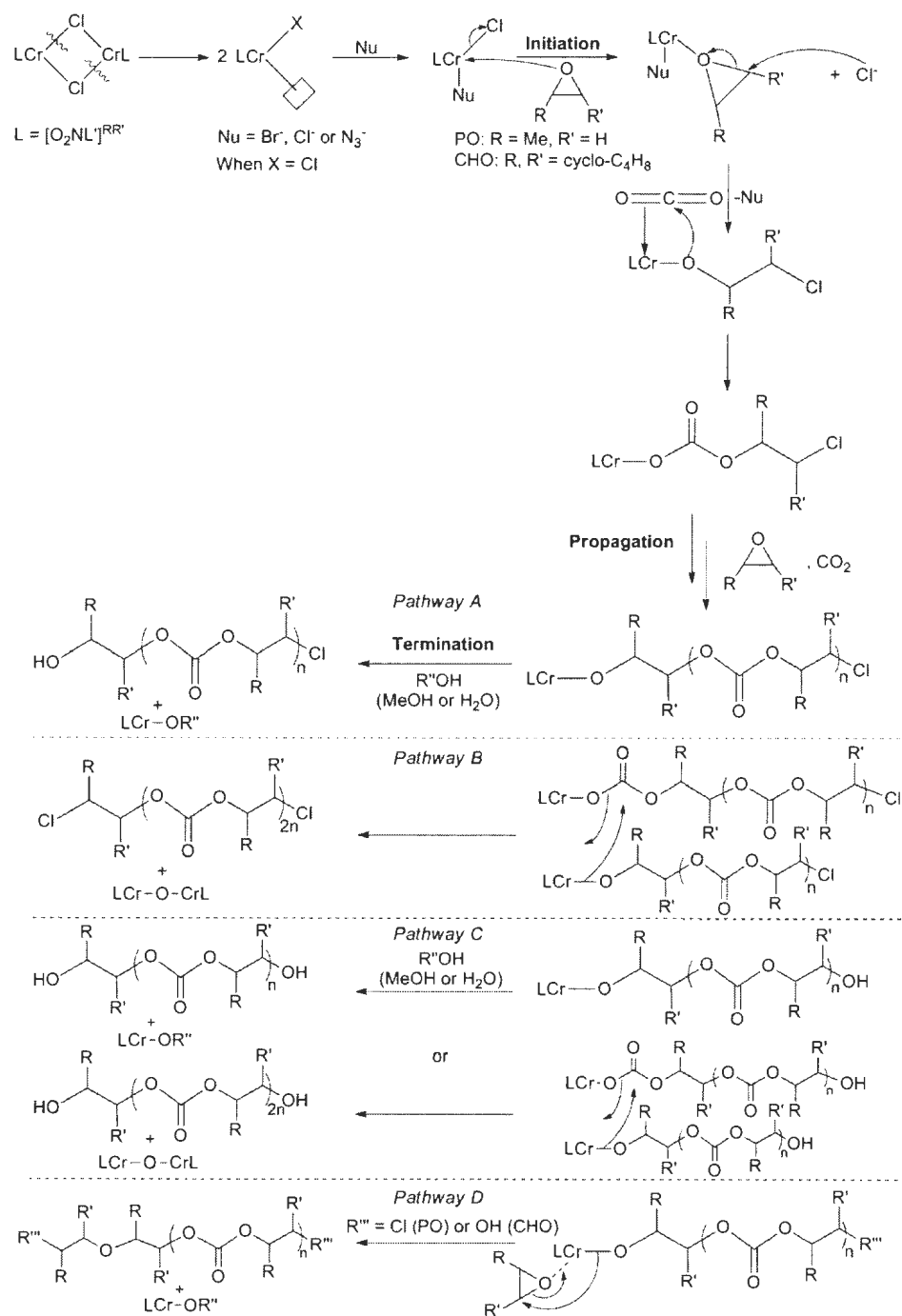
^aAll reactions were carried out in neat SO (4 mL). ^bCalculated by ¹H NMR. ^cTurnover frequency is moles of SC produced per mol of Cr per hour. ^dNA = not applicable (no SC obtained).

5.2.5 Mechanistic Proposal

The general mechanism proposed for epoxide/CO₂ copolymerization was presented in Chapter 1, Scheme 1.11. This coordination-insertion mechanism, when employing chromium as the active metal catalyst has been proposed to occur *via* a monometallic single site or through a bimetallic dual site fashion. Darensbourg and co-workers for example, have performed detailed mechanistic studies for Cr(salen)X and Cr(salan)X complexes towards epoxide/CO₂ copolymerization.³

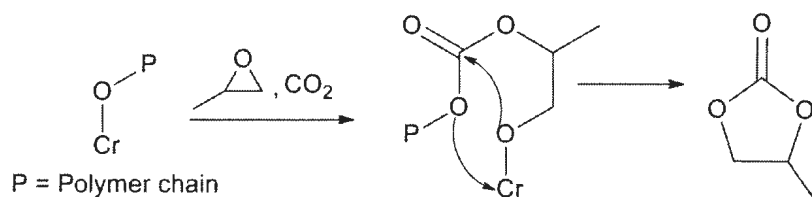
The proposed mechanism for this system is shown in Scheme 5.5. Based on the results obtained, preliminary mechanistic insights can be proposed. For instance, experimental findings from MALDI-TOF MS have suggested that a chloride (originating from the Cr complex) can initiate the ring-opening of the epoxide whether a neutral or ionic co-catalyst is utilized. In the copolymerization of PO/CO₂ only chloride end groups were observed as possible initiators in the MALDI-TOF MS. However, for the CHO monomer, hydroxyl and chloride initiators were observed. The presence of the OH end groups along with lower than expected M_n values suggests chain transfer reactions are occurring, likely due to trace water.^{41,46} Therefore, the first step in the mechanism, initiation, should involve the co-catalyst (Nu) binding to Cr, displacing the Cl⁻ from the metal. This Cl⁻ can now ring-open the bound epoxide at R' and start the polymerization process. Through this newly formed chromium alkoxide (Cr-OR) bond, CO₂ can insert at R producing a polycarbonate chain with HT regiochemistry. Sequential additions of epoxide and CO₂ allow propagation of the growing polymer chain. The copolymerization can then be terminated by addition of alcohol or water (Pathway A, Scheme 5.5). Again,

from the MALDI-TOF MS analysis end groups corresponding to the termination consisted of OH and Cl for both PO and CHO monomers. The presence of OH termination was expected, as acidic methanol (MeOH) was used to quench the reaction. However, chloride end groups were also found to end-cap these polymers. To the best of our knowledge such chloride termination has not been observed before. The possible route to this polymer chain may be a result of chain transfer occurring between two similar growing polymer fragments. This would therefore produce a polymer with two starting groups (Cl) as the chain ends as shown in pathway B. The hydroxyl end groups on the polymer chains could arise due to the presence of trace water, as mentioned, where either termination occurs through the expected route of the addition of water/alcohol or the formation of a new Cr(OH) species giving two OH chain ends (Pathway C). The formation of ether end groups is likely produced through double epoxide insertion (Pathway D).



Scheme 5.5. Proposed mechanism for the copolymerization of CO_2 with PO and CHO with Cr amine-bis(phenolate) complexes.

Although cyclic carbonate is not formed in the presence of the CHO monomer, PO was found to produce propylene carbonate. The cyclic product is likely formed as a result of back-biting at the metal center, where the Cr alkoxide attacks the carbonyl carbon next to it to form the five-membered ring (Scheme 5.6).^{3,7} A similar mechanism is expected to produce the depolymerization observed when NMR aliquot samples were left over time, as introduced in Section 5.2.2.1.



Scheme 5.6. Formation of propylene carbonate *via* back-biting mechanism.

5.3 Experimental

5.3.1 General Experimental Conditions

Unless otherwise stated, all manipulations were performed under an atmosphere of dry oxygen-free nitrogen by means of standard Schlenk techniques or using an MBraun Labmaster glove box. PO, CHO and SO were purchased from Aldrich and freshly distilled from CaH_2 and vacuum transferred into a sealed ampule prior to use. All solvents were purified by an MBraun Manual Solvent Purification System. PPNN_3 was prepared according to the literature procedure.⁴⁷ 4.8 Supercritical Fluid Chromatography Grade CO_2 was supplied from Praxair in a high-pressure cylinder equipped with a liquid dip tube. All ^1H and ^{13}C NMR were performed in CDCl_3 purchased from Cambridge Isotope

Laboratories, Inc. ^1H NMR spectra were recorded on either a Bruker AVANCE 500 MHz or Bruker AVANCE III 300 MHz spectrometer. All ^{13}C NMR spectra were recorded on a Bruker AVANCE III 300 MHz spectrometer at 75.487 MHz. Chemical shifts are given in ppm relative to TMS. All copolymerization reactions were carried out in a 300 mL stainless steel Parr[®] 5500 autoclave reactor with a Parr[®] 4836 controller. N.B. Caution should be taken when operating such high pressure equipment.

5.3.2 Polymerization Procedure

For all reactions carried out in neat epoxide, the appropriate amount of monomer was added to the catalyst (0.05 g) and co-catalyst in a glove box. The reactant solution was added via a long-needled syringe to a 300 mL Parr[®] autoclave, which was pre-dried under vacuum overnight at 80 °C. The autoclave was then charged with the appropriate pressure of CO_2 and left to stir at the desired temperature and time period. After the desired time the autoclave was cooled in an ice bath and vented in the fume hood. An aliquot for NMR was taken immediately after opening for the determination of % yield and conversion. The copolymer was extracted with CH_2Cl_2 and re-precipitated in cold acidic methanol. For reactions done in the presence of onium salts, complex **4.4** and the co-catalyst were first activated in 4 mL of CH_2Cl_2 and allowed to stir for 30 minutes and then dried *in vacuo*. The remaining procedure was followed in the same manner as the neat reactions.

5.3.3 Mass Spectrometry

MALDI-TOF MS. An Applied Biosystems 4800 MALDI TOF/TOF Analyzer equipped with a reflectron, delayed ion extraction and high performance nitrogen laser (200 Hz operating at 355 nm) was used for polymer analysis. 2,5-dihydroxybenzoic acid (DHBA) was used as the matrix. Mass spectra of the polymers were therefore modeled as $[M + H]^+$ cations resulting from protonation by DHBA. The matrix was dissolved in THF at a concentration of 10 mg/mL. Polymer was dissolved in THF at approximately 1 mg/mL. The matrix and polymer solutions were mixed together at a ratio of 5 to 1, respectively; 1 μ L of this was spotted on the MALDI plate and left to dry.

Inductively Coupled Plasma Mass Spectrometry (ICPMS). Analysis of 100 mg of purified and dried PCHC sample was dissolved in distilled concentrated nitric acid. The sample was heated on a hot plate overnight. This was followed by dilution of the sample to 60 g with Nanopure water. The solution was centrifuged and diluted to 10%. Analysis was carried out on an Elan DRCII ICP-MS.

5.3.4 Gel Permeation Chromatography

Gel permeation chromatography (GPC) analysis was performed on a Viscotek VE 2001 GPCMax at 35 °C equipped with a Viscotek VE 3580 RI Detector, and two phenogel 5 μ Linear Mixed Bed columns purchased from Phenomenex (300 x 4.60 mm column in series with a 100 Å, 300 x 4.60 mm column). Samples were prepared at a concentration of 2 mg/mL and left to equilibrate for ~ 2 h. The samples were filtered

through syringe filters before analysis. The GPC columns were eluted with chloroform (HPLC grade) at a flow rate of 0.35 mL/min with an 100 μ L injection volume. Six polystyrene standards were used in making the calibration curve, bracketing molecular weight ranges from 1050 to 3 800 000 Da. No further corrections were performed on the molecular weights obtained.

5.3.5 Differential Scanning Calorimetry

Glass transition (T_g) temperatures were measured using a Mettler Toledo DSC 1 STAR^c System equipped with a Julabo FT 100 immersion cooling system, using a R1150 refrigerant in an EtOH bath with a working range of -100 to $+20$ $^{\circ}$ C. Samples (~ 4 mg) were weighed into 40 μ L aluminum pans and subjected to two heating cycles. The first heating cycle consisted of heating from 0 to 100 $^{\circ}$ C at a rate of 10 $^{\circ}$ C/min, held for 2 min at 100 $^{\circ}$ C and then cooled back to 0 $^{\circ}$ C at 10 $^{\circ}$ C/min. The sample was held at this temperature for 2 min and subjected to a second heating cycle from 0 to 180 $^{\circ}$ C at a rate of 10 $^{\circ}$ C/min.

5.3.6 Thermal Gravimetric Analysis

TGA was performed with a TA Instrument Q500. Samples (8 mg) were loaded onto a platinum pan and subjected to a dynamic high resolution scan, with an initial heating rate of 20 $^{\circ}$ C/min. Each sample was heated from room temperature to 400 $^{\circ}$ C.

5.4 Conclusions

In conclusion, chromium diamine-bis(phenolate), $\{\text{CrCl}[\text{O}_2\text{NN}^{\text{tBuBu}}]\}_2$ (**4.4**) was shown to effectively copolymerize PO and CHO with CO_2 in the presence of various co-catalysts (DMAP, PPNCI, PPNN₃). When the PO monomer was examined, PPC was found to form at room temperature and the catalyst appeared to have good activity for this reaction. Furthermore, selectivity of the system to form cyclic product or copolymer could be tuned by varying the temperature of the reaction or co-catalyst. Cyclohexene oxide was found to copolymerize more effectively compared with PO when using this catalyst system, with no evidence of cyclic carbonate being formed and with a high degree of carbonate linkages. The number average molecular weights were shown to be lower than expected, but the polydispersities observed were generally narrow. The amount of Cr contaminants in the resulting polymer was also found to be relatively low given the simple method of purification. Preliminary results suggest the chloride on the Cr complex plays an important role in the initiation of the epoxides in order to generate polycarbonate. Further investigation into the influence of the pendant donor and substituents on the phenolate fragments of the amine-bis(phenolate) ligand are currently being undertaken by other members in the Kozak group.

5.5 References

- (1) Coates, G. W.; Moore, D. R. *Angew. Chem. Int. Ed.* **2004**, *43*, 6618-6639.
- (2) Darensbourg, D. J. *Chem. Rev.* **2007**, *107*, 2388-2410.
- (3) Darensbourg, D. J. *Inorg. Chem.* **2010**, *49*, 10765-10780.
- (4) Kember, M. R.; Buchard, A.; Williams, C. K. *Chem. Commun.* **2011**, *47*, 141-163.
- (5) Klaus, S.; Lehenmeier, M. W.; Anderson, C. E.; Rieger, B. *Coord. Chem. Rev.* **2011**, *255*, 1460-1479.
- (6) Lu, X.; Darensbourg, D. J. *Chem. Soc. Rev.* **2012**, *41*, 1462-1484.
- (7) Darensbourg, D. J.; Bottarelli, P.; Andreatta, J. R. *Macromolecules* **2007**, *40*, 7727-7729.
- (8) Darensbourg, D. J.; Mackiewicz, R. M.; Rodgers, J. L.; Phelps, A. L. *Inorg. Chem.* **2004**, *43*, 1831-1833.
- (9) Darensbourg, D. J.; Ulusoy, M.; Karroonnirum, O.; Poland, R. R.; Reibenspies, J. H.; Çetinkaya, B. *Macromolecules* **2009**, *42*, 6992-6998.
- (10) Guo, L.; Wang, C.; Zhao, W.; Li, H.; Sun, W.; Shen, Z. *Dalton Trans.* **2009**, 5406-5410.
- (11) Nakano, K.; Nakamura, M.; Nozaki, K. *Macromolecules* **2009**, *42*, 6972-6980.
- (12) Kruper, W. J.; Dellar, D. D. *J. Org. Chem.* **1995**, *60*, 725-727.
- (13) Mang, S.; Cooper, A. I.; Colclough, M. E.; Chauhan, N.; Holmes, A. B. *Macromolecules* **2000**, *33*, 303-308.
- (14) Stamp, L. M.; Mang, S. A.; Holmes, A. B.; Knights, K. A.; de Miguel, Y. R.; McConvey, I. F. *Chem. Commun.* **2001**, 2502-2503.
- (15) Kojima, F.; Aida, T.; Inoue, S. *J. Am. Chem. Soc.* **1986**, *108*, 391-395.
- (16) Darensbourg, D. J.; Holtcamp, M. W. *Macromolecules* **1995**, *28*, 7577-7579.

- (17) Darensbourg, D. J.; Holtcamp, M. W.; Struck, G. E.; Zimmer, M. S.; Niezgoda, S. A.; Rainey, P.; Robertson, J. B.; Draper, J. D.; Reibenspies, J. H. *J. Am. Chem. Soc.* **1999**, *121*, 107-116.
- (18) Darensbourg, D. J.; Wildeson, J. R.; Yarbrough, J. C.; Reibenspies, J. H. *J. Am. Chem. Soc.* **2000**, *122*, 12487-12496.
- (19) Cheng, M.; Lobkovsky, E. B.; Coates, G. W. *J. Am. Chem. Soc.* **1998**, *120*, 11018-11019.
- (20) Darensbourg, D. J.; Yarbrough, J. C. *J. Am. Chem. Soc.* **2002**, *124*, 6335-6342.
- (21) Darensbourg, D. J.; Yarbrough, J. C.; Ortiz, C.; Fang, C. C. *J. Am. Chem. Soc.* **2003**, *125*, 7586-7591.
- (22) Darensbourg, D. J.; Mackiewicz, R. M. *J. Am. Chem. Soc.* **2005**, *127*, 14026-14038.
- (23) Cohen, C. T.; Thomas, C. M.; Peretti, K. L.; Lobkovsky, E. B.; Coates, G. W. *Dalton Trans.* **2006**, 237-249.
- (24) Ren, W.; Zhang, X.; Liu, Y.; Li, J.; Wang, H.; Lu, X. *Macromolecules* **2010**, *43*, 1396-1402.
- (25) Buchard, A.; Kember, M. R.; Sandeman, K. G.; Williams, C. K. *Chem. Commun.* **2011**, *47*, 212-214.
- (26) Nakano, K.; Kobayashi, K.; Nozaki, K. *J. Am. Chem. Soc.* **2011**, *133*, 10720-10723.
- (27) Darensbourg, D. J.; Phelps, A. L. *Inorg. Chem.* **2005**, *44*, 4622-4629.
- (28) Shen, Y.-M.; Duan, W.-L.; Shi, M. *Eur. J. Org. Chem.* **2004**, 3080-3089.
- (29) North, M.; Pasquale, R.; Young, C. *Green Chem.* **2010**, *12*, 1514-1539.
- (30) Decortes, A.; Castilla, A. M.; Kleij, A. W. *Angew. Chem. Int. Ed.* **2010**, *49*, 9822-9837.
- (31) Rao, D.; Li, B.; Zhang, R.; Wang, H.; Lu, X. *Inorg. Chem.* **2009**, *48*, 2830-2836.
- (32) Qin, Z.; Thomas, C. M.; Lee, S.; Coates, G. W. *Angew. Chem. Int. Ed.* **2003**, *42*, 5484-5487.
- (33) S, S.; Min, J. K.; Seong, J. E.; Na, S. J.; Lee, B. Y. *Angew. Chem. Int. Ed.* **2008**, *47*, 7306-7309.

- (34) Nakano, K.; Hashimoto, S.; Nozaki, K. *Chem. Sci.* **2010**, 369-373.
- (35) Chisholm, M. H.; Navarro-Llobet, D.; Zhou, Z. *Macromolecules* **2002**, *35*, 6494-6504.
- (36) Allen, S. D.; Moore, D. R.; Lobkovsky, E. B.; Coates, G. W. *J. Am. Chem. Soc.* **2002**, *124*, 14284-14285.
- (37) Darensbourg, D. J.; Poland, R. R.; Strickland, A. L. *J. Polym. Sci., Part A: Polym. Chem.* **2012**, *50*, 127-133.
- (38) Paddock, R. L.; Nguyen, S. T. *J. Am. Chem. Soc.* **2001**, *123*, 11498-11499.
- (39) Darensbourg, D. J.; Rodgers, J. L.; Mackiewicz, R. M.; Phelps, A. L. *Catal. Today* **2004**, *98*, 485-492.
- (40) Sugimoto, H.; Ohtsuka, H.; Inoue, S. *J. Polym. Sci., Part A: Polym. Chem.* **2005**, *43*, 4172-4186.
- (41) Jutz, F.; Buchard, A.; Kember, M. R.; Fredriksen, S. B.; Williams, C. K. *J. Am. Chem. Soc.* **2011**, *133*, 17395-17405.
- (42) Hongfa, C.; Tian, J.; Andreatta, J.; Darensbourg, D. J.; Bergbreiter, D. E. *Chem. Commun.* **2008**, 975-977.
- (43) Wu, G.; Wei, S.; Lu, X.; Ren, W.; Darensbourg, D. J. *Macromolecules* **2010**, *43*, 9202-9204.
- (44) Hirahata, W.; Thomas, R. M.; Lobkovsky, E. B.; Coates, G. W. *J. Am. Chem. Soc.* **2008**, *130*, 17658-17659.
- (45) Thomas, R. M.; Widger, P. C. B.; Ahmed, S. M.; Jeske, R. C.; Hirahata, W.; Lobkovsky, E. B.; Coates, G. W. *J. Am. Chem. Soc.* **2010**, *132*, 16520-16525.
- (46) Darensbourg, D. J.; Fitch, S. B. *Inorg. Chem.* **2009**, *48*, 8668-8677.
- (47) Demadis, K. D.; Meyer, T. J.; White, P. S. *Inorg. Chem.* **1998**, *37*, 3610-3619.

Chapter 6

Conclusions and Future Projects

6.1 Conclusions and Future Directions

Homogeneous catalysis, coupled with renewable feedstocks to produce environmentally friendly consumer goods has become an important and active area of research around the world. The use of non-precious, non-toxic and inexpensive metals for catalysis is a goal worth pursuing, particularly for large scale industrial applications. The incorporation of easily synthesized and inexpensive amine-bis(phenolate) ligands together with high yielding lithium and chromium complexes provides justification for continuation of this research.

Chapter 1 of this thesis introduced an overview of important and precedent research involving amine-bis(phenolate) ligands; catalysis by chromium; salen/salan and BDI complexes for use in the copolymerization of epoxides/ CO_2 and ethene polymerization, respectively; and lithium-catalyzed reactions, specifically for the ring-opening polymerization of lactide.

Chapter 2 described the synthesis of amine-bis(phenolate) ligands and their lithium complexes. In addition, their solution and solid-state properties were investigated. The lithium complexes of the tetradentate ligands exhibited dimeric (tetralithium) base-free solid-state structures when obtained from non-coordinating solvents. Solution NMR results provided evidence that the dimeric structure persisted in solution when studied in

non-coordinating solvents. Interestingly, a monomeric (dilithium) complex was observed upon the addition of a coordinating solvent. The dilithium species was shown to have two symmetric ^7Li environments in solution NMR studies.

Various modifications to these amine-bis(phenol) ligands (Figure 6.1) are currently being explored in the Kozak group, where electron withdrawing halides (Cl or F) and electron donating groups (OMe) on the phenolates may affect catalytic activity. Some of these ligands have been used in the Kozak group with other transition metals such as iron and cobalt. Additionally, altering of the pendant donor on the ligand to give tri- (i.e. ^nPr or ^iPr) or tetradentate (i.e. $\text{CH}_2\text{CH}_2\text{NMe}_2$ or $\text{CH}_2\text{CH}_2\text{OMe}$) coordination around the metal could generate more reactive complexes. In particular, increasing the steric properties on the phenol substituents *via* the introduction of *tert*-amyl or side arm groups may allow for a monomeric complex to be produced rather than a dimeric complex. Solution and solid state NMR studies of tridentate lithium amine-bis(phenolate) complexes have yet to be studied and contrasted to the tetradentate complexes presented in this chapter. Based on the observation of THF coordinated to the metal center in the solid-state, the tridentate system may be expected to dissociate easier in solution.

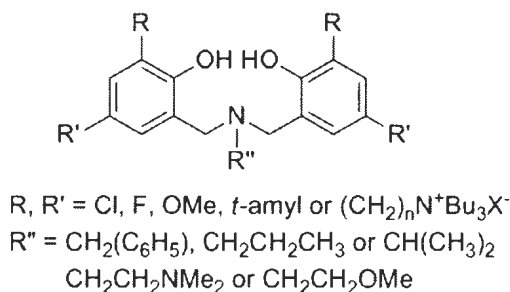


Figure 6.1. Potential examples of amine-bis(phenol) ligands for Li and Cr complexes.

In Chapter 3, dimeric lithium complexes were used to study the catalytic activity of the ring-opening polymerization of cyclic esters. Results found that both tri- and tetradentate complexes initiated the ROP of *rac*-lactide in toluene solutions. Kinetic studies on the tetradentate lithium complexes found that at low temperatures a first-order dependence on monomer concentration was observed, while at higher temperatures the kinetics were found to be second-order. Rates were generally observed to be fast, but the polymerizations proceeded in an uncontrolled manner. The domination of transesterification was evident for all complexes examined. Low molecular weights, broad polydispersities and cyclic species observed in the MALDI-TOF MS all indicated that transesterification was occurring.

Further refinement of the catalyst design is necessary to inhibit transesterification in the reaction. For example, modification of the substituents on the ligand to include more steric bulk or changing the electron donating capacity on the pendent donor may help reduce transesterification side reactions.¹ Future investigations of the source of contaminant (i.e. water) causing transesterification could also assist in solving this problem. NMR scale ROP reactions may also be helpful in order to monitor the reaction in more detail. Furthermore, changing the solvent in the reaction to THF or CH₂Cl₂ may offer better control as a result of a less crowded initiator being produced. Recently, Hayes and co-workers^{2,3} reported Zn cationic complexes which were found to give rapid, controlled and living ROP of lactide. Alkali metal initiators are known to suffer from unwanted side-reactions; therefore examination of this ligand with a Zn-based system may provide a route towards a single site initiator helping to circumvent these issues.

The synthesis, structure, spectroscopic and magnetic behaviour of mono- and bimetallic chromium(III) amine-bis(phenolate) complexes was described in Chapter 4. Seven solid-state structures were presented, five of which were synthesized through either a salt metathesis or protonolysis/oxidation route giving six-coordinate distorted octahedral complexes. Two monometallic complexes and one chloride-bridged dimer were obtained when prepared and purified under strictly anhydrous conditions. Two bimetallic complexes were obtained in the presence of air and were found to react with adventitious water resulting in a hydroxide bridge between the two Cr(III) centres and protonation of one of the phenolate groups. These paramagnetic Cr(III) amine-bis(phenolate) complexes were characterized by mass spectrometry, elemental analysis, IR, UV-Vis spectroscopy, magnetometry and cyclic voltammetry. MALDI-TOF MS showed characteristic monomeric and bimetallic fragments where applicable, for all complexes. Elemental and IR data were found to support the structures obtained and showed characteristic bands for OH stretching (3200 cm^{-1}). Electronic spectroscopy data and magnetic measurements confirmed all Cr complexes were in +3 oxidation states. The electronic absorption spectra for these complexes were shown to have multiple intense bands in the UV and visible region. Magnetic data for monometallic ($3.8\ \mu_{\text{B}}$) and bimetallic ($5.8\ \mu_{\text{B}}$) complexes exhibited moments common for Cr(III) d^3 centres having g -values slightly lower than 2. The cyclic voltammograms of the Cr(III) complexes showed two reversible ligand centred oxidations. Two additional chromium complexes were structurally isolated from attempted Cr amide and alkyl synthesis.

As a result of the interesting structural and physical properties of these Cr complexes additional studies continuing to explore Cr(III) complexes supported by a

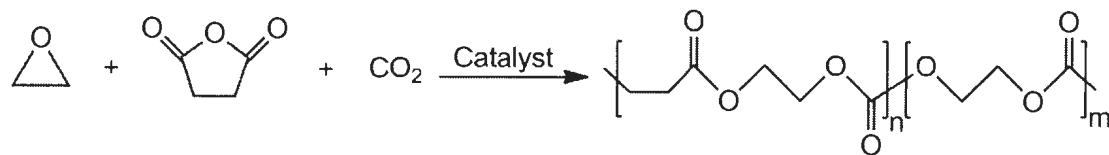
variety of amine-bis(phenolate) ligands would be valuable. Changing the ancillary ligand may also influence the structure and activity of the complex providing new analogues to use for catalysis. The study of Cr amine-bis(phenolate) complexes is still in its infancy in the Kozak group but related Fe complexes have shown that a variety of analogues are capable of being produced with this ligand framework.⁴⁻⁸ Furthermore, a comprehensive study including additional characterization of the attempted Cr alkyl and amide complexes could be conducted and attempts made to test their activity as polymerization catalysts.

The reactions of propylene oxide and cyclohexene oxide with CO₂ were found to effectively produce copolymer when employing a chromium(III) diamine-bis(phenolate) catalyst as discussed in Chapter 5. In the presence of a suitable co-catalyst (PPNN₃, PPNCI or DMAP), poly(propylene carbonate) could be synthesized with good selectivity, at low temperatures and narrow polydispersities. By varying the temperature or co-catalyst the system could be tuned to produce cyclic carbonate or polycarbonate. When the monomer cyclohexene oxide was examined only copolymer and no cyclic carbonate was obtained. Polymerization at 80 °C and at moderately low pressure (20 bar) gave polymer with narrow polydispersity. Preliminary end group analysis of the polymer suggests the chloride on the Cr complex is acting as the initiator in the ring-opening of the epoxide. Additionally, a relatively low amount of Cr contaminant was observed in the copolymer after limited purification. Initial reactions with styrene oxide and CO₂ produced only cyclic by-products and no copolymer was observed.

The results obtained from this research project provide a good starting point for future advancements, such as the development of more active catalysts and production of

higher molecular weight polymers. In order to achieve these goals a deeper mechanistic understanding is required. For example, *in situ* ATR/FTIR studies could help identify reaction intermediates and obtain critical kinetic data through real time analysis.⁹ An additional experiment which may provide further insight into the chain transfer process would involve examining the bimetallic chromium hydroxide bridged analogue (complex 4.6) of the chromium chloride-bridged complex (4.4) to observe whether similar end groups are obtained in the MALDI-TOF MS. If similar polymer chains are observed than the chain transfer reaction is most likely being caused from another source (i.e. one of the reactants). Furthermore, the addition of water to the reaction mixture could also determine if a related phenomenon observed by Williams and co-workers¹⁰ is at work here. As discussed in Chapter 5, the authors reported that polymerization was not directly inhibited by the addition of water, but instead led to chain transfer. In the short term, different co-catalysts, such as PPNX, where X = acetate or 2,4-dinitrophenoxide, could be screened to determine if there is any potential increase in catalytic activity or selectivity similar to results obtained by Darensbourg¹¹ and Coates.¹² The development of a single component catalyst with an anionic or neutral nucleophile, such as Cl⁻, Br⁻, N₃⁻ or DMAP as an ancillary ligand or side-arm attached at the phenolate group also has shown great improvements in activities.¹³⁻¹⁶ Terpolymerization, the reaction of two different monomers with CO₂, can be used to further enhance the physical properties of the polymer.¹⁶⁻¹⁹ For example, Darensbourg and co-workers¹⁹ recently studied the polymerization of cyclic monomers, cyclohexene oxide and vinylcyclohexene oxide, with CO₂. In their work, the terpolymer produced had a higher glass transition temperature than polymers derived from the copolymerization of either monomer with CO₂.

Over the long term the utilization of different, unexplored epoxides will open avenues for new polymers to be prepared. Related to this, poly(ester-*co*-carbonate)s (Scheme 6.1), synthesized by reacting cyclic esters with epoxides and CO₂ has been recently gaining in interest. For example, Coates and co-workers^{20,21} and more recently Darensbourg and co-workers²² reported the successful one pot reaction of di-block poly(ester-*co*-carbonate)s with Zn and Cr(III) complexes. As well, Duchateau and co-workers^{23,24} have utilized Cr(III) porphyrinate and salen complexes for co- and terpolymerization of CHO and SO with a series of cyclic anhydrides. Finally, the transition metal Fe is actively being explored for cross-coupling^{4,6-8} in the Kozak research group and of late for controlled radical polymerization.²⁵ A recent report of the copolymerization of CHO and CO₂ by a bimetallic Fe(III) complex²⁶ provides a hopeful future for Fe catalysts supported by amine-bis(phenolate) ligands to be also used for epoxide/CO₂ copolymerization.



Scheme 6.1. Generic synthesis of a poly(ester-*co*-carbonate).

6.2 References

- (1) Sutar, A. K.; Maharana, T.; Dutta, S.; Chen, C.; Lin, C. *Chem. Soc. Rev.* **2010**, *39*, 1724-1746.
- (2) Wheaton, C. A.; Hayes, P. G. *Chem. Commun.* **2010**, *46*, 8404-8406.
- (3) Sun, H.; Ritch, J. S.; Hayes, P. G. *Inorg. Chem.* **2011**, *50*, 8063-8072.
- (4) Chowdhury, R. R.; Crane, A. K.; Fowler, C.; Kwong, P.; Kozak, C. M. *Chem. Commun.* **2008**, 94-96.
- (5) Hasan, K.; Fowler, C.; Kwong, P.; Crane, A. K.; Collins, J. L.; Kozak, C. M. *Dalton Trans.* **2008**, 2991-2998.
- (6) Reckling, A. M.; Martin, D.; Dawe, L. N.; Decken, A.; Kozak, C. M. *J. Organomet. Chem.* **2011**, *696*, 787-794.
- (7) Qian, X.; Dawe, L. N.; Kozak, C. M. *Dalton Trans.* **2011**, *40*, 933-943.
- (8) Hasan, K.; Dawe, L. N.; Kozak, C. M. *Eur. J. Inorg. Chem.* **2011**, 4610-4621.
- (9) Darensbourg, D. J.; Rodgers, J. L.; Mackiewicz, R. M.; Phelps, A. L. *Catal. Today* **2004**, *98*, 485-492.
- (10) Jutz, F.; Buchard, A.; Kember, M. R.; Fredriksen, S. B.; Williams, C. K. *J. Am. Chem. Soc.* **2011**, *133*, 17395-17405.
- (11) Wu, G.; Wei, S.; Lu, X.; Ren, W.; Darensbourg, D. J. *Macromolecules* **2010**, *43*, 9202-9204.
- (12) Hirahata, W.; Thomas, R. M.; Lobkovsky, E. B.; Coates, G. W. *J. Am. Chem. Soc.* **2008**, *130*, 17658-17659.
- (13) Darensbourg, D. J.; Mackiewicz, R. M. *J. Am. Chem. Soc.* **2005**, *127*, 14026-14038.
- (14) Darensbourg, D. J.; Phelps, A. L. *Inorg. Chem.* **2005**, *44*, 4622-4629.
- (15) Darensbourg, D. J.; Moncada, A. I. *Inorg. Chem.* **2008**, *47*, 10000-10008.
- (16) Ren, W.; Zhang, X.; Liu, Y.; Li, J.; Wang, H.; Lu, X. *Macromolecules* **2010**, *43*, 1396-1402.

- (17) Seong, J. E.; Na, S. J.; Cyriac, A.; Kim, B.-W.; Lee, B. Y. *Macromolecules* **2010**, *43*, 903-908.
- (18) Huijser, S.; HosseiniNejad, E.; Sablong, R.; de Jong, C.; Koning, C. E.; Duchateau, R. *Macromolecules* **2011**, *44*, 1132-1139.
- (19) Darensbourg, D. J.; Poland, R. R.; Strickland, A. L. *J. Polym. Sci., Part A: Polym. Chem.* **2012**, *50*, 127-133.
- (20) Jeske, R.; Rowley, J.; Coates, G. *Angew. Chem. Int. Ed.* **2008**, *47*, 6041-6044.
- (21) DiCiccio, A. M.; Coates, G. W. *J. Am. Chem. Soc.* **2011**, *133*, 10724-10727.
- (22) Darensbourg, D. J.; Poland, R. R.; Escobedo, C. *Macromolecules* **2012**, *45*, 2242-2248.
- (23) Hosseini Nejad, E.; van Melis, Carlo G. W.; Vermeer, T. J.; Koning, C. E.; Duchateau, R. *Macromolecules* **2012**, *45*, 1770-1776.
- (24) Hosseini Nejad, E.; Paoniasari, A.; Koning, C. E.; Duchateau, R. *Polym. Chem.* **2012**, *3*, 1308-1313.
- (25) Allan, L. E. N.; MacDonald, J. P.; Reckling, A. M.; Kozak, C. M.; Shaver, M. P. *Macromol. Rapid. Commun.* **2012**, *33*, 414-418.
- (26) Buchard, A.; Kember, M. R.; Sandeman, K. G.; Williams, C. K. *Chem. Commun.* **2011**, *47*, 212-214.

Appendix A: NMR Spectroscopy

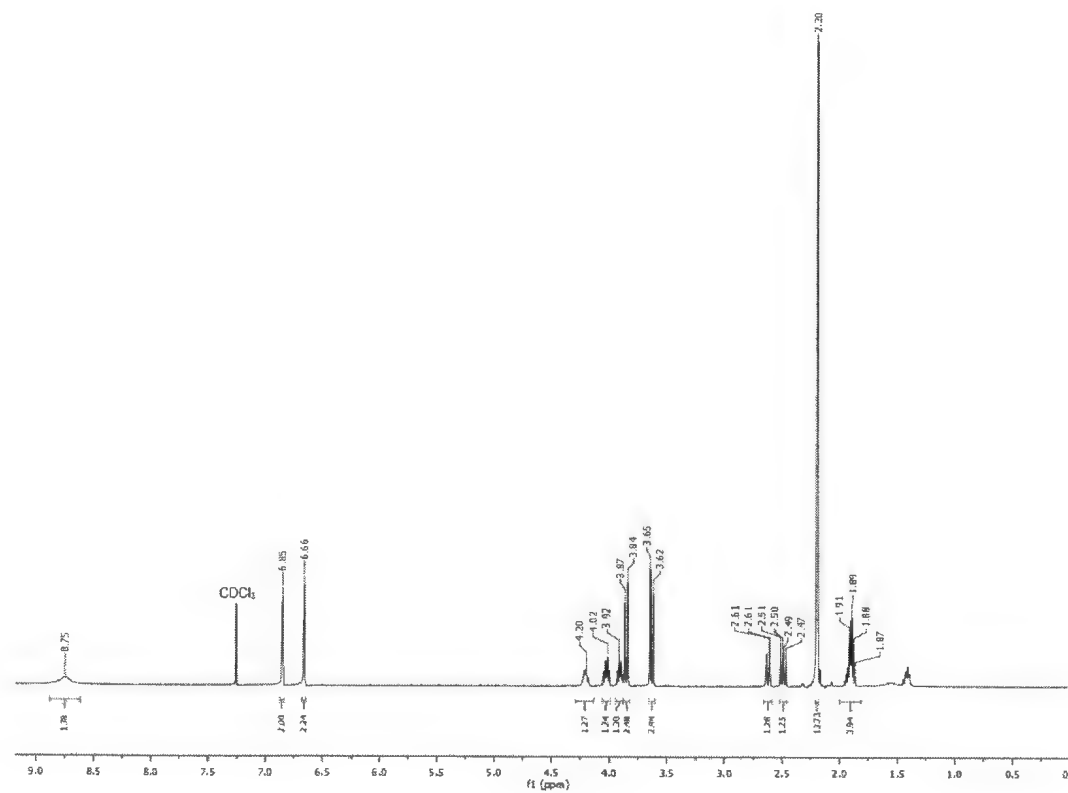


Figure A1.1. ^1H NMR spectrum of L1.

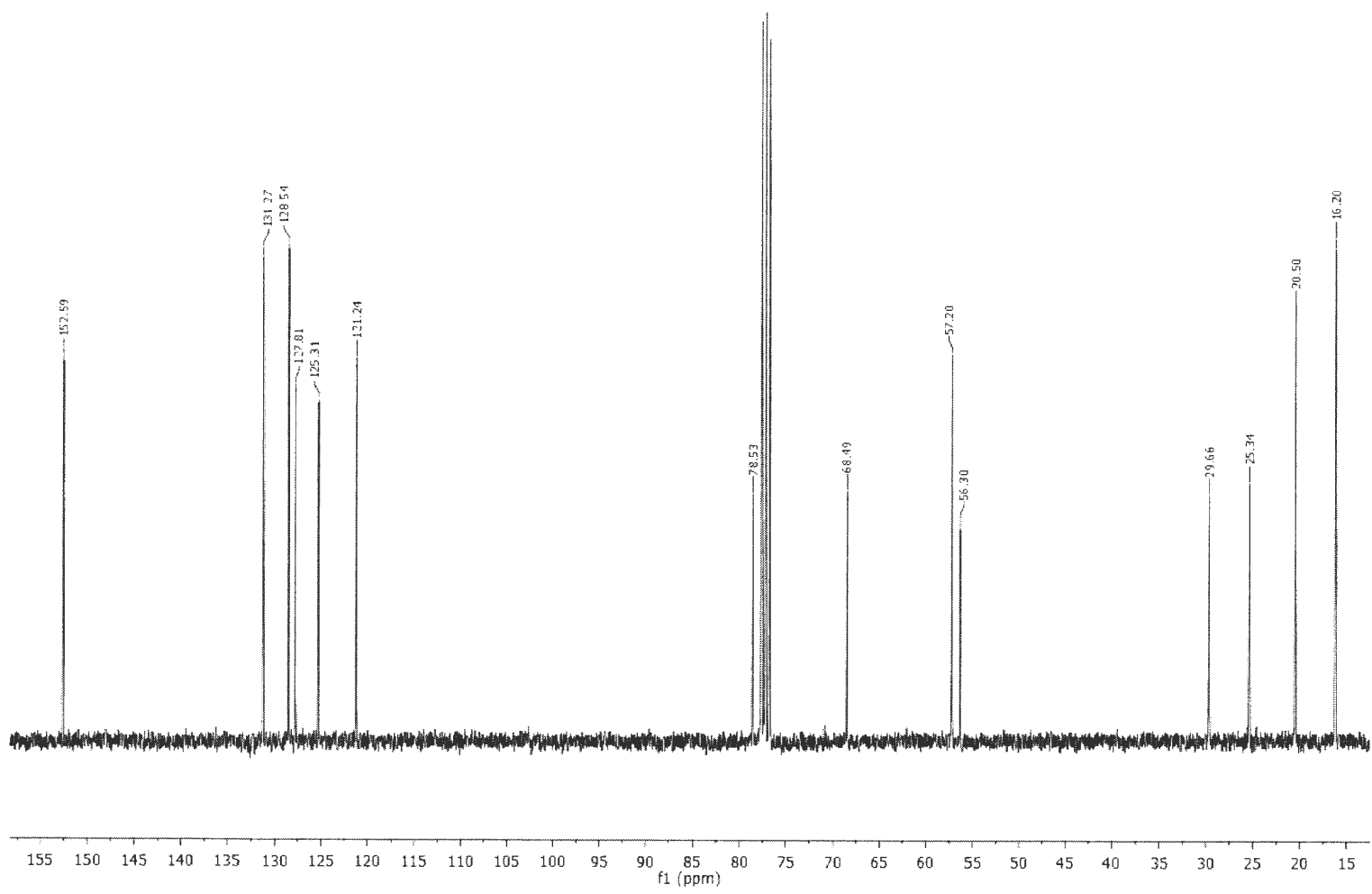


Figure A1.2. ^{13}C NMR spectrum of L1.

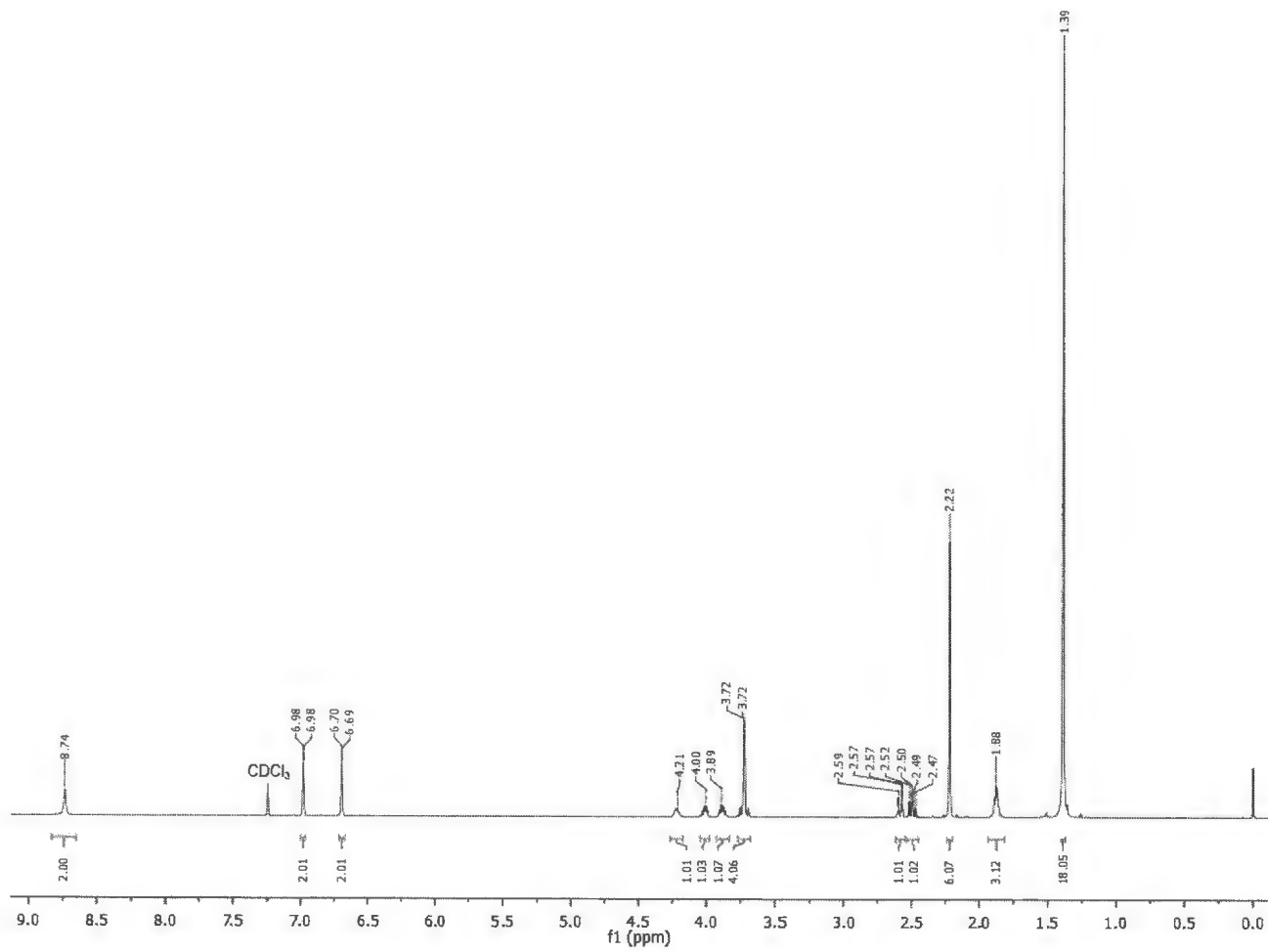


Figure A1.3. ^1H NMR spectrum of L2.

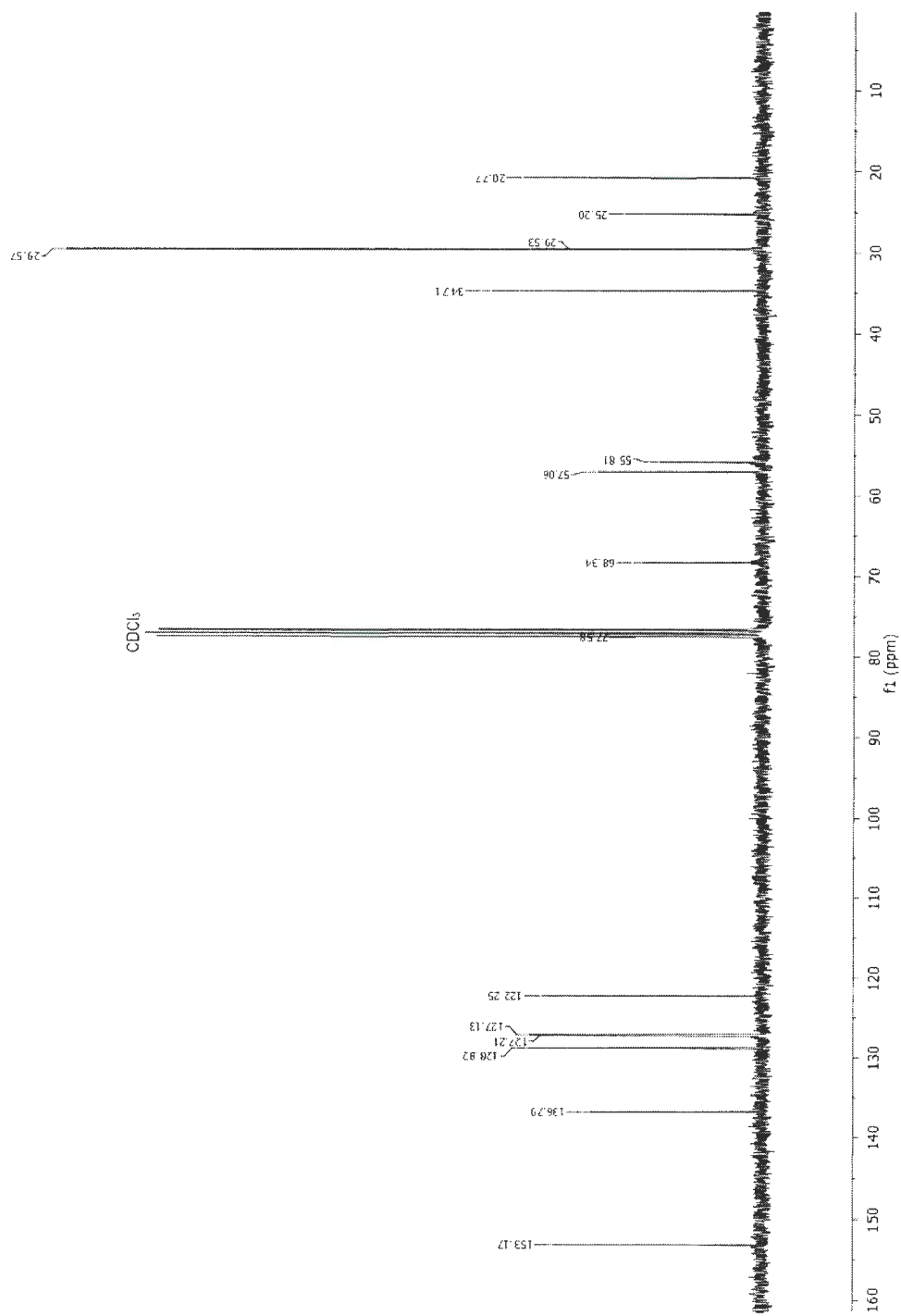


Figure A1.4. ¹³C NMR spectrum of L2.

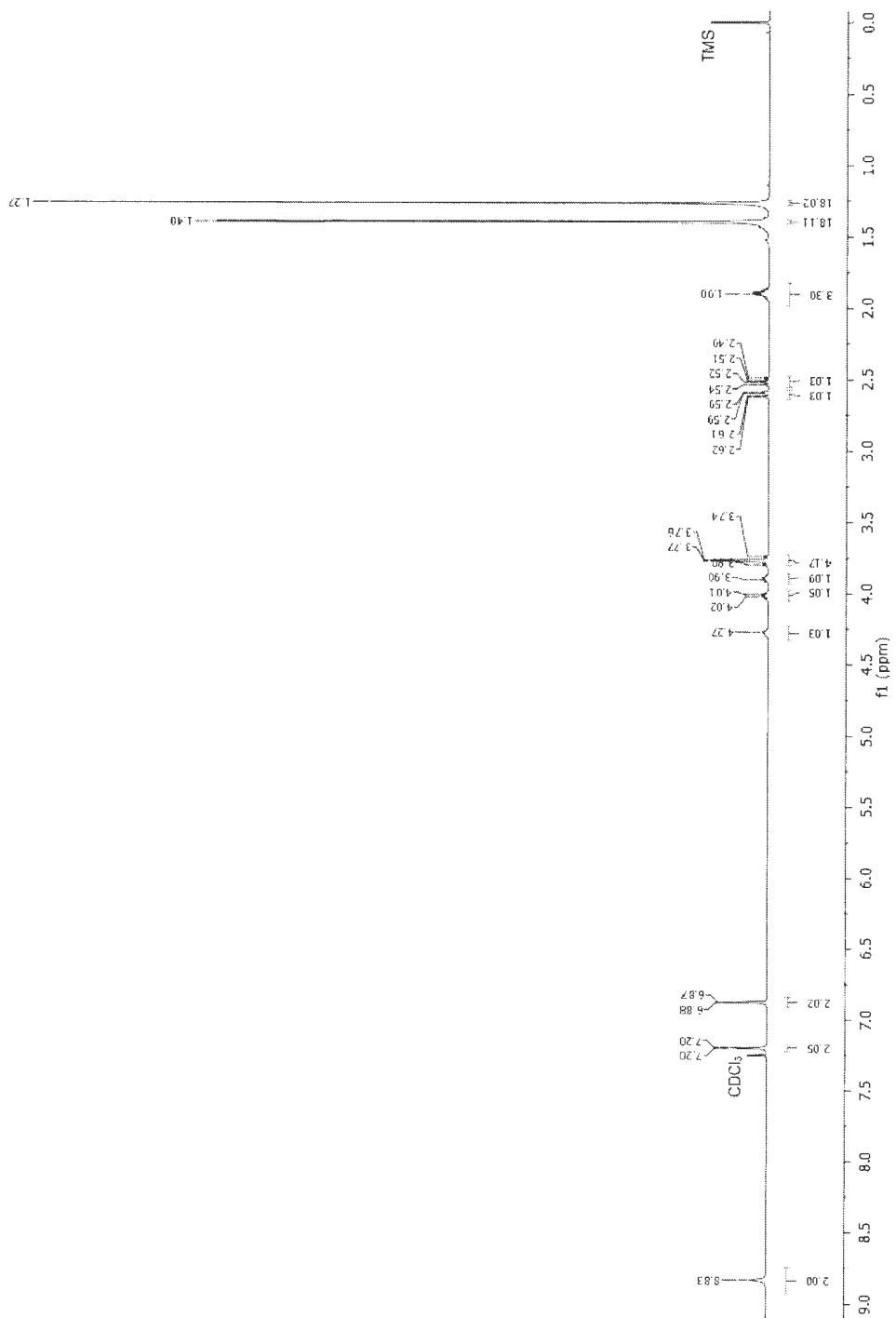


Figure A1.5. ¹H NMR spectrum of L3.

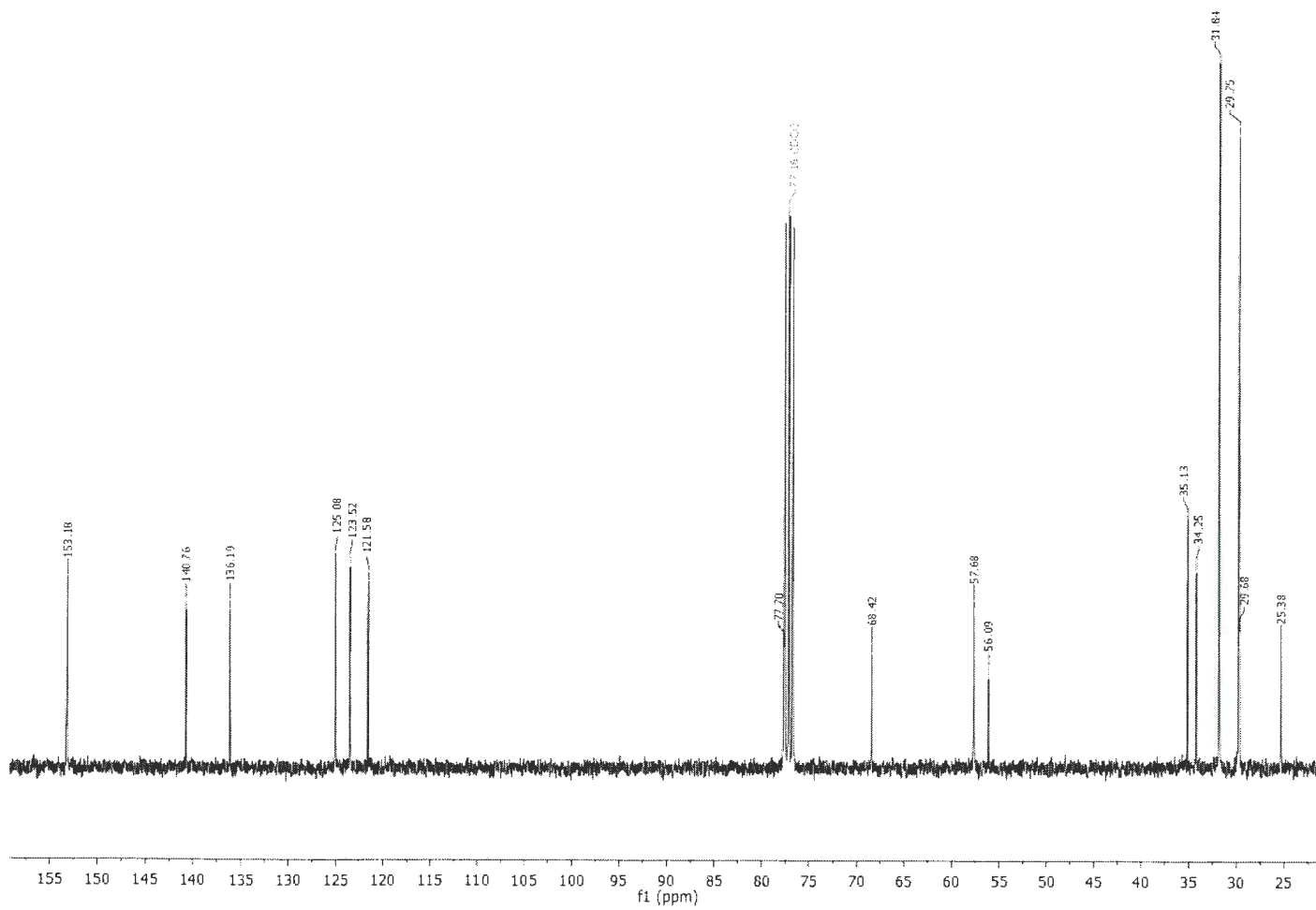


Figure A1.6. ^{13}C NMR spectrum of L3.

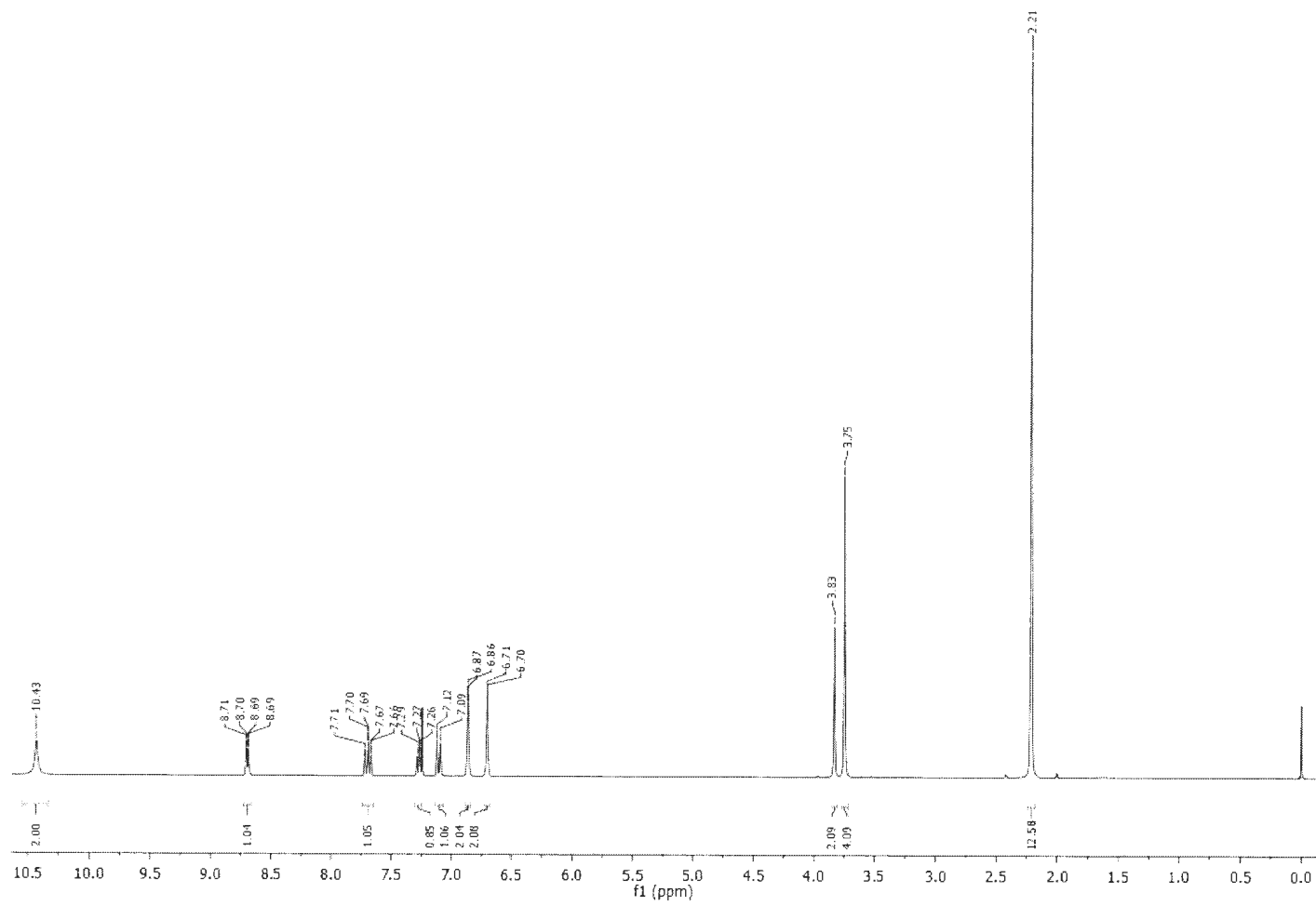


Figure A1.7. ¹H NMR spectrum of L4.

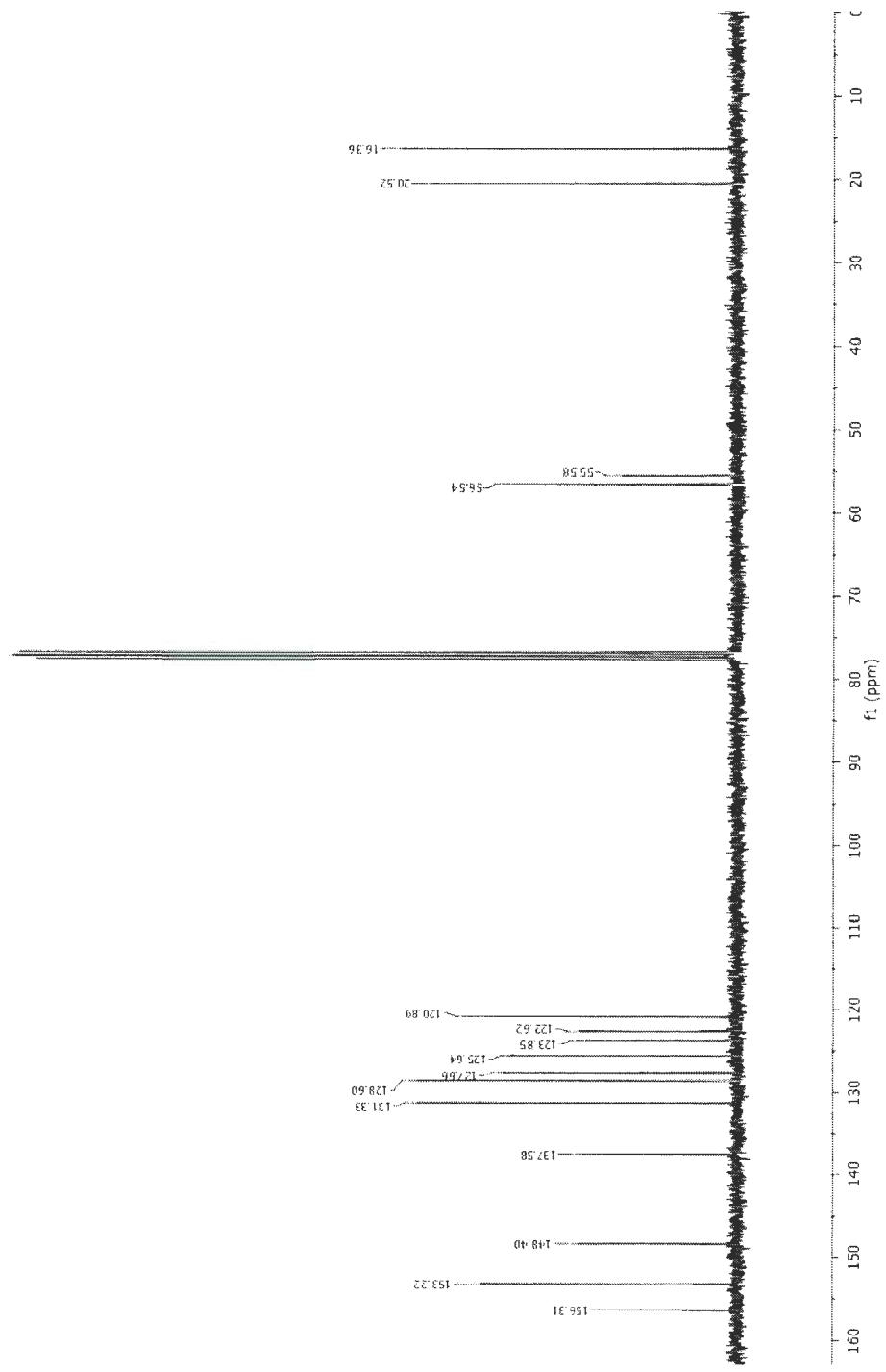


Figure A1.8. ¹³C NMR spectrum of L4.

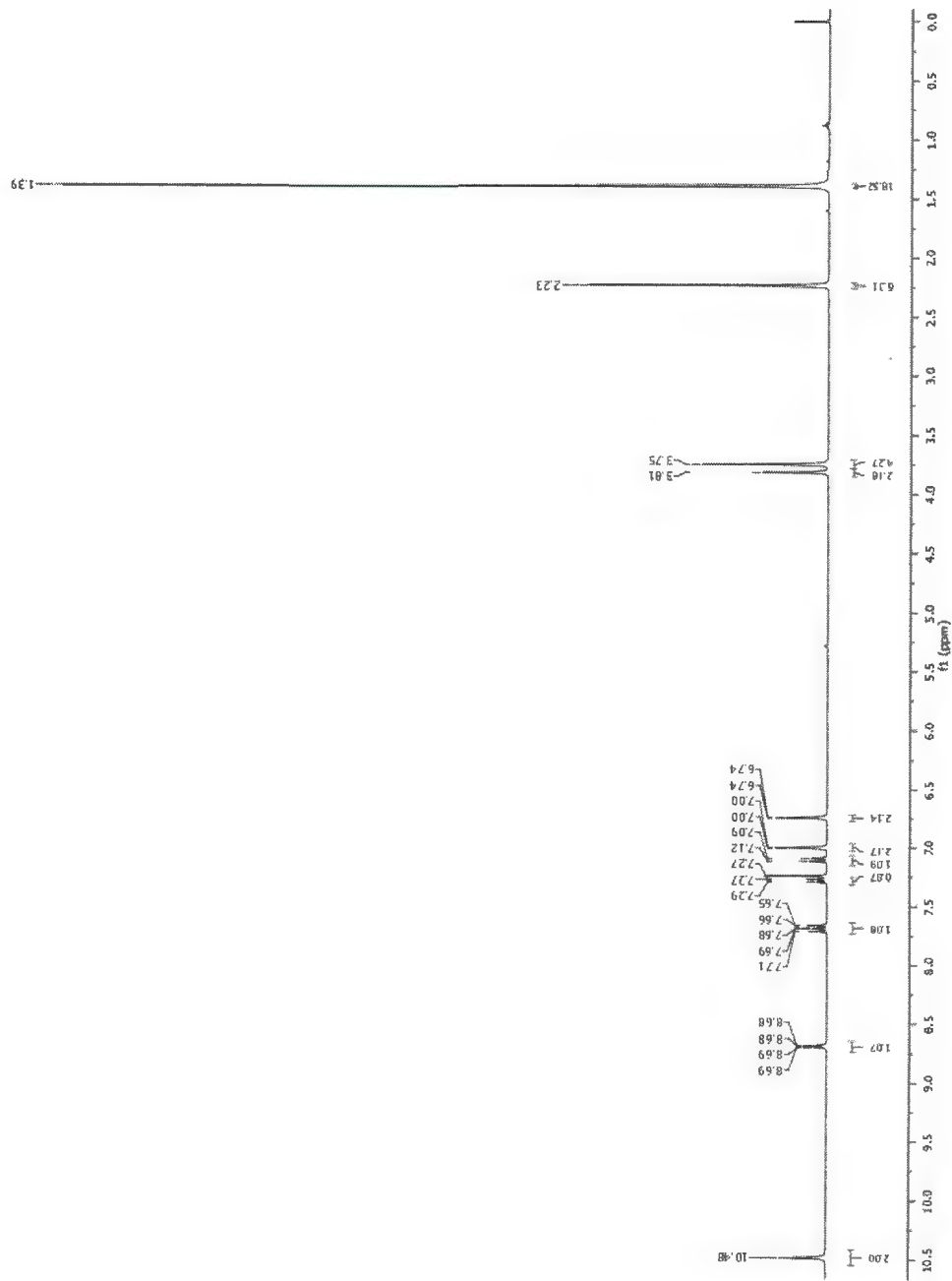


Figure A1.9. ¹H NMR spectrum of L5.

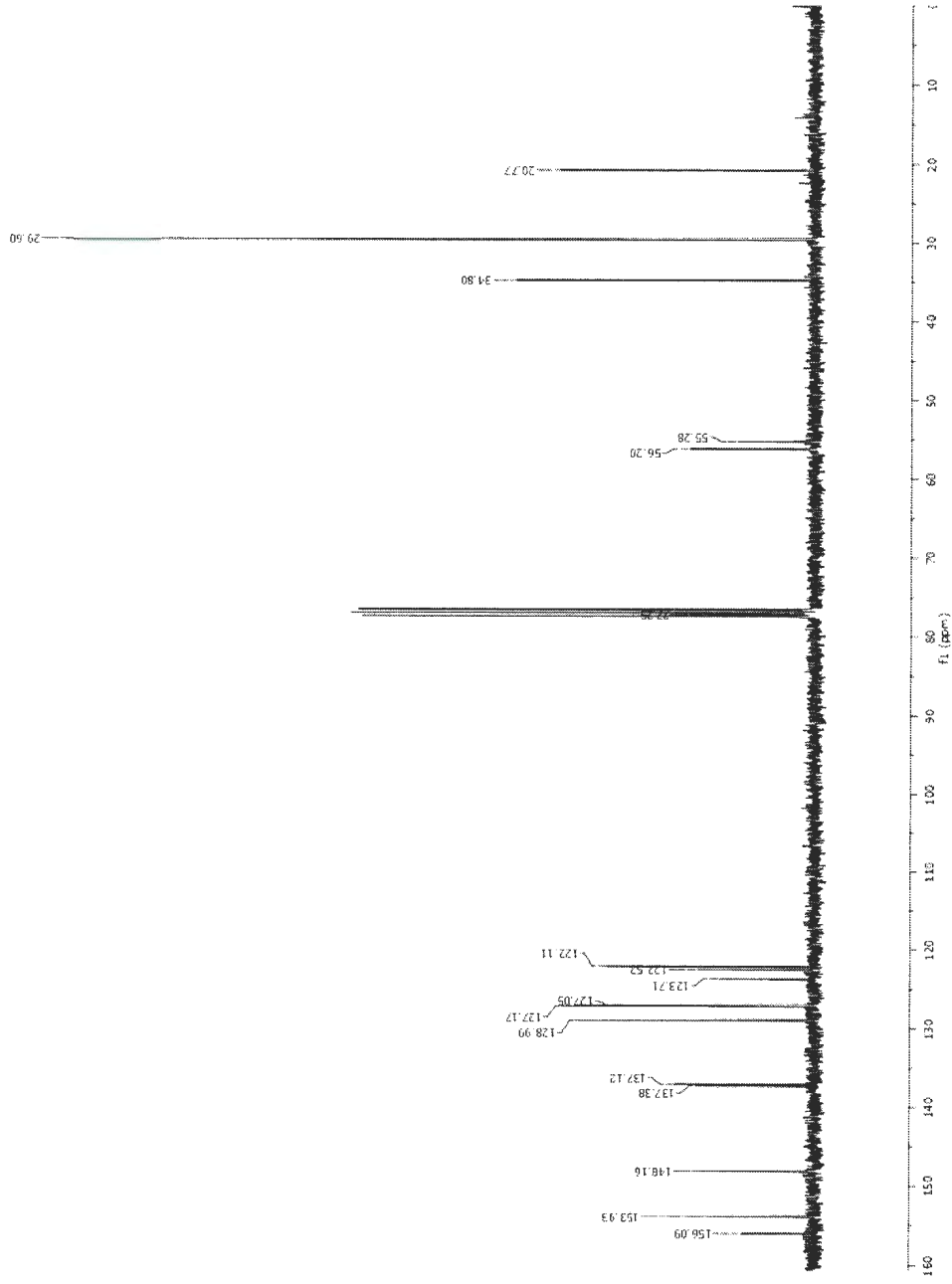


Figure A1.10. ¹³C NMR spectrum of L5.

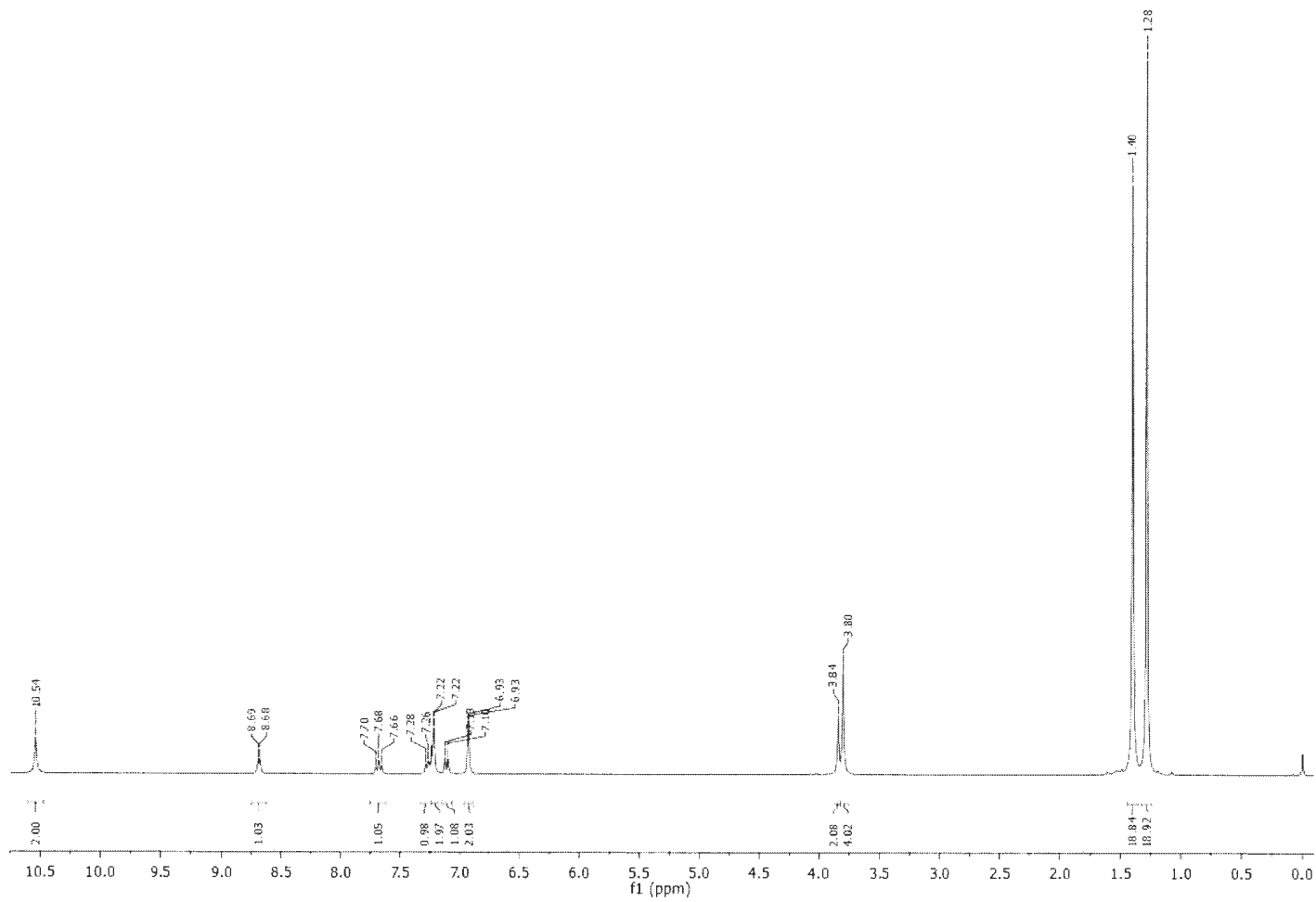


Figure A1.11. ¹H NMR spectrum of L6.

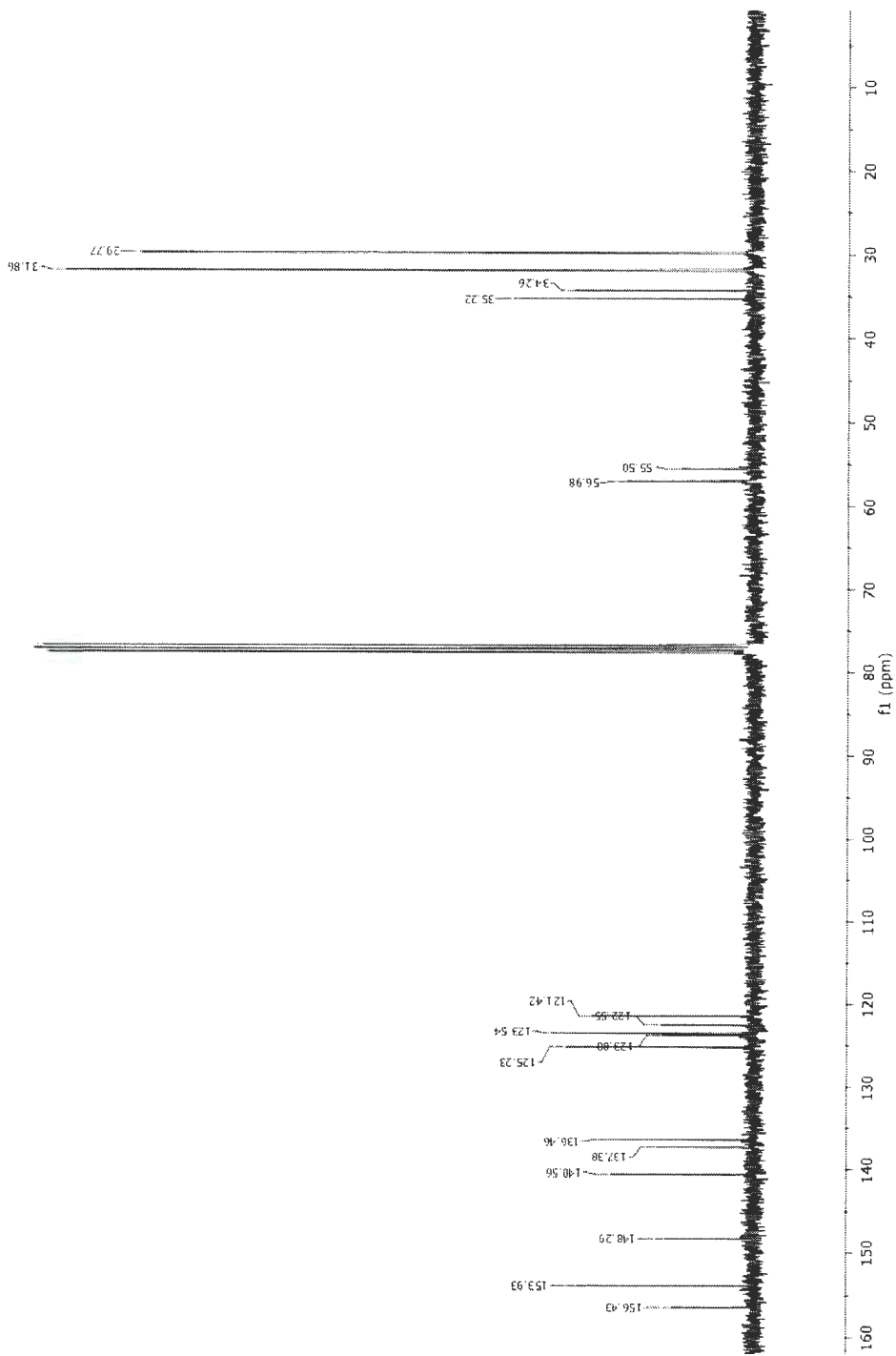


Figure A1.12. ¹³C NMR spectrum of L6.

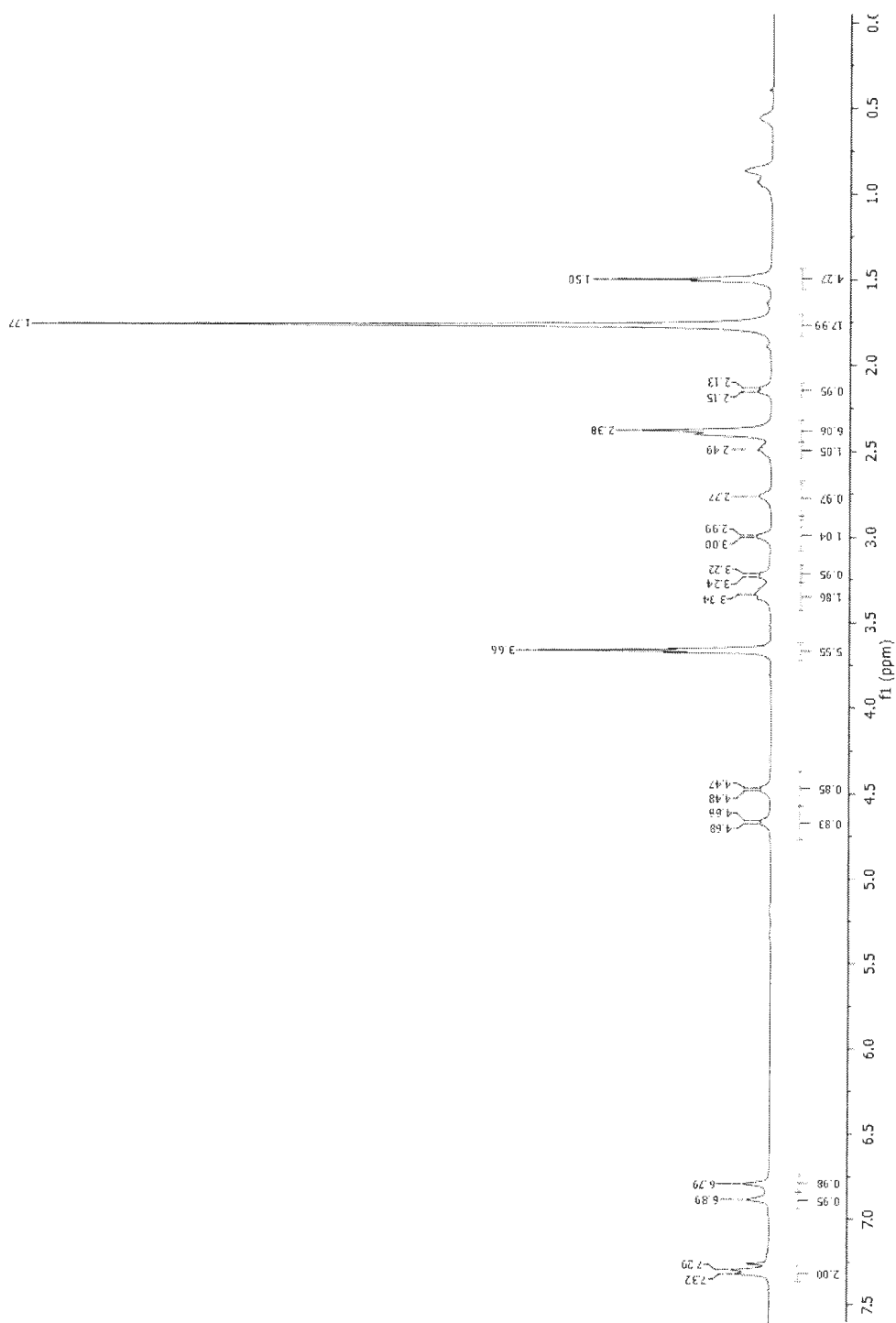


Figure A1.13. ¹H NMR spectrum of **2.1** in CDCl₃.

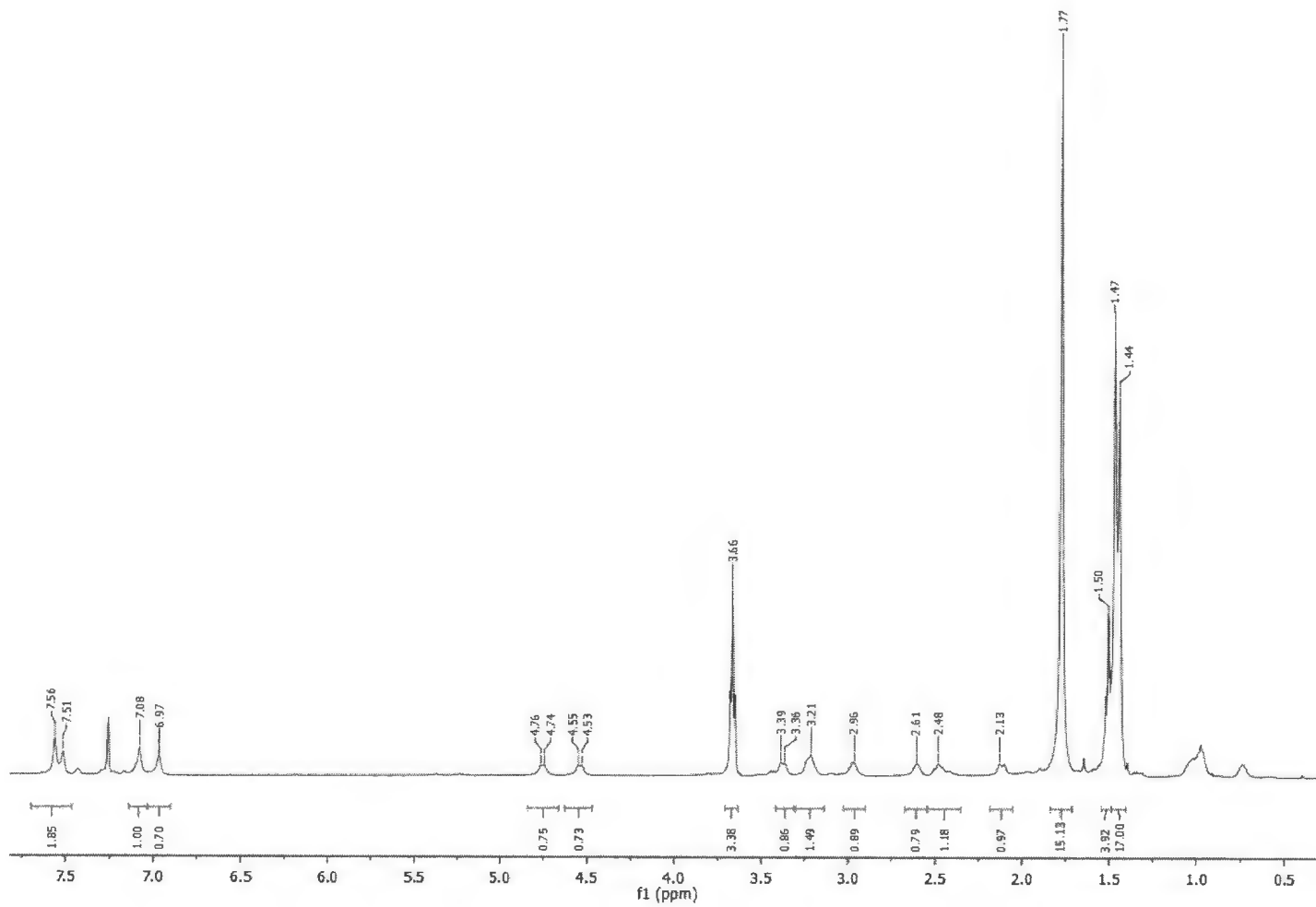


Figure A1.14. ^1H NMR spectrum of **2.2** in CDCl_3 .

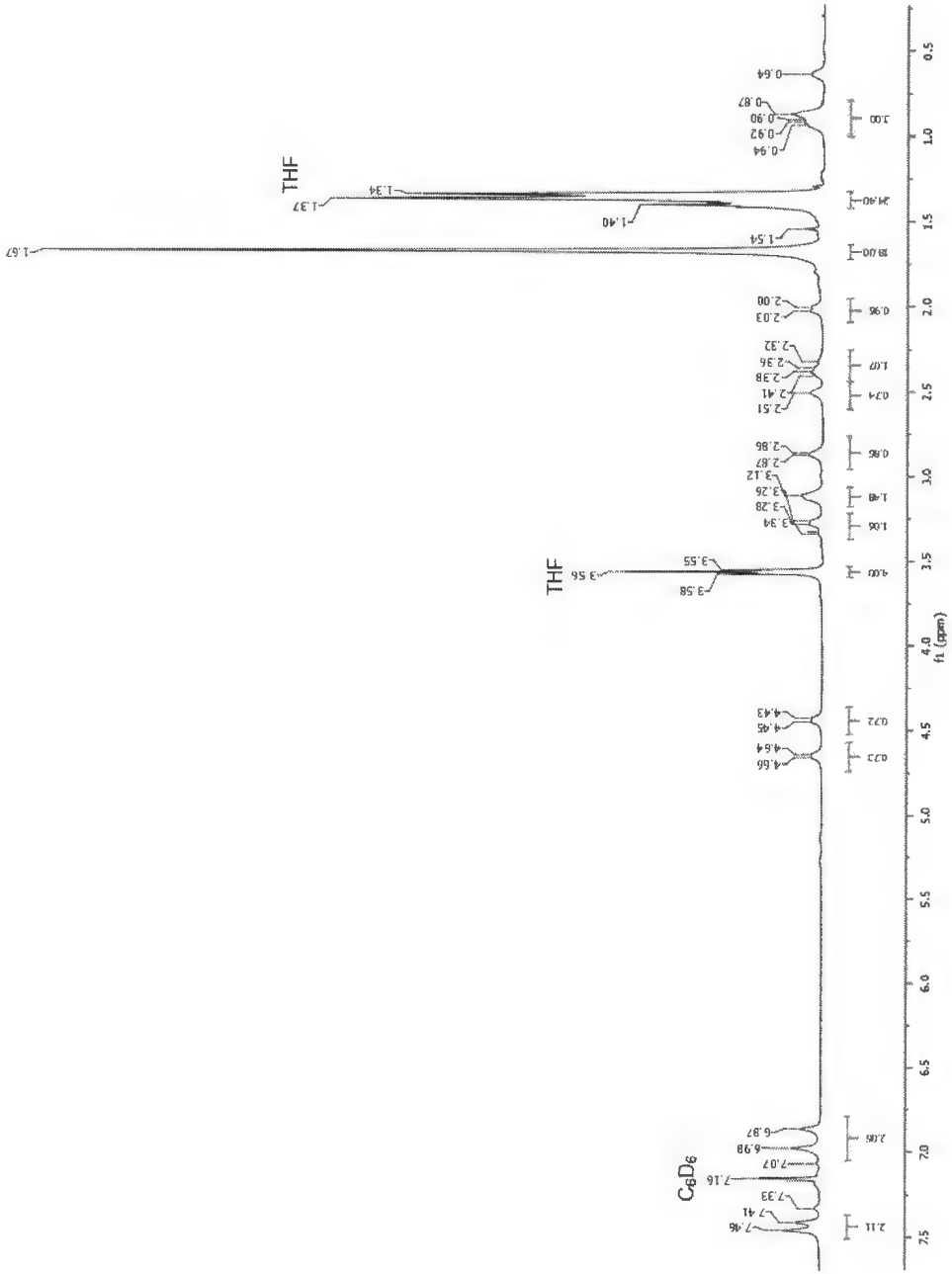


Figure A1.15. ¹H NMR spectrum of 2.2 in C₆D₆.

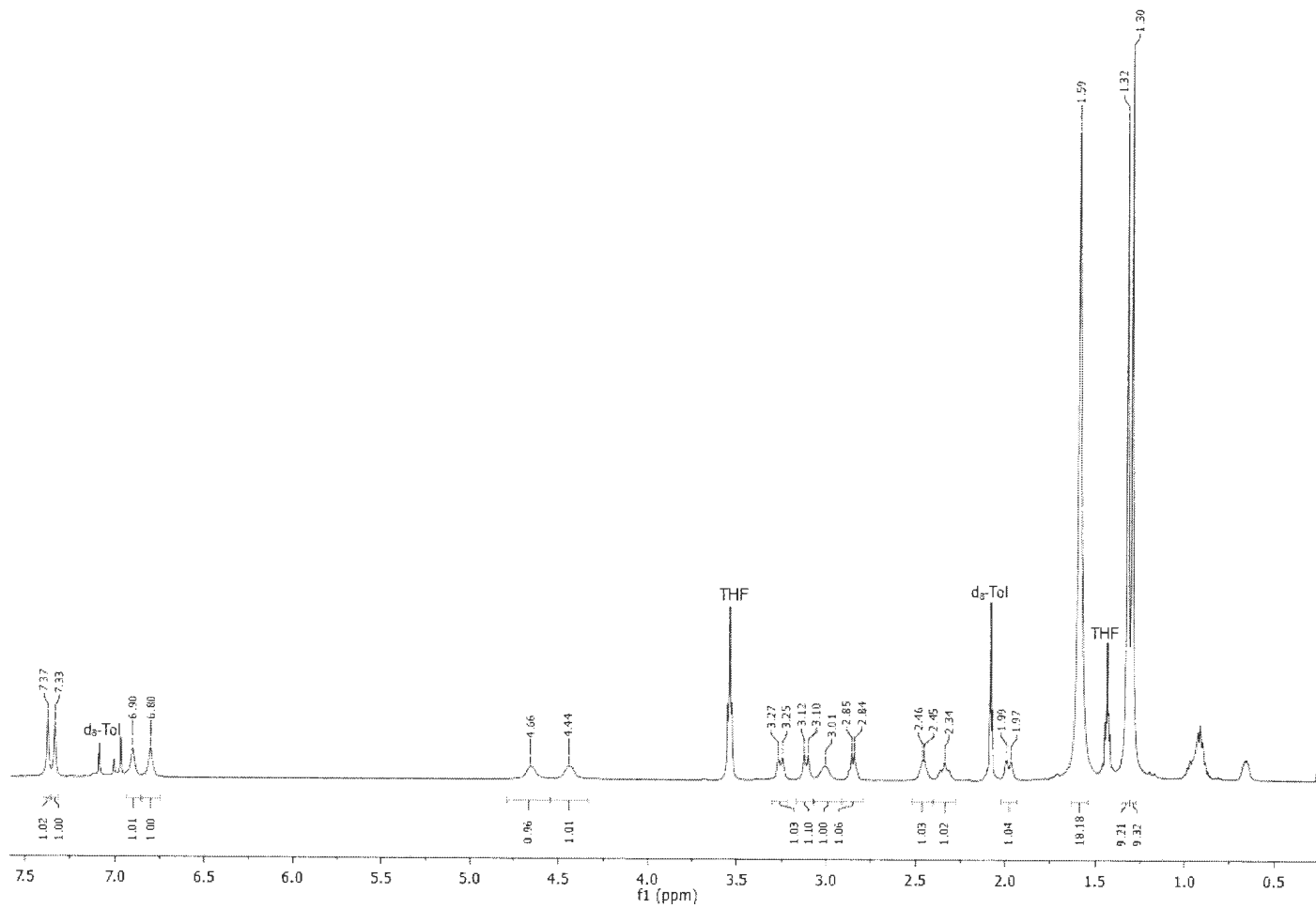


Figure A1.16. ^1H NMR spectrum of 2.2 in D_8 -toluene.

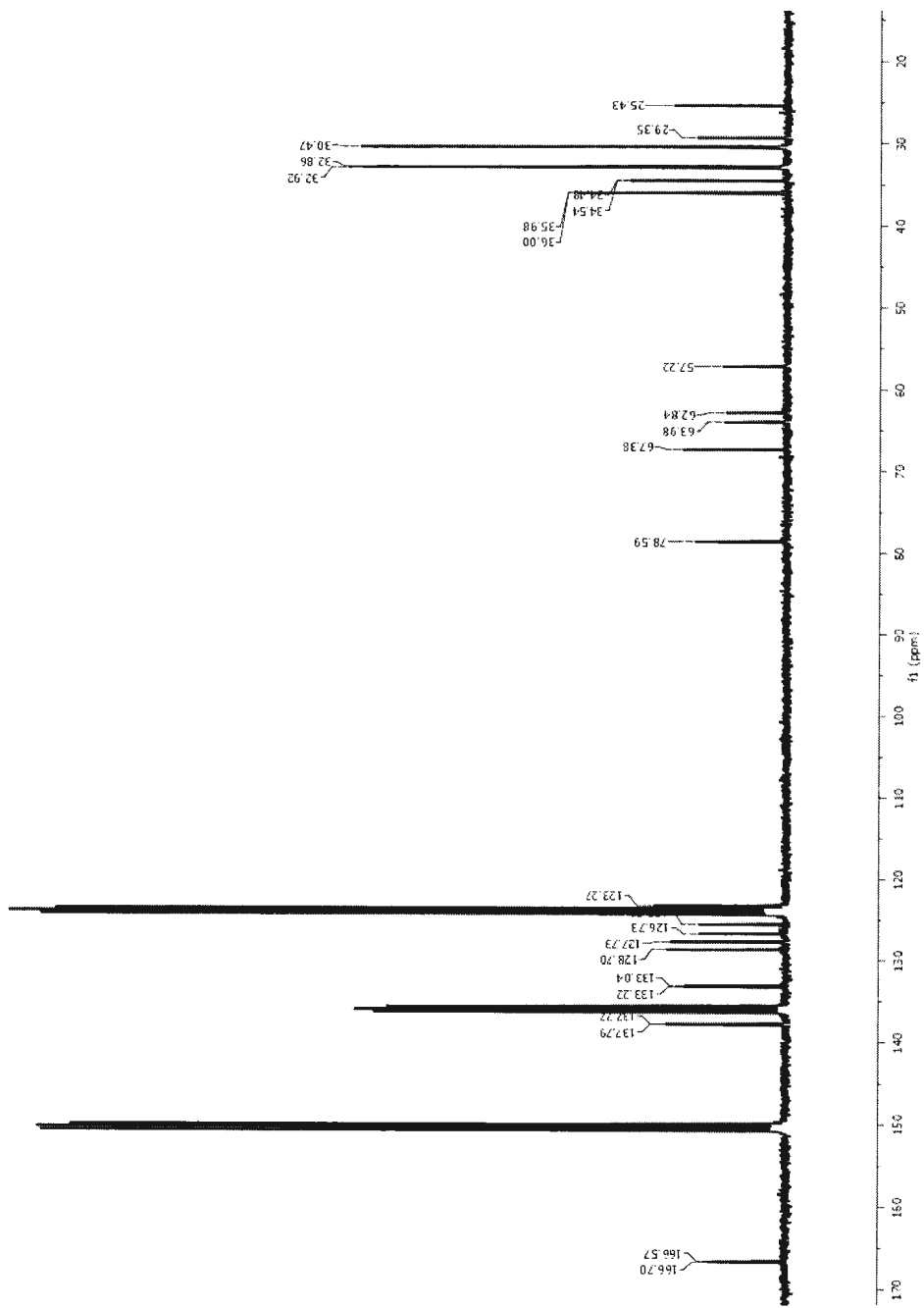


Figure A1.18. ¹³C NMR spectrum of 2.2 in D₅-pyridine.

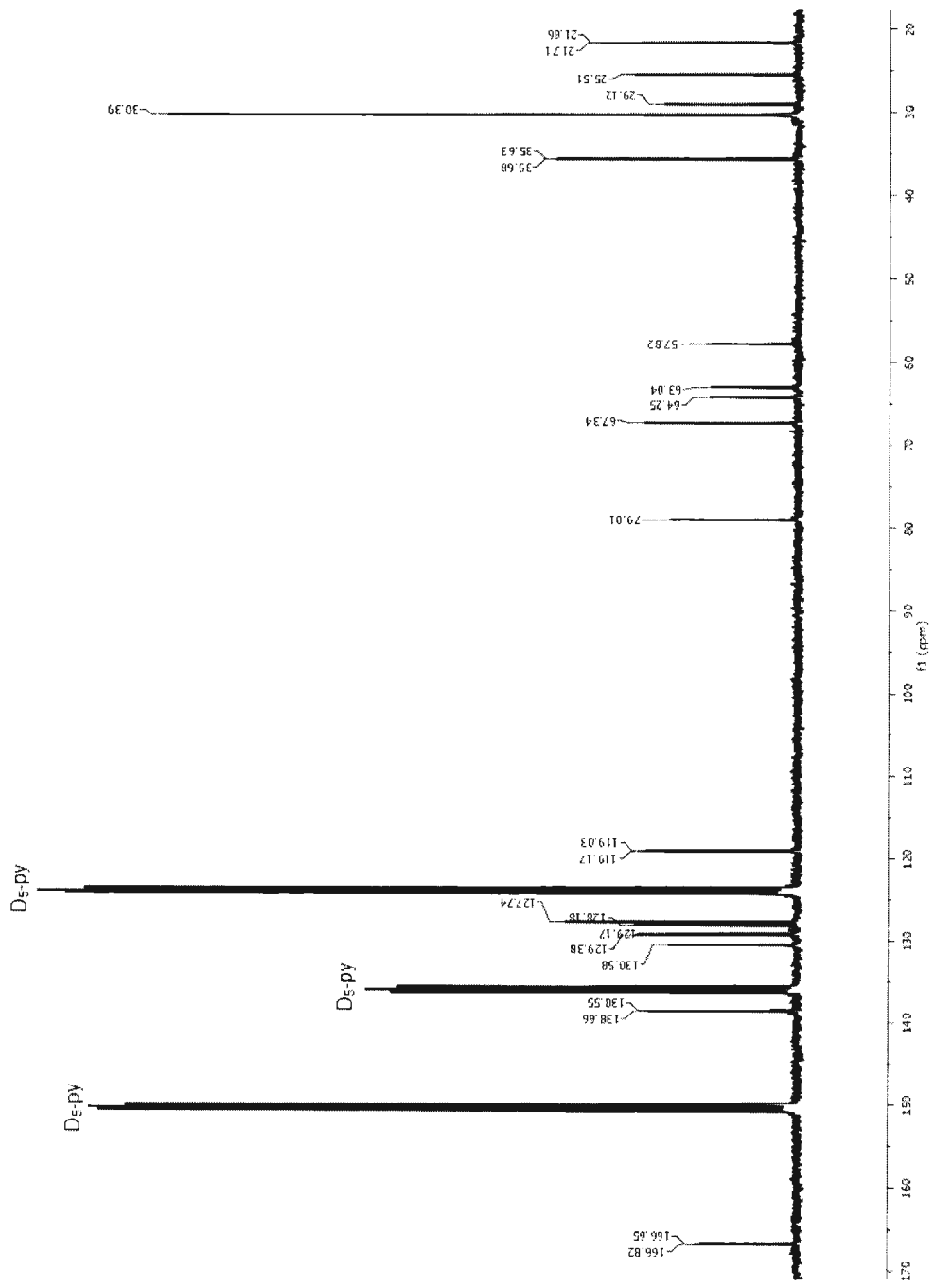


Figure A1.19. ^{13}C NMR spectrum of 2.1 in D_5 -pyridine.

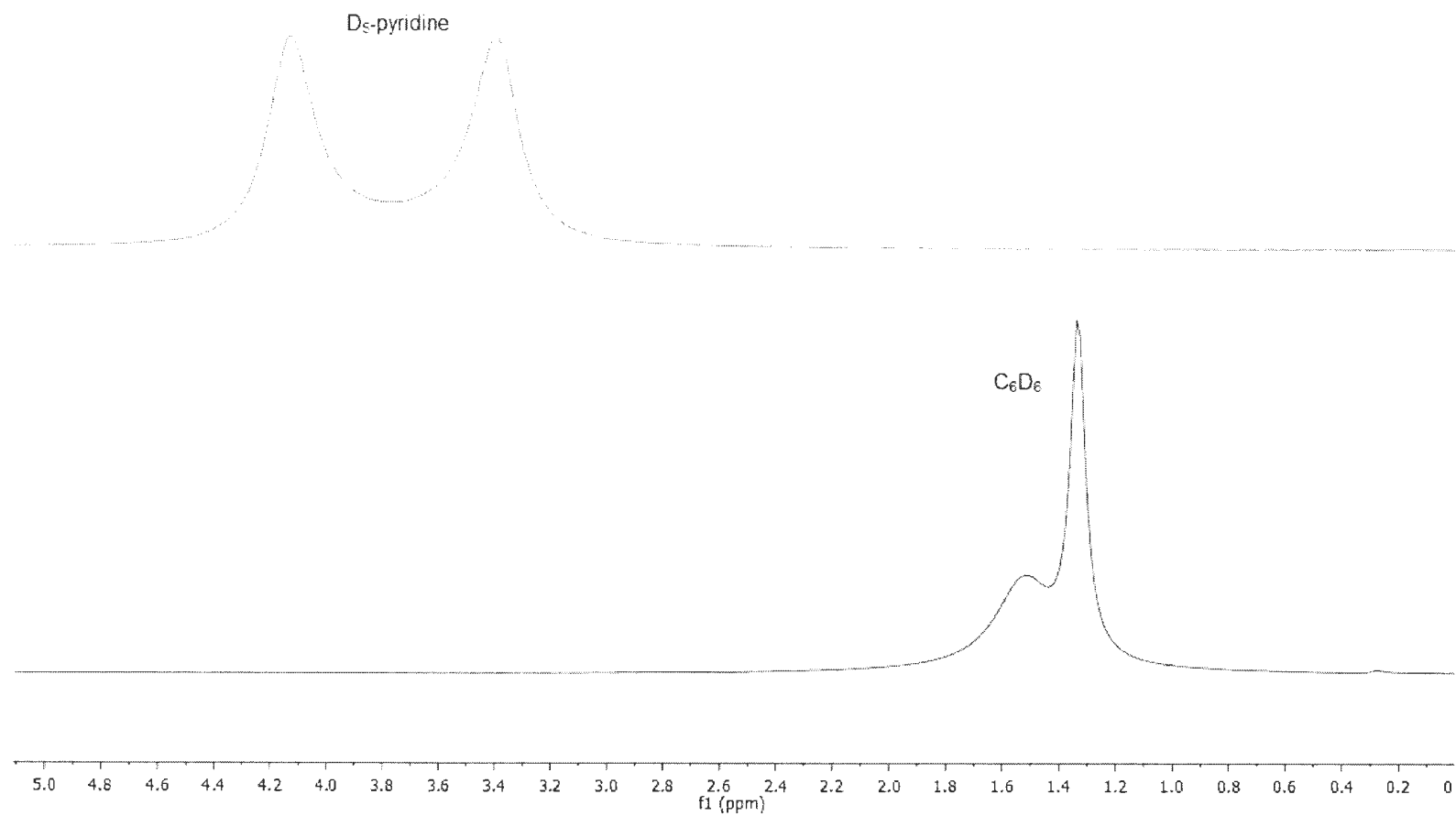


Figure A1.20. ^7Li NMR spectra at 7.04 T for complex **2.1** in $\text{D}_5\text{-pyridine}$ (top) and C_6D_6 (bottom).

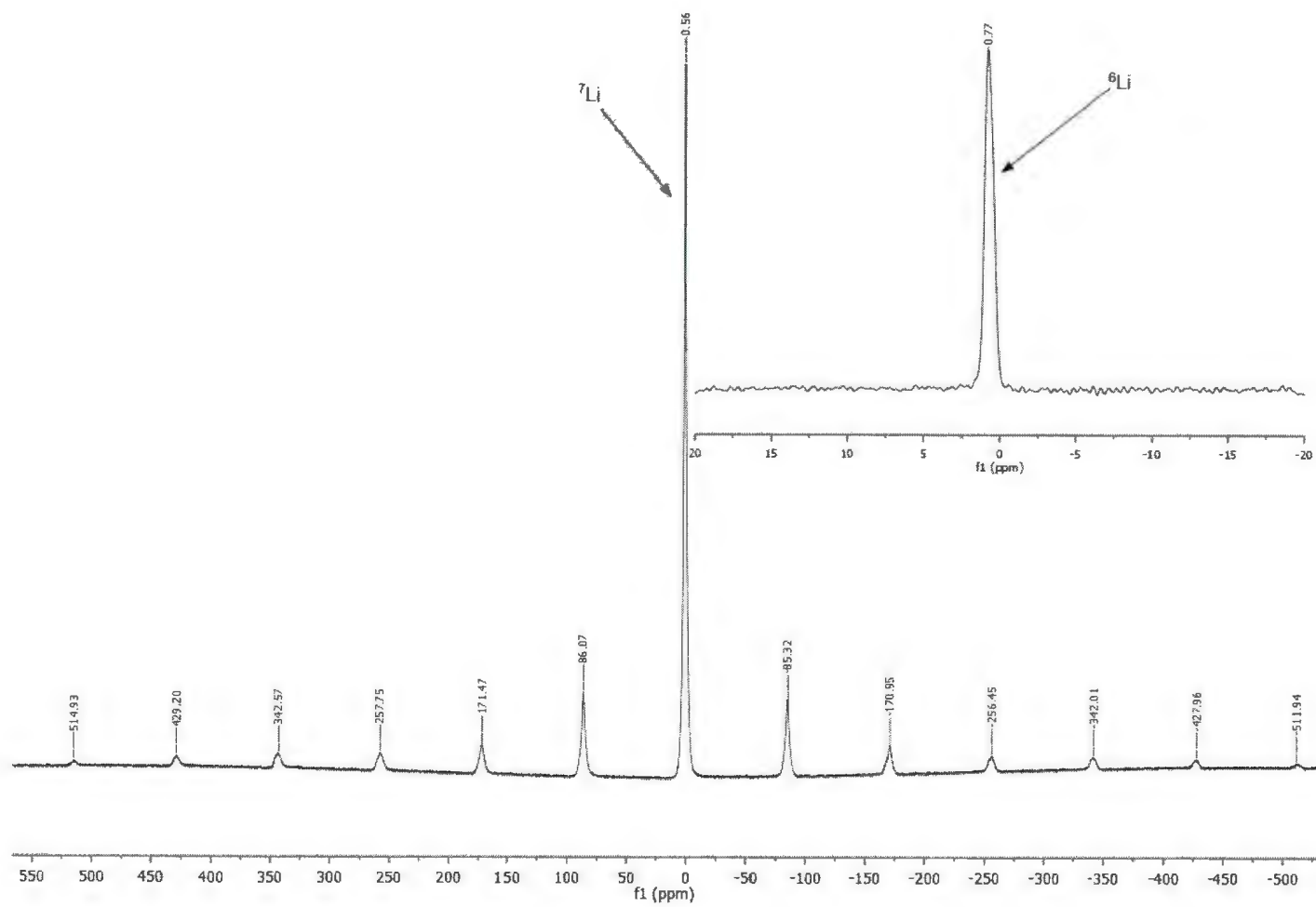


Figure A1.21. ^7Li MAS (20 kHz) and ^6Li MAS (15 kHz) spectra of complex **2.1** at 14 T.

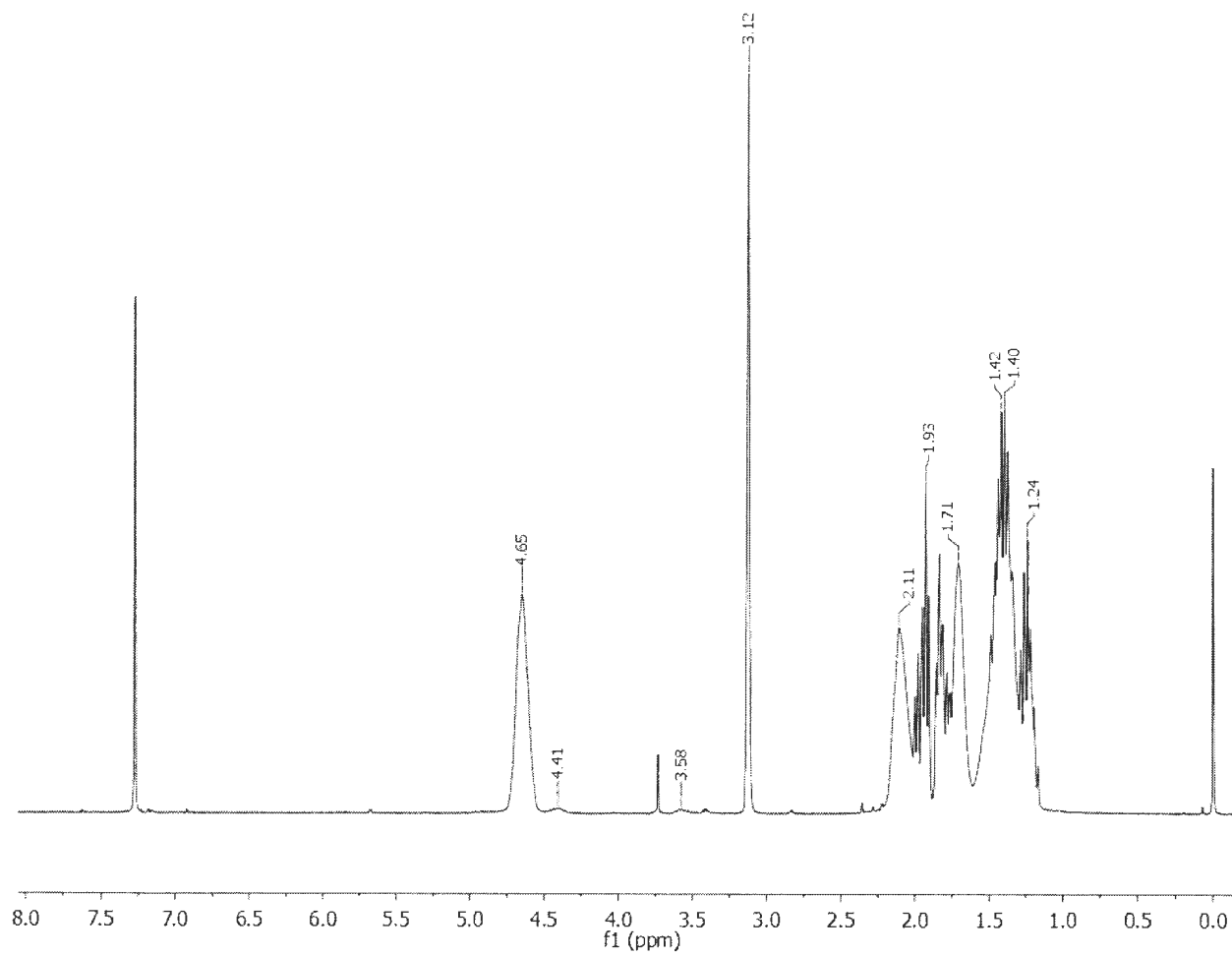


Figure A1.22. ^1H NMR spectrum from aliquot sample of PCHC in CDCl_3 (Table 5.5, entry 1).

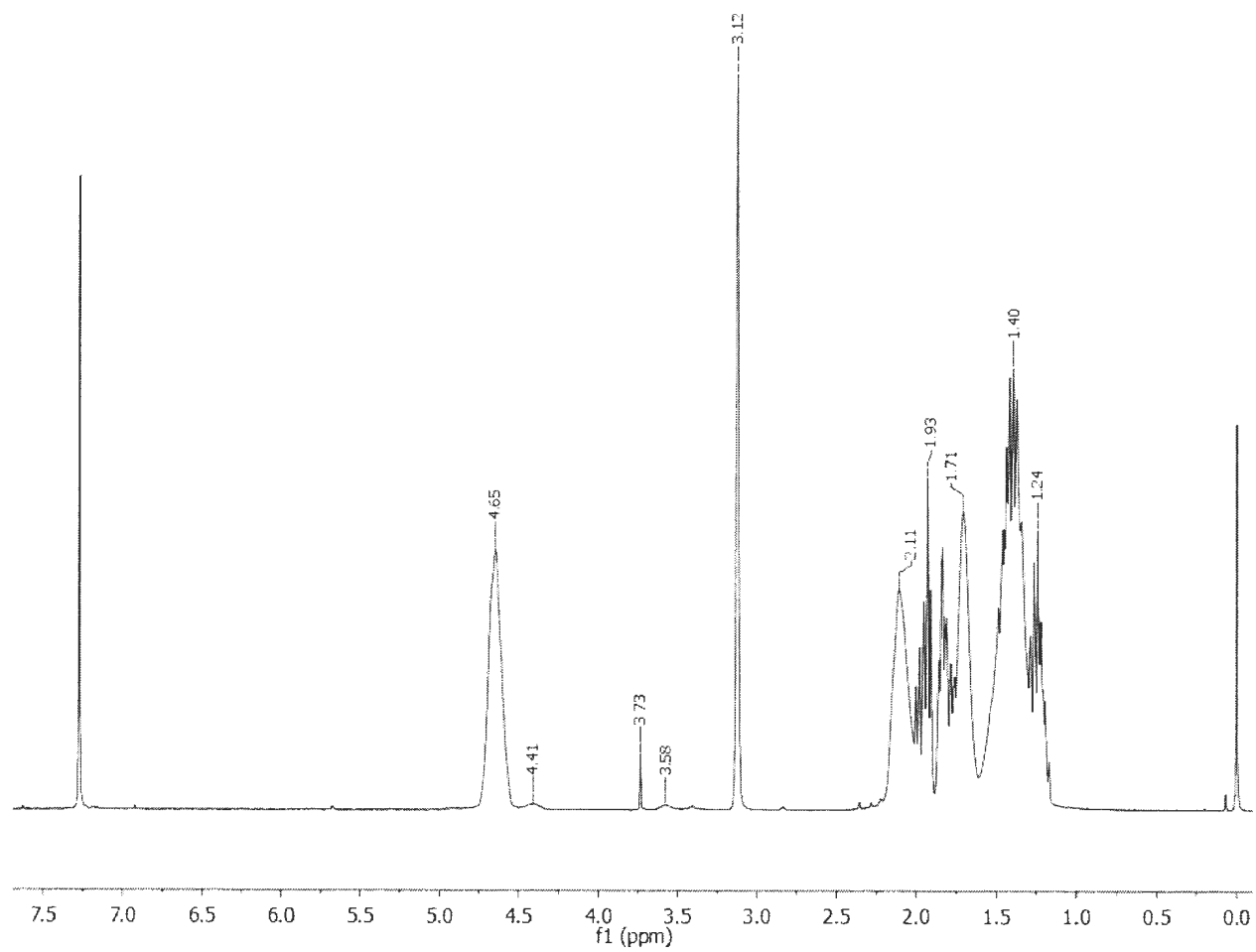


Figure A1.23. ^1H NMR spectrum from aliquot sample of PCHC in CDCl_3 (Table 5.5, entry 2).

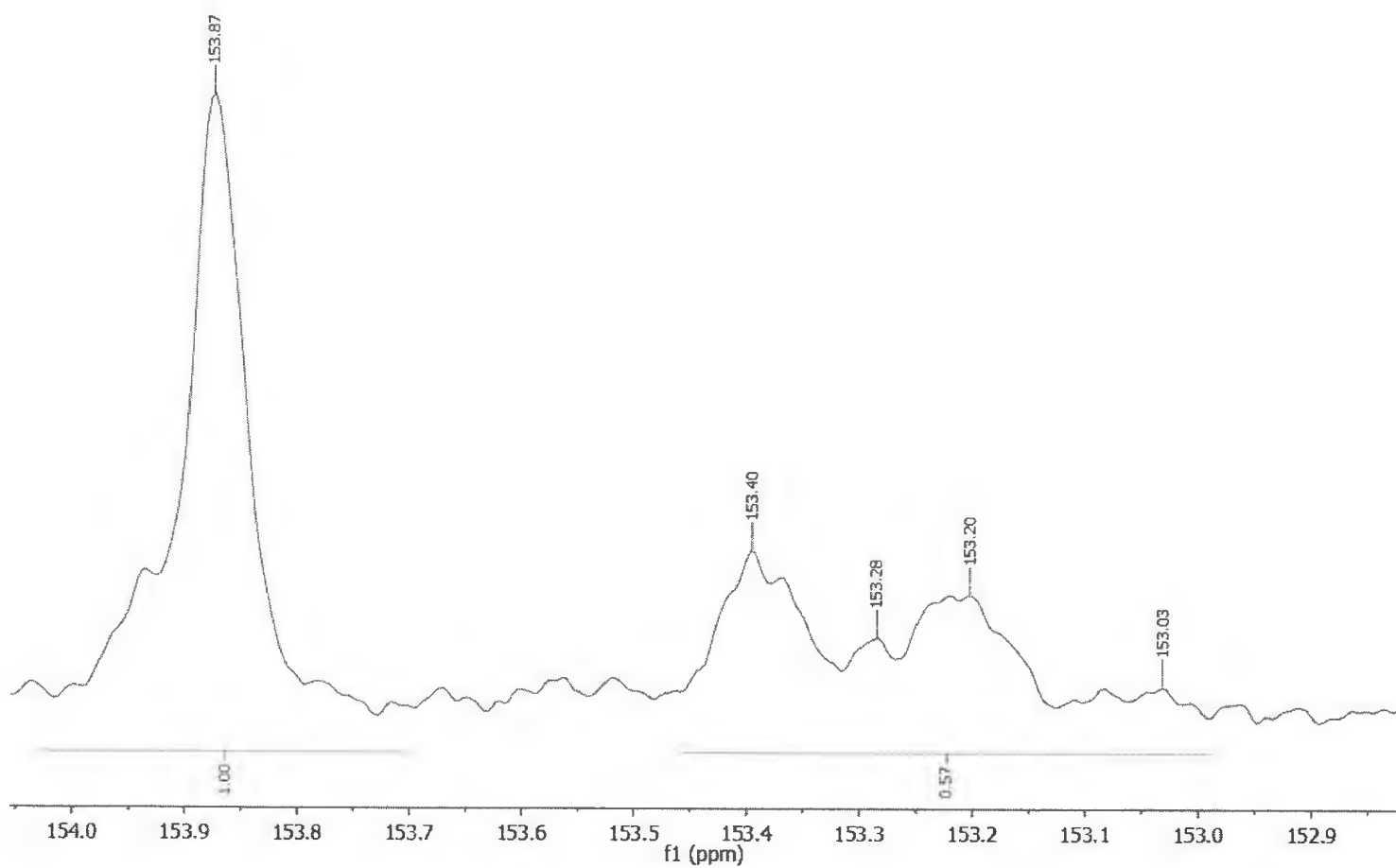


Figure A1.24. Carbonyl region of the ^{13}C NMR spectrum (75.5 MHz, CDCl_3) of CHO/CO₂ copolymer prepared with PPNCI (Table 5.3, entry 6).

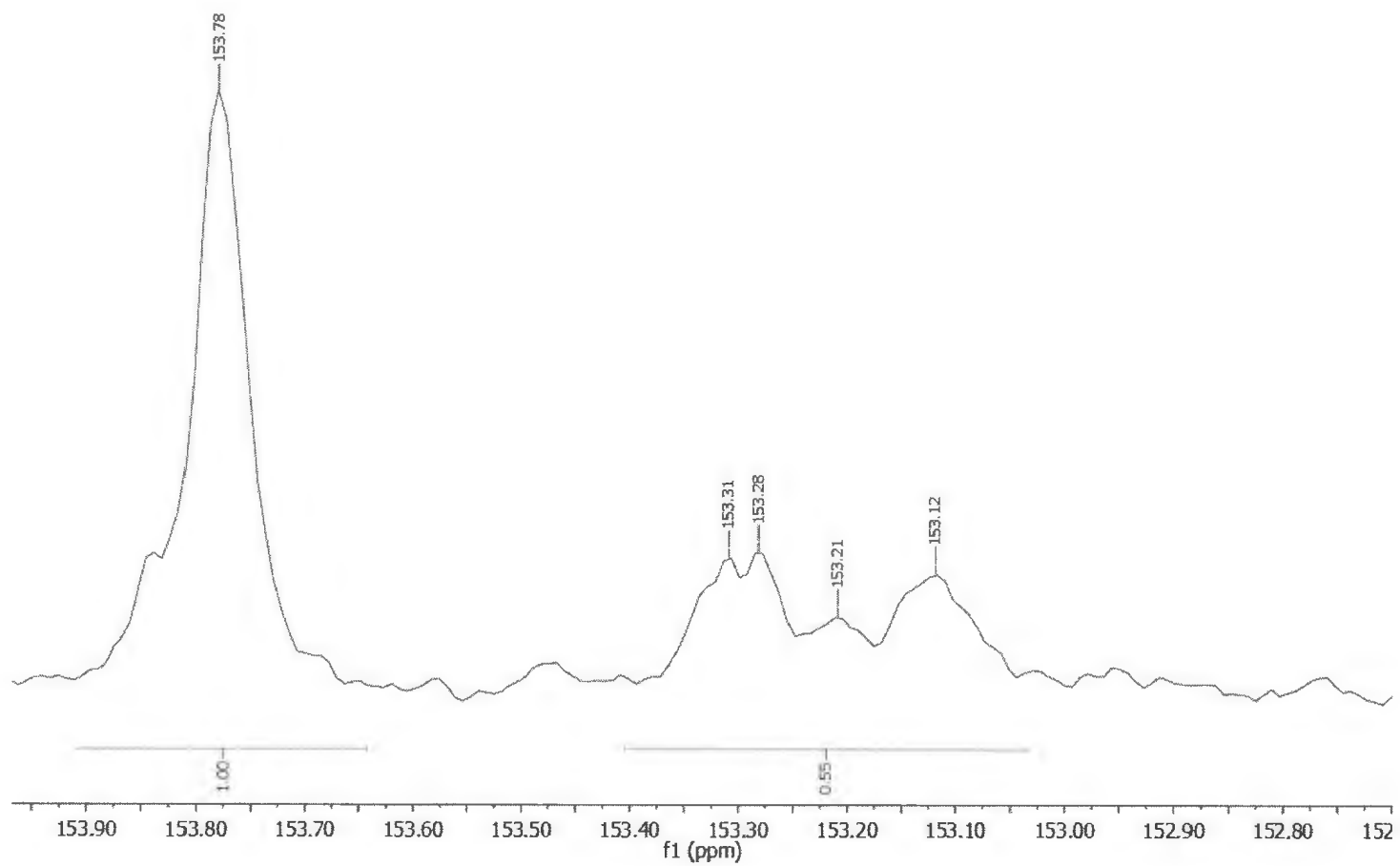


Figure A1.25. Carbonyl region of the ^{13}C NMR spectrum (75.5 MHz, CDCl_3) of CHO/CO₂ copolymer prepared with PPNN₃ (Table 5.3, entry 12).

Appendix B: MALDI-TOF MS

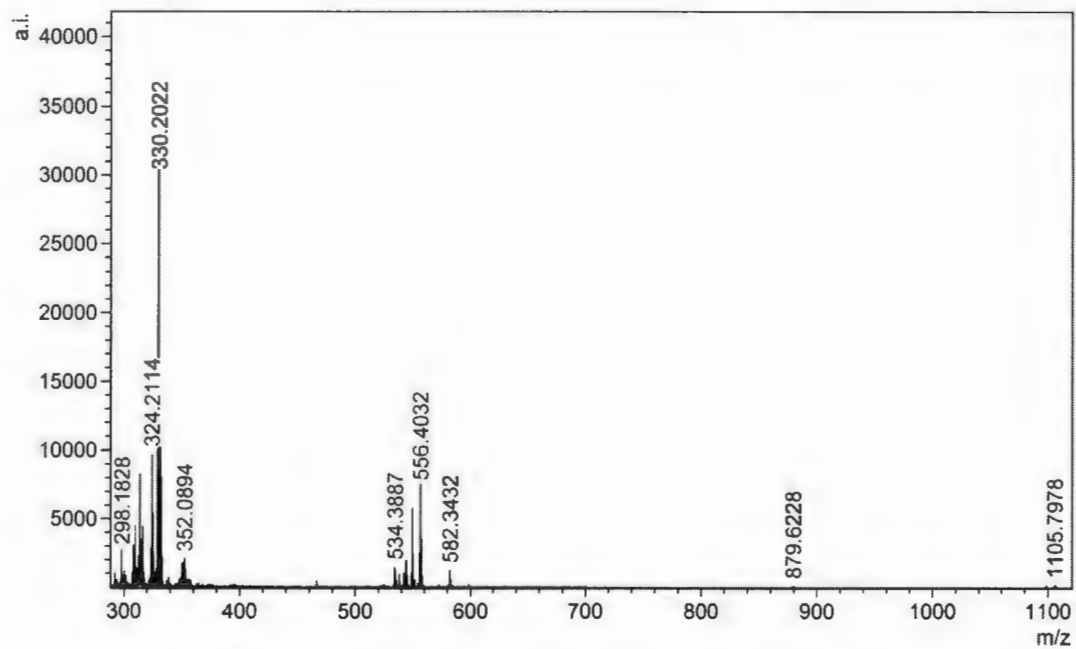


Figure B1.1. MALDI-TOF mass spectrum of $\{\text{Li}_2[\text{O}_2\text{NO}]^{\text{BuBu}}\}_2$ (2.2).

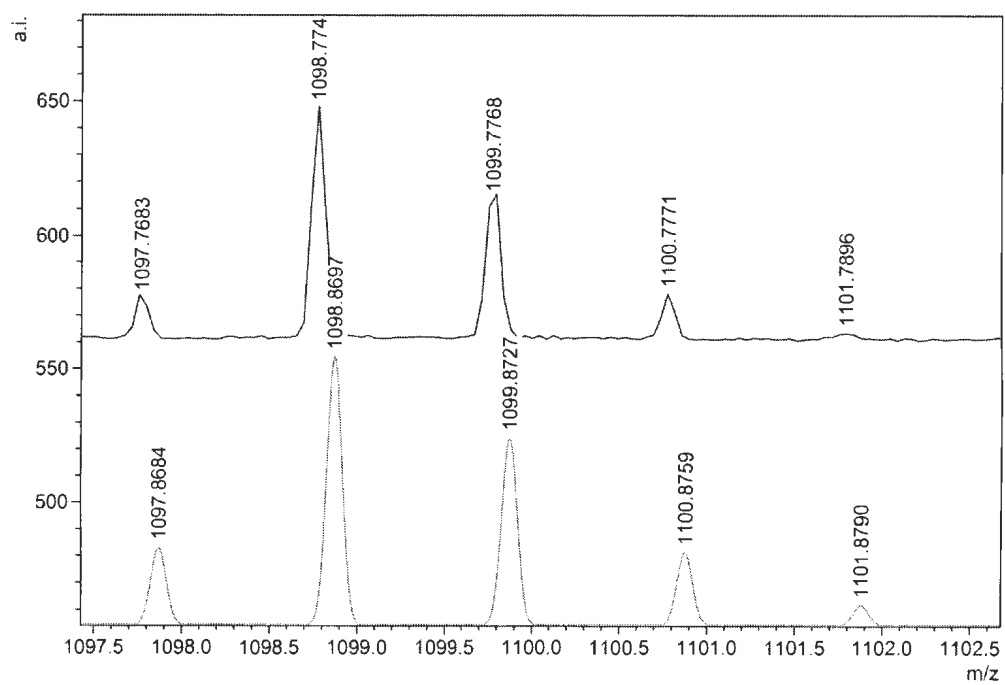
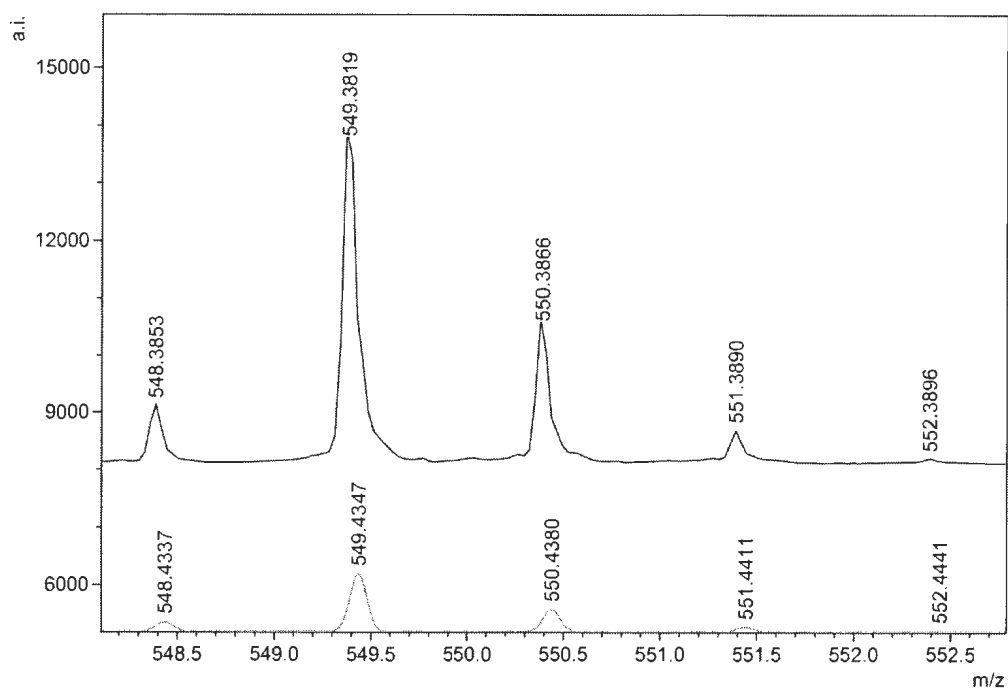


Figure B1.2. Experimental and theoretical MALDI-TOF MS isotopic distribution pattern for **2.2** (top = monomer, bottom = dimer).

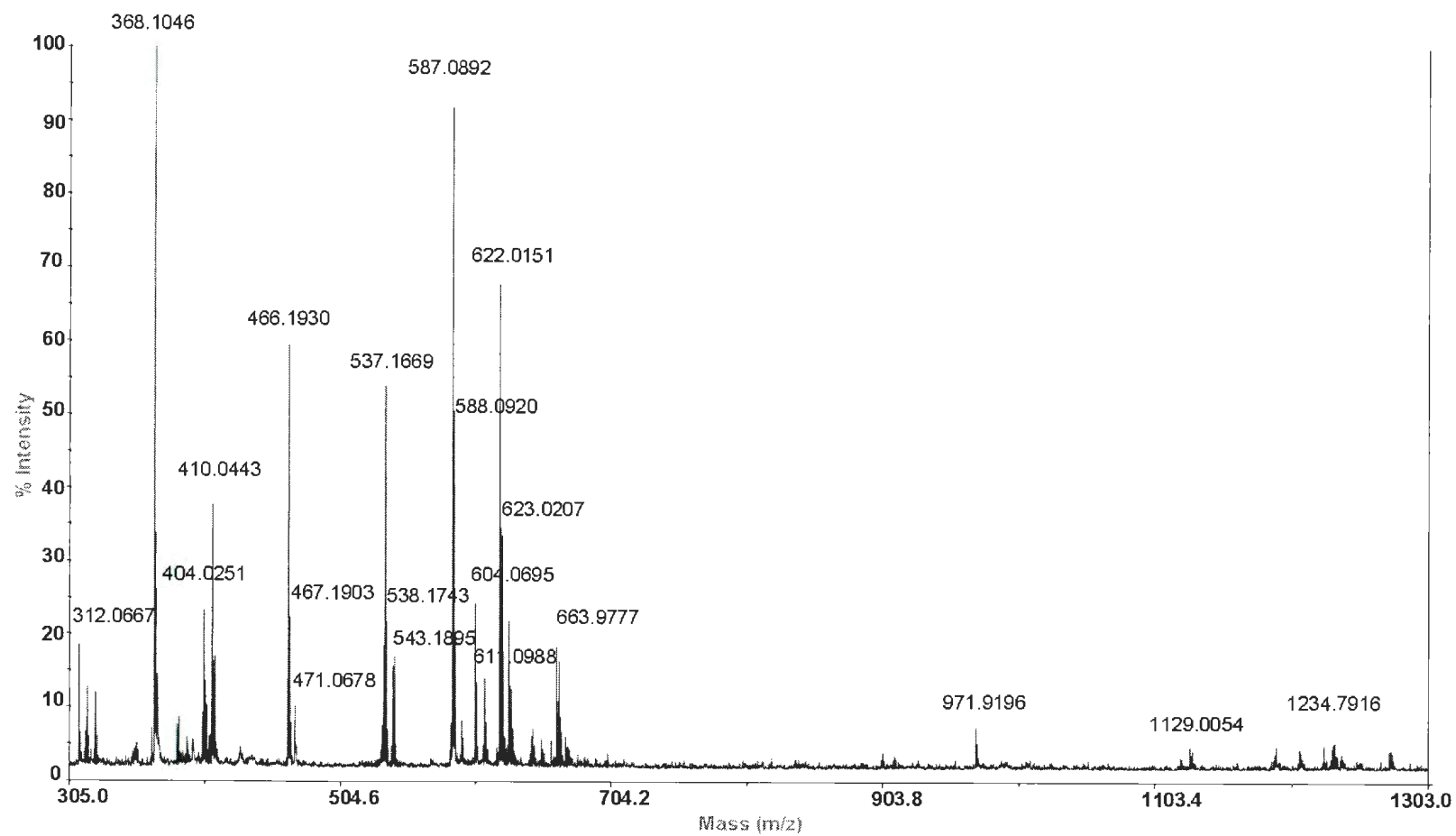


Figure B1.3. MALDI-TOF mass spectrum of $\text{CrCl}(\text{THF})[\text{O}_2\text{NO}]^{\text{BuBu}}$ (4.2).

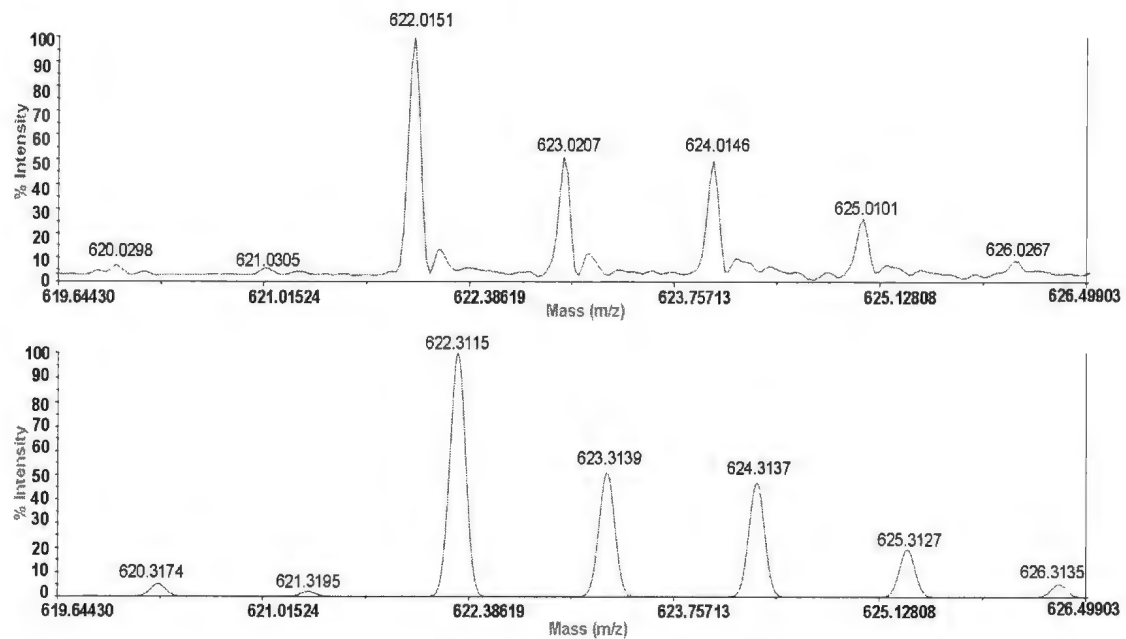


Figure B1.4. Experimental and theoretical MALDI-TOF MS isotopic distribution pattern for 4.2.

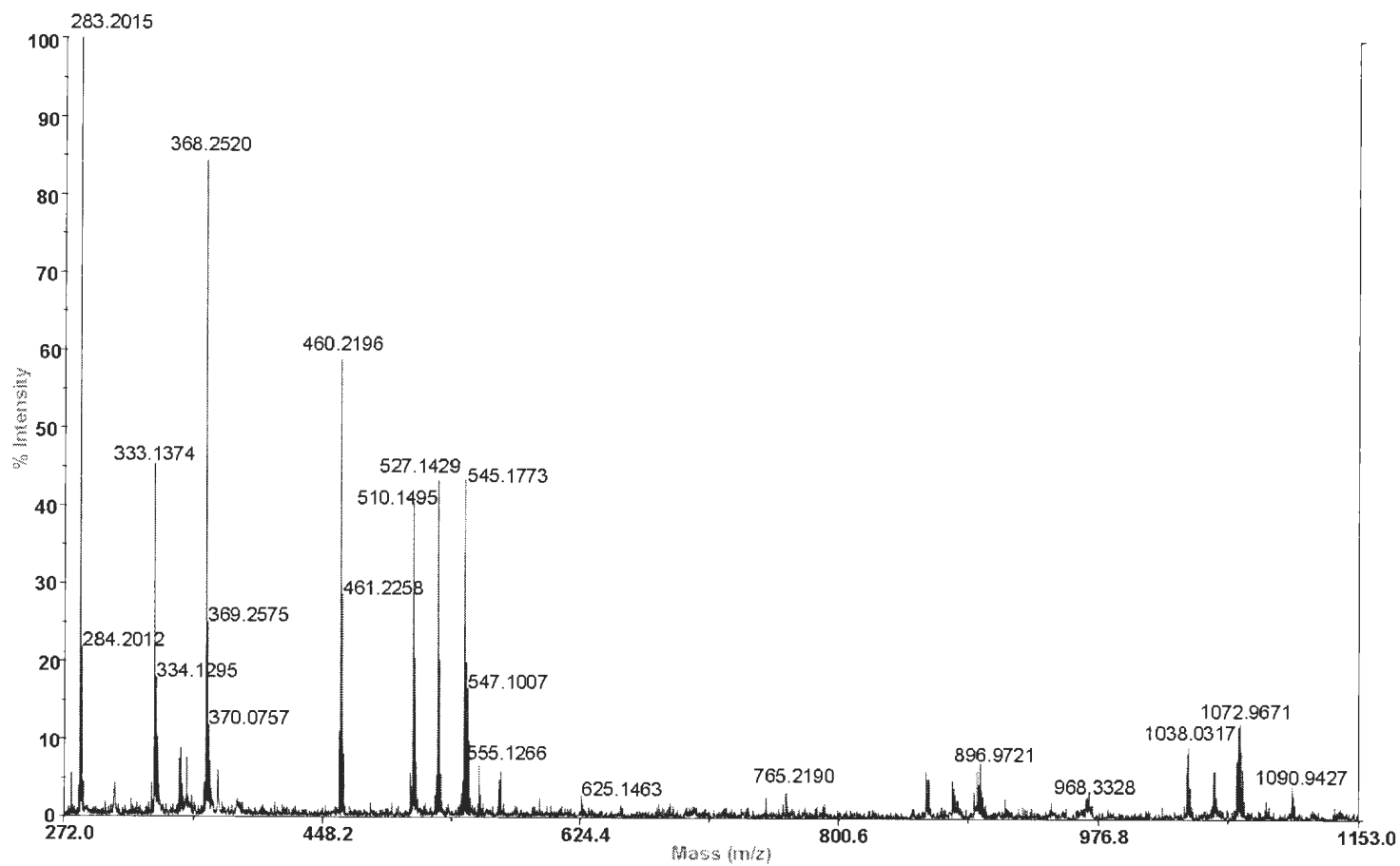


Figure B1.5. MALDI-TOF mass spectrum of $\text{CrCl}[\text{O}_2\text{NN}]^{\text{BuMc}}$ (4.3).

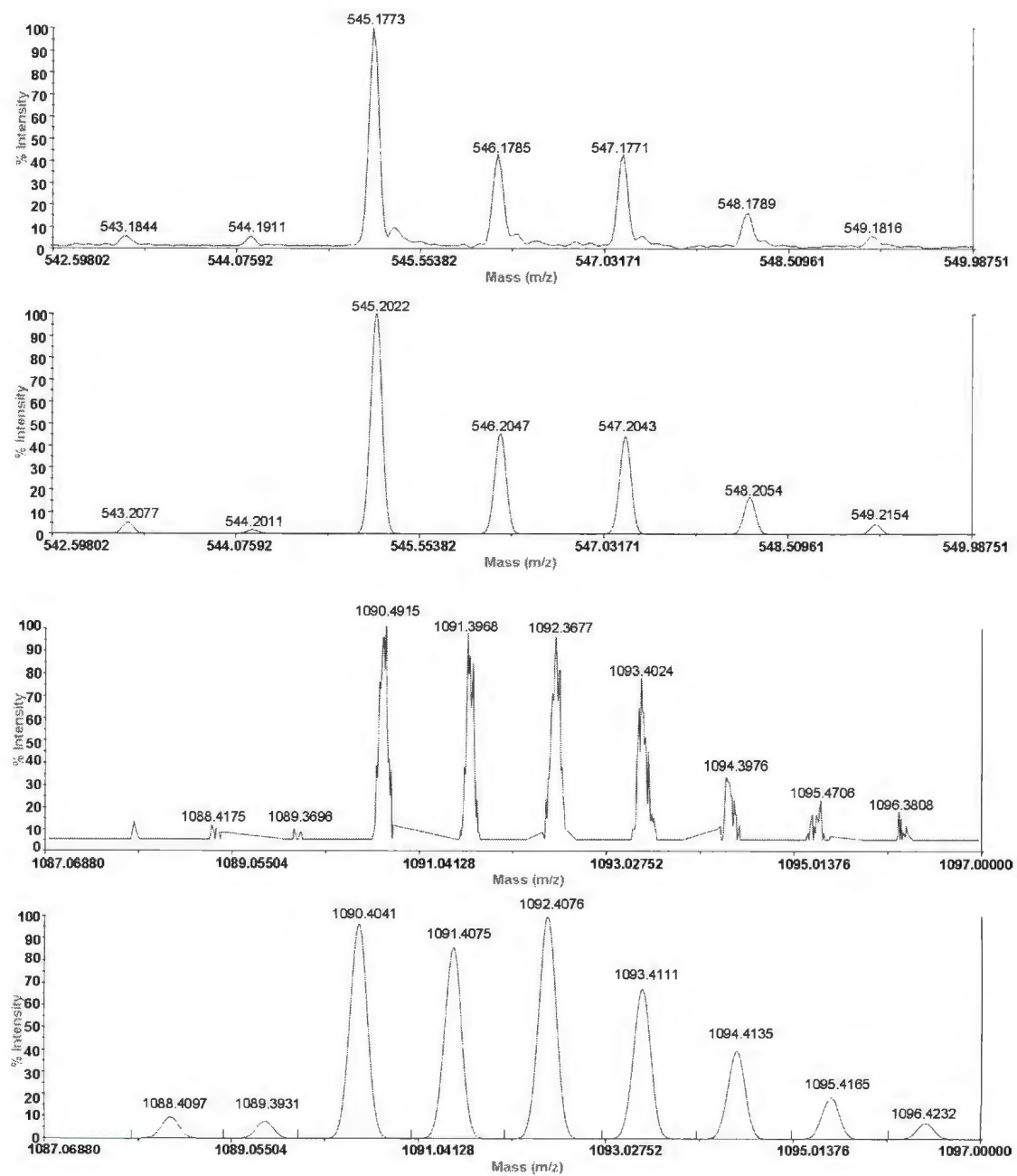


Figure B1.6. Experimental and theoretical MALDI-TOF MS isotopic distribution pattern for **4.3** (top = monomer, bottom = dimer).

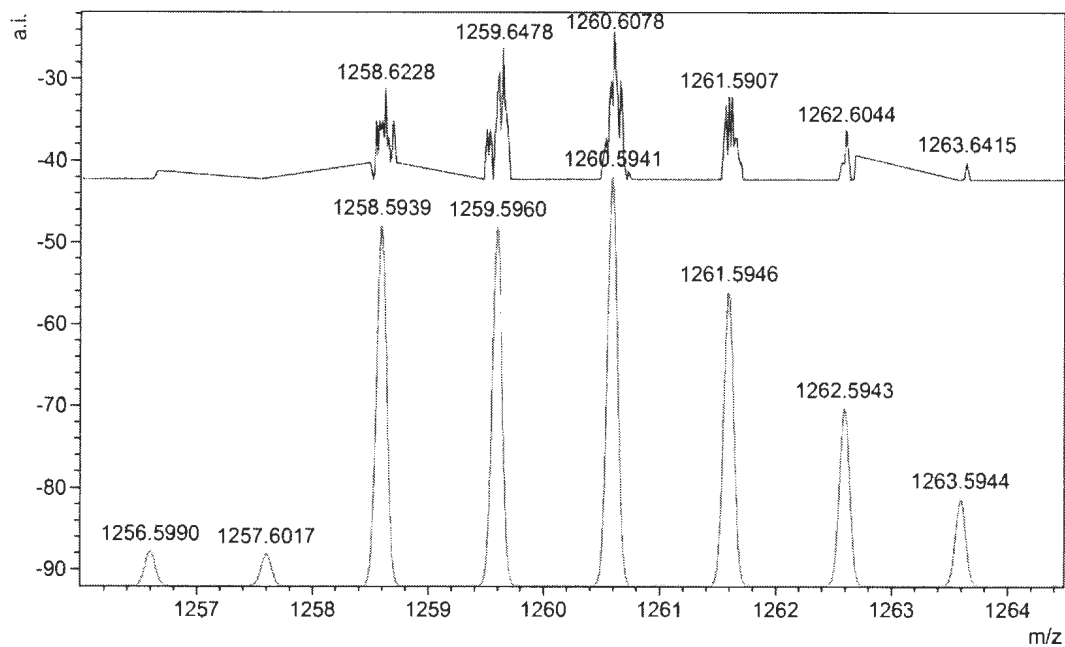


Figure B1.7. Experimental and theoretical MALDI-TOF MS isotopic distribution pattern for dimer fragment in 4.4. Poor resolution is due to very weak signal intensity.

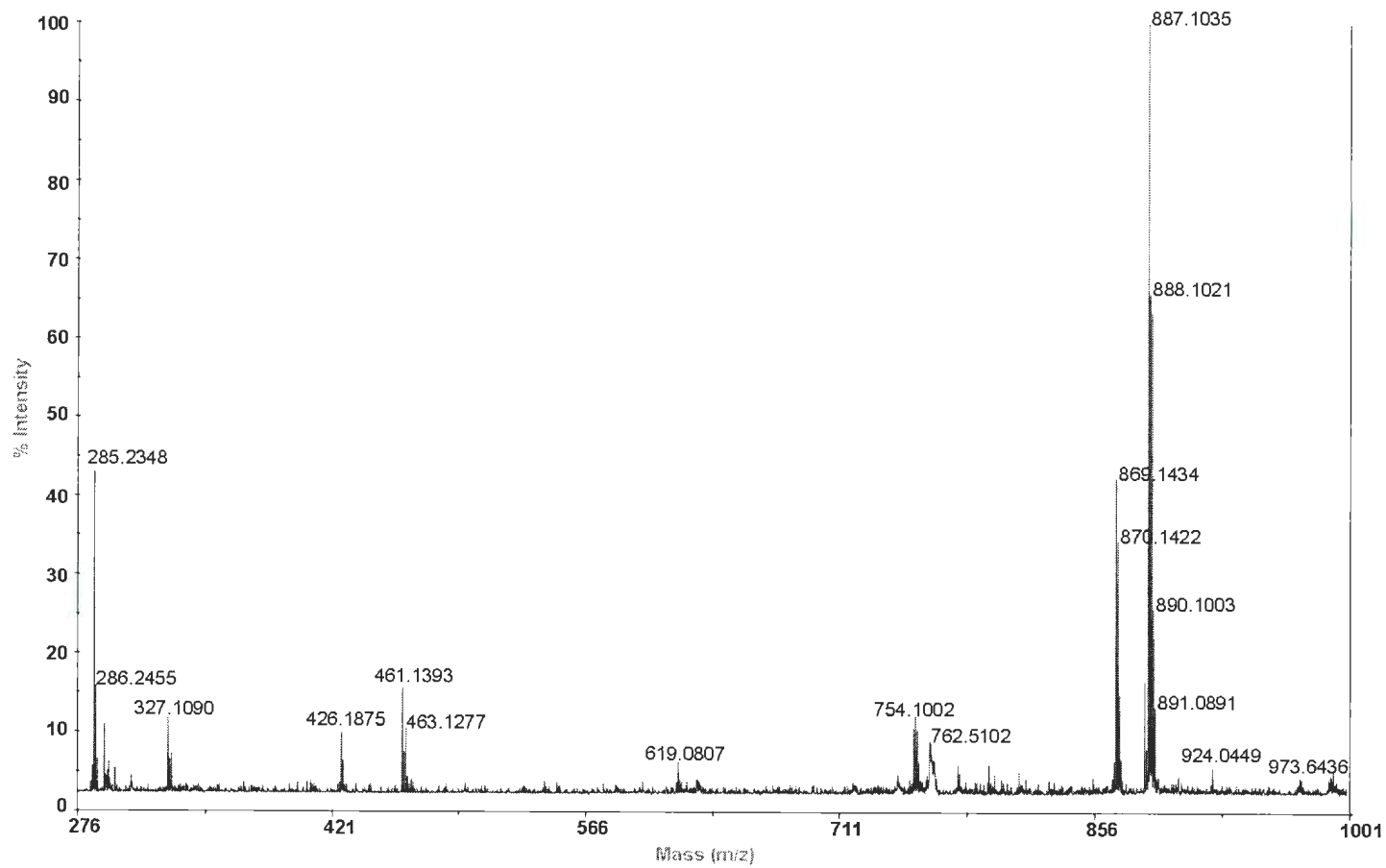


Figure B1.8. MALDI-TOF mass spectrum of $\{\text{CrCl}[\text{O}_2\text{NN}^{\text{MeMe}}]\}(\mu\text{-HO})\{\text{CrCl}[\text{HO}_2\text{NN}^{\text{MeMe}}]\}$ (**4.5**).

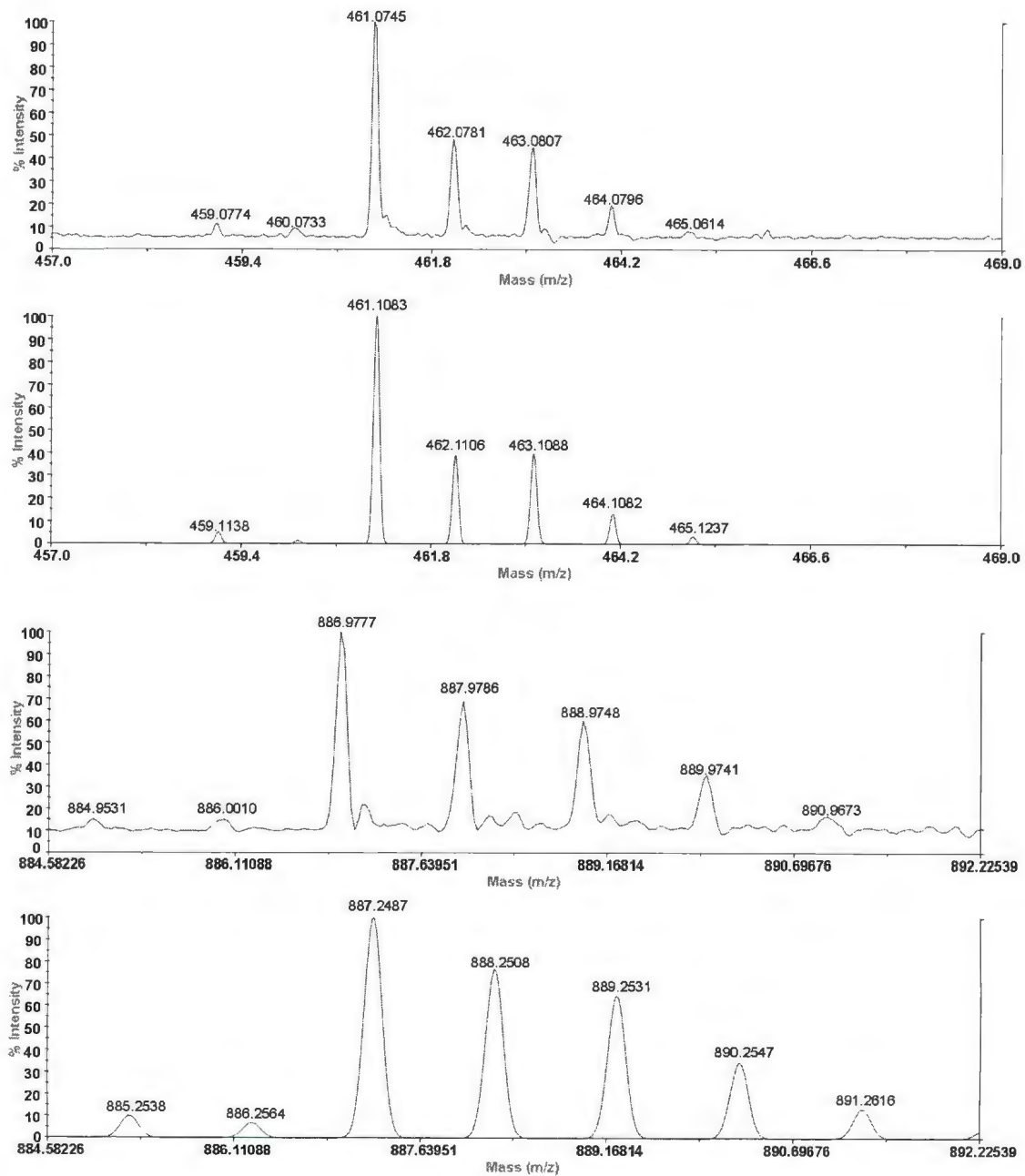


Figure B1.9. Experimental and theoretical MALDI-TOF MS isotopic distribution pattern for 4.5 (top = monomer, bottom = dimer).

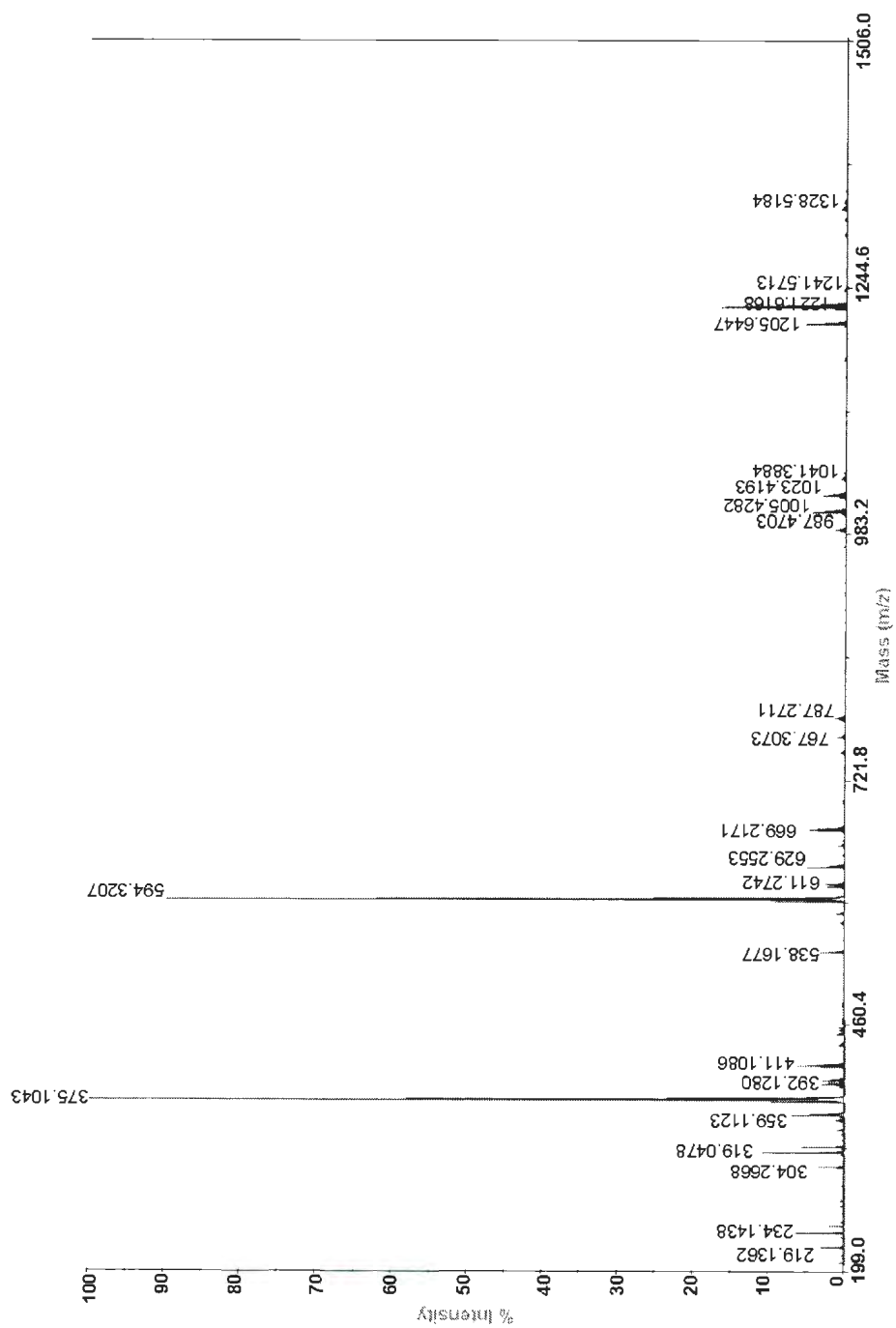


Figure B1.10. MALDI-TOF mass spectrum of $\{CrCl[O_2NN]^{nBuBu}\}(\mu-HO)\{CrCl[HO_2NN]^{nBuBu}\}$ (4.6).

Appendix C: Conversion Plots for the ROP of LA

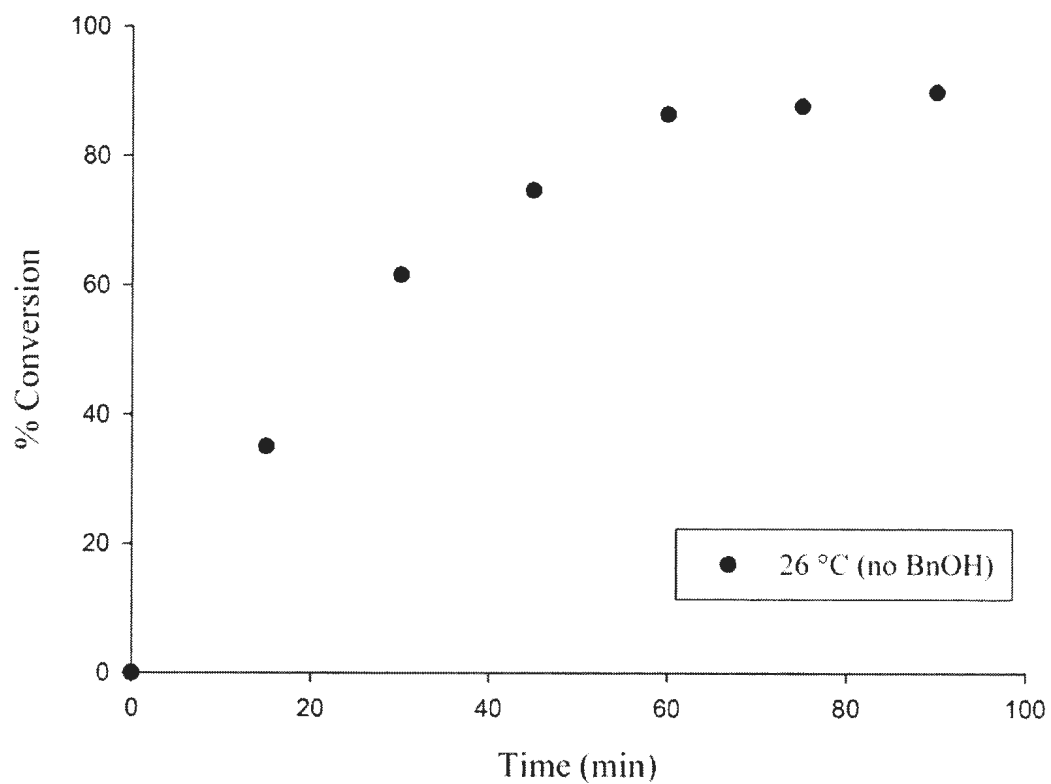


Figure C1.1. % conversion vs. time for the ROP of LA at 26 °C initiated by **2.1** without BnOH.

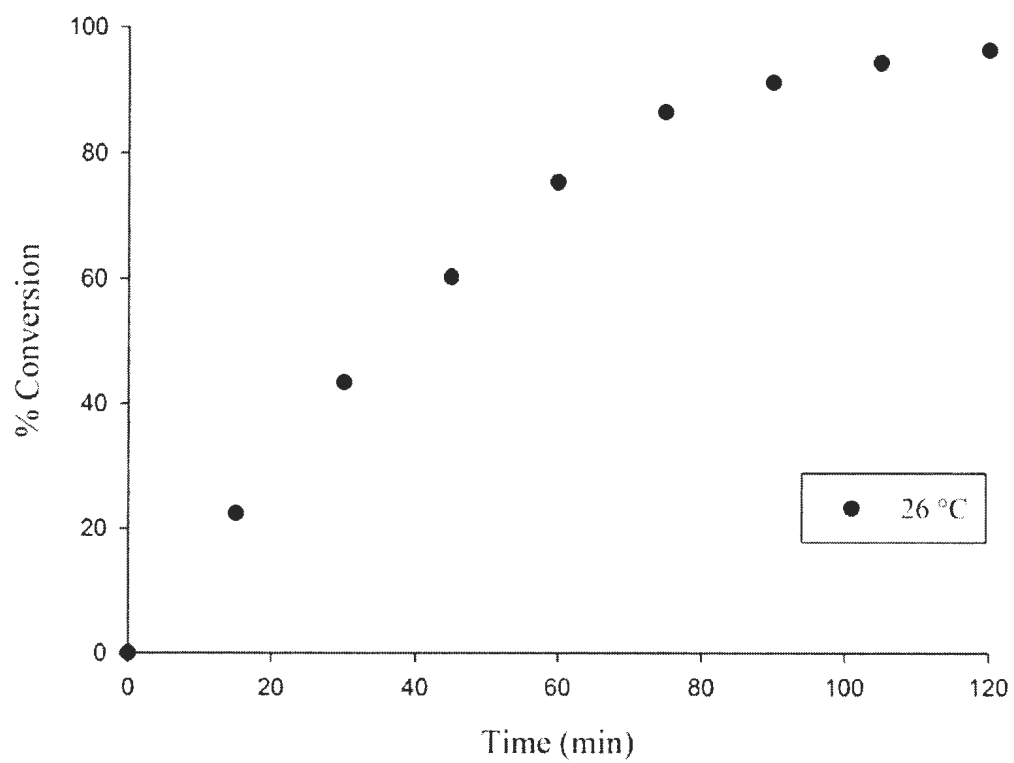


Figure C1.2. % conversion vs. time for the ROP of LA at 26 °C initiated by **2.1**.

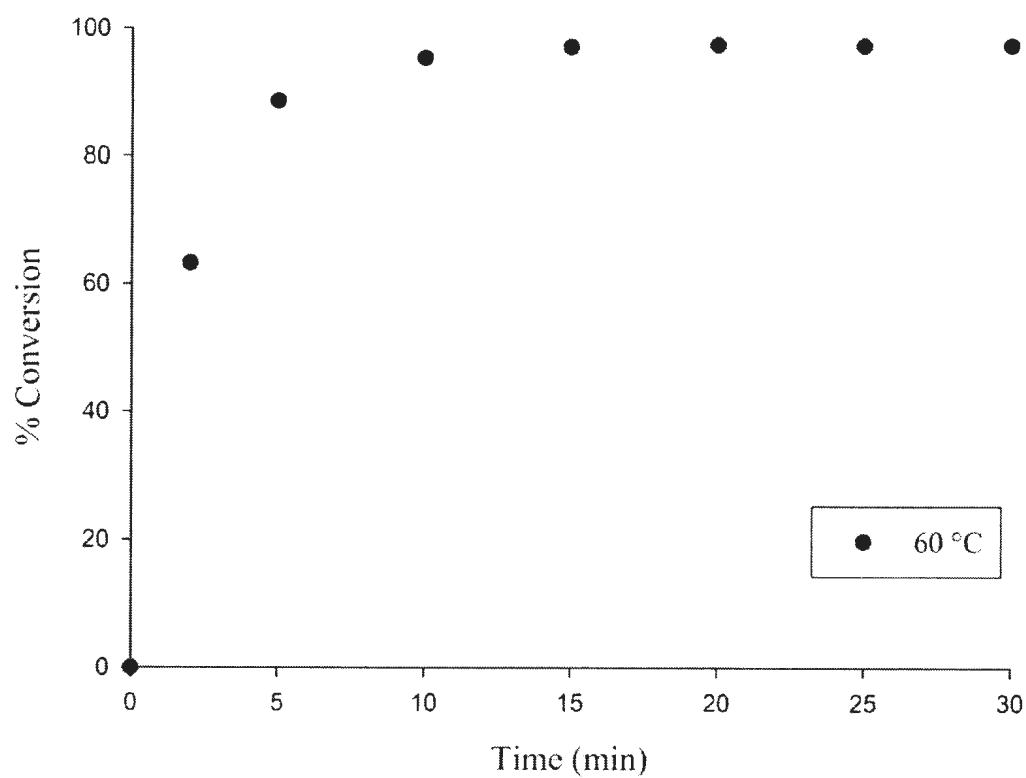


Figure C1.3. % conversion vs. time for the ROP of LA at 60 °C initiated by **2.1**.

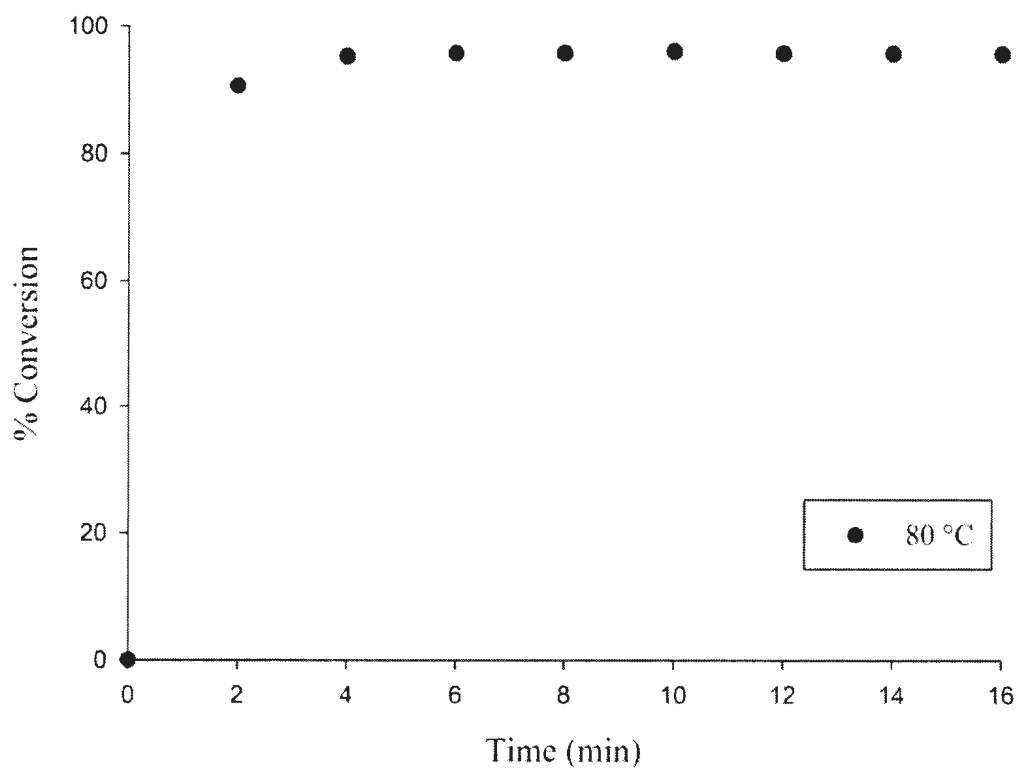


Figure C1.4. % conversion vs. time for the ROP of LA at 80 °C initiated by 2.1.

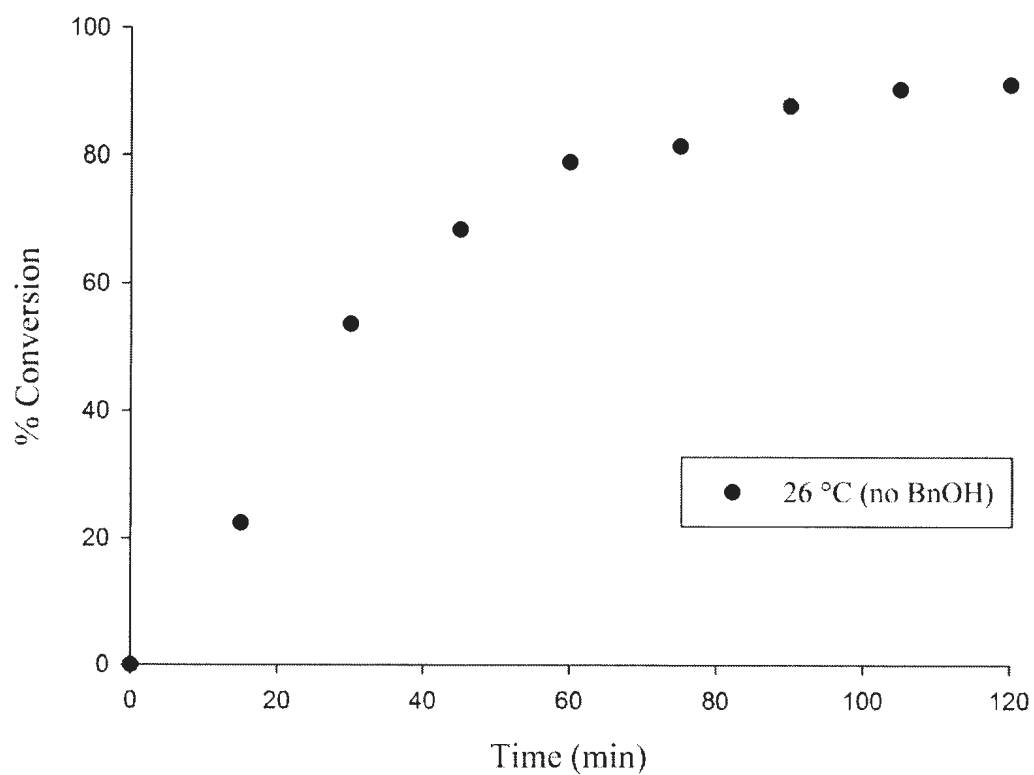


Figure C1.5. % conversion vs. time for the ROP of LA at 26 °C initiated by **2.2** without BnOH.

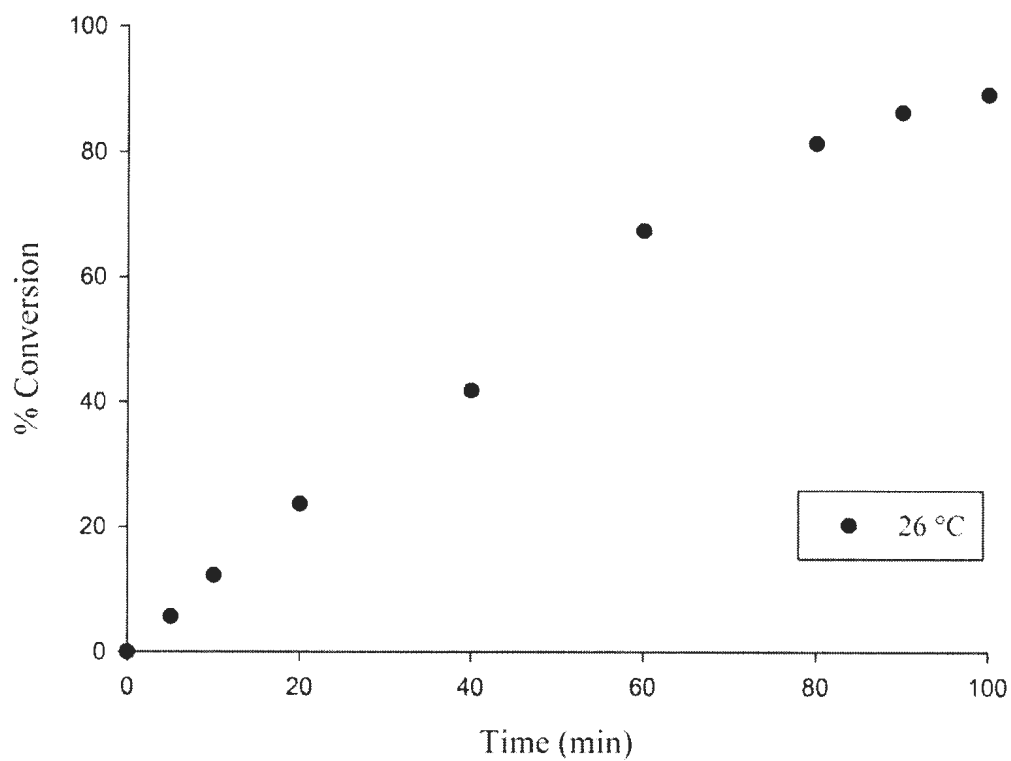


Figure C1.6. % conversion vs. time for the ROP of LA at 26 °C initiated by **2.2**.

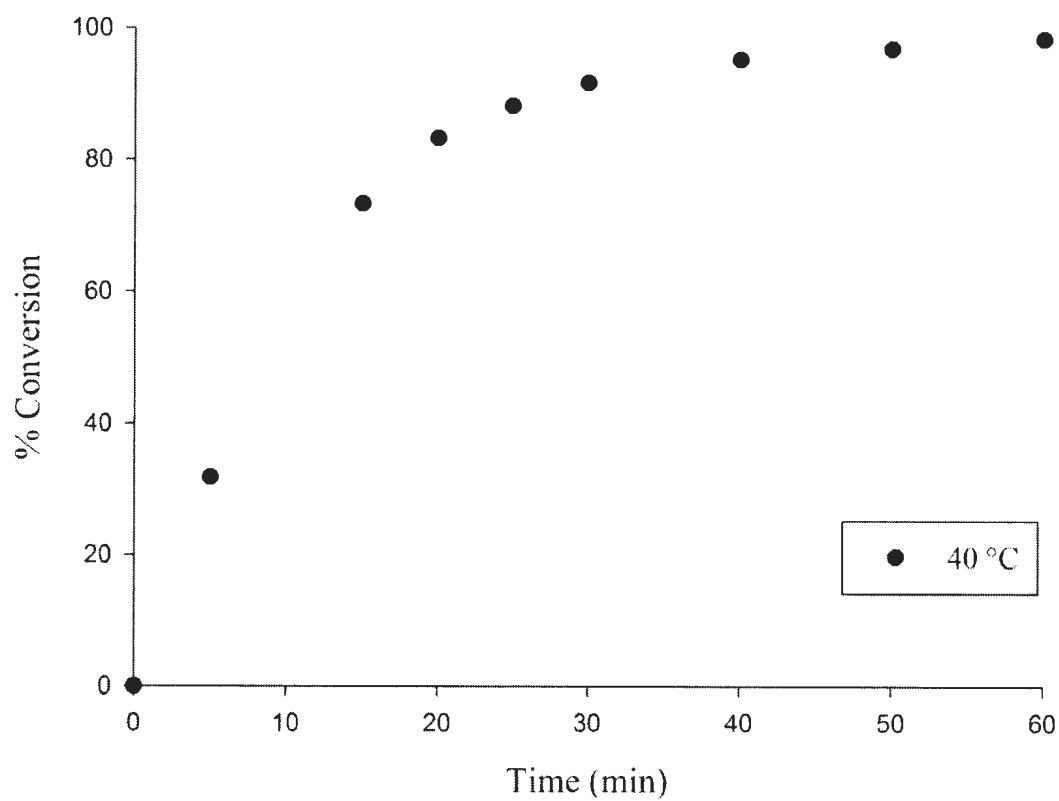


Figure C1.7. % conversion vs. time for the ROP of LA at 40 °C initiated by **2.2**.

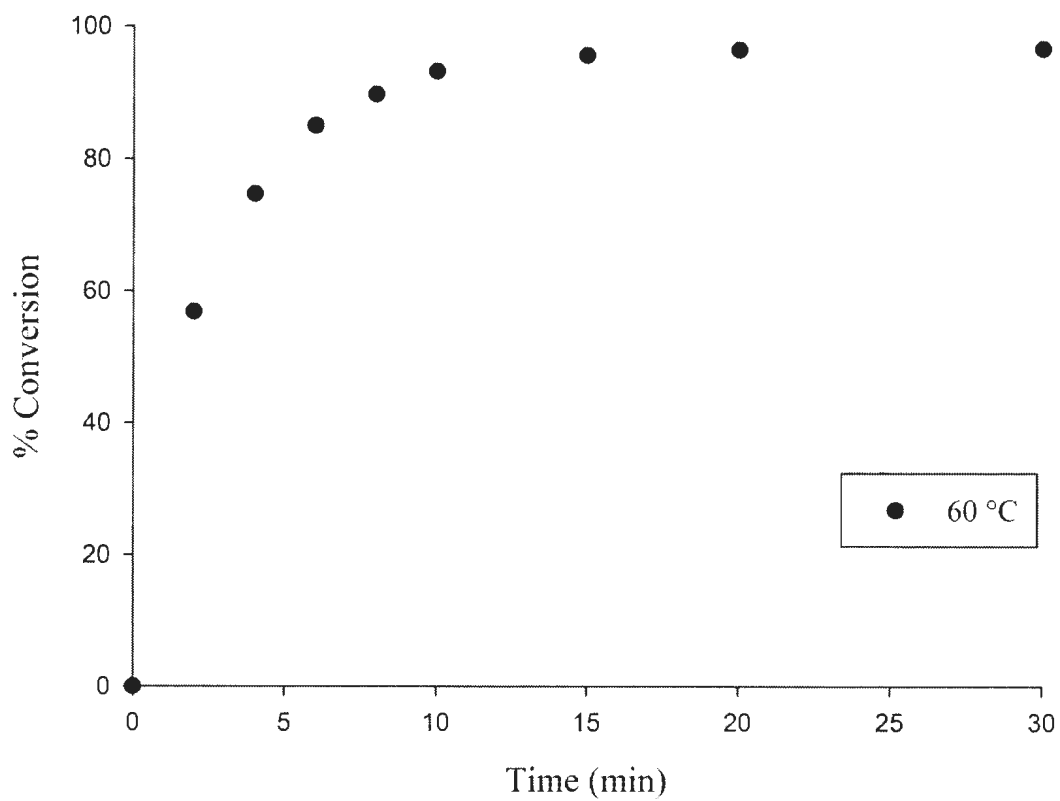


Figure C1.8. % conversion vs. time for the ROP of LA at 60 °C initiated by **2.2**.

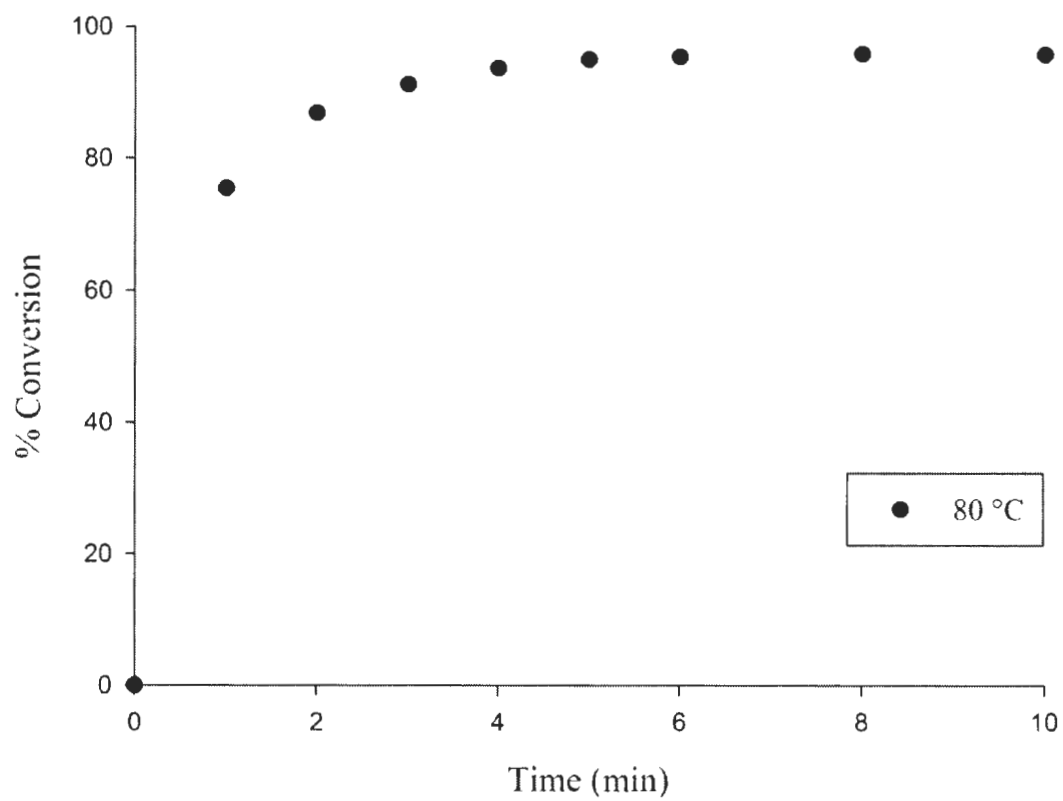


Figure C1.9. % conversion vs. time for the ROP of LA at 80 °C initiated by **2.2**.

Appendix D: UV-Visible Spectroscopy

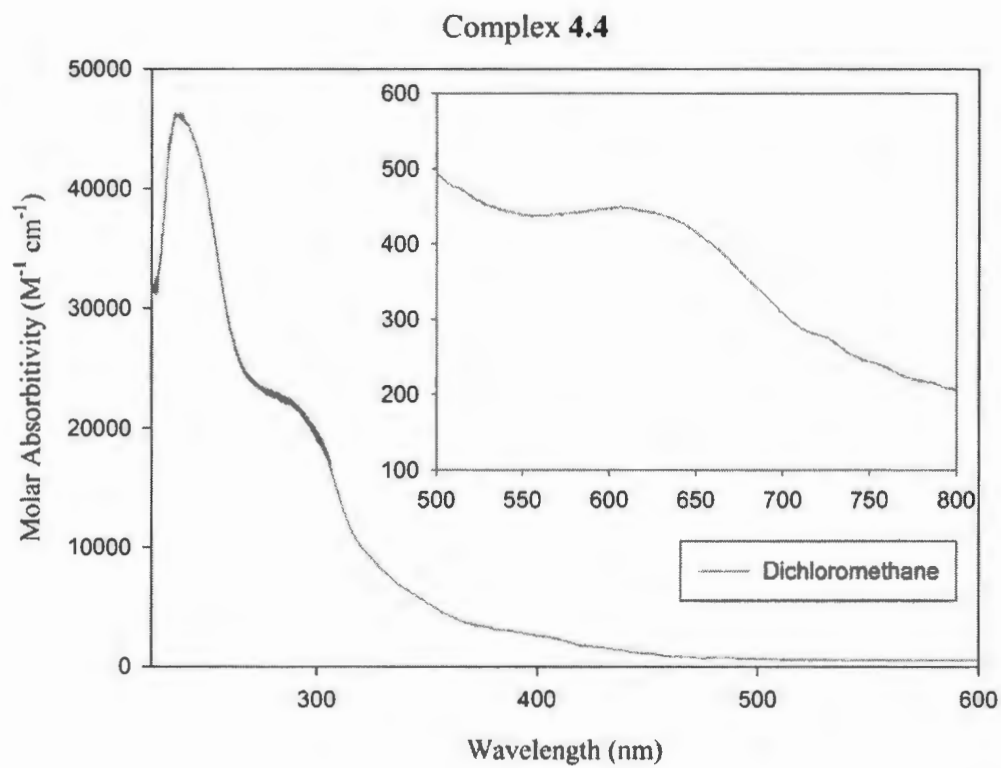


Figure D1.1. UV-Vis absorption spectrum of **4.4**.

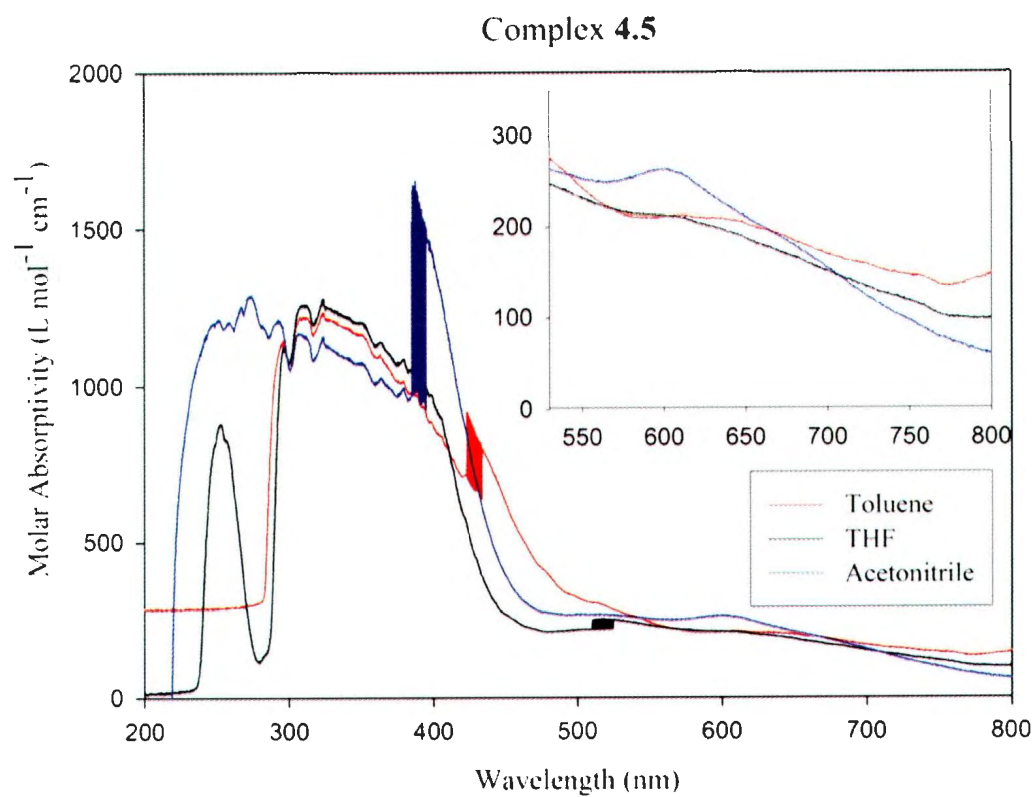


Figure D1.2. UV-Vis absorption spectrum of **4.5**.

Appendix E: Infrared Spectra

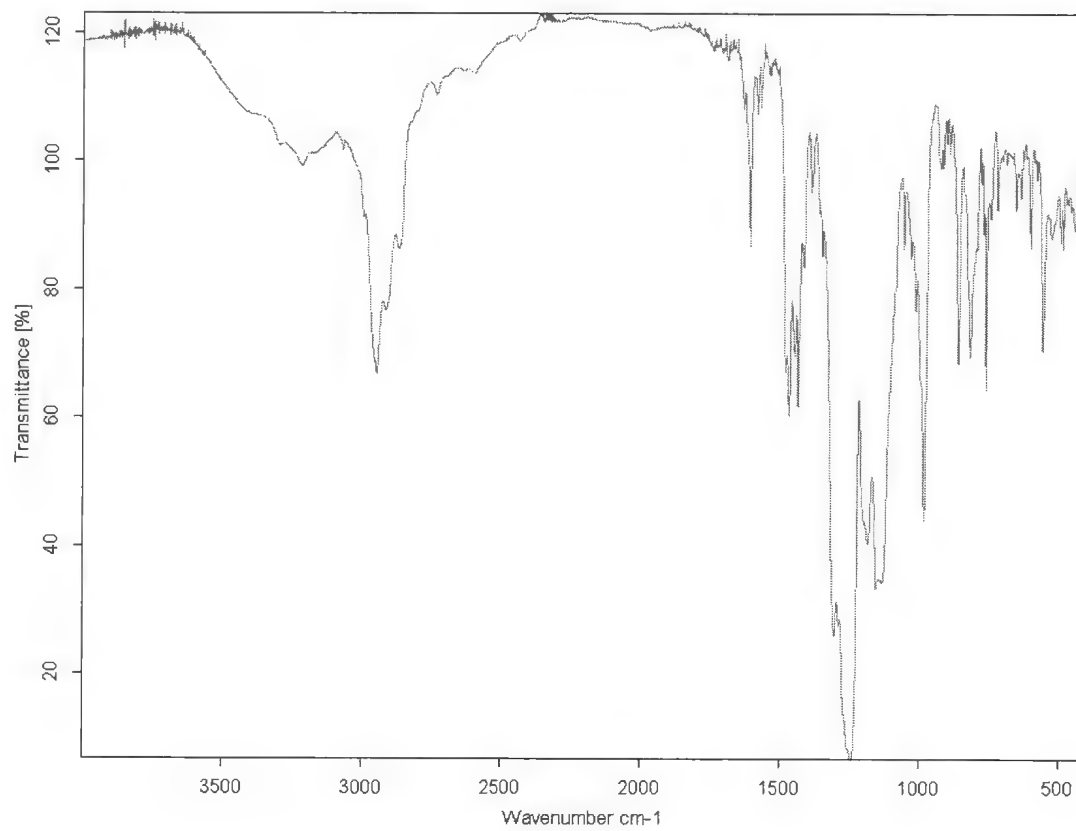


Figure E1.1. IR spectrum of complex 4.3.

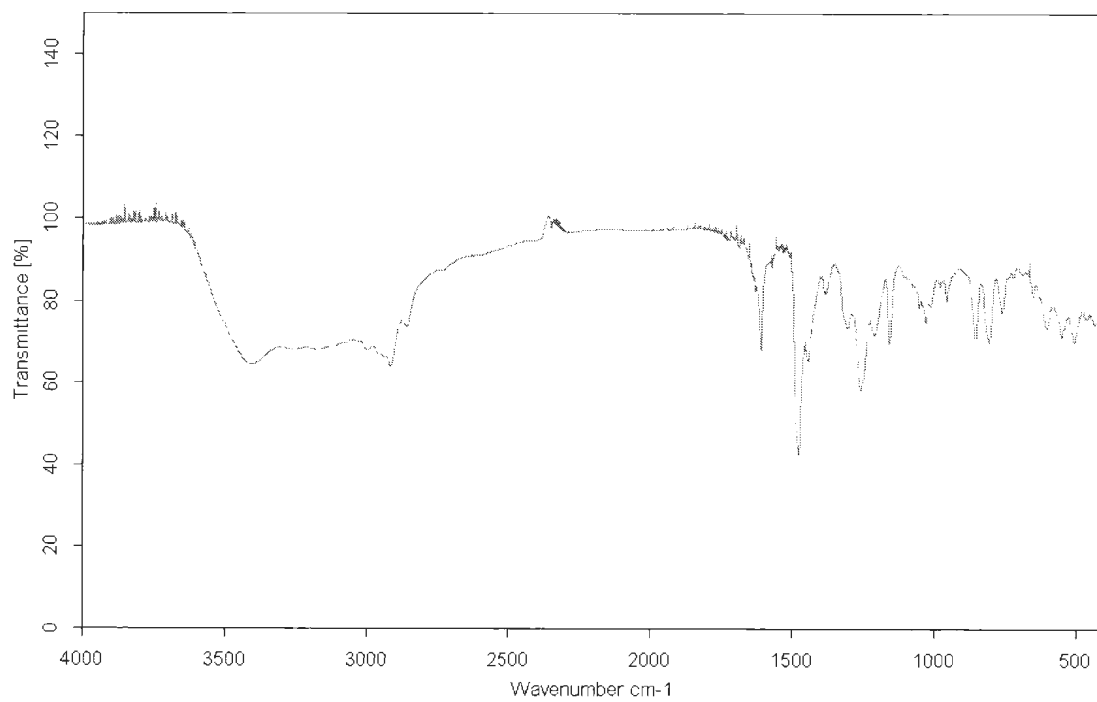


Figure E1.2. IR spectrum of complex **4.5**.

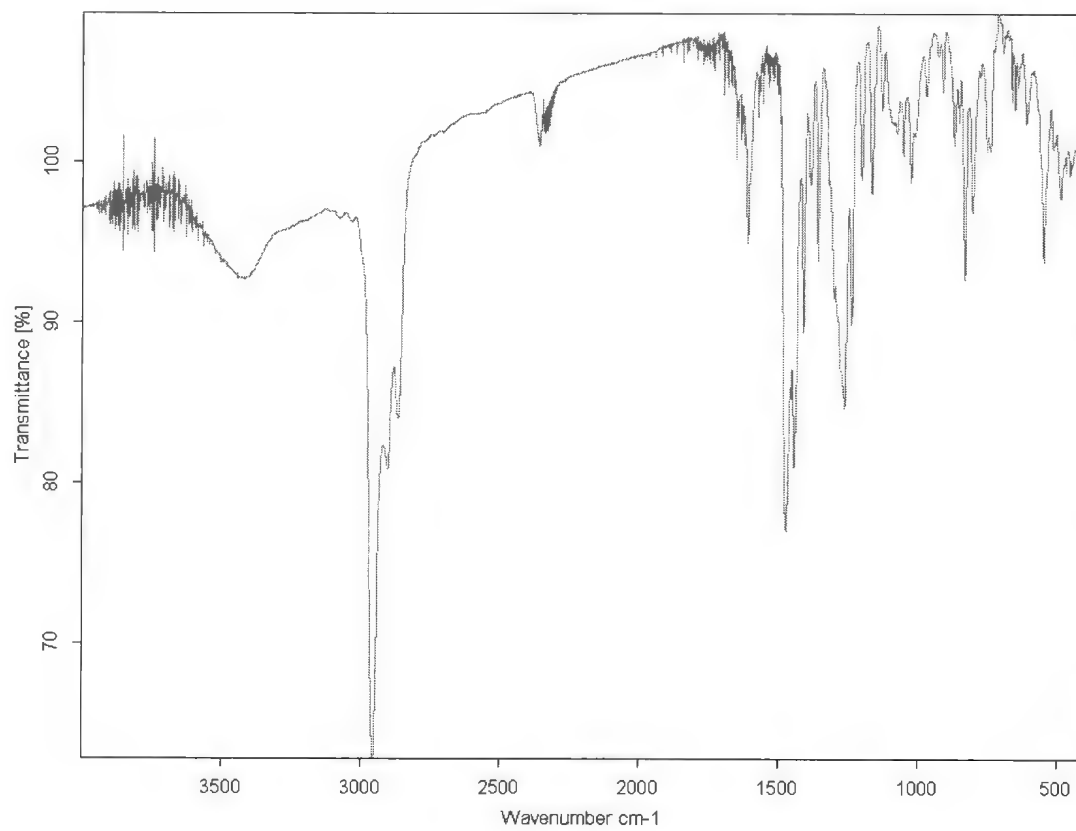


Figure E1.3. IR spectrum of complex **4.6**.

